SYNTHESIS OF CONJUGATED MOLECULES FOR TWO PHOTON ABSORPTION MATERIALS AND N-TYPE ORGANIC FIELD EFFECT TRANSISTORS

SHAO JINJUN

NATIONAL UNIVERSITY OF SINGAPORE

2013

Synthesis of Conjugated Molecules for Two Photon Absorption Materials and N-type Organic Field Effect Transistors

SHAO JINJUN

(B.Sc. Soochow University)

A THESIS SUBMITTED

FOR THE DEGREE OF DOCTOR OF PHILOSOPHY

DEPARTMENT OF CHEMISTRY

NATIONAL UNIVERSITY OF SINGAPORE

2013

To my parents, my wife,

for their love, support, and encouragement

Acknowledgements

This PhD thesis marks the end of a long journey, and I would like to take this opportunity to thank all the people who have given their invaluable assistance for making this journey possible.

First of all, I would like to express my most sincere gratitude to my supervisor, Dr. Chi Chunyan, for her guidance and encouragement during my PhD research and study. It is my honour to work under her supervision, and her suggestions, especially her optimistic attitude to research and life, are valuable to me, not only for my PhD study, but also for my future career life.

Secondly, I would like to extend my heartfelt thanks to Dr. Wu Jishan, as well as all the members in Chi and Wu's group, for their great support during group meetings and seminar discussions. I had a wonderful and unforgettable time working with them in/outside the lab for the last four years.

Particular thanks should be given to Mr. Chang Jingjing, who fabricated devices and measured the charge mobility for my compounds in chapter 3, 4 and 5, and to our collaborator, Prof. Xu Qinghua, who measured the two photon absorption and fluorescence lifetimes for my compounds in chapter 2.

I am also grateful to the staff in the Department of Chemistry for their kind assistance during my PhD career, Mdm Han, Mr. Wu for their assistance in NMR analysis, Mdm Wong, Mdm Lai and Dr. Liu for their assistance in Mass analysis. I also owe my thanks to many other people in Department of Chemistry in NUS, for their kind help from time to time. My warmest thanks also go to National University

of Singapore (NUS) and Singapore government for providing me with financial support.

Last but not least, I am profoundly indebted to my parents, Mr. Shao Qijin and Mrs. Xu Nianfen, and my wife Ms. Wan Mingyi who always support me, love me, without their encouragement, understanding and support, it would have been impossible for me to finish my PhD studies.

Thesis Declaration

I here declare that this thesis is my original work and it has been written by me in its entirety, under the supervision of Assistant Professor Chi Chunyan, (in the laboratory of Organic Electronics), Chemistry Department, National University of Singapore, between 2008 and 2013.

I have duly acknowledged all the sources of information which have been used in the thesis.

This thesis has also not been submitted for any degree in any university previously.

The contents of the thesis have been partly published in:

1. **Jinjun Shao**, Zhenping Guan, Yongli Yan, Chongjun Jiao, Qing-Hua Xu, Chunyan. Chi*, Synthesis and Characterizations of Star-shaped Octupolar Triazatruxenes Based Two-photon Absorption Chromophores, *J. Org. Chem*. **2011**, *76*, 780-790.
2. **Jinjun Shao**, Jingjing Chang, Chunyan Chi*, Linear and Star-shaped Pyrazine-containing Acene Dicarboximides with High Electron-affinity. *Org. Biomol. Chem.*, **2012**, 10, 7045-7052.

SHAO JINJUN _____ _____

Name Signature Date

Table of Contents

Chapter 2

Synthesis and Characterizations of Star-shaped Octupolar Triazatruxenes Based Two-photon Absorption Chromophores

SUMMARY

The aim of this study is to develop new π-conjugated organic molecules for two photon absorption (2PA) materials and organic field effect transistors (OFETs). In chapter 1, a brief historic overview of 2PA and OFETs was provided, and different types 2PA active molecules and different methods to construct n-channel semiconductores were introduced as well. A selection of conjugated molecules as the examples were shown in this chaper to highlight the recent development of 2PA materials and n-channel semiconductors, so as to elucidate how to design good 2PA active materials and n-channel organic semiconductors. A series of conjugated molecules for efficient 2PA response materials and n-channel OFETs have been synthesized and systematically investigated in this PhD work.

In chapter 2, a new synthetic route was developed to prepare six octupolar compounds based on triazatruxene. Solvent polarity has little effect on the UV-vis absorption spectra, while significant bathochromic shift of the emission spectra was observed together with a larger Stokes shift in polar solvents due to intramolecular charge transfer (ICT). Chromophores show high two-photon absorption cross section with the maxima ranging from 280 GM to 1620 GM. meanwhile, the largest 2P action cross section (δΦ) is up to 564 GM, so they could be the potential 2PEF probes. In addition, all chromophores show good thermal and photo-stability.

In chapter 3, a series of electron-deficient pyrazine-containing linear and

star-shaped acene molecules end functionalized with dicarboximide groups have been synthesized, and their optical properties, electrochemical properties and thermal behavior were investigated in detail. Due to the attachment of carboximide groups and the fusion of pyrazine units, these conjugated compounds showed high electron affinities, with the low-lying LUMO energy level up to -4.01 eV. Moderate electron mobilities in thin films were obtained via the Space-Charge Limited-Current (SCLC) technique.

In chapter 4, a family of electron-deficient naphthalene imide derivatives have been designed and synthesized; their optical properties, electrochemical properties, thermal behavior were fully investigated. All the semiconductors have been used as active components for high performance, solution-processed *n*-channel organic field effect transistors. The fabricated devices exhibit electron mobility of up to 0.016 $cm^2 V^{-1}s^{-1}$ under nitrogen atmosphere, with current on/off ratios of 10^4-10^5, and threshold voltages of 10-20 V. Moreover, they show excellent air and operating stability.

In chapter 5, a phthalimide-fused naphthalene diimde (**NDIIC24**) with low-lying LUMO energy level (-4.21 eV) and moderate solubility was synthesized. OFETs based on solution processed thin films showed typical *n*-channel characteristics with a high electron mobility of 0.056 $cm^2V^{-1}s^{-1}$ and a high on/off current ratio of 10^5-10^6. The devices exhibited very good air stability and operating stability. Complementary inverters based on *n*-type NDIIC24 and *p*-type TIPS-pentacene demonstrated a

maximum voltage gain ($-dV_{OUT}/dV_{IN}$) of 64.

Key Words: conjugated molecules, two-photon absorption (2PA), triazatruxene, field effect transistors (FETs), pyrazine, naphthalene diimide (NDI)

List of Abbreviations

AcOH	acetic acid
Ac	acetyl
aq.	aqueous
Ar	aryl
t-Bu	*tert*-butyl
c	concentration
^{o}C	degrees (Celcius)
CMOS	complementary metal–oxide–semiconductor
CV	cyclic voltammetry
δ	chemical shift in parts per million
DCM	dichloromethane
DMF	*N*, *N*-dimethylformaldehyde
DMSO	dimethyl sulfoxide
DPV	differential pulse voltammetry
DSC	differential scanning calorimetry
dd	doublet of doublet
EA	ethyl acetate
EI	electron impact ionization
ESI	electro spray ionization
Et	ethyl
FAB	fast atom bombardment ionization

g	grams
h	hour(s)
Hex	hexane
HBC	hexa-*peri*-hexabenzocoronene
HOMO	highest occupied molecular orbital
HR-MS	high resolution mass spectroscopy
Hz	hertz
ICT	Intremolecular charge transfer
J	coupling constant
LUMO	lowest unoccupied molecular orbital
MALDI-TOF	matrix-assisted laser desorption/ionization-time-of-flight
Me	methyl
MeOH	methanol
M	$mol \cdot L^{-1}$
mg	milligram
MHz	megahertz
min.	minute(s)
mL	milliliter
μL	microliter
mmol	millimole
MS	mass spectroscopy
NBS	*N*-bromosuccinimide

NDA	1,4,5,8-Naphthalenetetracarboxylic dianhydride
NDI	Naphthalene diimide
NIR	near-infrared
NMR	nulcear magnetic resonance
ODTS	octadecyltrichlorosilane
OFET	organic field-effect transistor
OSC	organic semiconductor
OTMS	octadecyltrimethoxysilane
ppm	parts per million
i-Pr	isopropyl
PDI	perylene tetracarboxylic diimide
Ph	phenyl
PL	photoluminesence
POM	polarized optical microscopy
QY	quantum yield
RT	room temperature
TGA	thermogravimetric analysis
THF	tetrahydrofuran
TLC	thin layer chromatography
2PEF	two-photon excited fluorescence
TsCl	*para*-toluenesulfonyl chloride
Ts	*para*-toluenesulfonyl

TsOH	*para*-toluenesulfonic acid
UV	ultraviolet
vis	visable
XRD	X-ray diffraction

LIST OF PUBLICATIONS AND CONFERENCES

Publications during PhD studies

1. **J. Shao**, Z. Guan, Y. Yan, C. Jiao, Q-H. Xu, C. Chi*. Synthesis and Characterizations of Star-shaped Octupolar Triazatruxenes Based Two-photon Absorption Chromophores*, J. Org. Chem*. **2011**, *76*, 780–790.
2. **J. Shao**, J. Chang, C. Chi*. Linear and Star-shaped Pyrazine-containing Acene Dicarboximides with High Electron-affinity. *Org. Biomol. Chem.,* **2012**, 10, 7045-7052.
3. **J. Shao,** J. Chang, J. Wu, C. Chi*. Unsymmetrical Naphthalene Imides with High Electron Affinity for Airstable and Soluble-Processible n-Channel Field Effect Transistors. *Org. Lett.,* **2013**, submitted.
4. J. Chang, **J. Shao,** J. Zhang, J. Wu, C. Chi*. A Phthalimide-fused Naphthalene Dimide With High Electron Affinity for High Performance n-Channel Field Effect Transistor. *Chem Comm*, **2013**, submitted.
5. **J. Shao,** J. Chang, J. Wu, C. Chi*. Pyromellitic diimide-based copolymers for air-stable field effect transistors: synthesis, characterization and device performance. *J. Mater. Chem.,* **2013**, to be submitted
6. Q. Ye, J. Chang, **J. Shao**, C. Chi*. Large core-expanded triazatruxene-based discotic liquid crystals: synthesis, characterization and physical properties, *J. Mater. Chem.,* **2012,** 22, 13180-13186.
7. J. Luo, B. Zhao, **J. Shao**, H. S. O. Chan, C. Chi*, Room-temperature Discotic Liquid Crystals Based on Oligothiophenes – Attached and Fused Triazatruxenes, *J. Mater. Chem.,* **2009,** 19, 8327-8334.
8. B. Zhao, B. Liu, **J. Shao**, P. K. H. Ho, C. Chi*, J. Wu*. New Discotic

Mesogens Based on Triphenylene-fused Triazatruxenes: Synthesis, Physical Proeprties, and Self-assembly, *Chem. Mater.*, **2010,** *22*, 435-449.

9. H. Qu, W. Cui, J. Li, **J. Shao, C. Chi*.** "6, 13-Dibromopentacene [2,3:9,10]-Bis(dicarboximide): A Versatile Building Block for Stable Pentacene Derivatives" *Org. Lett.,* **2011**, 13, 924-927, (**highlighted in SYNFACTS 2011, 5, 0492**).

Conferences

1. **J. Shao**, Z, Guan, Q-H, Xu, C, Chi*, Synthesis and Characterizations of Star-shaped Octupolar Triazatruxenes Based Two-photon Absorption Chromophores, *International chemical congress of pacific basin societies*, 15-20 Dec, 2010, Hawaii, USA.
2. **J. Shao**, C, Chi*, Pyrazine-containing Linear and Star-shaped n-type Acenes, *10th International Symposium on Functional π-Electron Systems (F-π-10)*, 13-17 Oct, 2011, Beijing, China

List of Tables

List of Figures

Figure 4.6 POM images for **4-1a**–**b** and **4-2** – **4-4**. a) **4-1a**, at 338 ^{o}C upon slow cooling; b) **4-1b**, at 227 ^{o}C upon slow cooling; c) **4-2**, at 205 ^{o}C upon slow cooling; d) **4-3**, at 270 ^{o}C upon slow cooling; e) **4-4**, at 100 ^{o}C upon slow cooling.

Figure 4.7 Powder X-ray diffraction (XRD) patterns of compounds **4-1a**, **4-1b**, **4-2** – **4-5** at different temperatures.

Figure 4.8 Transfer (V_D = 70 V, left) and output (right) characteristics of OFET devices from **4-1a** (a), **4-1b** (b), **4-2** (c), **4-3** (d) and **4-4** (e)

Figure 4.9 X-ray diffraction patterns for the thin films of **4-1a**, **4-1b** (as-spun), **4-2** – **4-3** (annealed at 150 ^{o}C) and **4-4** (annealed at 100 ^{o}C).

Figure 4.10 AFM images (height and amplitude images, 2μm×2μm) of the thin films of a) **4-1a** (as-spun), b) **4-1b** (as spun), c) **4-2** (annealed at 150 ^{o}C), d) **4-3** (annealed at 150 ^{o}C) and e) **4-4** (annealed at 100 ^{o}C).

Figure 4.11 Transfer characteristics of thin films **4-2** (a) and **4-3** (b) on OTMS treated substrates annealed at 150 ^{o}C for as spun conditions (red) and after storing in N_2 for three months (blue).

Figure 5.7 (a) Schematic representation of the inverter; (b) Chemical structures of the TIPS-pentacene and **NDIIC24**; (c) Voltage transfer characteristics of a complementary inverter with various supplied voltages and the plots of gains ($-dV_{OUT}/dV_{IN}$) that correspond to the voltage transfer curves.

List of Schemes

Chapter 1

Introduction

1.1 Introduction

Organic molecules are the chemicals of life, which found in and produced by living organisms, they contain carbon-hydrogen bonds, which distinguish them from inorganic molecules. Conjugated organic molecules were found to be acted as electrical conductors 30 years ago. Afterwards a tremendous research effort has been devoted towards the development of organic semiconducting molecules for photonic/electronic applications since the pioneering study from Wudl and Müllen.[1]

With few exceptions, organic semiconducting molecules are divided into two types, conjugated organic small molecules (oligomers),[2] and organic conjugated polymers (macromolecules),[3] both offering distinct advantages and disadvantages in terms of processability and device performance.[4] Conjugated organic small molecule materials having well defined chemical structures can be obtained in high purity levels through conventional purification techniques, such as chromatography, sublimation, and recrystallization. Furthermore, they can be provided in large amounts through reproducible and well-established synthetic protocols. Thin films with good characteristics can be easily produced by vacuum deposition, spin-coating, casting, or printing under ambient conditions to fabricate large-area devices with high performances. Nevertheless, organic small molecule semiconductors generally lack good solution film-forming properties, due to the limited achievable solution viscosities, presenting a challenge to widespread

applications in printed electronics. In contrast, polymers are polydisperse material systems for which large-scale purification methods are generally limited to reprecipitation or extraction (e.g., Soxhlet). Trace impurities from polymers are difficult to remove which may greatly compromise device performance. Furthermore, due to molecular weight and polydispersity variations, their device performance reproducibility from polymer batch to batch can be problematic.[5] Nevertheless, polymeric semiconductors typically exhibit good film-forming properties, which are essential for fabrication of large-area devices by printing.[6]

The π-conjugated organic molecules can serve as potential candidates for organic photonic/electronic applications, such as organic light emitting diode (OLEDs), organic photovoltaic solar cells (OPVs), organic field effect transistors (OFETs) and two photon absorption (2PA) materials.

1.2 Recent Development in Two-Photon Absorption (2PA) Materials

1.2.1 Introduction

2PA process was first proposed by M. Goeppert-Mayer (1906-1972) in her doctoral dissertation in 1931.[7] In her thesis, she theoretically predicted that a simultaneous 2PA process should also lead to a transition between a lower and a higher energy level of an atom or a molecule, which is different from one-photon absorption. In 1961, Kaiser and Garrett reported the first observation of a 2PA induced frequency-up-conversion fluorescence in a CaF_2:Eu^{2+}crystal sample.[8]

Since then, a new major research area of two-photon processes has been opened to scientists and engineers. During the 1970s and 1980s, the main research topic in this new area focused on two-photon spectroscopy of simple atomic and molecular gaseous systems, organic solvents and compounds, as well as inorganic crystals and semiconductors. From the 1990s onwards, research effort started to focus on developing various two-photon active materials and seeking for their applications. Recently, 2PA has attracted growing interest due to its potential application in material science and in biological imaging, including three-dimensional optical data storage, lithographic micro-fabrication, optical power limiting, two photon fluorescence imaging, and localized photodynamic therapy.[9] These applications depend considerably on the high 2PA cross-section values displayed by the specifically engineered organic molecules.

The 2PA properties are measured by two-photon excited fluorescence (2PEF),[10] nonlinear transmission (NLT),[11] open aperture Z-scan,[12] and femtosecond (fs) white light continuum (WLC) pump-probe[13] methods, employing nanosecond (ns), picosecond (ps), and fs pulses. The 2PEF method has been often employed, due to the experimental convenience and good data reproducibility. The 2PA cross section (δ) measured through NLT method varied by orders of magnitude depending on the pulse width. Z-scan and WLC methods are used as well but not as commonly as the 2PEF method due to the experimental difficulties. Moreover, the δ values checked by the WLC method are usually larger than those measured via the 2PEF method.

For applications that require high 2PA cross section, such as optical limiting and 3D microfabrication or strong 2PEF such as bioimaging, molecules with large 2PA cross section per molecular weight (δ_{max}/M_w) or large 2P action cross section per molecular weight ($\Phi\delta_{max}/M_W$) are needed. Moreover, molecules with $\delta_{max}/M_W > 1.0$ have been found to be useful for such applications.[14]

The most frequently employed structural motifs for 2PA response materials are donor–bridge–acceptor (D–π–A) dipoles, donor–bridge–donor (D–π–D) and donor–acceptor–donor (D–A–D) quadrupoles, octupoles with π-centers and functional groups of electron-donating and/or electron-withdrawing groups at the terminal sites.[15] A large number of dipolar/quadrupolar molecules have been synthesized and characterized, however, octupolar molecules with high 2PA cross section and good stability are relatively rare.

1.2.2 Dipolar 2PA Molecules

The first dipolar Donor–bridge–Acceptor (D–π–A) 2PA active molecules were reported by Reinhardt et al.[16] However, the δ obtained by the NLT method using ns pulses were overestimated. Recently, a more reasonable 2PA value utilizing a fs NLT method was reported by Prasad's group.[17] The δ/M_W value for the pentafluorostilbene derivatives increases with the conjugation length with a concomitant increase in the δ_{max} (**1-2** – **1-4**, Figure 1.1, Table 1.1). This indicates a parallel increase in the δ with the intramolecular charge transfer (ICT) between the donor (D) and acceptor (A).

However, strong ICT process results in low fluorescence quantum yields (Φ), so that these compounds are not useful for applications that use 2PEF.

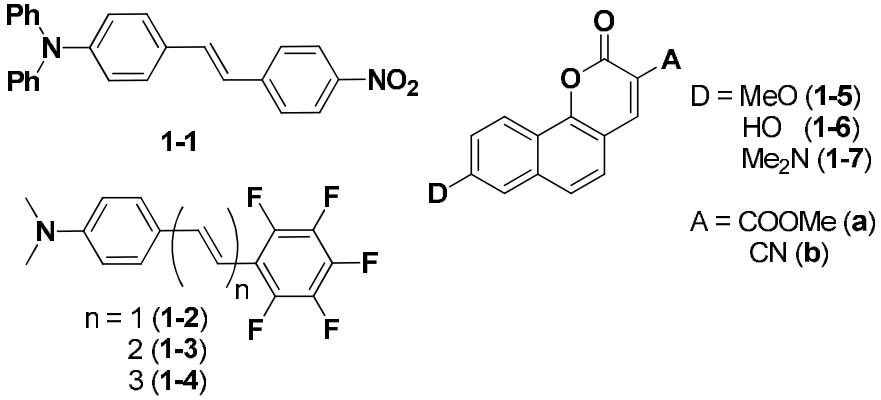

Figure 1.1 Chemical structures of dipolar molecules **1-1** – **1-7**

Table 1.1 Photophysical data for dipolar molecules **1-1** – **1-7**

	sol	λ^1_{max} [a]	Φ [b]	λ^2_{max} [c]	δ_{max} [d]	δ_{max}/M_W [e]	$\Phi\delta_{max}/M_W$ [e]
1-1	THF	431	0.022	840	125	0.32	
1-2	Tol	370		750	120	0.38	0.0084
1-3	Tol	396	0.025	825	300	0.88	0.0022
1-4	Tol	412	0.026	850	500	1.37	0.036
1-5a	H_2O	391	0.82	780	140	0.49	0.40
1-6a	H_2O	397	0.48	780	270	1.00	0.48
1-7a	H_2O	453	0.19	880	350	1.30	0.25
1-7b	H_2O	457	0.050	940	470	1.60	0.079

[a] λ_{max} of the one photon absorption spectra in nm; [b] Fluorescence quantum yield; [c] λ_{max} of the two-photon excitation spectra in nm; [d] The peak two-photon absorptivity in 10^{-50} cm^4 s/photon (GM); [e] When alkyl groups were larger than Me, the molecular weight was calculated by assuming that R = Me; the unit is GM/g.

Among all dipolar molecules reported in the literature, chromene derivatives (**1-5** – **1-7**, Figure 1.1) appear to be most promising in bioimaging. They show appreciable

water solubility, significant $\Phi\delta_{max}/M_W$ and high photostability, and emit strong 2PEF when labeled in giant unilamellar vesicles and cells.[18] Here, a parallel increase in the δ_{max}/M_W and δ_{max} values with a stronger donor group was observed. **1-7a** showed high quantum yield of 0.19 in water, with significant δ_{max}/M_W value of 1.30, as indicates that it would be an efficient 2PEF probe. However, its 2PA cross section is only at 350 GM.

1.2.3 Quadrupolar 2PA molecules

D–π–D, D–A–D, A–π–A quadrupoles are the most frequently investigated structural motifs for two-photon active molecules, in which phenyl, fluorene, and anthracenyl are employed as the core and C=C bonds are employed as the conjugation bridge.

When an anthryl group was used as the core, 9,10-Phenyl substituents at the anthryl group decreased δ_{max}/M_W and $\Phi\delta_{max}/M_W$ as a result of smaller δ_{max} and larger M_W (**1-8 vs. 1-9**, Figure 1.2, Table 1.2), whereas 9,10-π-cyanophenyl substituents did not appreciably change these values (**1-8 vs. 1-10**).[19] In comparison with **1-8**, λ_{max} and δ_{max}/M_W of **1-11** increased by around 190 nm and nearly twofold, respectively.[19] However, the quantum yield of **1-11** was lowered to 0.11, which may be due to strong ICT between the donor and acceptor groups, as a result, the $\Phi\delta_{max}/M_W$ value decreased by around three fold.

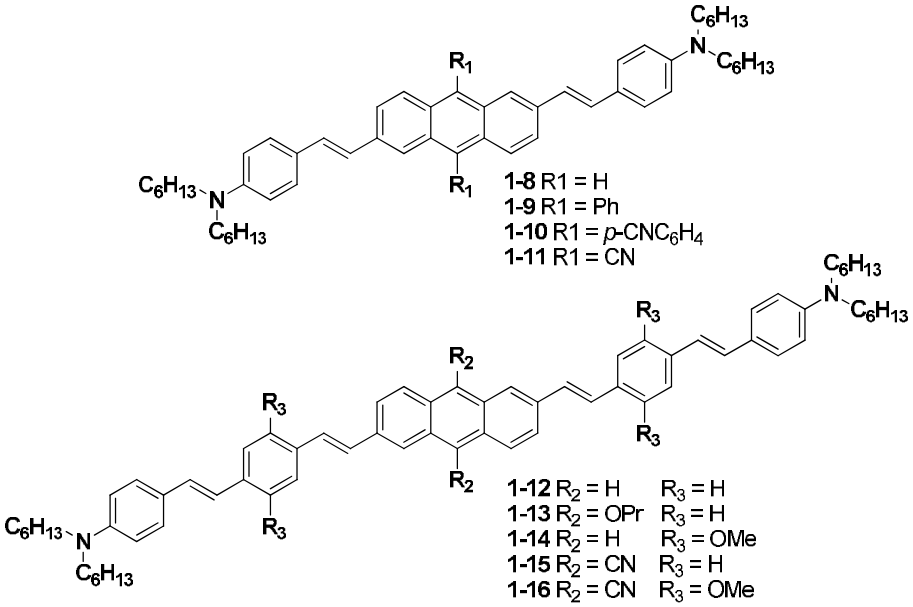

Figure 1.2 Chemical structures of quadrupolar molecules **1-8** – **1-16**

Table 1.2 Photophysical data for dipolar molecules **1-8** – **1-16**

	sol	λ^1_{max} [a]	Φ [b]	λ^2_{max} [c]	δ_{max} [d]	δ_{max}/M_W [e]	$\Phi\delta_{max}/M_W$ [e]
1-8	Tol	455	0.78	800	1100	2.35	1.83
1-9	Tol	466	1.0	780	770	1.28	1.28
1-10	Tol	488	0.64	840	1570	2.34	1.50
1-11	Tol	587	0.11	990	2290	4.41	0.49
1-12	Tol	427	0.64	800	1140	1.69	1.08
1-13	Tol	476	0.75	800	1900	2.59	1.94
1-14	Tol	478	0.66	800	2400	3.14	2.07
1-15	Tol	531	0.13	980	5530	7.65	0.99
1-16	Tol	575	0.064	980	3650	4.33	0.28

[a] λ_{max} of the one photon absorption spectra in nm; [b] Fluorescence quantum yield; [c] λ_{max} of the two-photon excitation spectra in nm; [d] The peak two-photon absorptivity in 10^{-50} cm^4 s/photon (GM); [e] When alkyl groups were larger than Me, the molecular weight was calculated by assuming that R = Me; the unit is GM/g.

Chromophore **1-12**, in comparison with **1-8**, the conjugation bridge was extended, resulting in a slight increase of δ_{max}, but a significant decrease in $\Phi\delta_{max}/M_W$, probably due to its distorted structure (Figure 1.2, Table 1.2).[20] Substitution of the OR groups at the core or at the intervening phenyl groups significantly increased the values of δ_{max}, δ_{max}/M_W and $\Phi\delta_{max}/M_W$ (**1-12 vs. 1-13** and **1-14**). When CN groups were introduced at the 9,10-positions, the λ_{max} and δ_{max}/M_W increased by 180 nm and by about five-fold, respectively, presumably because of the enhanced ICT (**1-12 vs. 1-15**). The OMe groups at the intervening phenyl groups further facilitated the ICT as indicated by the large increase in the δ_{max} (**1-15 vs. 1-16**). Here again, the $\Phi\delta_{max}/M_W$ value of **1-15** was smaller than those of **1-13** and **1-14** due to the large decrease in Φ.

1.2.4 Octupolar 2PA molecules

Multibranched structure would significantly increase the 2PA cross section in comparison to their singlebranched counterpart was first reported by Prasad.[21] The value of δ_{max}/M_W for **1-17a – 1-19a** increased from 0.17 to 0.36 to 0.58 as the number of branch increased (Figure 1.3, Table 1.3). A theoretical study has revealed that such an enhancement is mainly due to the vibronic coupling.[22] The electronic coupling is weak, probably because the central amino group is used as the connecting unit, which breaks the conjugation of the whole network. In other words, increasing the size of the π framework will increase the density of state, providing more effective coupling

channels, which would in turn increase the 2PA cross section.

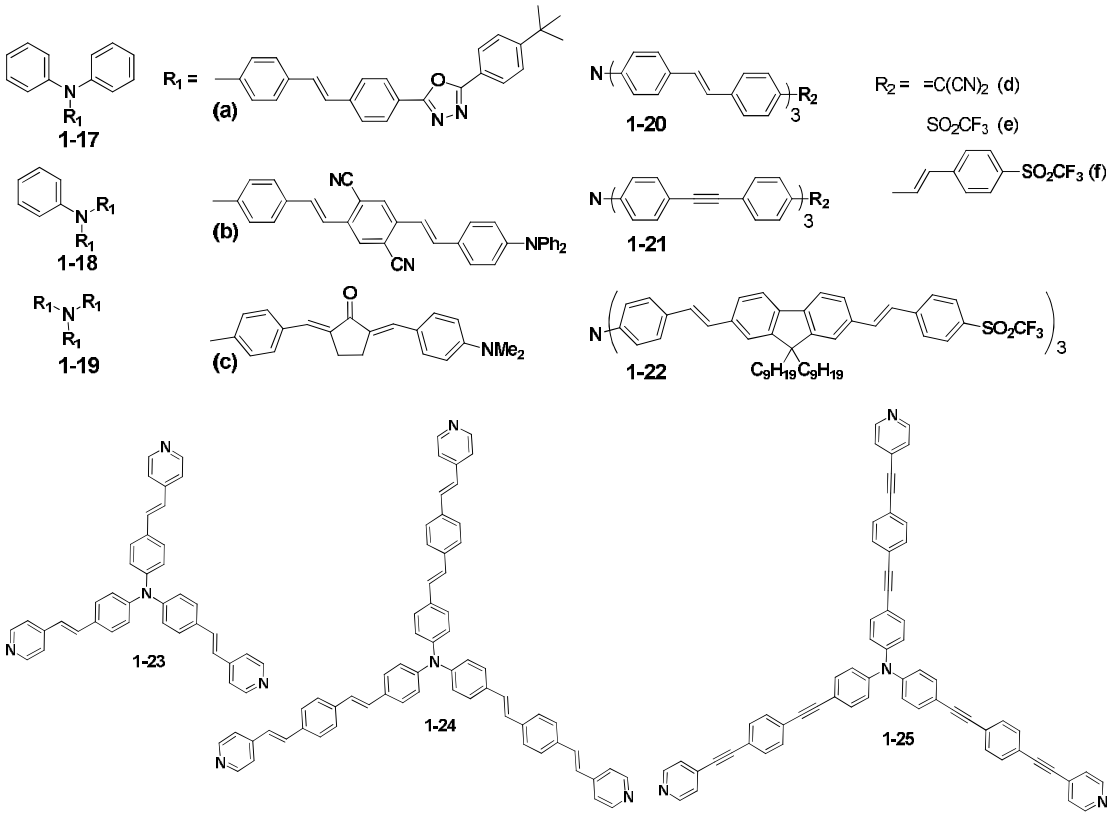

Figure 1.3 Chemical structures of octupolar molecules **1-17** – **1-25**

Table 1.3 Photophysical data for octupolar molecules **1-17** – **1-25**

	sol	λ^1_{max} [a]	Φ [b]	λ^2_{max} [c]	δ_{max} [d]	δ_{max}/M_W [e]	$\Phi\delta_{max}/M_W$ [e]
1-17a	TCE	399		796	88	0.17	
1-18a	TCE	417		796	275	0.36	
1-19a	TCE	426		796	600	0.58	
1-17b	Tol	473	0.73	840	1370	2.05	1.50
1-18b	Tol	492	0.69	840	3130	2.68	1.85
1-19b	Tol	495	0.67	840	5030	3.02	2.02
1-17c	$CHCl_3$	471	0.11	850	781	1.66	0.18

1-18c	$CHCl_3$	491	0.15	790	2474	3.56	0.53
1-19c	$CHCl_3$	492	0.16	790	3298	3.58	0.57
1-20d	Tol	487	0.41	890	1200	1.53	0.63
1-20e	Tol	435	0.71	740	1340	1.41	1.00
1-20f	Tol	435	0.84	800	2070	1.65	1.39
1-21e	Tol	405	0.78	740	495	0.53	0.41
1-21f	Tol	408	0.72	740	1080	0.87	0.63
1-22	Tol	440	0.83	740	2080	1.30	1.08
1-23	THF	406	0.23	800	370	0.71	0.16
1-24	THF	426	0.26	800	1037	1.22	0.32
1-25	THF	391	0.55	800	280	0.32	0.18

[a] λ_{max} of the one photon absorption spectra in nm; [b] Fluorescence quantum yield; [c] λ_{max} of the two-photon excitation spectra in nm; [d] The peak two-photon absorptivity in 10^{-50} cm^4 s/photon (GM); [e] When alkyl groups were larger than Me, the molecular weight was calculated by assuming that R = Me; the unit is GM/g.

Cho's group and others have observed similar results as well.[23,24] Hence, the δ_{max}/M_W for **1-17b – 1-19b** and **1-17c – 1-19c** (Figure 1.3, Table 1.3) increased with the number of branching to reach the maximum values of 3.02 and 3.58 for **1-19b** and **1-19c**, respectively, demonstrating significant enhancement in the multi-branched structure.[25] Moreover, the $\Phi\delta_{max}/M_W$ value of 2.02 for **1-19b** is among the largest values in the reported literature. It is to be noted that all these molecules have D–A–D structure in each branch. On the other hand, while the molecules are composed of three dipolar D–π–A branches, δ_{max}/M_W values are becoming lower (**1-17b – 1-19b** and **1-17c – 1-19c** vs. **1-20d – 1-20f**), even with strong electron withdrawing substituents at the periphery sites. An extension in the conjugation length by

replacement of the phenyl to fluorenyl group slightly decreased δ_{max}/M_W (**1-20f vs. 1-22**, Figure 1.3, Table 1.3). When the conjugation bridge was changed from C=C to C≡C, δ_{max}, δ_{max}/M_W and $\Phi\delta_{max}/M_W$ values all decreased, as expected from the poorer conjugating ability (**1-20e**, **1-20f** vs. **1-21e**, **1-21f**). Use of the pyridine moiety as the acceptor decreased δ_{max}/M_W, this may be due to the weak electron-withdrawing property of the pyridine unit (**1-20d**, **1-20e** vs. **1-23**). Here again, the C≡C bond in the conjugation bridge induced a positive effect on the quantum yield, but a negative effect on the 2PA cross section (**1-24** vs. **1-25**).

1.2.5 Objectives

Among all the dipolar, quadrupolar and octupolar 2PA active molecules, octupolar molecules are the most promising ones for material application, due to the vibronic coupling, cooperative effect and good intramolecular charge transfer (ICT) property. To develop an ideal multi-branched or octupolar 2PA active chromophores, it is of great importance to introduce novel cores, novel arms or novel bridges into the designation of the molecular structures. Although many multi-branched or octupolar chromophores have been investigated, most of them are not suitable for material applications, because they exhibit moderate 2PA cross section values only, while the properties such as processability and photo-stability have not been examined yet. Therefore, in this thesis, we aim to synthesize a series of novel octupolar molecules as 2PA chromophores for the

following studies:

1) Introducing of a novel core, triazatruxene (TAT), into the molecular structure designation, and constructing of an octupolar molecular structure for 2PA response materials.
2) Studying the effect of ICT of 2PA response molecules, via the introduction of different electron-withdrawing groups at the periphery sites and the adjustment of conjugation length by insertion of a thiophene unit as the bridge;
3) Checking the photostability, and thermal-stability of our synthesized molecules.

In chapter 2, a novel core, triazatruxene, have been employed to construct 2PA active molecules, they show high 2PA cross sections and high 2P action cross section values with good thermal-stability and photo-stability, which means that they are promising to be used as 2PEF probe.

1.3 Recent Development in N-type Organic Semiconductors

1.3.1 Introduction

Organic field effect transistor (OFET) is an organic transistor that relies on an electric field to control the resistance and the conductivity of a 'channel' in a semiconductor channel material. An OFET device is consisted of three electrodes, gate, source, and drain electrodes, and a small change in gate voltage can cause a

large variation in current from the source electrode to the drain electrode. According to the adopted device configuration, OFETs can be divided into four different types as shown in Figure 1.4, the bottom gate bottom contact (A), the bottom gate top contact (B), the top gate top contact (C) and the top gate bottom contact (D). The device configuration plays a key role in the device performance, and it was found that both B and D type devices always give better performances than that of A and C. This was attributed to the improved contact between the organic semiconductor and the electrodes.[26]

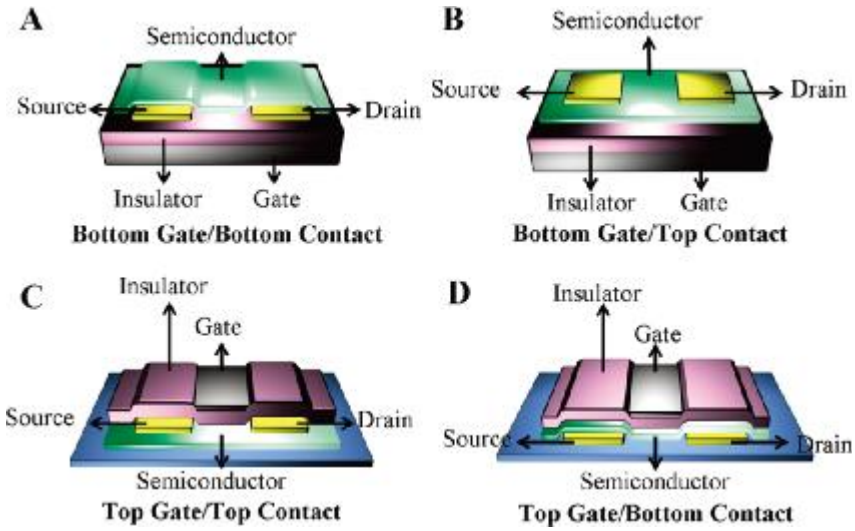

Figure 1.4 Four types of OFETs, (A) Bottom gate/bottom contact, (B) bottom gate/top contact, (C) top gate/top contact, and (D) top gate/bottom contact.

Based on the charge carrier which flowing through the organic semiconductors, the semiconductors are classified into three types, *p*-type (hole transporting), *n*-type (electron transporting) and ambipolar (both hole and electron transporting).[27] P-type semiconductors have been systematically studied during the past two decades, two kinds of promising p-type semiconductors are

oligoacenes and oligothiophenes, which have been prepared and used in organic electronics.[28] However only a limited number of n-type organic semiconductors have been synthesized and studied, which is desirable for the fabrication of *p*-*n* junction diodes, bipolar transistors, and complementary integrated circuits.[29] Therefore studies on *n*-type semiconductors have recently attracted increasing interest. The general design approaches to achieve *n*-type semiconductors include (1) attachment of electron-withdrawing substituents (e.g. fluorine, carboximide, cyano-) onto the traditional *p*-type semiconductors (e.g. acene, oligothiophene) and/or (2) replacement of the carbon atoms in the aromatic framework by electron-deficient atoms (e.g. imine nitrogen). Following this guidance, some *n*-type semiconductors have been successfully synthesized and applied for *n*-channel OFETs.

1.3.2 Fluorine-Containing N-type semiconductors

It is an important strategy to introduce strong electron withdrawing halogen atoms into organic semiconductor molecules to design n-channel semiconductors. Fluorine is one of the most widely used substituents to realize n-type behaviors.[30] For instance, pentacene is a benchmark molecule for p-channel semiconductors, while perfluoropentacene (**1-26a**)[31] shows n-type characteristics (Figure 1.5). Transistors based on evaporated thin films of **1-26b** exhibited electron mobility as high as 0.11 $cm^2\ V^{-1}s^{-1}$, while pentacene films deposited under the same

conditions showed p-type behavior with a hole mobility of 0.45 $cm^2\ V^{-1}s^{-1}$. Their comparable mobilities have made pentacene and **1-26a** suitable for the application of ambipolar OFETs and complementary circuits. The tetrafluoro (**1-26b**) and octafluoro (**1-26c**) substituted Pentacene derivatives were also synthesized and characterized.[32] OFETs based on **1-26b**–**c** showed ambipolar behaviors under N_2 (for **1-26b**, μ_e = 0.105 $cm^2\ V^{-1}s^{-1}$, μ_h = 0.07 $cm^2\ V^{-1}s^{-1}$; for **1-26c**, μ_e = 0.41 $cm^2\ V^{-1}s^{-1}$, μ_h = 0.33 $cm^2\ V^{-1}s^{-1}$). Transistors based on vacuum deposited films of **1-27** showed electron mobility of 0.016 $cm^2\ V^{-1}s^{-1}$ and a current on/off ratio of 10^4.

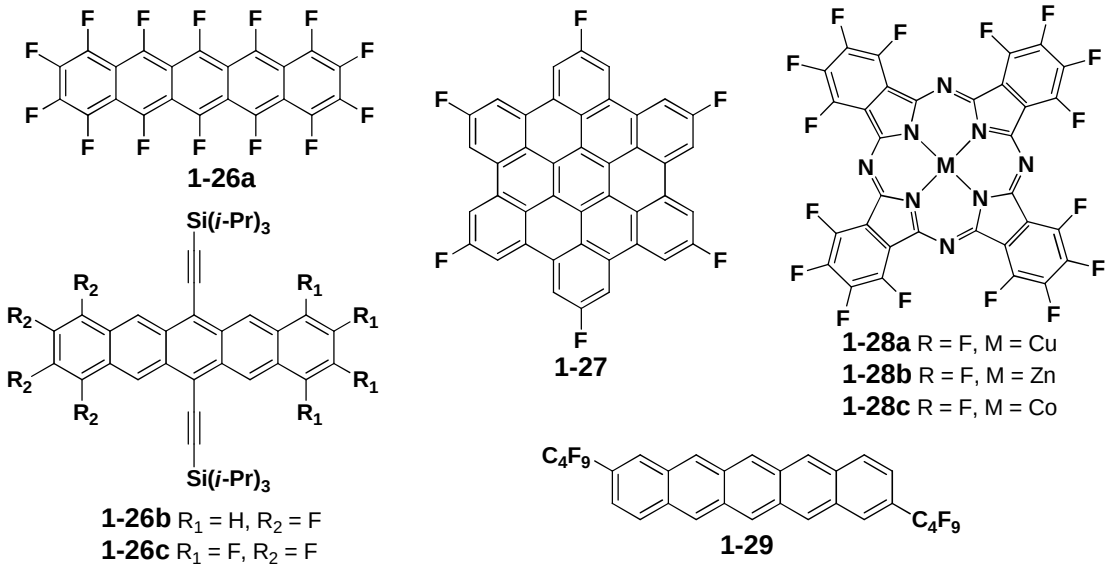

Figure 1.5 Chemical structures of fluorinated semiconductors **1-26** – **1-29**

A series of perfluorometallophthalocyanines (**1-28a**–**c**)[33a] were also designed for OFETs, they showed n-type behaviors with good air stability. For example, copper hexadecafluorophthalocyanine (F_{16}CuPc, **1-28a**), it showed an electron

mobility at 0.03 cm^2 $V^{-1}s^{-1}$ (Figure 1.5). Single crystalline nanoribbons of **1-28a** were obtained by Hu's group, and the fabricated transistors showed a mobility of 0.2 cm^2 $V^{-1}s^{-1}$.[33b]

Many perfluoroalkyl and perfluorophenyl substituted derivatives were synthesized and examined in OFETs as well, and most of them exhibited n-channel behaviors. For example, the perfluorobutyl substituted pentacene (**1-29**)[33c] showed an electron mobility of 1.7×10^{-3} cm^2 $V^{-1}s^{-1}$ (Figure 1.5).

1.3.3 Cyano-Containing N-type semiconductors

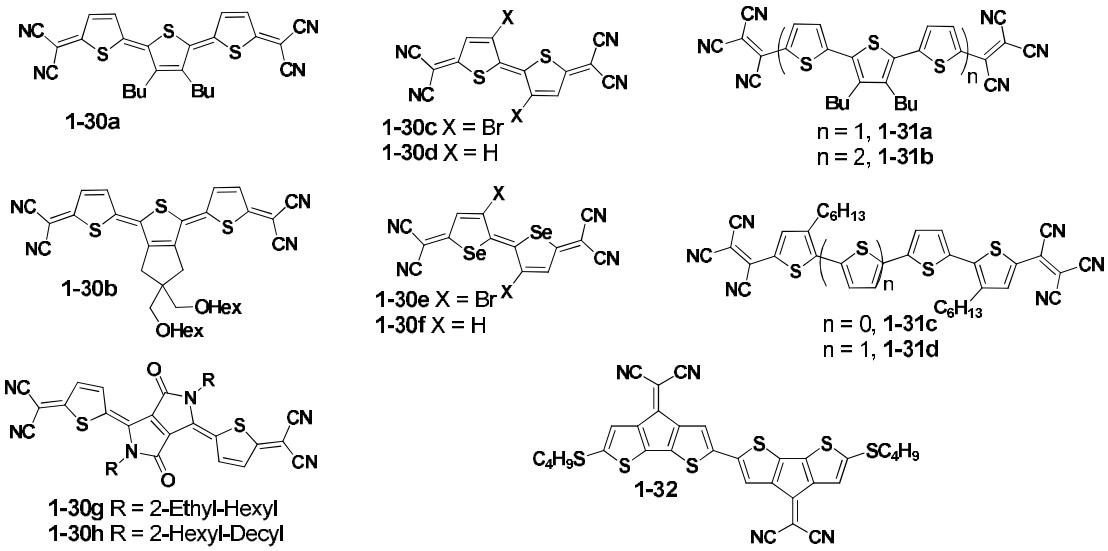

Figure 1.6 Chemical structures of CN-substituted semiconductors **1-30** – **1-32**

A terthiophene-based quinoidal molecule (**1-30a**, Figure 1.6) was reported by Frisbie et al, its cast films[34] showed electron mobility at about 0.002 cm^2 $V^{-1}s^{-1}$ and its vacuum deposited films [35] exhibited a mobility of 0.20 cm^2 $V^{-1}s^{-1}$. **1-30b**

was air stable and its spin-coated films [36] exhibited a mobility of 0.16 cm^2 $V^{-1}s^{-1}$ after annealing at 150 ^oC (Figure 1.6). Normally, derivatives with alkylated thiophene rings were not suitable for use in OFETs due to the steric effects hampering the ordering of the molecules.[37] The quinoidal biselenophene derivatives (**1-30e**–**f**)[37] were also employed as the active components of n-channel OFETs, they showed higher performance than their bithiophene counterparts (**1-30c**–**d**). Recently, two diketopyrrolopyrrole (DPP)-containing quinoidal molecules **1-30g**–**h** were reported by Qiao et al,[38] they exhibited maximum electron mobility up to 0.55 cm^2 $V^{-1}s^{-1}$with I_{on}/I_{off} values of 10^6 for **1-30g** by vapor evaporation, and 0.35 cm^2 $V^{-1}s^{-1}$ with I_{on}/I_{off} values of 10^5-10^6 for **1-30h** by solution process technique in ambient air.

Oligothiophenes end-capped with tricyanovinyl groups were supposed to be highly attractive, because the strong electron-withdrawing tricyanovinyl groups might inverse the transport ability of majority carriers.[39] Except for the sexithiophene derivative (**1-31b**), **1-31a** and **1-31c**–**d** showed n-channel behaviors and the highest performance was obtained from **1-31a** with an electron mobility at 0.02 cm^2 $V^{-1}s^{-1}$ (Figure 1.6). CN-groups substituted into the backbone of the acenes or heteroarenes have also been reported. The oligomer **1-32** showed fascinating n-type performance with an electron mobility of 0.34 cm^2 $V^{-1}s^{-1}$.[40]

1.3.4 Carboximide-Containing N-type Semiconductors

Carbonyl-containing semiconductors reported as being suitable for use in n-channel OFETs are most often combined with halogen atoms or cyano-groups as the electron-withdrawing units. Carboximide is one of the most important classes of n-channel semiconductors. Some of the dicarboximide that have been reported as active layers in n-channel OFETs include naphthalene diimides (NDI), perylene diimides (PDI), pyromellitic diimides (PMDI), anthracene diimides (ADI), and so on.

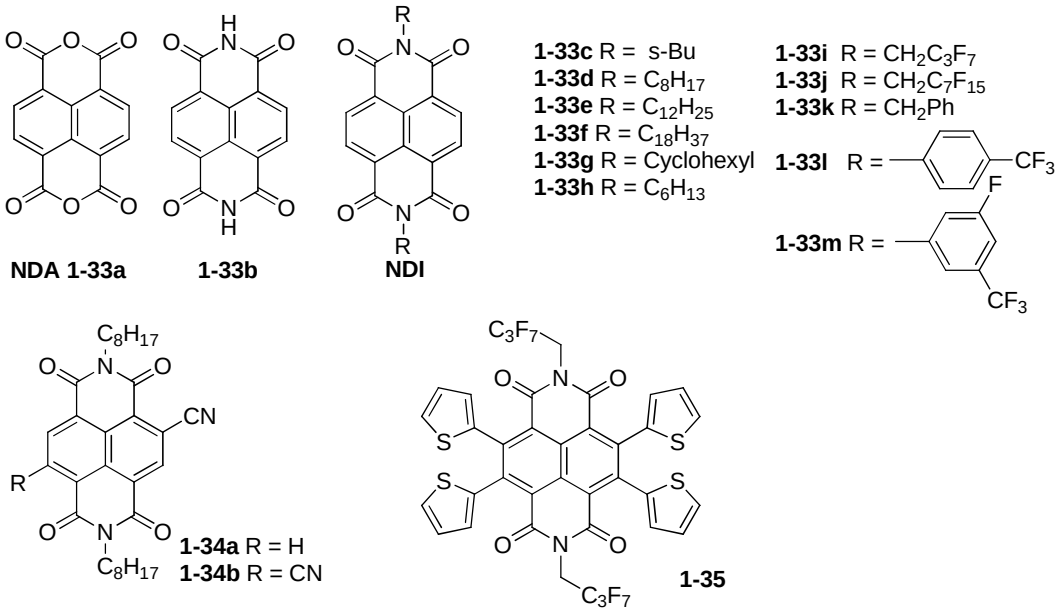

Figure 1.7 Chemical structures of NDI based semiconductors **1-33** – **1-35**

Naphthalene tetracarboxylic dianhydride (NDA, **1-33a**) is one of the first successes of n-channel materials (Figure 1.7). NDA showed an electron mobility of 3×10^{-3} $cm^2V^{-1}s^{-1}$ via vacuum deposited films.[41] The unsubstituted naphthalene diimides (NDI, **1-33b**) showed n-channel properties as well, with mobility at

about 10^{-4} $cm^2V^{-1}s^{-1}$; nonetheless, NDI with alkyl substitutents on the N atoms (**1-33c**–**h**) exhibited high electron mobility (Figure 1.7).[42] For example, the octyl substituted NDI derivative (**1-33d**) showed an electron mobility at 0.16 $cm^2V^{-1}s^{-1}$, and the sec-butyl (**1-33c**) and dodecyl functionalized NDI (**1-33e**) derivatives showed mobilities at 0.04 and 0.01 cm^2 $V^{-1}s^{-1}$, respectively.

Recently, Shukla et al.[43] reported a cyclohexyl substituted NDI (**1-33g**), its thin film transistors exhibited typical n-channel behavior with electron mobility up to 6.2 cm^2 $V^{-1}s^{-1}$ (Figure 1.7). In addition, the mobility increased up to 7.5 cm^2 $V^{-1}s^{-1}$ when devices were measured in argon atmosphere under low humidity conditions. It is one of the highest values reported for n-type semiconductors so far. In contrast, the hexyl substituted derivative (**1-33h**) showed a mobility of 0.70 cm^2 $V^{-1}s^{-1}$, lower than that of **1-33g**. This phenomenon could be ascribed to their different molecular arrangements in the films, although they both showed lamellar packing motifs with strong intermolecular π-π stacking. **1-33g** gives a 2D lamellar π-π stacking which results in efficient charge transport and extremely high device performance. However, **1-33h** shows only 1D lamellar stacking, and less π-π interactions lead to lower mobility.

When fluorine atom was introduced into NDI molecules, they exhibited n-type performances under ambient conditions. For example, the derivatives of **1-33i**–**k**[42b] showed electron mobility at 0.01 cm^2 $V^{-1}s^{-1}$ (Figure 1.7). The fluorinated derivative **1-33m**[45] showed similar mobility as **1-33l**. However, after

being stored in air for one month, **1-33l** devices showed significant degradation, while no obvious degradation was observed for **1-33m** devices (Figure 1.7).

Two CN-substituted NDI semiconductors (**1-34a**–**b**)[46] were synthesized to improve the environmental stability of these semiconductors. The average electron mobility of NDI-CN (**1-34a**) films was only at 4.7×10^{-3} $cm^2 V^{-1}s^{-1}$ while the mobility of NDI-CN2 (**1-34b**) was at 0.15 $cm^2 V^{-1}s^{-1}$. Although the performance of **1-34b** was comparable to the derivative **1-33d** which is unsubstituted by CN-groups, the mobility could be maintained as high as 0.11 $cm^2 V^{-1}s^{-1}$ when tested in air. It suggests excellent environmental stability of the compounds. The thiophene-substituted NDI derivatives **1-35**[47] (at 2,3,6,7-positions) exhibited only low transistor performance (Figure 1.7).

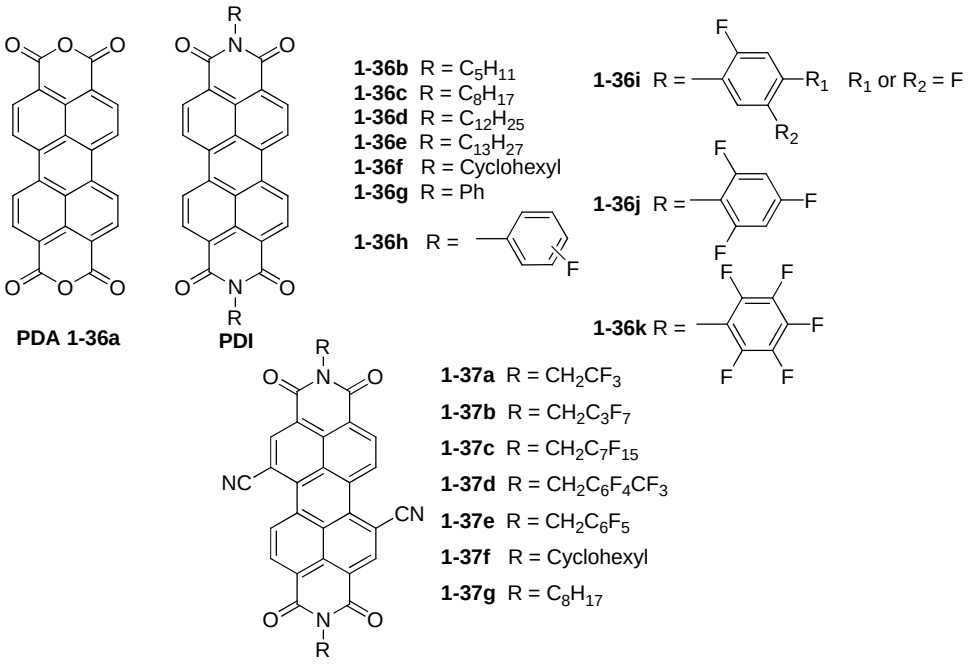

Figure 1.8 Chemical structures of PDI based semiconductors **1-36** – **1-37**

With results similar to those for NDA, PDA (**1-36a**) exhibited n-type behaviors with an electron mobility of 10^{-4} cm^2 $V^{-1}s^{-1}$ under vacuum (Figure 1.8).[48] In addition, single crystal transistors of PDA showed a mobility at 5×10^{-3} cm^2 $V^{-1}s^{-1}$, which was one order of magnitude higher than that for its thin film devices under vacuum.[49] Using polycrystalline films of octyl-substituted PDI (**1-36c**) to fabricate devices, a mobility up to 1.7 cm^2 $V^{-1}s^{-1}$ was obtained.[50] In other results, the pentyl (**1-36b**)[51] and dodecyl (**1-36d**)[50b] substituted derivatives showed mobilities up to 0.1 and 0.52 cm^2 $V^{-1}s^{-1}$, respectively. The tridecyl-substituted PDI (**1-36e**)[52] showed mobility around 0.58 cm^2 $V^{-1}s^{-1}$, and this could be improved up to 2.1 cm^2 $V^{-1}s^{-1}$ when devices were annealed at 140 ^oC.[53] However, the cyclohexyl (**1-36f**)[54] and phenyl (**1-36g**)[55] substituted derivatives exhibited lower values of only 1.9×10^{-4} and 0.017 cm^2 $V^{-1}s^{-1}$, respectively.

Fluorinated alkyl and aryl substituents were also introduced onto PDI molecules in the nitrogen atom positions. A series of fluorophenyl substituted PDI derivatives (**1-36h**–**k**) were prepared by Chen et al (Figure 1.8).[55b] The monofluoro-substituted derivative showed low mobility in the range of 10^{-3} - 10^{-4} cm^2 $V^{-1}s^{-1}$. The difluoro-, trifluoro-, and perfluorophenyl- substituted derivatives (**1-36i**–**k)** were usually over 10^{-2} cm^2 $V^{-1}s^{-1}$, and the perfluorophenyl PDI (**1-36k**) had a mobility at 0.068 cm^2 $V^{-1}s^{-1}$ with a current on/off ratio of 10^5. With the

introduction of the fluorine atoms, both the stability and mobility of the materials are improved.

CN-substituted PDIs at core positions (**1-37a**–**g**) were also synthesized and applied for n-channel OFETs with good air stability (Figure 1.8). The evaporated films of core-cyanated PDI derivatives **1-37b**, **1-37f**, and **1-37g** showed mobilities at 0.64, 0.10, and 0.16 $cm^2\ V^{-1}s^{-1}$, respectively.[56] On the other hand, the other materials (**1-37a**, **1-37c**, **1-37d**, and **1-37e**)[56c] gave rather low mobility. Recently, transistors based on **1-37b**[57] with spin-coated films showed electron mobility at around 0.15 $cm^2\ V^{-1}s^{-1}$ under vacuum.

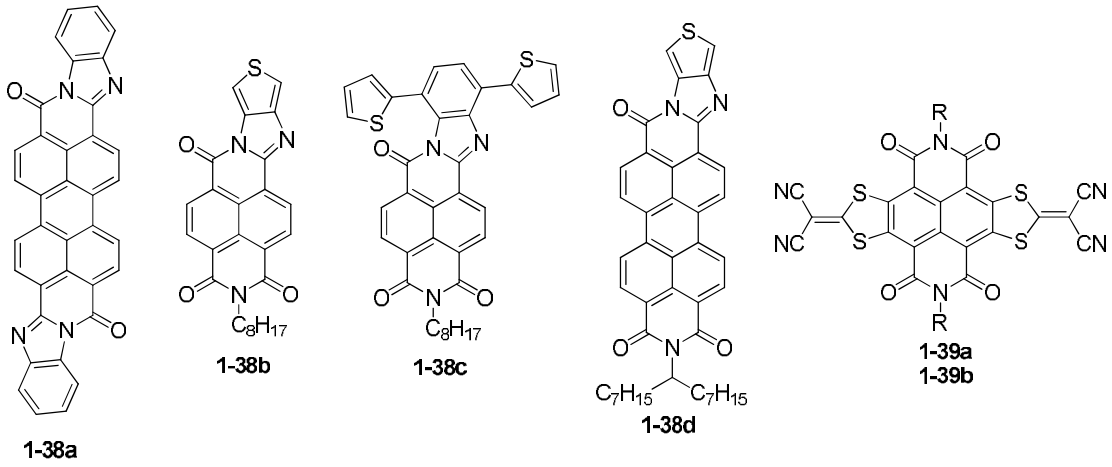

Figure 1.9 Chemical structures of imide-containing semiconductors **1-38** – **1-39**

The 3,4,9,10-perylenetetracarboxylic bis-benzimidazole (PTCBI, **1-38a**) is usually used as an electron acceptor in organic photovoltaic cells, its mobility reached 0.05 $cm^2\ V^{-1}s^{-1}$ with the highly ordered ODTS self-assembled monolayer

(SAM) (Figure 1.9).[58] Recently, a series of arylenediimidethiophene derivatives (**1-38b**–**d**) were reported by Marks et. al,[59] the highest performance was obtained from **1-38c** with an electron mobility at 0.35 $cm^2\ V^{-1}s^{-1}$ (**1-38b** and **1-38d** displayed mobility at 0.10 and 0.15 $cm^2\ V^{-1}s^{-1}$, respectively) from vapor deposited film, the solution processed films showed the electron mobility at only 4×10^{-5} to 3×10^{-3} $cm^2\ V^{-1}\ s^{-1}$ under vacuum.

Several core-expanded NDI derivatives (**1-39a**–**b**) were reported recently by Gao et al (Figure 1.9).[60] The core-expanded π-system facilitated π-π stacking and the rich electron withdrawing groups (such as malonitrile) lowered the LUMO energy levels, and the electron mobility of solution-processed devices (**1-39b**) reached 0.51 $cm^2\ V^{-1}s^{-1}$ under ambient conditions.

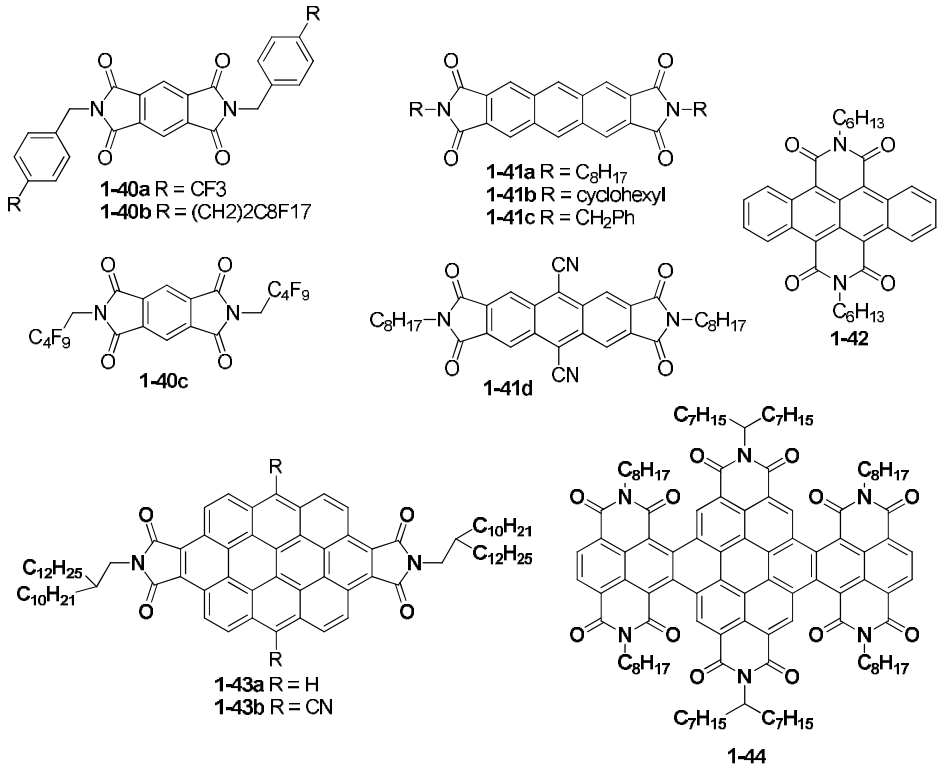

Figure 1.10 Chemical structures of imide-containing semiconductors **1-40** – **1-44**

A series of pyromellitic dimides (PMDI) derivatives (**1-40a**–**c**) contained minimal cores for n-channel semiconductors have been synthesized (Figure 1.10).[61] The maximum mobilities were about 0.074, 0.079, and 0.03 $cm^2 V^{-1}s^{-1}$ for **1-40a**, **1-40b**, and **1-40c**, respectively, with on/off ratios in the range of 10^4-10^5. A family of anthracenedicarboximides derivatives (ADIs, **1-41a**–**c**) were reported by Marks' group, an electron mobility of 0.02 $cm^2 V^{-1}s^{-1}$ and an on/off ratio at 10^7 were achieved.[62] Further studies on the CN-substituted ADIs (**1-41d**) gave a electron mobility of 0.02 $cm^2 V^{-1}s^{-1}$ when tested in air, with an on/off ratio over 10^7.When devices of **1-41d** were measured under vacuum, a similar mobility of 0.03 $cm^2 V^{-1}s^{-1}$ was observed.

Tetracene dimide **1-42** with the imide groups at the zig-zag edges was reported by Yamada's group (Figure 1.10).[63] A top-contact OFET was fabricated by vapor deposition of **1-42** under nitrogen. The device performance was moderate, showing an electron mobility at 3.3×10^{-3} $cm^2 V^{-1}s^{-1}$. Ovalene diimide (ODI, **1-43a**) and its cyanated derivative (ODI-2CN, **1-43b**) were designed and synthesized by Wu's group.[64] Although **1-43a** showed ordered self-assembly behavior, it did not show any obvious OFET activity in air or nitrogen atmosphere. However, its cyanated derivative **1-43b** exhibited typical n-channel semiconducting behavior in solution processed OFET devices, showing high electron mobility up to 1.0 $cm^2 V^{-1}s^{-1}$ under nitrogen, and 0.51 $cm^2 V^{-1}s^{-1}$ in air.

Recently, a hybrid rylene array **1-44** was synthesized by Wang et. al (Figure 1.10).[65] Thin films of **1-44** spin-coated from chloroform solution were fabricated for devices under ambient conditions, the as casted thin-film devices showed a moderate electron mobility of 0.02 cm^2 $V^{-1}s^{-1}$. After annealing the thin film at 220 °C, device performance was significantly improved with the electron mobility reaching 0.25 cm^2 $V^{-1}s^{-1}$ accompanied by a high current on/off ratio of 10^7. However, the synthesis of **1-44** was via toxic organic tin intermediate.

1.3.5 Nitrogen-Containing Heterocyclic N-type semiconductors

Nitrogen-containing π-conjugated molecules in which some of the C-H groups are replaced with sp^2-hybridized nitrogen atoms (=N-), have been shown both experimentally and theoretically to be featured with a less negative reductive potential, high electron affinity, and ambient stability.[66]

As a typical nitrogen-containing heterocyclic compound, pyrazine containing two nitrogen atoms (=N-) has been proven as a valuable building block for thermally stable polymers and electron-accepting π-conjugated polymers. Recently, pyrazine is frequently used in the design and synthesis of *n*-type organic semiconductors, such as pyrazinoquinoxaline derivatives, N-heteroacenes, owing to its electron deficient characteristics. The electron affinity of the resultant compounds is noticeably higher than that of analogous polycyclic aromatic hydrocarbons and can be adjusted by altering molecular structures or substitution

patterns.

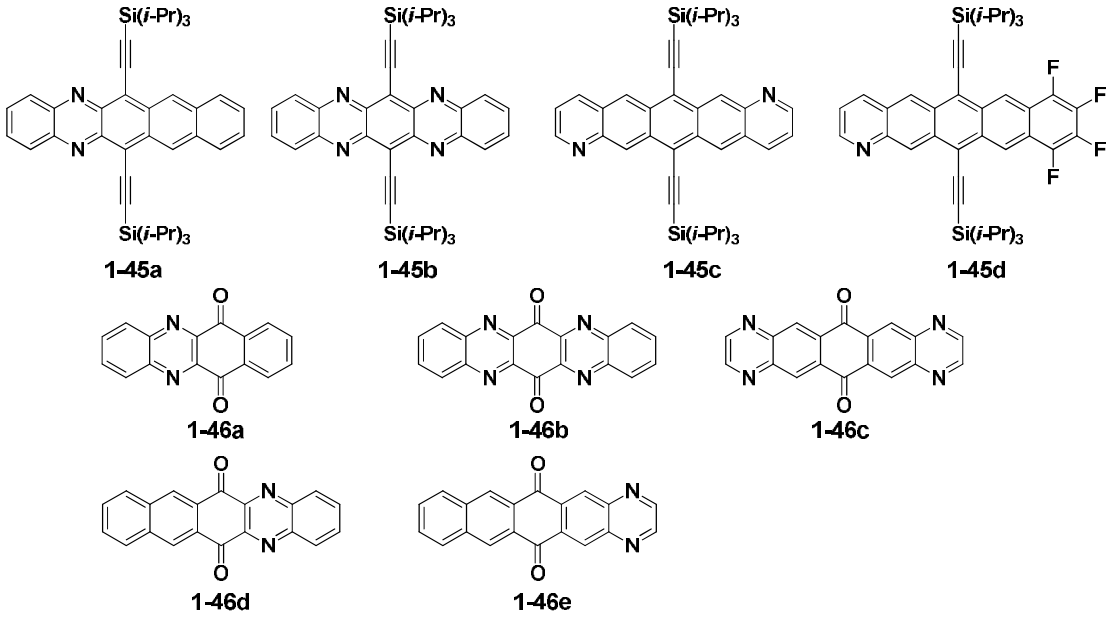

Figure 1.11 Chemical structures of N-containing acene based semiconductors **1-45** – **1-46**

A series of soluble and stable N-heteropentacenes were designed and prepared by Miao's and Gong's group.[67] One pyrazine containing N-heteropentacene **1-45a** functioned as an ambipolar semiconductor, showing hole mobility at 0.02-0.05 $cm^2\ V^{-1}s^{-1}$, and electron mobility at 2–4 × 10^{-4} $cm^2\ V^{-1}s^{-1}$ via films deposited at a substrate temperature of 100 °C (Figure 1.11). However, two pyrazine containing N-heteropentacene **1-45b** functioned as an n-type semiconductor, with electron mobility in the range of 1.0 – 3.3 $cm^2\ V^{-1}s^{-1}$ via vacuum deposited films under vacuum. When the transistors of **1-45b** were investigated in ambient atmosphere, the measured electron mobility decreased to 0.3–0.5 $cm^2\ V^{-1}s^{-1}$. The highest

field-effect mobility measured from the solution processed films was 3×10^{-3} cm^2 $V^{-1}s^{-1}$ for **1-45b**, the low mobility of **1-45b** in the solution-cast films can be attributed to the electron trapping by hydroxyl groups of SiO_2 surface. Two pyridine containing N-heteropentacene **1-45c** was functioned as an ambipolar semiconductor, with a hole mobility at 0.008-0.11 cm^2 $V^{-1}s^{-1}$, and electron mobility at 0.15 cm^2 $V^{-1}s^{-1}$. The tetra-fluorinated N-heteropentacene **1-45d** was also functioned as an ambipolar semiconductors, with a hole mobility at 0.0015-0.08 cm^2 $V^{-1}s^{-1}$, and electron mobility at 0.09 cm^2 $V^{-1}s^{-1}$ (Figure 1.11).

In addition, N-substituted acene quinones (**1-46a**–**e**) were also synthesized and used for n-channel devices (Figure 1.11).[68] Vacuum deposited thin films of **1-46b** performed as n-channel transistors with electron mobility at 0.04-0.12 cm^2 $V^{-1}s^{-1}$ under vacuum, and 2×10^{-3} cm^2 $V^{-1}s^{-1}$ in air. On the other hand, **1-46a** showed a much lower electron mobility of 10^{-6} cm^2 $V^{-1}s^{-1}$ due to the low crystalline films. **1-46c** and **1-46d** showed similar electron mobility at 10^{-5} cm^2 $V^{-1}s^{-1}$, while **1-46e** did not show any obvious OFET activity in air or nitrogen atmosphere, the poor performances of **1-46c-e** can be attributed to the amorphous nature of their films, since it is well known that the field effect mobility is very sensitive to the crystallinity of the thin film.

All of these N-containing acene based semiconductors gave ambipolar or n-channel behavior. The best mobility was achieved from vacuum deposited films, while the solution processed films at low temperature gave only moderate

mobility, or even no OFET behavior.

1.3.6 Objectives

N-channel semiconductors are of significant importance. Nonetheless, the research for n-channel molecules is not so mature, and only a limited number of n-type semiconductors have been achieved. The general design approaches to obtain *n*-channel semiconductors include introduction of electron-withdrawing substituents, such as fluorine, carboximide, CN groups onto the traditional *p*-type semiconductors, and replacement of the carbon atoms in the π-conjugated system by electron-deficient imine nitrogen atoms. According to this guidance, some *n*-type semiconductors have been successfully synthesized and applied for *n*-channel OFETs. However, for large scale fabrication of low-cost devices, solution based film deposition processes at low temperature with high charge mobility are highly desirable.

The purposes of this study were,

1) To combine all the methods available to convert normal p-type semiconductors to n-type semiconductors, by introducing different electron withdrawing groups, or introducing the nitrogen imine into the acene framework, and make it suitable for fabrication of n-channel devices with high performance and good stability;
2) To study the structure-property relationships for understanding the

fundamental chemical aspects behind the structural design and realization of desired properties.

In chapter 3-5, a series of electron deficient molecules have been synthesized via attachment of carboximide, pyrazine and cyano groups. Their electronic, electrochemical properties, thermal behavior, molecular packing in the solid state, and OFET performances have been studied. The LUMO energy levels of these molecules are tuned ranging from -3.43 to -4.21eV, the electron mobility shows up to 0.056 cm^2 $V^{-1}s^{-1}$ via as-spun solution-processed films under ambient condition.

1.4 References:

1. a) Bendikov, M.; Wudl, F.; Perepichka, D. F. *Chem. Rev.* **2004**, *104*, 4891; b) Wu, J.; Pisula, W.; Müllen, K. *Chem. Rev.* **2007**, *107*, 718;
2. Murphy, A. R.; Frechet, J. M. *J. Chem. Rev*. **2007**, *107*, 1066.
3. Osaka, I.; McCullough, R. D. *Acc. Chem. Res*. **2008**, *41*, 1202.
4. a) Liu, S.; Wang, W.; Briseno, A. L.; Mannsfeld, S. C. B.; Bao, Z. Adv. Mater. 2009, 21, 1217. b) Facchetti, A. *Mater. Today* **2007**, *10*, 28.
5. a) Kline, R. J.; McGehee, M. D.; Kadnikova, E. N.; Liu, J.; Frechet, J. M. J. Adv. Mater. 2003, 15, 1519. b) Kline, R. J.; McGehee, M. D.; Kadnikova, E. N.; Liu, J.; Frechet, J. M. J.; Toney, M. F. *Macromolecules* **2005**, *38*, 3312. c) Ahmed, E.; Kim, F. S.; Xin, H.; Jenekhe, S. A. *Macromolecules* **2009**, *42*,

8615.

6. Allard, S.; Forster, M.; Souharce, B.; Thiem, H.; Scherf, U. *Angew. Chem., Int. Ed*. **2008**, *47*, 4070.
7. Goppert-Mayer. M. *Ann. Phys.* **1931**, *9*, 273.
8. Kaiser, W.; Garrett, C. G. B. *Phys. Rev. Lett*. **1961**, *7*, 229
9. a) Parthenopoulos, D. A.; Rentzepis, P. M. *Science* **1989**, *245*, 843. (b) Strickler, J. H.; Webb, W. W. *Opt. Lett.* **1991**, *16*, 1780. b) Zhou, W.; Kuebler, S. M.; Braun, K. L.; Yu, T.; Cammack, J. K.; Ober, C. K.; Perry, J. W.; Marder, S. R. *Science* **2002**, *296*, 1106. c) He, G. S.; Xu, G. C.; Prasad, P. N.; Reinhardt, B. A.; Bhatt, J. C.; Dillard, A. G. *Opt. Lett.* **1995**, *20*, 435. d) Denk, W.; Strickler, J. H.; Webb, W. W. *Science* **1990**, *248*, 73.
10. a) Xu, C.; Webb, W. W. *J. Opt. Soc. Am. B*, **1996**, *13*, 481; b) Xu, C.; W. Zipfel, J. B. Shear, R. M. Williams and Webb, W. W. *Proc. Natl. Acad. Sci. U. S. A.*, **1996**, *93*, 10763.
11. Boggess, T. F.; Bohnert, K. M.; Mansour, K.; Moss, S. C.; Boyd I. W.; Smirl, A. L. *IEEE J. Quantum Electron.*, **1986**, *22*, 360.
12. a) Yu, B.; Zhu, C.; Gan, F.; Wu, X.; Zhang, G.; Tang G.; Chen, W. *Opt. Mater.*, **1997**, *8*, 249; b) Attias, A. J.; Cavalli, C.; Lemaitre, N.; Cherioux, F.; Maillotte, H.; Ledoux I.; Zyss, J. *J. Opt. Appl. Phys.*, **2002**, *4*, S212; c) Guo, S. L.; Xu, L.; Wang, H. T.; You X. Z.; Ming, N. B. *Opt. Quantum Electron.*, **2003**, *35*, 693; d) Gopinath, J. T.; Soljacic, M.; Ippen, E. P.; Fuflyigin, V. N.; King, W. A.;

Shurgalin, M. *J. Appl. Phys.*, **2004**, *96*, 6931.

13. Negres, A. R.; Stryland, E. W.; Hagan, Van D.; Belfield, J. K.; Schafer, D. K. J.; Przhonska, O. V.; Reinhardt, B. A. *Proc. SPIE*, **1999**, 3796.
14. a) Kim, H. M.; Jung, C.; Kim, B. R.; Jung, S.-Y.; Hong, J. H. ; Ko, Y.-G.; Lee, K. J.; Cho, B. R. *Angew. Chem., Int. Ed.*, **2007**, *46*, 3460; b) Kim, H. M.; Kim, B. R.; Hong, J. H.; Park, J.-S.; Lee, K. J.; Cho, B. R. *Angew. Chem., Int. Ed.*, **2007**, *46*, 7445; c) Kim, H. M.; Yang, P. R.; Seo, M. S.; Yi, J.-S.; Hong, J. H.; Jeon, S.-J.; Ko, Y.-G.; Lee, K. J.; Cho, B. R. *J. Org. Chem.*, **2007**, *72*, 2088; d) Kim, H. M.; Choo, H.-J.; Jung, S.-Y.; Ko, Y.-G.; Park, W.-H.; Jeon, S.-J.; Kim, C. H.; Joo, T.; Cho, B. R. *ChemBioChem*, **2007**, *8*, 553.
15. a) He, G. S.; Tan. L.-S.; Zheng, Q.; Prasad, P. N. *Chem. Rev.* **2008**, *108*, 1245. b) Kim, H. M.; Cho, B. R. *Chem. Commun.* **2009**, 153. c) Kim, H. M.; Cho, B. R. *Acc. Chem. Res.*, **2009**, *42*, 863. d) Terenziani, F.; Katan, C.; Badaeva, E.; Tretiak, S.; Blanchard-Desce, M. *Adv. Mater.* **2008**, *20*, 4641. e) Pawlicki, M.; Collins, H. A.; Denning, R. G.; Anderson, H. L. *Angew. Chem. Int. Ed.* **2009**, *48*, 3244.
16. a) Reinhardt, B. A.; Brott, L. L.; Clarson, S. J.; Dillard, A. G.; Bhatt, J. C.; Kannan, R.; Yuan, L. X.; He G. S.; Prasad, P. N. *Chem. Mater.*, **1998**, *10*, 1863.
17. Lin, T. C.; He, G. S.; Prasad, P. N.; Tan, L. S. *J. Mater. Chem.*, **2004**, *14*, 982.
18. Kim, H. M.; Fang, X. Z.; Yang, P. R.; Yi, J. S.; Ko, Y. G.; Piao, M. J.; Chung, Y. D.; Park, Y. W.; Jeon S. J.; Cho, B. R. *Tetrahedron Lett.*, **2007**, *48*, 2791.

19. a) Yang, W. J.; Kim, D. Y.; Jeong, M. Y.; Kim, H. M.; Lee, Y. K. ; Fang, X.; Jeon, S. J. ; Cho, B. R. *Chem.–Eur. J.*, **2005**, *11*, 4191; b) Yang, W. J.; Kim, D. Y.; Jeong, M. Y.; Kim, Jeon, S. J. ; Cho, B. R. *Chem. Commun.*, **2003**, 2618.

20. Lee, S. K.; Yang, W. J.; Choi, J. J.; Kim, C. H.; Jeon, S. J.; Cho, B. R. *Org. Lett.*, **2005**, *7*, 323.

21. Chung, S. J.; Kim, K. S.; Lin, T. C.; He, G. S.; Swiatkiewicz, J.; Prasad, P. N. *J. Phys. Chem. B*, **1999**, *103*, 10741.

22. Macak, P.; Luo, Y.; Norman P.; Agren, H. *J. Chem. Phys.*, **2000**, *113*, 7055.

23. a) Chung, S. J.; Kim, K. S.; Lin, T. C.; He, G. S.; Swiatkiewicz, J.; Prasad, P. N. *J. Phys. Chem. B*, **1999**, *103*, 10741. b) Yoo, J.; Yang, S. K.; Jeong, M. Y.; Ahn, H. C.; Jeon, S. J.; Cho, B. R. *Org. Lett.*, **2003**, *5*, 645. c) Wu, J.; Zhao, Y. X.; Li, X.; Shi, M. Q.; Wu, F. P.; Fang, X. Y. *New J. Chem.*, **2006**, *30*, 1098.

24. a) Yang, W. J.; Kim, D. Y.; Kim, C. H.; Jeong, M. Y.; Lee, S. K.; Jeon, S. J.; Cho, B. R. *Org. Lett.*, **2004**, *6*, 1389. b) Le Droumaguet, C.; Mongin, O.; Werts, M. H. V.; Blanchard-Desce, M. *Chem. Commun.*, **2005**, 2802. c) Porres, L.; Mongin, O.; Katan, C.; Charlot, M.; Pons, T. ; Mertz, J.; Blanchard-Desce, M. *Org. Lett.*, **2004**, *6*, 47.

25. a) Bhaskar, A.; Ramakrishna, G.; Lu, Z. K.; Twieg, R.; Hales, J. M.; Hagan, D. J. E.; Stryland, Van; Goodson, T. J. *Am. Chem. Soc.*, **2006**, *128*, 11840. b) Woo, H. Y.; Hong, J. W.; Liu, B.; Mikhailovsky, A.; Korystov, D.; Bazan, G. C. *J. Am. Chem. Soc.*, **2005**, *127*, 820.

26. Di, C. A.; Liu, Y. Q.; Yu, G.; Zhu, D. B. *Acc. Chem. Res*. **2009**, *42*, 1573.

27. (a) Katz, H. E.; Bao, Z.; Gilat, S. L. *Acc. Chem. Res.* **2001**, *34*, 359; (b) Pascal, R. A. Jr. *Chem. Rev.* **2006**, *106*, 4809; (c) Anthony, J. E. *Angew. Chem. Int. Ed.* **2008**, *47*, 452.

28. Anthony, J. E. *Chem. Rev*. **2006**, *106*, 5028.

29. a) Yoon, M.-H.; Dibeneddetto, S. A.; Facchetti, A.; Marks, T. J. *J. Am. Chem. Soc.*, **2005**, *127*, 1348; b) Sun, Y.; Liu, Y.; Zhu, D. *J. Mater. Chem.*, **2005**, *15*, 53; c) Di, C.; Yu, G.; Liu, Y.; Zhu, D. *J. Phys. Chem. B*, **2007**, *111*, 4083.

30. Heidenhain, S. B.; Sakamoto, Y.; Suzuki, T.; Miura, A.; Fujikawa, H.; Mori, T.; Tokito, S.; Taga, Y. *J. Am. Chem. Soc.* **2000**, *122*, 10240.

31. Sakamoto, Y.; Suzuki, T.; Kobayashi, M.; Gao, Y.; Fukai, Y.; Inoue, Y.; Sato, F.; Tokito, S. *J. Am. Chem. Soc.* **2004**, *126*, 8138.

32. a) Swartz, C. R.; Parkin, S. R.; Bullock, J. E.; Anthony, J. E.; Mayer, A. C.; Malliaras, G. G. Org. Lett. **2005**, 7, 3163. b) Tang, M. L.; Oh, J. H.; Reichardt, A. D.; Bao, Z. *J. Am. Chem. Soc*. **2009**, *131*, 3733.

33. a) Bao, Z.; Lovinger, A. J.; Brown, J. *J. Am. Chem. Soc.* **1998**, *120*, 207. b) Tang, Q.; Li, H.; Liu, Y.; Hu, W. *J. Am. Chem. Soc*. **2006**, *128*, 14634. c) Okamoto, K.; Ogino, K.; Ikari, M.; Kunugi, Y. *Bull. Chem. Soc. Jpn.* **2008**, *81*, 530.

34. Pappenfus, T. M.; Chesterfield, R. J.; Frisbie, C. D.; Mann, K. R.; Casado, J.; Raff, J. D.; Miller, L. L. *J. Am. Chem. Soc.* **2002**, *124*, 4184.

35. Chesterfield, R. J.; Newman, C. R.; Pappenfus, T. M.; Ewbank, P. C.; Haukaas, M. H.; Mann, K. R.; Miller, L. L.; Frisbie, C. D. *Adv. Mater.* **2003**, *15*, 1278.

36. Handa, S.; Miyazaki, E.; Takimiya, K.; Kunugi, Y. *J. Am. Chem. Soc.* **2007**, *129*, 11684.

37. a) Takahashi, T.; Matsuoka, K.-i.; Takimiya, K.; Otsubo, T.; Aso, Y. *J. Am. Chem. Soc.* **2005**, *127*, 8928. b) Kunugi, Y.; Takimiya, K.; Toyoshima, Y.; Yamashita, K.; Aso, Y.; Otsubo, T. *J. Mater. Chem.* **2004**, *14*, 1367.

38. Qiao, Y.; Guo, Y.; Yu, C.; Zhang, F.; Xu, W.; Liu, Y.; Zhu, D. *J. Am. Chem. Soc.* **2012**, *134*, 4084

39. Cai, X.; Burand, M. W.; Newman, C. R.; da Silva Filho, D. A.; Pappenfus, T. M.; Bader, M. M.; Bredas, J.-L.; Mann, K. R.; Frisbie, C. D. *J. Phys. Chem. B* **2006**, *110*, 14590.

40. Ortiz, R. P.; Facchetti, A.; Marks, T. J.; Casado, J.; Zgierski, M. Z.; Kozaki, M.; Hernandez, V.; Navarrete, J. T. L. *Adv. Funct. Mater.* **2009**, *19*, 386.

41. a) Laquindanum, J. G.; Katz, H. E.; Dodabalapur, A.; Lovinger, A. J. *J. Am. Chem. Soc.* **1996**, *118*, 11331. b) Tanida, S.; Noda, K.; Kawabata, H.; Matsushige, K. *Thin Solid Films* **2009**, *518*, 571.

42. a) Katz, H. E.; Lovinger, A. J.; Johnson, J.; Kloc, C.; Siegrist, T.; Li, W.; Lin, Y. Y.; Dodabalapur, A. *Nature.* **2000**, *404*, 478. b) Gawrys, P.; Boudinet, D.; Zagorska, M.; Djurado, D.; Verilhac, J. M.; Horowitz, G.; Pecaud, J.; Pouget,

S.; Pron, A. *Synth. Met.* **2009**, *159*, 1478.

43. Shukla, D.; Nelson, S. F.; Freeman, D. C.; Rajeswaran, M.; Ahearn, W. G.; Meyer, D. M.; Carey, J. T. *Chem. Mater*. **2008**, *20*, 7486.
44. Katz, H. E.; Johnson, J.; Lovinger, A. J.; Li, W. J. *J. Am. Chem. Soc.* **2000**, *122*, 7787.
45. Lee, Y.-L.; Hsu, H.-L.; Chen, S.-Y.; Yew, T.-R. *J. Phys. Chem. C* **2008**, *112*, 1694.
46. Jones, B. A.; Facchetti, A.; Marks, T. J.; Wasielewski, M. R. *Chem. Mater.* **2007**, *19*, 2703.
47. Kruger, H.; Janietz, S.; Sainova, D.; Dobreva, D.; Koch, N.; Vollmer, A. *Adv. Funct. Mater.* **2007**, *17*, 3715.
48. Ostrick, J. R.; Dodabalapur, A.; Torsi, L.; Lovinger, A. J.; Kwock, E. W.; Miller, T. M.; Galvin, M.; Berggren, M.; Katz, H. E. *J. Appl. Phys.* **1997**, *81*, 6804.
49. Yamada, K.; Takeya, J.; Takenobu, T.; Iwasa, Y. *Appl. Phys. Lett.* **2008**, *92*, 253311.
50. a) Malenfant, P. R. L.; Dimitrakopoulos, C. D.; Gelorme, J. D.; Kosbar, L. L.; Graham, T. O.; Curioni, A.; Andreoni, W. *Appl. Phys. Lett*. **2002**, *80*, 2517. b) Chesterfield, R. J.; McKeen, J. C.; Newman, C. R.; Ewbank, P. C.; da Silva Filho, D. A.; Bredas, J.-L.; Miller, L. L.; Mann, K. R.; Frisbie, C. D. *J. Phys. Chem. B* **2004**, *108*, 19281.

51. Chesterfield, R. J.; McKeen, J. C.; Newman, C. R.; Frisbie, C. D.; Ewbank, P. C.; Mann, K. R.; Miller, L. L. *J. Appl. Phys.* **2004**, *95*, 6396.

52. a) Gundlach, D. J.; Pernstich, K. P.; Wilckens, G.; Gruter, M.; Haas, S.; Batlogg, B. *J. Appl. Phys.* **2005**, *98*, 064502. b) Rost, C.; Gundlach, D. J.; Karg, S.; Riess, W. *J. Appl. Phys.* **2004**, *95*, 5782.

53. Tatemichi, S.; Ichikawa, M.; Koyama, T.; Taniguchi, Y. *Appl. Phys. Lett.* **2006**, 89, 112108.

54. Locklin, J.; Li, D. W.; Mannsfeld, S. C. B.; Borkent, E. J.; Meng, H.; Advincula, R.; Bao, Z. *Chem. Mater.* **2005**, *17*, 3366.

55. a) Horowitz, G.; Kouki, F.; Spearman, P.; Fichou, D.; Nogues, C.; Pan, X.; Garnier, F. *Adv. Mater.* **1996**, *8*, 242. b) Chen, H. Z.; Ling, M. M.; Mo, X.; Shi, M. M.; Wang, M.; Bao, Z. *Chem. Mater*. **2007**, *19*, 816.

56. a) Yoo, B.; Jung, T.; Basu, D.; Dodabalapur, A.; Jones, B. A.; Facchetti, A.; Wasielewski, M. R.; Marks, T. J. *Appl. Phys. Lett.* **2006**, *88*, 082104. b) Weitz, R. T.; Amsharov, K.; Zschieschang, U.; Villas, E. B.; Goswami, D. K.; Burghard, M.; Dosch, H.; Jansen, M.; Kern, K.; Klauk, H. *J. Am. Chem. Soc.* **2008**, *130*, 4637. c) Rivnay, J.; Jimison, L. H.; Northrup, J. E.; Toney, M. F.; Noriega, R.; Lu, S.; Marks, T. J.; Facchetti, A.; Salleo, A. *Nat. Mater.* **2009**, *8*, 952.

57. Piliego, C.; Jarzab, D.; Gigli, G.; Chen, Z. H.; Facchetti, A.; Loi, M. A. *Adv. Mater.* **2009**, *21*, 1573.

58. a) Yakimov, A.; Forrest, S. R. *Appl. Phys. Lett.* **2002**, *80*, 1667. b) Kumashiro, R.; Tanigaki, K.; Ohashi, H.; Tagmatarchis, N.; Kato, H.; Shinohara, H.; Akasaka, T.; Kato, K.; Aoyagi, S.; Kimura, S.; Takata, M. *Appl. Phys. Lett.* **2004**, *84*, 2154.

59. Zheng, Y.; Segura, J. L. *J. Am. Chem. Soc.* **2010**, *132*, 8440.

60. Gao, X.; Di, C.-a.; Hu, Y.; Yang, X.; Fan, H.; Zhang, F.; Liu, Y.; Li, H.; Zhu, D. *J. Am. Chem. Soc.* **2010**, *132*, 3697.

61. Zheng, Q. D.; Huang, J.; Sarjeant, A.; Katz, H. E. *J. Am. Chem. Soc.* **2008**, *130*, 14410.

62. Wang, Z.; Kim, C.; Facchetti, A.; Marks, T. J. *J. Am. Chem. Soc.* **2007**, *129*, 13362.

63. Katsuta, S.; Tanaka, K.; Maruya, Y.; Mori, S.; Masuo, S.; Okujima, T.; Uno, H.; Nakayma, K.; Yamada, H. *Chem. Commun*. **2011**, *47*, 10112.

64. Li, J.; Chang, J.; Tan, P.; Jiang, H.; Chen, X.; Chen, Z.; Zhang, J.; Wu, J. *Chem. Sci.* **2012**, *3*, 846.

65. Yue, W.; Lv, A.; Gao, J.; Jiang, W.; Hao, L.; Li, C.; Li, Y.; Polander, L. E.; Barlow, S.; Hu, W.; Di Motta, S.; Negri, F.; Marder, S. R.; Wang, Z. *J. Am. Chem. Soc.* **2012**, *134*, 5770.

66. a) Miao, S.; Brombosz, S. M.; Schleyer, P. v. R.; Wu, J. I.; Barlow, S.; Marder, S. R.; Hardcastle, K. I.; Bunz, U. H. F. *J. Am. Chem. Soc.* **2008**, *130*, 7339. b) Gao, B.; Wang, M.; Cheng, Y.; Wang, L.; Jing, X.; Wang, F. *J. Am. Chem.*

Soc. **2008**, *130*, 8297.c) Winkler, M.; Houk, K. N. *J. Am. Chem. Soc.* **2007**, *129*, 1805.

67. a) Liang, Z.; Tang, Q.; Xu, J.; Miao, Q. *Adv. Mater.* **2011**, *23*, 1535. b) Liu, Y.-Y.; Song, C.-L.; Zeng, W.-J.; Zhou, K.-G.; Shi, Z.-F.; Ma, C.-B.; Yang, F.; Zhang, H.-L.; Gong, X. *J. Am. Chem. Soc.* **2010**, *132*, 16349.
68. a) Tang, Q.; Liang, Z.; Liu, J.; Xu, J.; Miao, Q. *Chem. Commun.* **2010**, *46*, 2977. b) Liang, Z.; Tang, Q.; Liu, J.; Li, J.; Yan, F.; Miao, Q. *Chem. Mater.* **2010**, *22*, 6438.

Chapter 2

Synthesis and Characterizations of Star-shaped Octupolar Triazatruxenes Based Two-photon Absorption Chromophores

2.1 Introduction

In recent years, two-photon absorption (2PA) has attracted growing interest due to its potential applications in materials science and in biological imaging,[1] including three-dimensional optical data storage,[2] lithographic micro-fabrication,[3] optical power limiting,[4] two photon fluorescence imaging,[5] and photodynamic therapy.[6] These applications strongly depend on the high 2PA cross-section displayed by the specifically engineered organic molecules. This has led to a great number of works on building π-conjugated dipolar-,[6] quadrupolar-[7] and octupolar-[8] molecules with π-centers and functional groups of electron-donating and/or electron-withdrawing groups at the terminal sites.

Design of a star-shaped multipolar molecular structure is one of the strategies[7a, 9] to obtain a large 2PA cross-section. The coherent coupling between the branches will significantly increase the 2PA cross-section. In addition, it was also found that a planar, extended π-conjugated core usually afforded better performance than the three-dimensionally twisted, non-conjugated cores. Star-shaped octupolar triphenyl amines and dendrimers based on planar truxene molecules[10] have proved to be good 2PA chromophores. To further exploit good 2PA active materials, we expect that the C_3-symmetric molecule, triazatruxene (TAT) could be another good candidate (Figure 2.1). This idea is based on the following considerations: (1) TAT can be considered as an extended delocalized π-system in which three carbazole units share one aromatic ring; (2) in

comparison with its analogue truxene, triazatruxene contains three nitrogen atoms which can serve as good electron donating groups like those in triphenyl amines; (3) selective chemical functionalizations around the TAT core allow us to introduce electron withdrawing groups to form star-shaped octupolar chromophores such as **2-1 - 2-6** (Figure 2.1). So this design combines the advantages of the electron donating properties of aryl amines and the branched feature of truxene. The additional thienylene vinylene units in **2-4** – **2-6** can further improve the π-conjugation in each arm and tune the 2PA properties. Although some research has been done for the TAT-based materials,[11] this interesting building block has not been used to develop 2PA chromophores. In this chapter, for the first time, we report the synthesis of a series of TAT-based octupolar chromophores which show large 2PA cross-section in the near infrared (NIR) range.

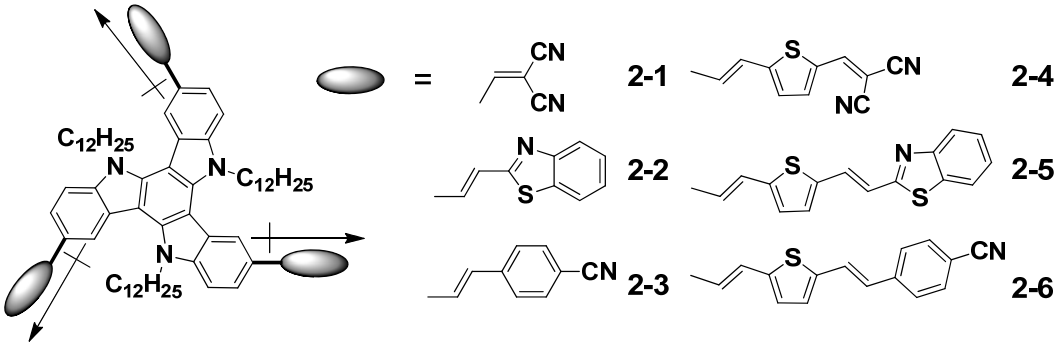

Figure 2.1 Molecular structures of star-shaped octupolar triazatruxenes **2-1** – **2-6**.

2.2 Results and Discussion

2.2.1 Synthesis

The synthesis of the octupolar TAT molecules **2-1** – **2-6** is shown in Scheme 2.1. Three different electron-withdrawing groups are introduced onto the TAT core at the periphery sites to form a C_3-symmetric structure and this results in three dipoles at three directions with a net zero permanent dipole moment. The synthesis started from alkylation of the known hexabromotriazatruxene **2-7**[11a] with 1-bromododecane in the presence of KOH to give compound **2-8** in a 90% yield. Three dodecyl groups were introduced onto the TAT core to increase the solubility and to facilitate the subsequent synthesis and purification.[11h] The reductive debromination of **2-8** was performed in refluxing THF in the presence of 10% Pd/C, providing **2-9** in a 95% yield. The key step is the selective introduction of three –CHO groups onto the *para*-positions of the nitrogen atoms in **2-9**. The Vilsmeier-Haack condition[12] ($POCl_3$/DMF) was first tested, but it failed to give the trisformylated compound **2-10** even by increasing the reaction temperature or prolonging the reaction time. Therefore more reactive condition, $CHCl_2OCH_3/SnCl_4$ system,[13] was performed and compound **2-10** was obtained in a 55% yield. Compound **2-1** was then prepared as a red powder in an 83% yield by three-fold condensation reaction between the –CHO groups and excessive malononitrile (**2-11**) in the presence of $TiCl_4$ and pyridine in dichloromethane (DCM).[14] Horner–Wadsworth–Emmons reaction[15] between **2-10** and compounds

2-12[14c], **2-13**[16] and **2-14**[17] in dry THF afforded compounds **2-2**, **2-3** and **2-15** in 84%, 72% and 85% yield, respectively.

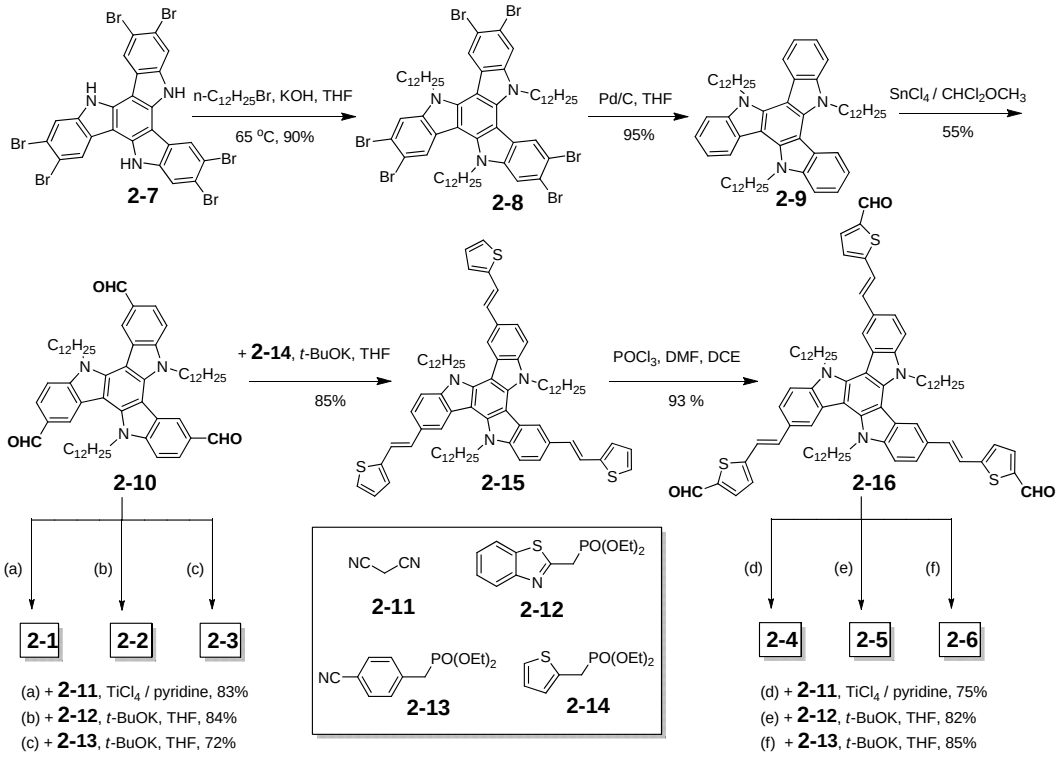

Scheme 2.1 Synthetic route of chromophores **2-1** – **2-6**.

Due to the high reactivity of the alpha-position of the periphery thiophene molecule, the key intermediate compound **2-16** was easily obtained in a 93% yield by treating **2-15** with Vilsmeier-Haack condition ($POCl_3$/DMF).[12] Afterwards, the chromophore **2-4** was prepared through three-fold condensation reaction between **2-16** and malononitrile (**2-11**) with $TiCl_4$/pyridine in dichloroethane (DCE) instead of DCM because higher temperature was necessary to complete the conversion. Chromophores **2-5** and **2-6** were synthesized via Horner–Wadsworth–Emmons reaction[17] between **2-16** and compounds **2-12**[14c] and

2-13[16] by using *t*-BuOK as the base in 82% and 85% yield, respectively. It is worth noting that **2-1**, **2-2** and **2-3** were prepared via only 4 steps with an overall yield of 39%, 40% and 34%, respectively and **2-4**, **2-5** and **2-6** were synthesized via 6 steps with a good overall yield of 28%, 30% and 32%, respectively. In addition, all the double bond formed under Horner–Wadsworth–Emmons reaction condition in the chromophores **2-2**, **2-3**, **2-15**, **2-16**, **2-4**, **2-5**, and **2-6** were *E*-configured which could be confirmed from the ^{1}H-^{1}H coupling constants of the protons of the vinylene π-bridges (J = ~16 Hz) in their ^{1}H NMR spectra.[18] ^{1}H NMR, ^{13}C NMR spectroscopy, mass spectrometry (MS) and elemental analysis were used to identify the chemical structure and purity of all of these chromophores.

2.2.2 One-photon spectral properties

The one-photon UV-vis absorption and fluorescence spectra of chromophores **2-1** - **2-6** were recorded in different solvents and the data are shown in Figure 2.2, Figure 2.3, and Table 2.1 Compounds **2-1** - **2-3** in THF displayed broad intense absorptions with maxima at 428, 400, and 388 nm, and the emission peaks appeared at 575, 503 and 499 nm, respectively (Figure 2.2a), while chromophores **2-4** - **2-6** exhibited their absorption with maxima at 512, 454 and 441 nm and emission maxima at 671, 570 and 554 nm, respectively (Figure 2.2b). Interestingly, the absorption maxima of **2-5** and **2-6** are 54 nm and 53 nm

red-shifted from that of **2-2** and **2-3**, respectively, while that for **2-4** is 84 nm red-shifted from **2-1**, which probably because of the attachment of very strong electron withdrawing dicyanomethylene groups.

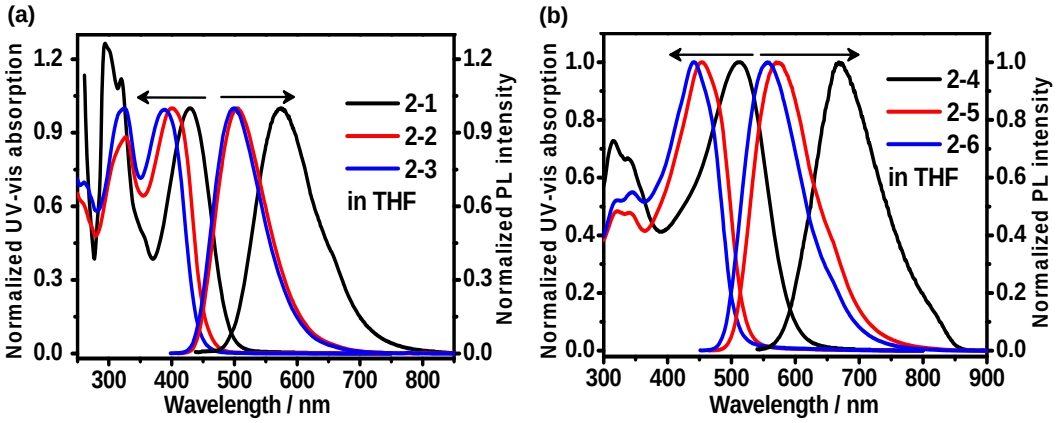

Figure 2.2 Normalized steady state UV-vis absorption and fluorescence spectra of chromophores (a) **2-1** – **2-3**, and (b) **2-4** – **2-6** in THF.

Table 2.1 Photophysical data of chromophores **2-1** – **2-6**

Cpd	solvent	λ_{abs} (nm) [a]	ε ($cm^{-1}M^{-1}$) [b]	λ_{em} (nm) [c]	Stokes shift (cm^{-1}) [d]	Φ [e] (%)	δ (GM) [f]	δΦ (GM) [g]
2-1	Toluene	436	67200	528	3996	3	730 [820nm]	22
	THF	428	65700	575	5970	4	840 [820nm]	34
2-2	Toluene	401	80700	480	4104	19	770 [800nm]	146
	THF	400	86000	503	5119	22	1110 [800nm]	244
2-3	Toluene	388	83200	462	4128	15	1050 [800nm]	158
	THF	388	89800	499	5733	16	1580 [800nm]	253
2-4	Toluene	514	48700	606	2950	8	540 [770nm]	43

	THF	512	59300	671	4628	2	280 [770nm]	6
2-5	Toluene	455	137500	524	2894	21	1620 [740nm]	340
	THF	454	142700	570	4482	22	1600 [740nm]	352
2-6	Toluene	444	122900	508	2837	34	1050 [740nm]	357
	THF	441	133000	554	4625	40	1410 [740nm]	564

[a] one-photon absorption maximum, the experimental uncertainty is ±1 nm. [b] molar extinction coefficient at the absorption maximun. [c] one-photon emission maximum, the experimental uncertainty is ±1 nm. [d] Stokes shift = $(1/\lambda_{abs} - 1/\lambda_{em})$. [e] fluorescence quantum yields by using fluorescein (pH ≈ 11, NaOH aqueous solution) as a standard the experimental uncertainty is ± 5-10%. [f] 2PA cross-section maximum in the measurable range; 1 GM = 10^{-50} cm^4 s $photon^{-1}$; the corresponding excitation wavelengths are shown in the square brackets; the experimental uncertainty on δ is of the order of (±) 12-15% of the corresponding values for **2-2**, **2-3**, **2-5** and **2-6** and (±) 25% of the corresponding values for **2-1** due to its low quantum yield. [g] 2P action cross section.

Although the solvent polarity has only little effect on the absorption spectra (Figure 2.3), significant bathochromic shift of the emission band was apparently observed for each chromophore with increasing solvent polarity. By taking compound **2-1** as an example, the fluorescence spectra show pronounced bathochromic shift with the increase of solvent polarity, i.e., from less polar toluene to highly polar DCM, the emission maximum red shifted from 528 nm to 591 nm (Figure 2.3). Such a positive solvatochromism was commonly observed for many 2PA chromophores due to the photo-induced intramolecular charge transfer (ICT)[1b] from the center to the periphery. This could be explained by that the symmetry of our octupolar molecules were broken in the excited state by

forming a relaxed, dipolar excited state localized on one of the donor-acceptor pairs.[8k] It could also be ascribed to the large steady state octupole moments in polar solvents.

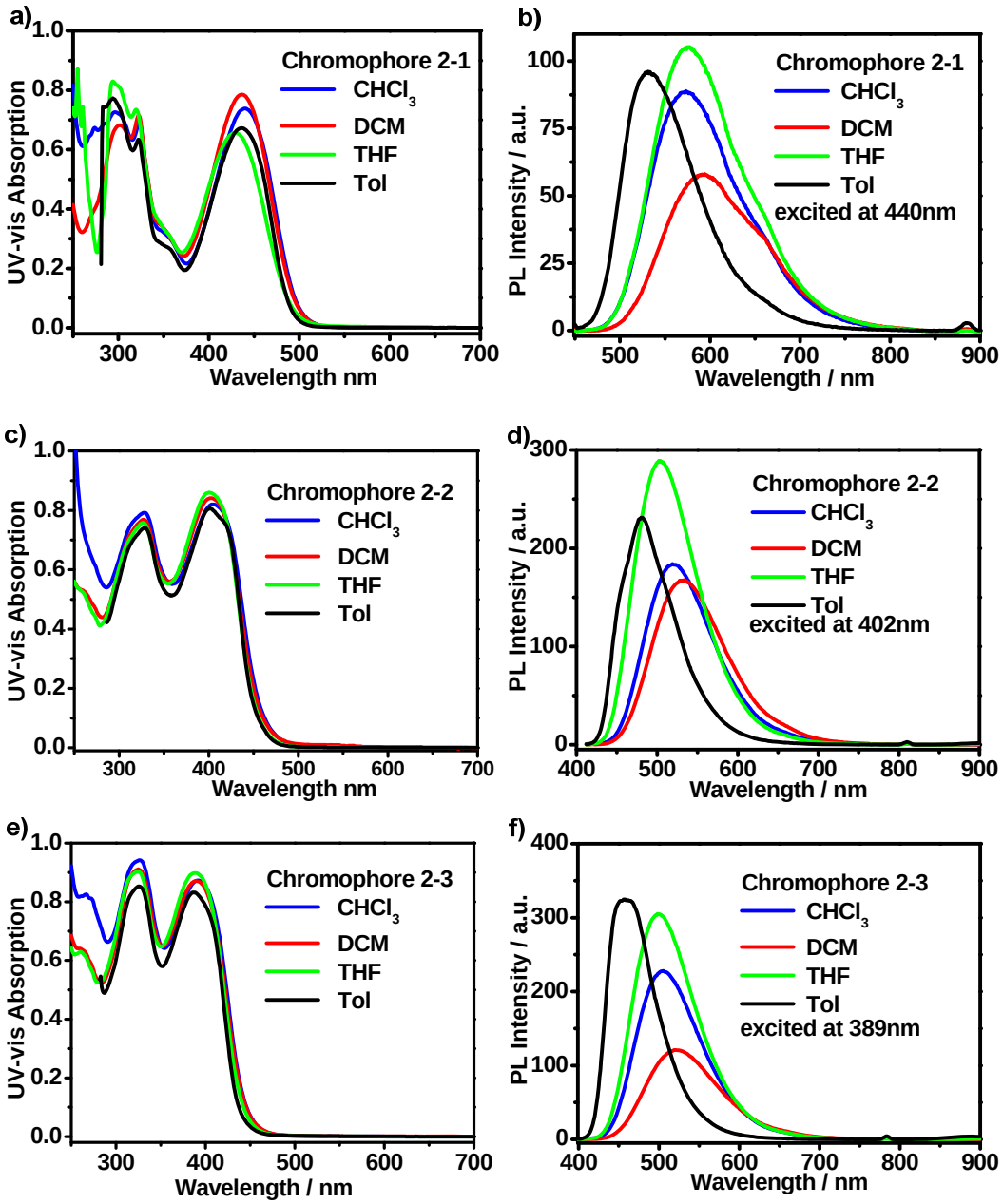

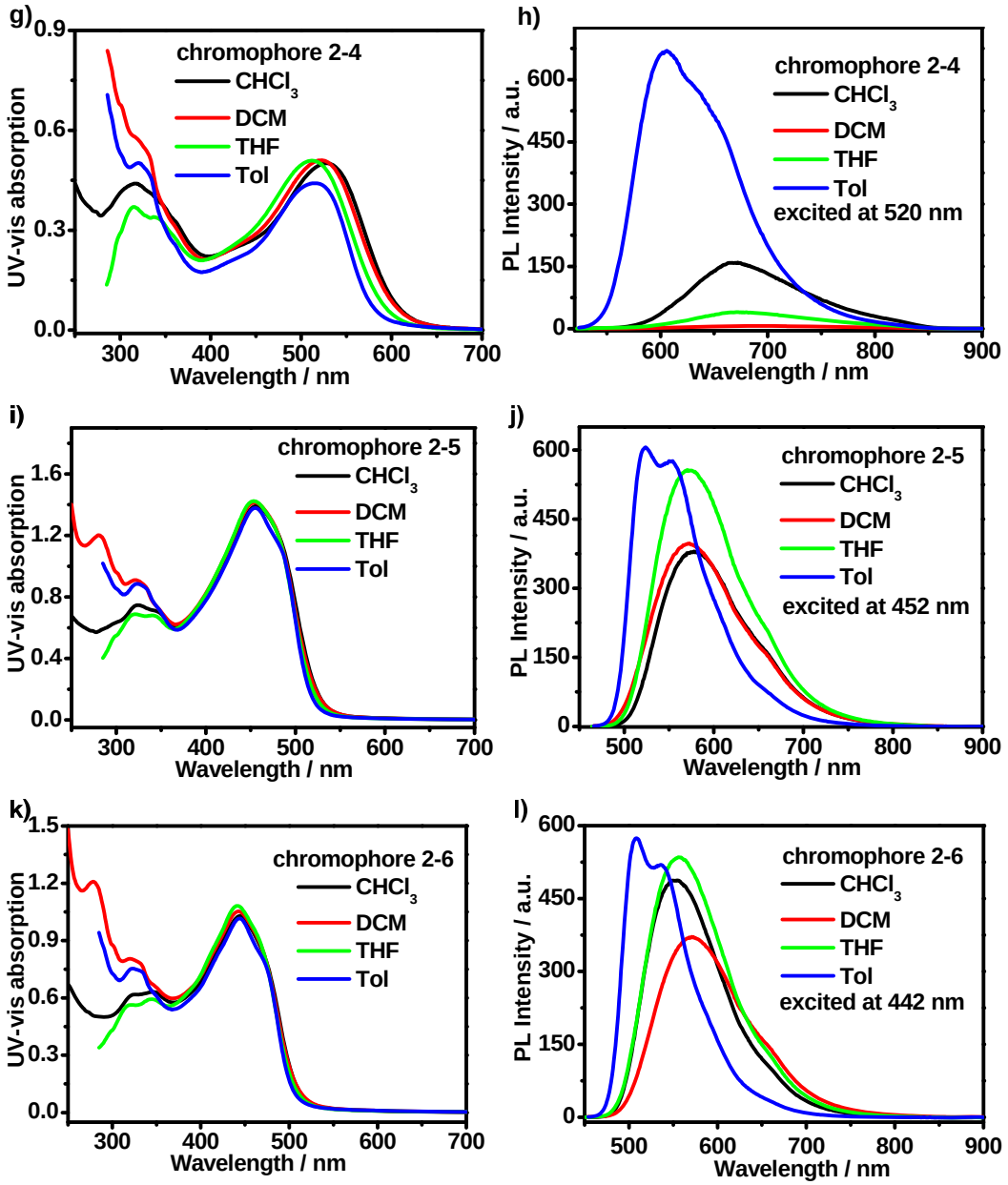

Figure 2.3 Steady state UV-vis absorption and fluorescence spectra of chromophores **2-1** – **2-6** in different solvents. For the UV-vis absorption spectra, the concentration of the solution is 1.0×10^{-5} M; and for fluorescence measurements, the solution concentration is 1.0×10^{-6} M; the excitation wavelengths for the chromophores **2-1** – **2-6** are 440, 402, 389, 520, 452 and 442 nm, respectively.

The observed large Stokes shifts (5970, 5119, 5733, 4628, 4482 and 4625 cm^{-1} for **2-1** – **2-6** in THF, respectively) indicate that significant charge

redistribution occurs upon excitation, prior to emission, and that the emission originates from a strongly dipolar emissive state.[8k] Potentially large 2PA cross sections can be obtained for these chromophores. All compounds except **2-1** and **2-4** have moderate fluorescence quantum yields (Φ, Table 2.1), which also depend on the solvent polarity. The significant decrease in quantum yields for compounds **2-1** and **2-4** could be due to the strong intramolecular charge transfer. This would promote the solute-solvent interactions, by which the excited state of the chromophore would be readily quenched and the quantum yield decreases.[8i,19]

The fluorescence lifetime was measured by using a Time-Correlated Single Photon Counting (TCSPC) technique. The frequency-doubled output of a mode-locked Ti:sapphire laser (Tsunami, Spectra-Physics) at 400 nm was used for excitation of the sample. The output pulses from Ti:sapphire centered at 800 nm had a duration of 50 fs with a repetition rate of 80 MHz. The fluorescence intensity was collected by an optical fiber which is directed to an avalanche photodiode (APD). The signals were processed by a PicoHarp 300 module (PicoQuant) with a temporal resolution of ≈ 150 ps. Mono-exponential decays were observed for all compounds (Figure 2.4) and the fluorescence lifetimes were 1.78 ns, 1.35 ns, 2.24 ns, 1.20 ns, 1.44 ns and 1.29 ns for **2-1** – **2-6**, respectively.

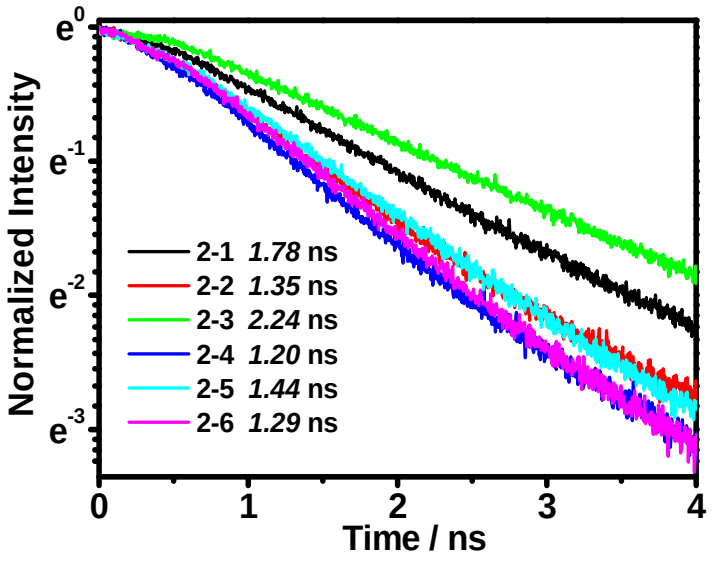

Figure 2.4 Fluorescence decay curves of chromophores **2-1** – **2-6** in toluene.

2.2.3 Electrochemical Properties

The electrochemical properties of compounds **2-1** – **2-6** were investigated by cyclic voltammetry (CV) and differential pulse voltammetry (DPV) in DCM. One or two quasi-reversible oxidation wave observed for each chromophore (Figure 2.5). Their HOMO, LUMO energy levels and energy gaps are shown in Table 2.2. The HOMO energy levels derived from the onset of oxidation potential are -5.12, -5.15, -5.15, -5.11, -4.97 and -5.00 eV for **2-1** – **2-6**, respectively.[20] Accordingly, the respective LUMO energy levels are deducted as -2.61, -2.45, -2.36, -3.06, -2.60 and -2.57 eV based on equation LUMO = HOMO + E_g, where E_g is the optical energy gap.[20] One can see that compounds **2-1** – **2-3** have similar HOMO energy levels probably because they have a common electron rich TAT core, but their LUMO energy levels are different due to the attachment of different

electron-withdrawing groups. The stronger electron-withdrawing group such as dicyanomethylene pulls down the LUMO energy level and as a result, a smaller energy gap was observed for **2-1**. For compounds **2-4** – **2-6**, the additional thienylene vinylene units further increased the π-conjugation and led to a higher lying HOMO energy level and a convergence of the HOMO-LUMO energy gap in comparison to the corresponding chromophores **2-1** – **2-3**.

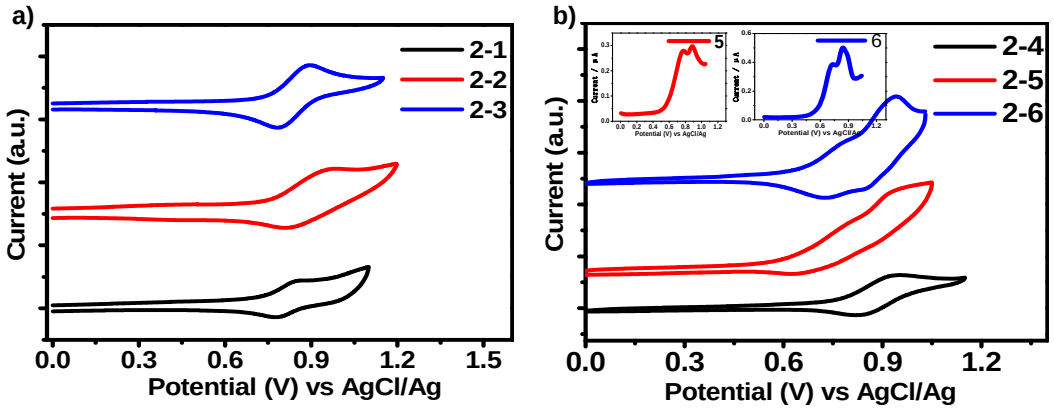

Figure 2.5 Cyclic voltammograms of chromophores **2-1** – **2-6** in DCM with 0.1 M Bu_4NPF_6 as the supporting electrolyte, AgCl/Ag as reference electrode, Au as working electrode, Pt wire as counter electrode, and scan rate at 50 mV/s. (Inset: the differential pulse voltammograms of chromophores **2-5** and **2-6** showing two distinguishable redox waves).

Table 2.2 Electrochemical properties of the chromophores **2-1** – **2-6**

Compound	[a] E_{ox}^{onset} / V	HOMO [b] / eV	LUMO [c] / eV	E_g [d] / eV
2-1	0.32	-5.12	-2.61	2.51
2-2	0.35	-5.15	-2.45	2.70
2-3	0.35	-5.15	-2.36	2.79

2-4	0.31	-5.11	-3.06	2.05
2-5	0.17	-4.97	-2.60	2.37
2-6	0.20	-5.00	-2.57	2.43

[a] E_{ox}^{onset} is the onset potential of the first oxidation wave relative to $E_{Fc^+/Fc}$. Fc^+/Fc was used as internal reference for these measurements, $E_{1/2} = 0.40$ V for Fc^+/Fc *vs* AgCl/Ag; [b] HOMO = – (4.8 + E_{ox}^{onset}); [c] LUMO = HOMO + E_g; [d] E_g (optical energy gap) calculated from the low-energy absorption edge.

2.2.4 Two-Photon Absorption (2PA) Characteristics

2PA spectra of the chromophores **2-1** - **2-6** were recorded in toluene and THF by two-photon excited fluorescence (2PEF) measurements in the range of 740-860 nm (Figure 2.6, Figure 2.7). The 2PEF spectra of these samples were compared with a reference solution of fluorescein at the corresponding excitation wavelengths.[21] All six chromophores exhibited maximum 2PA cross section (δ) ranging from 280 GM to 1620 GM in the two solvents (Table 2.1). A quadratic dependence of the 2PEF on the incident power was observed (Figure 2.8), indicating a two-photon absorption process.

A discernable trend of the two-photon absorption cross section (δ) was observed for chromophores **2-1** – **2-3**. The values in toluene increase from **2-1** to **2-3** with the maxima 2PA cross-section increasing from 730 GM to 1050 GM (Figure 2.6a). A similar trend was observed in THF (Figure 2.7). Since **2-1** – **2-3** have a common TAT core with the same electron donating effect, such a difference must be owing to the varied electron withdrawing groups and the

different effective π-conjugation length. Although the dicyanomethylene group shows the strongest electron-withdrawing property, **2-2** and **2-3** have more extended conjugation length than **2-1**, which results in larger 2PA cross-section than **2-1**. Chromophores **2-2** and **2-3** have the similar conjugation length, while **2-3** has the –CN group at the terminal site which may cause **2-3** to have the larger two-photon absorptivity than **2-2**.[7u,8j]

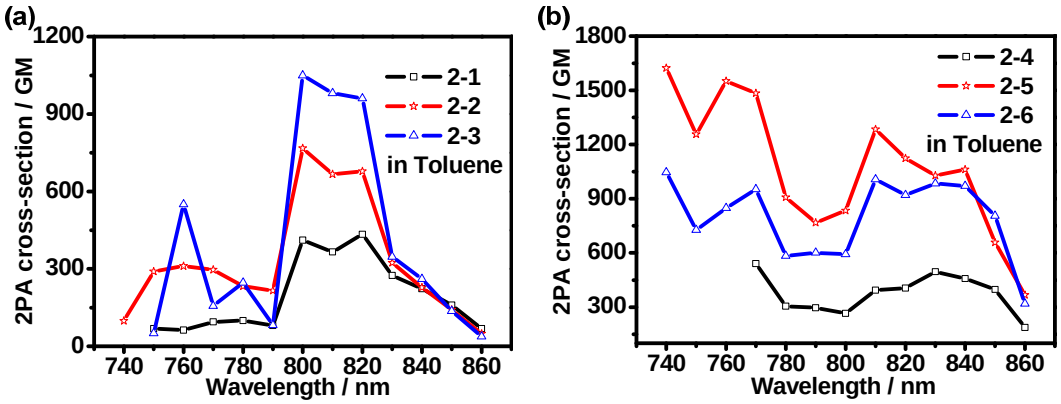

Figure 2.6 2PA spectra of the compounds **2-1** – **2-6** in toluene.

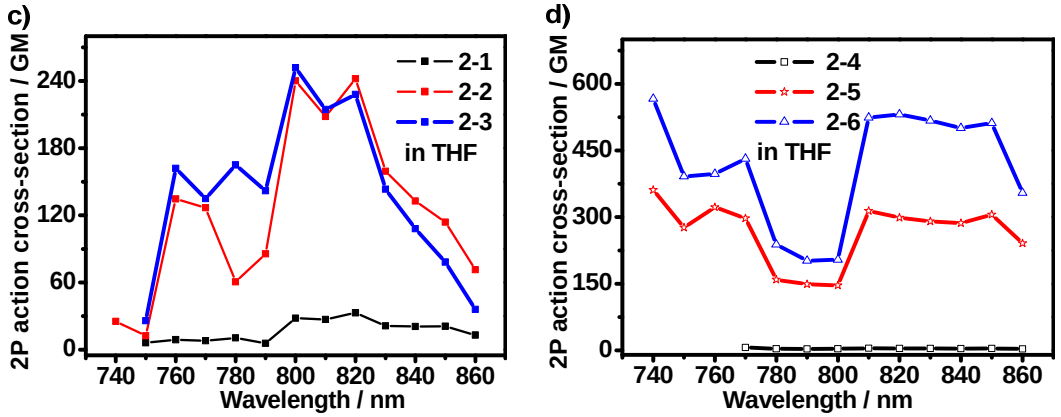

Figure 2.7 2PA spectra of the compounds **2-1** – **2-6** in THF

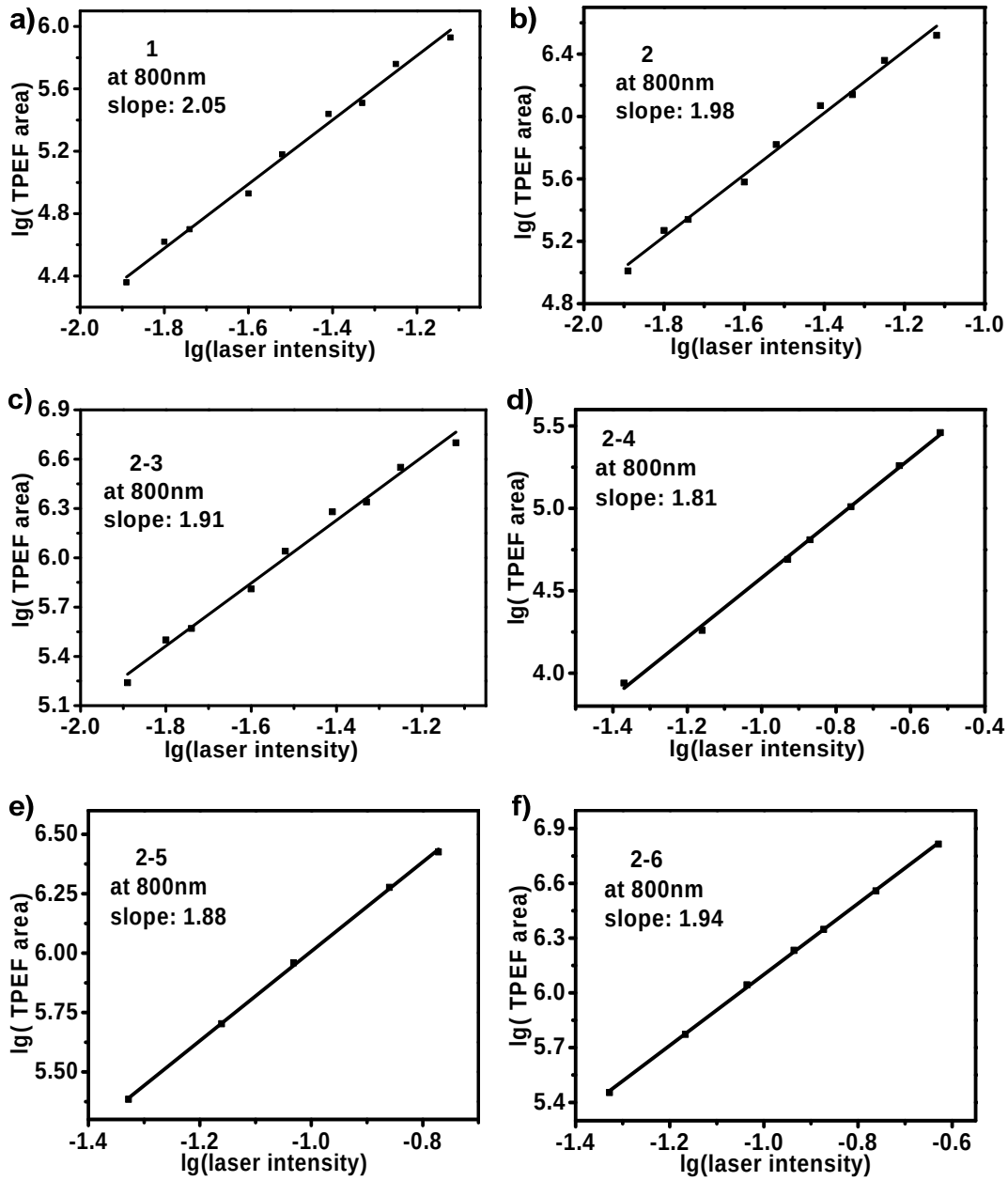

Figure 2.10 Quadratic dependence of two-photon excited fluorescence (2PEF) on the incident power: a) chromophore **2-1**; b) chromophore **2-2**; c) chromophore **2-3**; d) chromophore **2-4**; e) chromophore **2-5**; and f) chromophore **2-6**.

Compounds **2-4** – **2-6** in toluene show their maxima 2PA cross-section (δ) of 540 GM at 770 nm, 1620 GM at 740 nm and 1050 GM at 740 nm, respectively, which are larger than that of **2-1** – **2-3** (Figure 2.6). This trend could be explained as due to extended effective π-conjugation length after incorporating a thienylene

vinylene unit into the each branch. The longer π-conjugated compound may have a larger number of density of states which could provide more effective coupling channels between the ground states and two-photon allowed states, which in turn will enhance the 2PA cross-section.[8j] Chromophores **2-1** – **2-3** showed their 2PA cross section maxima in the sequence: **2-3** > **2-2** > **2-1**, and chromopores **2-5** and **2-6** exhibited comparable 2PA cross section values with both larger than that for **2-4**.

It is clearly to see the trend of 2P action cross section maximum values of the six chromophores, **2-3** > **2-2** > **2-1**, **2-6** > **2-5** > **2-4** in toluene as well as in THF (Figure 2.9, and Table 2.1). The 2P action cross section maxima of **2-2**, **2-3** are almost the same and much larger than that of **2-1**, and this is due to the relatively low quantum yield of **2-1**. In the measurement range from 740 to 860 nm, 2P action cross section of **2-6** is a little bit larger than that of **2-5**, and much larger than that of **2-4**. In addition, the 2P action cross section of **2-2**, **2-3**, **2-5**, and **2-6** are larger in THF than those in toluene (Table 2.1). It is worth noting that compared with rhodamine B, one common commercial fluorophore with 2PA cross section value of 200 GM and 2P action cross section (δΦ) of 140 GM at 840 nm in MeOH,[22] both compounds **2-5** and **2-6** have much higher 2PA cross section and TP action cross section values. Thus, compounds **2-5** and **2-6** could be potential efficient two-photon fluorescent (2PF) probes.

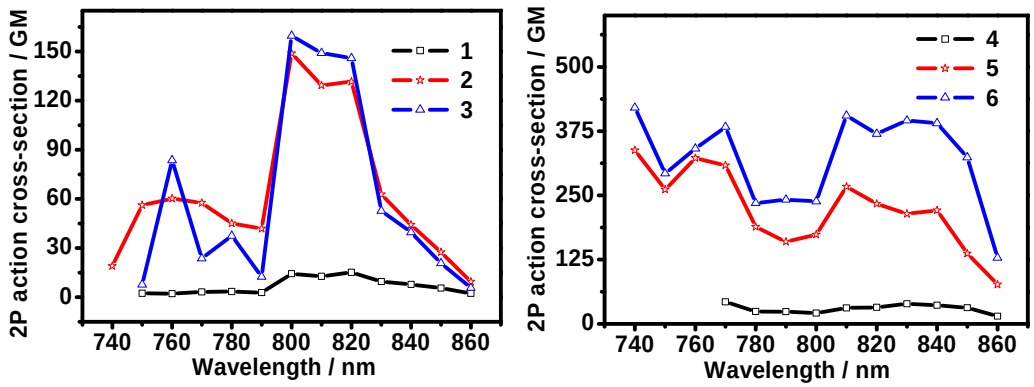

Figure 2.9 2P action cross-section spectra (δΦ) of **2-1** – **2-6** in toluene

There have been few theoretical studies to address the solvent effect, but unfortunately the published results still lack consensus.[23] One recent experimental study by using vinylbenzene[24a] and vinylfluorene[24b] derivatives revealed that, unlike one-photon transition, two-photon transition does not correlate with the polarity of the solvent. However, Bazan et al.[25] reported that the 2PA cross-section value of distyrylbenzene chromophores was solvent-dependent and nonmonotonic, and the maxima 2PA cross-section values were observed in the solvent with intermediate polarity. On the other hand, the 2PA cross-section values of octupolar molecules are expected to show little solvent dependence on account of a lack of permanent dipole moment. However, theoretical and computational studies indicate the influence of dipolar, quadrupolar, octupolar, and higher-order interactions with the solvent.[23c] In our TAT-based chromophores, no clear trend of the solvent dependence was observed. In the non-polar solvent such as toluene, the δΦ values are slightly smaller than those in polar solvents such as THF. The difference should be related

to the conformation of the chromophore molecules in excited states and solvation effect in different solvents. The small difference may be due to the rigid and planar core structure of these TAT-based chromophores.

2.2.5 Thermal Properties

The thermal stability is one of the key requirements for some practical applications of organic chromophores used in a solid matrix. The thermal stability of the compounds are examined by thermogravimetric analysis (TGA) in N_2 at a heating rate of 10 ^{o}C/min, and all the compounds have high thermal stability, with decomposition temperatures (T_d, corresponding to a 5% weight loss) at 330, 347, 378, 352, 393 and 420 ^{o}C for compounds **2-1** – **2-6**, respectively (Figure 2.10). These results confirm that the triazatruxene-containing chromophores are thermally stable.

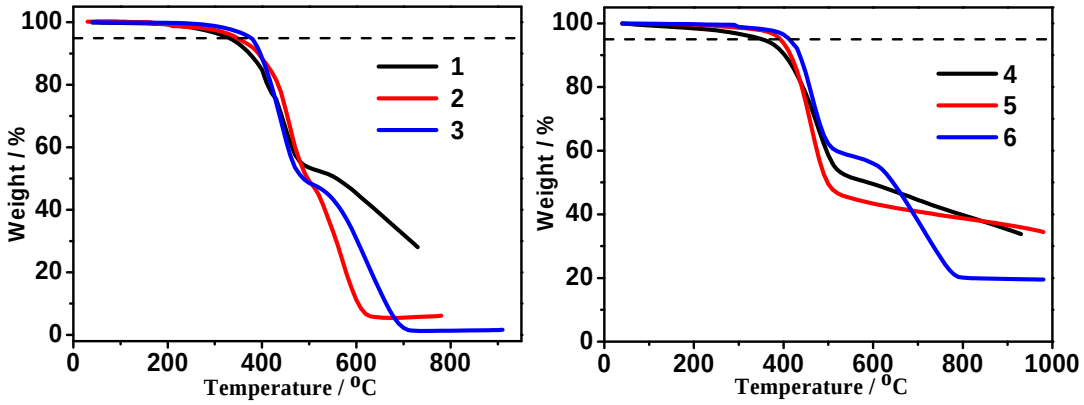

Figure 2.10 TGA curves of compounds **2-1** – **2-6**. TGA curves were obtained under N_2 at a heating rate of 10 ^{o}C/min.

2.2.6 Photostability Test

The photostability of a chromophore is of great importance regarding potential application for two-photon fluorescent microscopy (2PFM) probes. Herein the photostability and 2PA cross sections of chromophores **2-1** – **2-6** were compared with the commercially available Fluorescein via photodecomposition experiments using absorption method (Figure 2.11).[26] A figure of merit (F_M)[26b,26c] which probes for 2PFM was defined as two-photon action cross section (Φδ) normalized by their photodecomposition quantum yields (η) (see experimental section), i.e., F_M = Φδ/η, and the data are shown in Table 2.3. The F_M values of all chromophores are 1-3 orders of magnitude higher than that of fluorescein, providing strong support for the fidelity of chromophore **2-5** and **2-6** relative to commercial fluorescein probes for 2PFM biological imaging.

Table 2.3 Photostability test data for **2-1** – **2-6** and fluorescein

Compound	$\eta \times 10^{6}$ [a]	$\Phi\delta$ [b]	$F_M \times 10^{-6}$ [c]
2-1	0.04	22	550
2-2	1.22	146	120
2-3	9.0	158	18
2-4	0.28	43	154
2-5	0.07	340	4857
2-6	0.87	357	410

Fluorescein	7.16	33	5

[a] Photobleaching decomposition quantum yield, the experimental uncertainty is ± 15%. [b] 2P action cross section maximum in the measurable range in GM. [c] Figure of merit in GM, $F_M = \Phi\delta/\eta$.

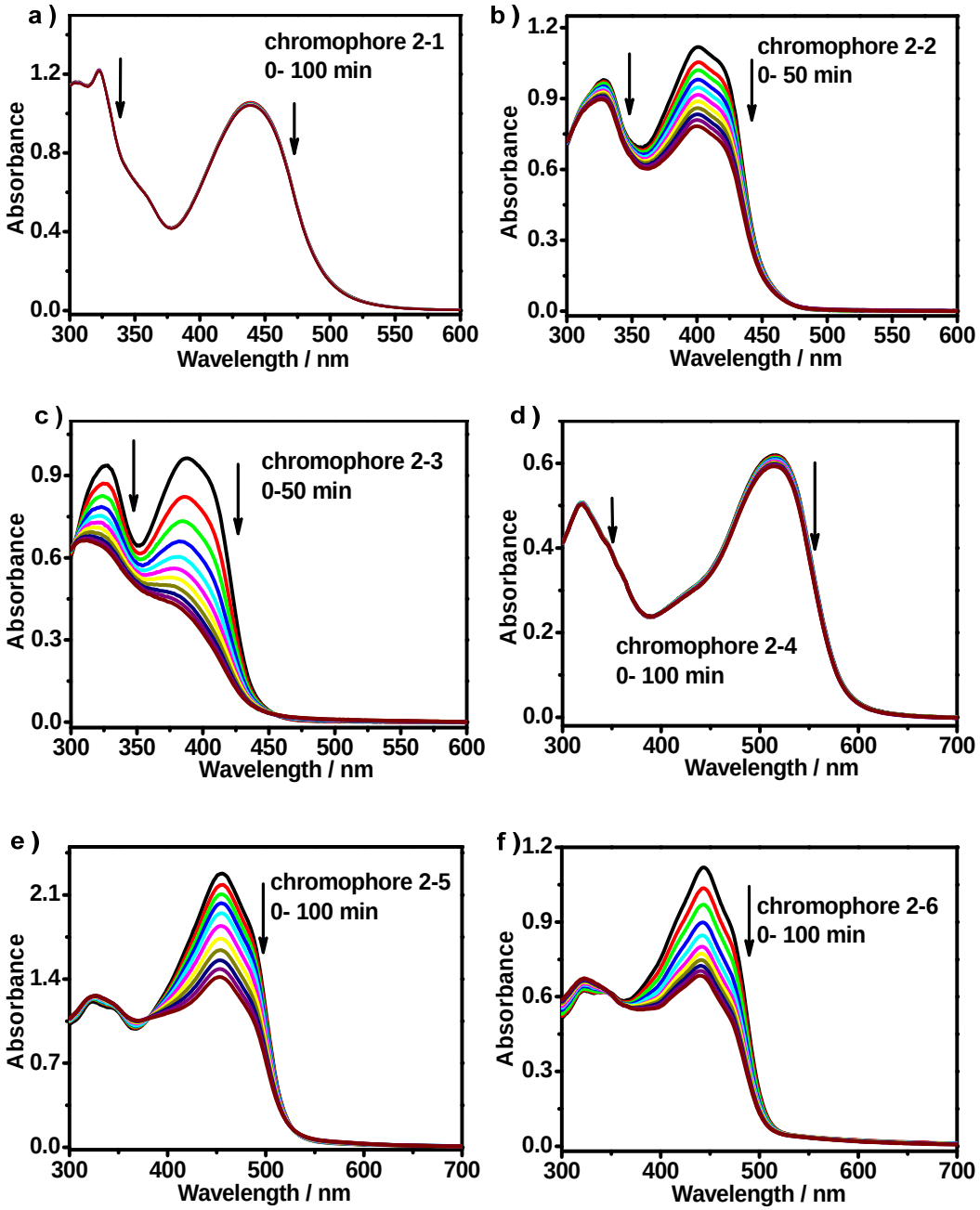

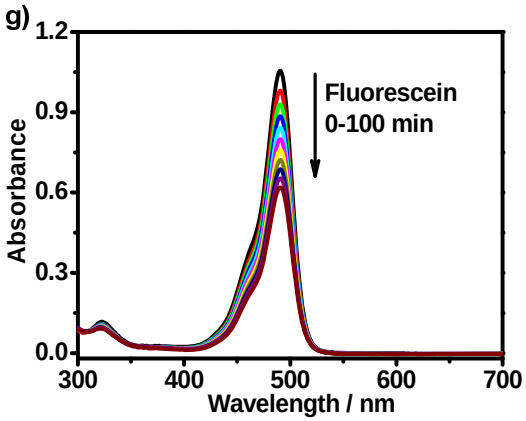

Figure 2.11 Absorbance spectra of (a) **2-1**, (b) **2-2**, (c) **2-3**, (d) **2-4**, (e) **2-5**, (f) **2-6** and (g) fluorescein by irradiation at 457, 400, 400, 457, 457, 457 and 457 nm, respectively.

2.3 Conclusions

A new synthetic route was developed to prepare six new star-shaped octupolar compounds based on triazatruxene. The synthesis of the trisformylated precursor **2-10** was the key for the synthesis of **2-1**, **2-2**, **2-3** and **2-15**. Direct formylation introduced three aldehyde groups onto **2-15**, which was the key intermediate to synthesize **2-4**, **2-5**, and **2-6**. In general, all the six chromophores were readily obtained with a good overall yield from the starting material **2-7**. Solvent polarity has little effect on the UV-vis absorption spectra, while significant bathochromic shift of the emission spectra was observed together with a larger Stokes shift in polar solvents due to intramolecular charge transfer. Chromophores **2-1** – **2-6** show high two-photon absorptivity with the maxima ranging from 280 GM to 1620 GM. At the same time, **2-5** and **2-6** exhibit the large 2P action cross section ($\delta\Phi$) and the figure of merit (F_M), so they could be the potential 2PF probes. In addition, all chromophores show good

thermal and photo-stability. We can also expect that many modifications can be done on this TAT core to further tune their 2PA properties by introducing multiple branched or dendritic structures with more extended π-conjugation in the future.

2.4 Experimental Section

2.4.1 General

Anhydrous tetrahydrofuran (THF) and DCM were obtained by distillation over sodium and CaH_2, respectively. Hexabromo-triazatruxene (**2-7**),[11a] diethyl(benzothiazol-2-yl)methylphosphonate (**2-12**),[14c] diethyl(4-cyanophenyl) methyl phosphonate (**2-13**)[16] and diethyl thiophen-2-yl methylphosphonate (**2-14**)[17] were prepared according to the literature procedure. All other chemicals were purchased from commercial supplies and used without further purification. Deuterated solvents for NMR spectroscopic analyses were used as received.

^1H NMR and ^{13}C NMR spectra were recorded in $CDCl_3$ or $CDCl_2CDCl_2$. All chemical shifts are quoted in ppm, relative to tetramethylsilane, using the residual solvent peak as a reference standard. MS were recorded in either EI mode or FAB mode and high resolution mass spectrometry were recorded with FAB ionization source. Matrix-assisted laser desorption ionization time-of-flight (MALDI-TOF) analysis was performed by using dithranol as matrix. UV-vis absorption and fluorescence spectra were recorded in HPLC pure solvents. Melting points were checked on the Buchi Melting Point B-540 instrument by using capillary method.

Cyclic voltammetry was performed on an electrochemical analyzer with a three-electrode cell in a solution of 0.1 M tetrabutylammonium hexafluorophosphate (Bu_4NPF_6) dissolved in dry DCM at a scan rate of 50 mV s^{-1}. A gold electrode with a diameter of 2 mm, a Pt wire and an Ag/AgCl electrode were used as the working electrode, the counter electrode and the reference electrode, respectively. The potential was calibrated against the ferrocene/ferrocenium couple. Thermogravimetric analysis (TGA) was carried out at a heating rate of 10 ºC/min under nitrogen flow.

The two-photon excited fluorescence (2PEF) method was used to measure the 2PA cross sections.[21] The excitation source was a femtosecond Ti:sapphire oscillator pumped by a 532 nm diode laser. The output laser pulses have pulse duration of 50 fs, a repetition rate of 80 MHz, and a center wavelength at 800 nm. The power of the laser beam before the samples was adjusted to 100 mW using neutral density filters for most measurements. The samples were excited by directing a tightly collimated, high intensity laser beam onto the sample. The emission from the sample was collected at a 90° angle by a pair of lens and optical fibers and directed to the spectrometer, which was a monochromator coupled CCD system. To avoid internal filter effects, the excited volume was located near the cell wall on the collection optics side. This configuration minimizes the fluorescence path inside the sample cell and thus reduces self-absorption. A short pass filter with cut-off wavelength at 700 nm was placed

before the spectrometer to minimize the intensity of pumping light scattering. Samples were dissolved in toluene and THF at the same concentration of 5×10^{-6} M and the two-photon induced fluorescence intensity was measured at 740-860 nm by using Fluorescein (5×10^{-6} M in water, pH = 11) as the reference. The intensities of the two-photon induced fluorescence spectra of the reference and sample under the same measurement conditions were determined and compared. The 2PA cross section of sample δs, measured by using the two-photon-induced fluorescence measurement technique, can be calculated by using the equation:

$$\delta_s = \frac{F_s \Phi_r C_r n_s^2}{F_r \Phi_s C_s n_r^2} \delta_r$$

where the subscripts s and r stand for the sample and reference molecules, respectively. F is the integral area of the two-photon fluorescence; Φ is the fluorescence quantum yield and *c* is the number density of the molecules in solution. δ_r is the 2PA cross section of the reference molecule; n is the refractive indices of the solvents. The measurements were conducted in a regime where the fluorescence signal showed a quadratic dependence on the intensity of the excitation beam, as expected for two-photon-induced emission.

The photostability of all the chromophores were determined by the absorption method[26]. For chromophore **2-1**, **2-4**, **2-5**, and **2-6**, a solution of which in toluene was irradiated in 1 mm path length quartz cuvettes with a 457 nm diode laser at 20 mW, and fluorescein in 0.1 M NaOH (aq) was tested with the same condition; for compounds **2-2** and **2-3**, a solution of which in toluene was irradiated in 1 mm

path length quartz cuvettes with a 400 nm diode laser at 20 mW. The values of photodecomposition quantum yields, η, were calculated according to equation 1, and the results listed in Table 2.3 are the average of ten pairs of adjacent absorbance maxima.

$$\eta = \frac{(A_1 - A_0)N_A}{10^3 \times \varepsilon \times \mathrm{I} \times (1 - 10^{(A_1 + A_0)/2})(t_1 - t_0)}$$ **equation 1**

Where η is the photobleaching decomposition quantum yield, A_1 is absorbance maximum at t_1, A_0 is absorbance maximum at t_0, N_A is Avogadro's number, ε is molar absorbance in $M^{-1}\cdot cm^{-1}$, t_1-t_0 is time exposed (s), and I is the intensity of laser in photon$\cdot cm^{-2}\cdot s^{-1}$.

2.4.2 Detailed Synthetic Procedures and Characterization Data

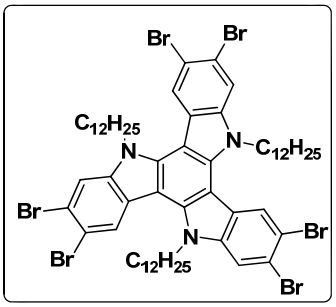

2,3,7,8,12,13-hexabromo-5,10,15-tridodecyl-10,15-dihydro-5H-diindolo[3, 2-*a*:3',2'-*c*] carbazole (2-8).

A mixture of hexabromo-triazatruxene **2-7** (2.45 g, 3.00 mmol) and KOH (1.68 g, 30.00 mmol) was heated to reflux in THF (30 mL) for 30 min. Then, 1-bromododecane (3.50 mL, 13.5 mmol) was added and the mixture was refluxed for 13 h before it was cooled to room temperature. The mixture was diluted with

DCM (50 mL) and washed with 10% aqueous HCl solution (50 mL × 2) and with saturated aqueous NaCl solution (50 mL × 2), dried over Na_2SO_4 and the solvent was removed under vacuum. The residue was purified by silica gel column chromatography using hexane as the eluent to give **2-8** as a yellow solid (2.3 g, 90%). ^{1}H NMR (500 MHz, $CDCl_3$): δ ppm = 7.95 (s, 3H), 7.49 (s, 3H), 3.97 (t, *J* = 7.5 Hz, 6H), 1.71 (br, 6H), 1.31 - 1.22 (m, 54H), 0.90 (t, *J* = 7.0 Hz , 9H); ^{13}C NMR (125 MHz, $CDCl_3$): δ ppm = 140.0, 138.6, 124.8, 122.7, 118.5, 115.2, 114.4, 101.2, 46.8, 32.0, 30.2, 29.69, 29.67, 29.60, 29.58, 29.4, 29.3, 26.5, 22.7, 14.1. FAB-MS (*m/z)*: calcd. for $C_{60}H_{81}Br_6N_3$: 1323.15; found: 1323.0 (M^+), 1243.1 (M^+ - Br). Elemental Analysis: calcd. for $C_{60}H_{81}Br_6N_3$: C, 54.44; H, 6.17; N, 3.17; found: C, 54.54; H, 6.01; N, 3.17.

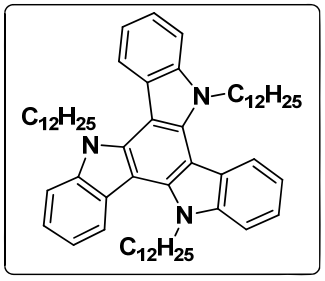

5,10,15-tridodecyl-10,15-dihydro-5H-diindolo[3,2-*a*:3',2'-*c*]carbazole (2-9).

A mixture of **2-8** (0.662 g, 0.50 mmol), Et_3N (0.55 mL, 4.00 mmol), HCOOH (0.16 mL, 4.00 mmol), and 10% Pd/C (160 mg, 0.15 mmol) in THF (10 mL) was heated at 70 ^{0}C overnight. The mixture was filtered through Celite, and the filtrate was diluted with DCM (30 mL), washed with 10% aqueous HCl (30 mL × 3),

dried over Na_2SO_4, and the solvent was removed under reduced pressure. The residue was purified by silica gel column chromatography using pure hexane as eluent to give **2-9** as a white solid (0.404 g, 95%). MP 63-65 ^oC. ^1H NMR (500 MHz, $CDCl_3$): δ ppm = 8.29 (d, *J* = 8.0 Hz, 3H), 7.64 (d, *J* = 8.0 Hz, 3H), 7.46 (t, *J* = 8.0 Hz, 3H), 7.35 (t, *J* = 8.0 Hz, 3H), 4.92 (t, *J* = 8.0 Hz, 6H), 2.00 (quin, 6H), 1.29 - 1.18 (m, 54H), 0.89 (t, *J* = 8.0 Hz, 9H); ^{13}C NMR (125 MHz, $CDCl_3$): δ ppm = 141.0, 138.9, 123.5, 122.6, 121.5, 119.6, 110.5, 103.2, 47.0, 31.9, 29.8, 29.59, 29.58, 29.5, 29.4, 29.3, 29.2, 26.7, 22.7, 14.1. EI-MS (*m/z)*: calcd. for $C_{60}H_{87}N_3$: 849.69; found: 849.9 (M^+). Elemental Analysis: calcd. for $C_{60}H_{87}N_3$: C, 84.75; H, 10.31; N, 4.94; found: C, 84.85; H, 10.20; N, 4.82.

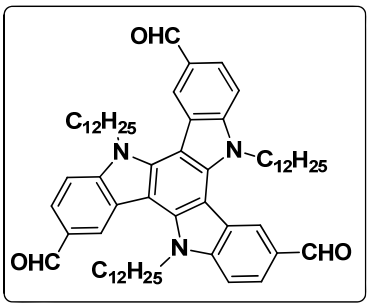

5,10,15-tridodecyl-10,15-dihydro-5H-diindolo[3,2-*a*:3',2'-*c*]carbazole-3,8,13-tricarbaldehyde (2-10).

Compound **2-9** (1.360 g, 1.60 mmol) was dissolved in dry DCM (10.0 mL) and cooled to 0 ^oC under an N_2 atmosphere. $SnCl_4$ (0.57 mL, 5.20 mmol, 3.25 equiv.) was added dropwise with stirring, followed by slow addition of dichloro-methyl methyl ether (0.47 mL, 5.20 mmol, 3.25 equiv.). After 30 min at 0 ^oC the

solution was warmed to room temperature and stirred for another 36 h. The dark solution was poured into a separatory funnel filled with 10 g of ice and shaken thoroughly. The layers were separated, and the aqueous phase was diluted with water (10 mL) and extracted with DCM (10 mL× 3). The combined organic layers were washed with water (50 mL × 2) and saturated aq. $NaHCO_3$ (50 mL × 2), diluted with ether (75 mL), and washed with brine (50 mL × 3). The solution was dried over Na_2SO_4, and the solvents were removed under reduced pressure to give the crude product as dark oil. Purification by flash chromatography (silica gel, hexane/EtOAc = 8:1) gave a deep-red solid (0.83 g, 55%). ^{1}H NMR (500 MHz, $CDCl_3$): δ ppm = 10.13 (s, 3H), 8.66 (s, 3H), 7.97 (d, *J* = 8.8 Hz, 3H), 7.63 (d, *J* = 8.8 Hz, 3H), 4.80 (t, *J* = 8.2 Hz, 6H), 1.97 (quin, 6H), 1.31 – 1.14 (m, 54H), 0.86 (t, *J* = 7.0 Hz, 9H); ^{13}C NMR (125 MHz, $CDCl_3$): δ ppm = 191.6, 144.4, 139.4, 129.5, 125.9, 124.07, 122.7, 110.7, 103.7, 47.2, 31.9, 30.1, 29.6, 29.5, 29.4, 29.32, 29.28, 26.5, 22.7, 14.1. EI-MS (*m/z)*: calcd. for $C_{63}H_{87}N_3O_3$: 933.67; found: 933.9 (M^+). Elemental Analysis: calcd. for $C_{63}H_{87}N_3O_3$: C, 80.98; H, 9.38; N, 4.50; found: C, 81.09; H, 9.26; N, 4.35.

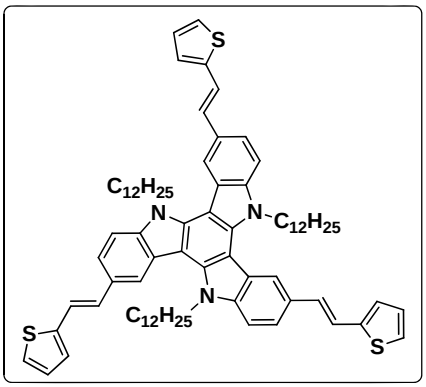

5,10,15-tridodecyl-3,8,13-tris((E)-2-(thiophen-2-yl)vinyl)-10,15-dihydro-5 H-diindolo[3,2-*a*:3',2'-*c*]carbazole (2-15).

Under N_2 atmosphere, *t*-BuOK (561 mg, 5.0 mmol, 5 equiv.) was added in small portion to a solution of **2-14** (1.173 g, 5.0 mmol, 5 equiv.) and **2-10** (0.934 g, 1.0 mmol) in dry THF (60 mL). After adding *t*-BuOK, the reaction solution turned red. The mixture was stirred at 65 ^{o}C overnight. After cooling to room temperature, the reaction solution was diluted with DCM (60 mL), washed with water (60 mL × 2) and brine (60 mL × 2), and the organic layer was dried over Na_2SO_4. After removal of solvents, the residue was purified by column chromatography (silica gel, hexane/$CHCl_3$= 4:1 - 3:1) to give the title compound **2-15** as a yellow solid (1.00 g, 85%). MP 137-139 ^{o}C. ^{1}H NMR (500 MHz, $CDCl_3$): δ ppm = 8.10 (s, 3H), 7.59 (d, *J* = 7.6 Hz, 3H), 7.48 (d, *J* = 8.2 Hz, 3H), 7.26 (d, *J* = 16.4 Hz, 3H), 7.20 (d, *J* = 5.0 Hz, 3H), 7.14 (d, *J* = 15.7 Hz, 3H), 7.10 (d, *J* = 3.2 Hz, 3H), 7.06 - 7.04 (m, 3H), 4.67 (t, *J* = 8.2 Hz, 6H), 1.99 (quin, 6H), 1.29 - 1.16 (m, 54H), 0.88 (t, *J* = 7.0 Hz, 9H); ^{13}C NMR (125 MHz, $CDCl_3$): δ ppm = 143.70, 140.74, 139.1, 130.0, 128.9, 127.6, 125.1, 123.5, 123.4, 120.8,

120.5, 119.4, 110.6, 103.1, 47.1, 31.9, 30.2, 29.7, 29.6, 29.5, 29.4 26.9, 22.7, 14.1. HR-FAB-MS (*m/z)*: calcd. for $C_{78}H_{99}N_3S_3$ (M^+): 1173.7001; found: 1173.6952 (error: -4.2 ppm); MALDI-TOF MS (*m/z)*: calcd. for $C_{78}H_{99}N_3S_3$: 1173.700; found: 1174.776 $(M + H)^+$. Elemental Analysis: calcd. for $C_{78}H_{99}N_3S_3$, C, 79.74; H, 8.49; N, 3.58; S, 8.19; found: C, 79.96; H, 8.27; N, 3.35; S, 8.36.

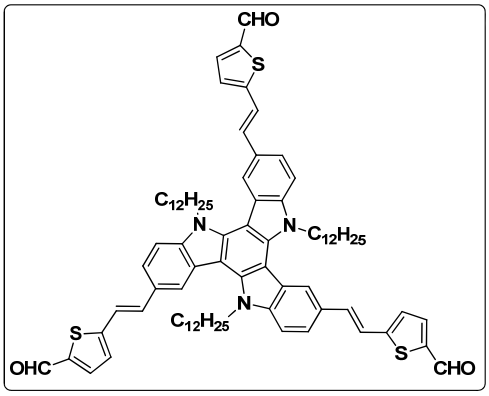

5,5',5''-(1E,1'E,1''E)-2,2',2''-(5,10,15-tridodecyl-10,15-dihydro-5H-diindolo[3,2-*a*:3',2'-*c*]carbazole-3,8,13-triyl)tris(ethene-2,1-diyl)trithiophene-2-carbaldehyde (2-16).

To a three-necked flask, $POCl_3$ (0.118 mL, 1.2 mmol) and dry DMF (0.116 mL, 1.5 mmol) were added dropwise to dry dichloroethane (DCE) (20 mL) at 0 ^oC with stirring. The mixture was warmed to room temperature, stirred for another 30 min and cooled back to 0 ^oC. A cooled solution of **2-15** (117.5 mg, 0.1 mmol) in DMF (2 mL) was added dropwise over 5 min with stirring. The reaction mixture was heated to 85 ^oC for 10 h and poured into a stirred solution of brine and crushed ice (30 mL). After 30 min, the whole was extracted with DCM (3 × 30 mL)

and the combined organic extracts were washed with brine (30 mL), dried over $MgSO_4$, filtered and concentrated in vacuo. Purification by flash chromatography on silica gel (ethyl acetate/hexane, 1:4) gave the title compound **2-16** as a red solid (117 mg, 93%). MP > 350 ^oC (the sample decomposes when the temperature is higher than 350 ^oC, the color of the solid changes from red to black.) ^1H NMR (500 MHz, $CDCl_3$): δ ppm = 9.88 (s, 3H), 8.03 (s, 3H), 7.68 (d, *J* = 3.8 Hz, 3H), 7.62 (d, *J* = 8.8 Hz, 3H), 7.48 (d, *J* = 8.8 Hz, 3H), 7.30 (d, *J* = 15.8 Hz, 3H), 7.19 (d, *J* = 15.8 Hz, 3H), 7.12 (d, *J* = 3.8 Hz, 3H), 4.62 (br, 6H), 1.93 (br, 6H), 1.25 - 1.12 (m, 54H), 0.85 (t, *J* = 7.5 Hz, 9H); ^{13}C NMR (125 MHz, $CDCl_3$): δ ppm = 182.2, 153.3, 141.0, 138.6, 137.3, 134.4, 127.7, 125.7, 123.0, 121.5, 121.1, 118.1, 110.6, 102.8, 46.9, 31.9, 30.2, 29.72, 29.66, 29.61, 29.5, 29.3, 26.9, 22.7, 14.1. MALDI-TOF MS (m/z): calcd. for 1257.685; found: 1258.737 (M^+ + H). Elemental Analysis: calcd. for $C_{81}H_{99}N_3O_3S_3$, C, 77.28; H, 7.93; N, 3.34; O, 3.81; S, 7.6; found: C, 77.58; H, 7.84; N, 3.41; S, 7.81.

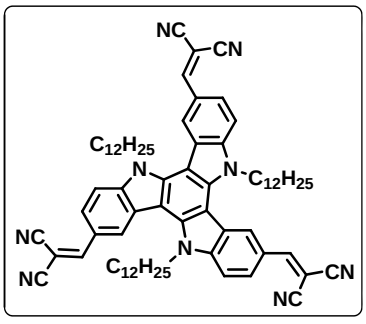

2,2',2''-(5,10,15-tridodecyl-10,15-dihydro-5H-diindolo[3,2-*a*:3',2'-*c*]carbazole-3,8,13-triyl)tris(methan-1-yl-1-ylidene) trimalononitrile (2-1).

Compound **2-10** (187 mg, 0.20 mmol) and malononitrile (**2-11**, 0.08 ml, 1.20 mmol, 6 equiv.) were dissolved in DCM (10 mL) under nitrogen atmosphere and then $TiCl_4$ (0.14 mL, 1.20 mmol, 6 equiv.) and pyridine (0.20 mL, 2.40 mmol, 12 equiv.) were slowly added at room temperature. The reaction mixture was heated to reflux and the reaction was monitored by TLC. After 12 h the reaction was cooled to room temperature and the mixture was poured into water (80 mL) and extracted with DCM (80 mL × 3). The organic layer was dried over Na_2SO_4, and the solvent was removed under vacuum. The crude concentrated extract was dropped into large amount of CH_3OH to give the title compound as a red precipitate (180 mg, 83%). MP 179-180 ^oC. ^1H NMR (500 MHz, $CDCl_3$): δ ppm = 8.93 (s, 3H), 7.95 (d, *J* = 8.8 Hz, 3H), 7.92 (s, 3H), 7.77 (d, *J* = 8.8 Hz, 3H), 5.07 (t, *J* = 8.0 Hz, 6H), 1.80 (quin, 6H), 1.26 - 1.01 (m, 54H), 0.85 (t, *J* = 7.5Hz , 9H); ^{13}C NMR (125 MHz, $CDCl_3$): δ ppm = 160.2, 144.7, 139.9, 128.2, 124.7, 123.7, 123.6, 114.7, 114.1, 112.1, 104.3, 77.9, 47.4, 31.8, 29.52, 29.47, 29.37, 29.26, 29.0, 26.4, 22.6, 14.1. HR-FAB-MS (*m/z)*: calcd. for $C_{72}H_{87}N_9$ $(M + H)^+$: 1078.7163; found: 1078.7172 (error: 0.83 ppm); MALDI-TOF MS (m/z): found 1078.571. Elemental Analysis: calcd. for $C_{72}H_{87}N_9$: C, 80.18; H, 8.13; N, 11.69; found: C, 80.35; H, 8.11; N, 11.51.

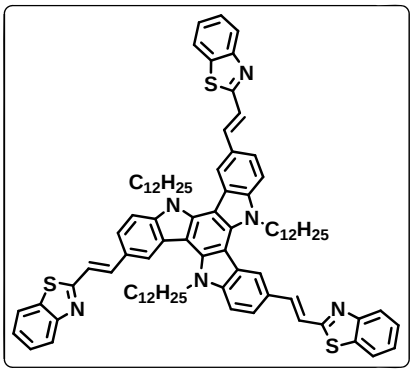

2,2',2''-(1E,1'E,1''E)-2,2',2''-(5,10,15-tridodecyl-10,15-dihydro-5H-diindolo[3,2-*a*:3',2'-*c*]carbazole-3,8,13-triyl)tris(ethene-2,1-diyl)tribenzo[*d*]thiazole (2-2).

Under N_2 atmosphere, potassium *tert*-butoxide (100 mg, 1.125 mmol, 9 equiv.) was added in portion to a solution of diethyl(benzo[d]thiazol-2-yl) methylphosphonate **2-12** (178 mg, 0.625 mmol, 5 equiv.) and **2-10** (117 mg, 0.125 mmol) in dry THF (20 mL). After adding potassium *tert*-butoxide, the reaction solution turned red. The mixture was stirred at 65 ^{o}C overnight. After cooling to room temperature, the reaction solution was diluted with DCM (30 mL) and the organic layer was washed with water (30 mL × 2) and brine (30 mL × 2), dried over Na_2SO_4 and the solution was concentrated under reduced pressure. The crude concentrated extract was dropped into large amount of CH_3OH to give the title compound as an orange powder (140 mg, 84%). MP 190-191 ^{o}C. ^{1}H NMR (500 MHz, $CDCl_3$): δ ppm = 8.25 (s, 3H), 8.01 (d, *J* = 8.0 Hz, 3H), 7.83 (d, *J* = 8.0 Hz, 3H), 7.74 - 7.67 (m, 6H), 7.57 (d, *J* = 8.0 Hz, 3H), 7.49 -7.46 (m, 6H), 7.36 (t, *J* = 7.5 Hz, 3H), 4.77 (br, 6H), 1.99 (br, 6H), 1.29 - 1.11 (m, 54H), 0.83 (t, *J* = 7.8 Hz , 9H); ^{13}C NMR (125 MHz, $CDCl_3$): δ ppm = 167.6, 154.0, 141.55, 139.2, 138.9,

134.2, 127.4, 126.2, 125.0, 123.1, 122.7, 122.0, 121.8, 121.4, 119.7, 110.8, 103.1, 47.1, 31.9, 30.3, 29.86, 29.77, 29.74, 29.71, 29.66, 29.64, 29.4, 27.0, 14.1. HR-FAB-MS (*m/z)*: calcd. for $C_{87}H_{102}N_6S_3$ $(M + H)^+$: 1327.7406; found: 1327.7387 (error: -1.4 ppm). MALDI-TOF MS (m/z): found: 1327.793. Elemental Analysis: calcd. for $C_{87}H_{102}N_6S_3$: C, 78.69; H, 7.74; N, 6.33; S, 7.24; found: C, 78.86; H, 7.62; N, 6.18; S, 7.16.

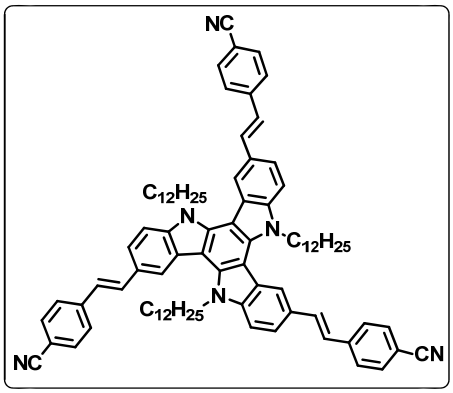

4,4',4''-(1E,1'E,1''E)-2,2',2''-(5,10,15-tridodecyl-10,15-dihydro-5H-diindolo[3,2-*a*:3',2'-*c*]carbaz-ole-3,8,13-triyl)tris(ethene-2,1-diyl)tribenzo-nitrile (2-3).

Under N_2 atmosphere, *t*-BuOK (200 mg, 2.25 mmol, 9 equiv.) was added in small portion to a solution of diethyl (4-cyanophenyl) methylphosphonate **2-13** (200 mg, 1.25 mmol, 5 equiv.) and **2-10** (234 mg, 0.25 mmol) in dry THF (30 mL). After adding *t*-BuOK, the reaction solution turned red. The mixture was stirred at 65 ^oC overnight. After cooling to room temperature, the reaction solution was diluted with DCM (30 mL), washed with water (30 mL × 2) and brine (30 mL × 2),

and the organic layer was dried over Na_2SO_4 and concentrated to afford a crude solid. The crude extract was dropped into CH_3OH to give the title compound as an yellow powder (220 mg, 72%). MP 200-201 ^{o}C. ^{1}H NMR (500 MHz, $CDCl_3$): δ ppm = 8.30 (s, 3H), 7.73 - 7.61 (m, 18H), 7.44 (d, *J* = 16.4 Hz, 3H), 7.13 (d, *J* = 16.4 Hz, 3H), 4.89 (t, *J* = 7.5 Hz, 6H), 2.05 (quin, 6H), 1.26 - 1.12 (m, 54H), 0.86 (t, *J* = 7.0 Hz, 9H); ^{13}C NMR (125 MHz, $CDCl_3$): δ ppm = 142.4, 141.3, 139.2, 133.7, 132.5, 128.5, 126.5, 124.3, 123.5, 121.5, 121.3, 119.1, 110.9, 110.0, 103.4, 47.2, 31.9, 30.1, 29.7, 29.64, 29.61, 29.58, 29.47, 29.3, 26.9, 22.7, 14.1. HR-FAB-MS (*m/z)*: calcd. for $C_{87}H_{102}N_6$ (M^+): 1230.8166; found: 1230.8187 (error: 1.7 ppm). MALDI-TOF MS (m/z): found: 1232.139. Elemental Analysis: calcd. for $C_{87}H_{102}N_6$: C, 84.83; H, 8.35; N, 6.82; found: C, 84.79; H, 8.27; N, 6.67.

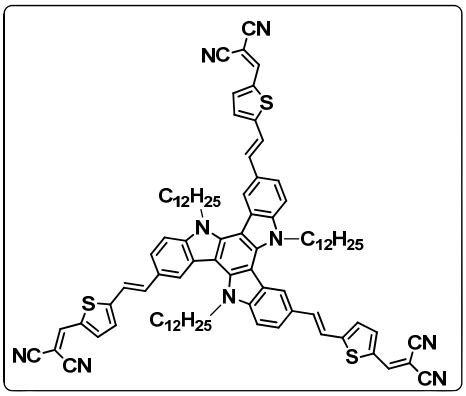

2,2',2''-(5,5',5''-(1E,1'E,1''E)-2,2',2''-(5,10,15-tridodecyl-10,15-dihydro-5 H-diindolo[3,2-*a*:3',2'-*c*]carbazole-3,8,13-triyl)tris(ethene-2,1-diyl)tris(thioph ene-5,2-diyl))tris(methan-1-yl-1-ylidene)trimalononitrile (2-4).

Compound **2-16** (377 mg, 0.30 mmol) and malononitrile (**2-11**, 119 mg, 1.80 mmol, 6 equiv.) were dissolved in dry dichloroethane (DCE) (20 mL) under nitrogen atomosphere and then $TiCl_4$ (0.2 mL, 1.80 mmol, 6 equiv.) and pyridine (0.29 mL, 3.60 mmol, 12 equiv.) were slowly added at room temperature. The reaction mixture was heated at 85 ^oC and the reaction was monitored by TLC. After 24 h the reaction was cooled to room temperature and the mixture was poured into water (200 mL) and extracted with DCM. The organic layer was dried over magnesium sulfate and the solvent was removed under reduced pressure to give the crude product as a red solid. Then 1.0 mL of $CHCl_3$ was added to dissolve the solid, and followed by addition of 15.0 mL of CH_3OH. The pure product was precipitated out as a purple-red solid (316 mg, 75%). MP 219-220 ^oC. ^1H NMR (500 MHz, $CDCl_3$, 323 K): δ ppm = 8.12 (s, 3H), 7.72 - 7.66 (m, 6H), 7.62 - 7.55 (m, 6H), 7.39 (d, J = 15.8 Hz, 3H), 7.23 (d, J = 15.8 Hz, 3H), 7.16 (d, J = 4.4 Hz, 3H), 4.75 (t, J = 7.5 Hz, 6H), 1.88 (br, 6H), 1.28 – 1.09 (m, 54H), 0.85 (t, J = 7.0 Hz, 9H); ^{13}C NMR (125 MHz, $CDCl_3$, 323K): δ ppm =155.8, 149.8, 141.9, 140.1, 139.1, 136.4, 133.2, 127.9, 126.2, 123.5, 122.2, 121.9, 117.8, 114.4, 113.8, 111.2, 103.7, 75.5, 47.2, 31.9, 29.8, 29.7, 29.59, 29.57, 29.5, 29.28, 29.26, 26.7, 22.6, 14.0. HR-FAB-MS (*m/z)*: calcd. for $C_{90}H_{99}N_9S_3$ $(M + H)^+$: 1402.7264.; found: 1402.7224 (error: -2.9 ppm). MALDI-TOF MS (m/z): found: 1402.762. Elemental Analysis: calcd. for $C_{90}H_{99}N_9S_3$: C, 77.05; H, 7.11; N, 8.99; S, 6.86; found: C, 77.16; H, 6.98; N, 8.76; S, 6.61.

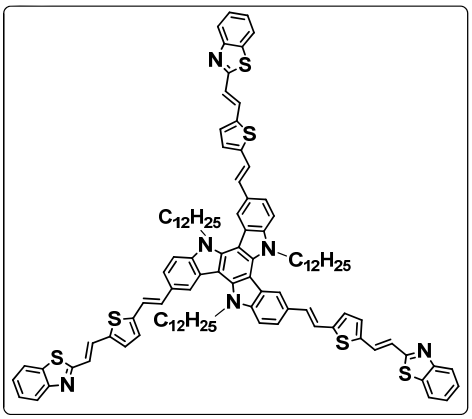

2,2',2''-(1E,1'E,1''E)-2,2',2''-(5,5',5''-(1E,1'E,1''E)-2,2',2''-(5,10,15-tridodecyl-10,15-dihydro-5H-diindolo[3,2-*a*:3',2'-*c*]carbazole-3,8,13-triyl)tris(ethene-2,1-diyl)tris(thiophene-5,2-diyl))tris(ethene-2,1-diyl)tribenzo[*d*]thiazole (2-5).

Under N_2 atmosphere, potassium *tert*-butoxide (253 mg, 2.25 mmol, 9 equiv.) was added in portion to a solution of diethyl(benzo[*d*]thiazol-2-yl)methylphosphonate **2-12** (357 mg, 1.25 mmol, 5 equiv.) and **2-16** (315 mg, 0.25 mmol) in dry THF (30 mL). After adding potassium *tert*-butoxide, the reaction solution turned red. The mixture was stirred at 85 ^{o}C overnight. After cooling to room temperature, the reaction solution was diluted with DCM, washed with water and brine. The organic layer was dried over Na_2SO_4 and the solution was concentrated under reduced pressure. The crude concentrated extract was dropped into large amount of CH_3OH to give the title compound as an red powder (338 mg, 82%). MP 231-233 ^{o}C. ^{1}H NMR (500 MHz, $Cl_2CDCDCCl_2$, 313 K): δ ppm = 8.17 (s, 3H), 7.99 (d, *J* = 8.0Hz, 3H), 7.85 (d, *J* = 8.0 Hz, 3H), 7.67 – 7.55 (m, 9H), 7.48 (t, *J* = 8.0 Hz, 3H), 7.37 (t, *J* = 8.0 Hz,

3H), 7.20 – 7.15 (m, 12H), 7.04 (d, *J* = 3.65 Hz), 4.76 (br, 6H), 2.09 (br, 6H), 1.37 - 1.18 (m, 54H), 0.82 (t, *J* = 7.1 Hz , 9H); ^{13}C NMR (125 MHz, $CCl_2CDCDCCl_2$): δ ppm = 165.8, 154.1, 145.5, 141.2, 139.1, 138.7, 134.5, 131.6, 129.8, 129.6, 128.8, 125.9, 125.7, 124.8, 123.6, 122.7, 121.3, 121.1, 120.5, 119.0, 110.6, 103.6, 47.2, 31.5, 29.7, 29.24, 29.21, 29.20, 29.1, 28.9, 26.6, 22.2, 13.5. HR-FAB-MS (*m/z)*: calcd. for $C_{105}H_{114}N_6S_6$ (M^+): 1651.7463; found: 1651.7460 (error: -0.2 ppm). MALDI-TOF MS (m/z): found: 1652.788. Elemental Analysis: calcd. for $C_{105}H_{114}N_6S_6$: C, 76.32; H, 6.95; N, 5.09; S, 11.64; found: C, 76.22; H, 6.72; N, 4.95; S, 11.56.

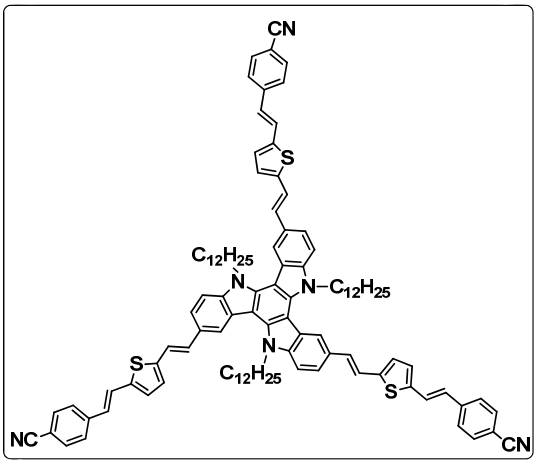

4,4',4''-(1E,1'E,1''E)-2,2',2''-(5,5',5''-(1E,1'E,1''E)-2,2',2''-(5,10,15-tridodecyl-10,15-dihydro-5H-diindolo[3,2-*a*:3',2'-*c*]carbazole-3,8,13-triyl)tris(ethene-2,1-diyl)tris(thiophene-5,2-diyl))tris(ethene-2,1-diyl)tribenzonitrile (2-6).

Under N_2 atmosphere, potassium *tert*-butoxide (240 mg, 2.0 mmol, 10 equiv.) was added in small portion to a solution of diethyl

(4-cyanophenyl)methylphosphonate **2-13** (254 mg, 1.0 mmol, 5 equiv.) and **2-16** (252 mg, 0.2 mmol) in dry THF (30 mL). After adding potassium *tert*-butoxide, the reaction solution turned red. The mixture was stirred at 85 ^{o}C overnight. After cooling to room temperature, the reaction solution was diluted with DCM, washed with water and brine, and the organic layer was dried over Na_2SO_4 and concentrated to afford a crude solid. The crude extract was dropped into CH_3OH to give the title compound as an orange powder (264.2 mg, 85%). MP 246-248 ^{o}C. ^{1}H NMR (500 MHz, $Cl_2CDCDCCl_2$, 343 K): δ ppm = 8.30 (s, 3H), 7.69 – 7.62 (m, 12H), 7.55 (d, *J* = 8.85 Hz, 6H), 7.32 – 7.25 (m, 9H), 7.11 (d, *J* = 3.75 Hz, 3H), 7.05 (d, *J* = 3.75 Hz, 3H), 6.91 (d, *J* = 15.75 Hz, 3H), 4.92 (t, *J* = 7.0 Hz, 6H), 2.13 (br, 6H), 1.42-1.21 (m, 54H), 0.87 (t, *J* = 7.0 Hz, 9H); ^{13}C NMR (125 MHz, $CDCl_3$, 323 K): δ ppm = 144.4, 141.6, 141.1, 139.9, 139.2, 132.4, 131.1, 128.9, 128.8, 126.5, 126.0, 125.7, 125.5, 123.7, 121.2, 120.7, 119.3, 118.8, 110.7, 110.5, 103.5, 47.3, 31.8, 30.1, 29.63, 29.58, 29.4, 29.31, 29.26, 29.20, 26.9, 22.6, 13.9. HR-FAB-MS (*m/z)*: calcd. for $C_{105}H_{114}N_6S_3$ $(M + H)^+$: 1556.8379; found: 1556.8376 (error: -0.2 ppm). MALDI-TOF MS (m/z): found: 1556.890. Elemental Analysis: calcd. for $C_{105}H_{114}N_6S_3$: C, 81.04; H, 7.38; N, 5.40; S, 6.18. found: C, 80.93; H, 7.21; N, 5.28; S, 6.34.

2.5 References

1. For a recent review, see: a) He, G. S.; Tan. L.-S.; Zheng, Q.; Prasad, P. N. *Chem. Rev*. **2008**, *108*, 1245. b) Kim, H. M.; Cho, B. R. *Chem. Commun.* **2009**, 153. c) Kim, H. M.; Cho, B. R. *Acc. Chem. Res.*, **2009**, *42*, 863. d) Terenziani, F.; Katan, C.; Badaeva, E.; Tretiak, S.; Blanchard-Desce, M. *Adv. Mater*. **2008**, *20*, 4641. e) Pawlicki, M.; Collins, H. A.; Denning, R. G.; Anderson, H. L. *Angew. Chem. Int. Ed*. **2009**, *48*, 3244.
2. a) Parthenopoulos, D. A.; Rentzepis, P. M. *Science* **1989**, *245*, 843. b) Strickler, J. H.; Webb, W. W. *Opt. Lett.* **1991**, *16*, 1780. c) Belfield, K. D.; Schafer, K. J. *Chem. Mater.* **2002**, *14*, 3656. d) Corredor, C. C.; Huang, Z.-L.; Belfield, K. D.; Morales, A. R.; Bondar, M. V. *Chem. Mater.* **2007**, *19*, 5165.
3. a) Zhou, W.; Kuebler, S. M.; Braun, K. L.; Yu, T.; Cammack, J. K.; Ober, C. K.; Perry, J. W.; Marder, S. R. *Science* **2002**, *296*, 1106. b) Kawata, S.; Sun, H.-B.; Tanaka, T.; Takada, K. *Nature* **2001**, *412*, 697. c) Maruo, S.; Nakamura, O.; Kawata, S. *Opt. Lett*. **1997**, *22*, 132. d) Cumpston, B. H.; Ananthavel, S. P.; Barlow, S.; Dyer, D. L.; Ehrlich, J. E.; Erskine, L. L.; Heikal, A. A.; Kuebler, S. M.; Lee, I. Y. S.; McCord-Maughon, D.; Qin, J.; Rockel, H.; Rumi, M.; Wu, X. L.; Marder, S. R.; Perry, J. W. *Nature* **1999**, *398*, 51. e) Joshi, M. P.; Pudavar, H. E.; Swiatkiewicz, J.; Prasad, P. N.; Reinhardt, B. A. *Appl. Phys. Lett.* **1999**, *74*, 170. f) Dvornikov, A. S.; Bouas-Laurent, H.; Desvergne, J.-P.; Rentzepis, P. M. *J. Mater. Chem*. **1999**, *9*, 1081. g) Sun, H.-B.; Kawakami, T.; Xu, Y.; Ye, J.-Y.; Matuso, S.; Misawa, H.; Miwa, M.; Kaneko, R. *Opt. Lett*.

2000, *25*, 1110. h) Wang, I.; Bouriau, M.; Baldeck, P. L.; Martineau, C.; Andraud, C. *Opt. Lett*. **2002**, *27*, 1348. i) Lu, Y.; Hasegawa, F.; Goto, T.; Ohkuma, S.; Fukuhara, S.; Kawazu, Y.; Totani, K.; Yamashita, T.; Watanabe, T. *J. Mater. Chem*. **2004**, *14*, 75. j) Nguyen, L. H.; Straub, M.; Gu, M. *Adv. Func. Mater.* **2005**, *15*, 209. k) Jhaveri, S. J.; McMullen, J. D.; Sijbesma, R.; Tan, L.-S.; Zipfel, W.; Ober, C. K. *Chem. Mater.* **2009**, *21*, 2003.

4. a) He, G. S.; Xu, G. C.; Prasad, P. N.; Reinhardt, B. A.; Bhatt, J. C.; Dillard, A. G. *Opt. Lett.* **1995**, *20*, 435. b) Ehrlich, J. E.; Wu, X. L.; Lee, I.-Y. S.; Hu, Z.-Y.; Röckel, H.; Marder, S. R.; Perry, J. W. *Opt. Lett.* **1997**, *22*, 1843. c) Bouit, P.-A.; Wetzel, G.; Berginc, G.; Loiseaux, B.; Toupet, L.; Feneyrou, P.; Bretonniere, Y.; Kamada, K.; Maury, O.; Andraud, C. *Chem. Mater.* **2007**, *19*, 5325.

5. a) Denk, W.; Strickler, J. H.; Webb, W. W. *Science* **1990**, *248*, 73. b) Larson, D. R.; Zipfel, W. R.; Williams, R. M.; Clark, S. W.; Bruchez, M. P.; Wise, F. W.; Webb, W. W. *Science* **2003**, *300*, 1434. c) Picot, A.; D'Aléo, A.; Baldeck, P. L.; Grichine, A.; Duperray, A.; Andraud, C.; Maury, O. *J. Am. Chem. Soc.* **2008**, *130*, 1532. d) Gao, Y.; Wu, J.; Li, Y.; Sun, P.; Zhou, H.; Yang, J.; Zhang, S.; Jin, B.; Tian, Y. *J. Am. Chem. Soc.* **2009**, *131*, 5208. e) Kim, H. J; Han, J. H.; Kim, M. K.; Lim, C. S.; Kim, H. M.; Cho, B. R. *Angew. Chem. Int. Ed*. DOI: 10.1002/anie.201002907. f) Kim, H. M.; Seo, M. S.; An, M. J.; Hong, J. H.; Tian, Y. S.; Choi, J. H.; Kwon, O.; Lee, K. J.; Cho, B. R. *Angew. Chem. Int.*

Ed. **2008**, *47*, 5167. g) Kim, M. K.; Lim, C. S.; Hong, J. T.; Han, J. H.; Jang, H.-Y.; Kim, H. M.; Cho, B. R. *Angew. Chem. Int. Ed*. **2010**, *49*, 364. h) Tian, Y. S.; Lee, H. Y.; Lim, C. S.; Park, J.; Kim, H. M.; Shin, Y. N.; Kim, E. S.; Jeon, H. J.; Park, S. B.; Cho, B. R. *Angew. Chem. Int. Ed.* **2009**, *48*, 8027. i) Kim, H. M; Jung, C.; Kim, B. R; Jung, S. Y.; Hong, J. H.; Ko, Y. G.; Lee, K. J; Cho, B. R. *Angew. Chem. Int. Ed*. **2007**, *46*, 3460. j) Kim, H. M.; An, M. J.; Hong, J. H.; Jeong, B. H.; Kwon, O.; Hyon, J. Y.; Hong, S. C.; Lee, K. J.; Cho, B. R. *Angew. Chem. Int. Ed.* **2008**, *47*, 2231. k) Kim, H. M.; Kim, B. R.; Hong, J. H.; Park, J. S.; Lee, K. J.; Cho, B. R. *Angew. Chem. Int. Ed*. **2007**, *46,* 7445. l) Lee, J. H.; Lim, C. S.; Tian, Y. S.; Han, J. H.; Cho, B. R. *J. Am. Chem. Soc.* **2010**, *132*, 1216. m) Morales, A. R.; Schafer-Hales, K. J.; Marcus, A. I.; Belfield, K. D. *Bioconjugate Chem.* **2008,** *19,* 2559. n) Morales, A. R.; Yanez, C. O.; Schafer-Hales, K. J.; Marcus, A. I.; Belfield, K. D. *Bioconjugate Chem.* **2009**, *20*, 1992. o) Mohan, P. S.; Lim, C. S.; Tian, Y. S.; Roh, W. Y.; Lee, J. H.; Cho, B. R. *Chem. Commun.* **2009**, 5365. p) Wang, X.; Nguyen, D. M.; Yanez, C. O.; Rodriguez, L.; Ahn, H.-Y.; Bondar, M. V.; Belfield, K. D. *J. Am. Chem. Soc.* **2010**, *132*, 12237.

6. a) Bhawalkar, J. D.; Kumar, N. D.; Zhao, C. F.; Prasad, P. N. *J. Clin. Laser Med. Surg.* **1997**, *15*, 201. b) Kim, S.; Ohulchanskyy, T. Y.; Pudavar, H. E.; Pandey, R. K.; Prasad, P. N. *J. Am. Chem. Soc.* **2007**, *129*, 2669. c) Ogawa, K.; Kobuke, Y. *Org. Biomol. Chem.* **2009**, *7*, 2241. d) Nielsen, C. B.; Arnbjerg, J.;

Johnsen, M.; Jorgensen, M.; Ogilby, P. R. *J. Org. Chem*. **2009**, *74*, 9094. e) Belfield, K. D.; Hagan, D. J.; Stryland, Eric W. V.; Schafer, K. J.; Negres, R. A. *Org. Lett.* **1999**, *1*, 1575.

7. a) Albota, M.; Beljonne, D.; Brédas, J.-L.; Ehrlich, J. E.; Fu, J.-Y.; Heikal, A. A.; Hess, S. E.; Kogej, T.; Levin, M. D.; Marder, S. R.; McCord-Maughon, D.; Perry, J. W.; Röckel, H.; Rumi, M.; Subramaniam, G.; Webb, W. W.; Wu, X.-L.; Xu, C. *Science* **1998**, *281*, 1653. b) Ventelon, L.; Charier, S.; Moreaux, L.; Mertz, J.; Blanchard- Desce, M. *Angew. Chem. Int. Ed.* **2001**, *40*, 2098. c) Frederiksen, P. K.; Jørgensen, M.; Ogilby, P. R. *J. Am. Chem. Soc.* **2001**, *123*, 1215. d) Mongin, O.; Porrés, L.; Moreaux, L.; Mertz, J.; Blanchard-Desce, M. *Org. Lett.* **2002**, *4*, 719. e) Abbotto, A.; Beverina, L.; Bozio, R.; Facchetti, A.; Ferrante, C.; Pagani, G. A.; Pedron, D.; Signorini, R. *Org. Lett.* **2002**, *4*, 1495. f) Yang, W. J.; Kim, D. Y.; Jeong, M.-Y.; Kim, H. M.; Jeon, S.-J.; Cho, B. R. *Chem. Commun.* **2003**, 2618. g) Cho, B. R.; Son, K. H.; Lee, S. H.; Song, Y. S.; Lee, Y. K.; Jeon, S. J.; Choi, J. H.; Lee, H.; Cho, M. *J. Am. Chem. Soc.* **2001**, *123*, 10039. h) Rumi, M; Ehrlich, J. E; Heikal, A. A.; Perry, J. W.; Barlow, S.; Hu, Z. Y.; McCord-Maughon, D.; Parker, T. C.; Rockel, H.; Thayumanavan, S.; Marder, S. R.; Beljonne D.; Brédas, J. L. *J. Am. Chem. Soc*. **2000**, *122*, 9500. i) Pond, S. J.; Rumi, K. M.; Levin, M. D.; Parker, C. T.; Beljonne, D.; Day, M. W.; Brédas, J.-L.; Marder, S. R.; Perry, J. W. *J. Phys. Chem. A*, **2002**, *106,* 11470. j) Huang, P. H.; Shen, J. Y.; Pu, S. C.; Wen, Y. S.; Lin, J. T.; Chou, P. T. M.; Yeh, C. P. *J. Mater.*

Chem. **2006**, *16*, 850. k) Chung, S.; Rumi, J. M; Alain, V.; Barlow, S.; Perry, J. W.; Marder, S. R. *J. Am. Chem. Soc*. **2005**, *127*, 10844. l) Mongin, O.; Porres, L.; Charlot, M.; Katan C.; Blanchard-Desce, M. *Chem.–Eur. J*. **2007**, *13*, 1481. m) Ventelon, L.; Moreaux, L.; Mertz, J.; Blanchard-Desce, M. *Chem. Commun.* **1999**, 2055; n) Ventelon, L.; Charier, S.; Moreaux, L.; Mertz, J.; Blanchard-Desce, M. *Angew. Chem. Int. Ed.*, **2001**, *40*, 2098. o) Werts, M. H.; Gmouh, S.; Mongin, O.; Pons, T.; Blanchard-Desce, M. *J. Am. Chem. Soc.* **2004**, *126*, 16294. p) Yang, W. J.; Kim, D. Y.; Jeong, M. Y.; Kim, H. M.; Lee, Y. K.; Fang, X.; Jeon S. J.; Cho, B. R. *Chem.–Eur. J.* **2005**, *11*, 4191. q) Kim, H. M.; Yang, W. J.; Kim, C. H.; Park, W. H.; Jeon, S. J.; Cho, B. R. *Chem.–Eur. J*. **2005**, *11*, 6386. r) Zheng, S. J.; Beverina, L.; Barlow, S.; Zojer, E.; Fu, J.; Padilha, L. A.; Fink, C.; Kwon, O.; Yi, Y. P.; Shuai, Z. G.; Stryland, E. W. V.; Hagan, D. J.; Brédas J.-L.; Marder, S. R. *Chem. Commun*. **2007**, 1372. s) Zheng, S. J.; Leclercq, A.; Fu, J.; Beverina, L.; Padilha, L. A.; Zojer, E.; Schmidt, K.; Barlow, S.; Luo, J. D.; Jiang, S. H.; Jen, A. K. Y.; Yi, Y. P.; Shuai, Z. G.; Stryland, E. W. V.; Hagan, D. J.; Brédas, J.-L.; Marder, S. R. *Chem. Mater.* **2007**, *19*, 432. t) Chung, S. J.; Zheng, S. J.; Odani, T.; Beverina, L.; Fu, J.; Padilha, L. A.; Biesso, A.; Hales, J. M.; Zhan, X. W.; Schmidt, K.; Ye, A. J.; Zojer, E.; Barlow, S.; Hagan, D. J.; Stryland, E. W. V.; Yi, Y. P. Z.; Shuai, Z. G.; Pagani, G. A.; Brédas, J.-L.; Perry, J. W.; Marder, S. R. *J. Am. Chem. Soc.* **2006**, *128*, 14444. u) Lee, S. K.; Yang, W. J.; Choi, J. J.; Kim, C. H.; Jeon, S.-J.; Cho, B. R. *Org. Lett.* **2005**, *7*, 323. v) Belfield, K. D.; Bondar, M. V.; Yanez, C.

O.; Hernandez, F. E.; Przhonska, O.V. *J. Mater. Chem*. **2009**, *19*, 7498. w) Yao, S.; Ahn, H.-Y.; Wang, X.; Fu, J.; Stryland, E. W. V.; Hagan, D. J.; Belfield, K. D. *J. Org. Chem*. **2010**, *75*, 3965. x) Andrade, C. D.; Yanez, C. O.; Rodriguez, L.; Belfield, K. D. *J. Org. Chem*. **2010**, *75*, 3975.

8. a) Joshi, M. P.; Swiakiewicz, J.; Xu, F.; Prasad, P. N.; Reinhardt, B. A.; Kannan, R. *Opt. Lett.* **1998**, *23*, 1742. b) Mongin, O.; Brunel, J.; Porres, L.; Blanchard-Desce, M. *Tetrahedron Lett.* **2003**, *44*, 2813. c) Beljonne, D.; Wenseleers, W.; Zojer, E.; Shuai, Z. G.; Vogel, H.; Pond, S. J. K.; Perry, J. W.; Marder, S. R.; Brédas, J.-L. *Adv. Funct. Mater.* **2002**, *12*, 631. d) Bordeau, G.; Lartia, R.; Metge, G.; Fiorini-Debuisschert, C.; Charra, F.; Teulade-Fichou, M.-P. *J. Am. Chem. Soc.* **2008**, *130*, 16836. e) Droumaguet, C. L.; Mongin, O.; Werts, M. H. V.; Blanchard- Desce, M. *Chem. Commun*. **2005**, 2802. f) Fang, Z.; Zhang, X.; Lai, Y. H.; Liu, B. *Chem. Commun.* **2009**, 920. g) Chung, S. J.; Kim, K. S.; Lin, T. C.; He, G. S.; Swiatkiewicz, J.; Prasad, P. N. *J. Phys. Chem. B* **1999**, *103*, 10741. h) Yoo, J.; Yang, S. K.; Jeong, M. Y.; Ahn, H. C.; Jeon, S. J.; Cho, B. R. *Org. Lett*. **2003**, *5*, 645. i) Wu, J.; Zhao, Y. X.; Li, X.; Shi, M. Q.; Wu, F. P.; Fang, X. Y. *New J. Chem*. **2006**, *30*, 1098. j) Yang, W. J.; Kim, D. Y.; Kim, C. H.; Jeong, M. Y.; Lee, S. K.; Jeon, S. J.; Cho, B. R. *Org. Lett.* **2004**, *6*, 1389. k) Porres, L.; Mongin, O.; Katan, C.; Charlot, M.; Pons, T. J.; Blanchard-Desce, M. *Org. Lett.* **2004**, *6*, 47. l) Bhaskar, A.; Ramakrishna, G.; Lu, Z. K.; Twieg, R. J.; Hales, M.; Hagan, D. J.; Stryland, E. V.; Goodson, T. *J. Am. Chem. Soc*. **2006**, *128*, 11840.

m) Cui, Y. Z.; Fang, Q.; Xue, G.; Xu, G. B.; Yin, L.; Yu, W. T. *Chem. Lett*. **2005**, *34,* 644. n) Lin, T.-C.; Hsu, C.-S.; Hu, C.-L.; Chen, Y. -F.; Huang. W. -J. *Tetrahedron Lett.* **2009**, *50*, 182. o) Lin, T.-C.; Huang, Y.-J.; Chen, Y.-F.; Hu, C.-L. *Tetrahedron* **2010**, *66*, 1375. p) Jiang, Y.; Wang, Y.; Hua, J.; Tang, J.; Li, B.; Qian, S.; Tian, H. *Chem. Commun*. **2010**, *46*, 4689.

9. a) McDonagh, A. M.; Humphrey, M. G.; Samoc, M.; Luther-Davies, B. *Organometallics* **1999**, *18*, 5195. b) Spangler, C. W. *J. Mater. Chem.* **1999**, *9*, 2013.
10. Zheng, Q. D.; He. G. S.; Prasad, P. N. *Chem. Mater.* **2005**, *17*, 6004.
11. a) Robertson, N.; Parsons, S.; MacLean, E. J.; Coxall, R. A.; Mount, A. R. *J. Mater. Chem.* **2000**, *10*, 2043. b) Gomez-Lor, B.; Alonso, B.; Omenat, A.; Serrano, J. L. *Chem. Commum.* **2006**, 5012. c) Gomez-Lor, B.; Echavarren, A. M. *Org. Lett.* **2004**, *6*, 2993. d) Gomez-Lor, B.; Gunther, H.; Beatriz, A.; Angeles, M.; Enrique, G-P.; Antonio, M. E. *Angew. Chem. Int. Ed.* **2006**, *45*, 4491. e) Lai, W.-Y.; Chen, Q.-Q.; He, Q.-Y.; Fan, Q.-L.; Huang, W. *Chem. Commun.* **2006**, 1959. f) Lai, W.-Y.; Zhu, R.; Fan, Q.-L.; Hou, L.-T.; Cao, Y.; Huang, W. *Macromolecules* **2006**, *39*, 3707. g) Talarico, M.; Termine, R.; Garcia-Frutos, E. M.; Omenat, A.; Serrano, J. L.; Gomez-Lor, B.; Golemme, A. *Chem. Mater.* **2008**, *20*, 6589. h) Lai, W.-Y.; He, Q.-Y.; Zhu, R.; Chen, Q.-Q.; Huang, W. *Adv. Funct. Mater*. **2008**, *18*, 265. i) García-Frutos, E. M.; Gómez-Lor, B. *J. Am. Chem. Soc.* **2008**, *130*, 9173. j) Luo, J.; Zhao, B. M.;

Shao, J.; Lim, K. A.; Chan, H. S. O.; Chi, C. *J. Mater. Chem.* **2009**, *19*, 8327. k) Zhao, B.; Liu, B.; Png, R. Q.; Zhang, K.; Lim, K. A.; Luo, J.; Shao, J.; Ho, K. H.; Chi, C.; Wu, J. *Chem. Mater.* **2010**, *22*, 435.

12. a) Vilsmeier, A.; Haack, A. *Ber.* **1927**, *60*, 119. b) Meth-Cohn, O.; Stanforth, S. P. *Comp. Org. Syn.* **1991**, *2*, 777. c) He, F.; Tian, L.; Tian, X.; Xu, H.; Wang, Y. H.; Xie, W.; Hanif, M.; Xia, J.; Shen, F.; Yang, B.; Li, F.; Ma, Y.; Yang, Y.; Shen, J. *Adv. Funct. Mater.* **2007**, *17*, 1551
13. Kedrowski, B. L.; Hoppe, R. W. *J. Org. Chem.* **2008**, *73*, 5177.
14. a) Kochurani, J.; Becker, J. Y.; Ellern, A.; Khodorkovsky, V. *Tetrahedron Lett.* **1999**, *40*, 8625. b) Sanguinet, L.; Williams, J. C.; Yang, Z.; Twieg, R. J.; Mao, G.; Singer, K. D.; Wiggers, G.; Petschek, R. G. *Chem. Mater.* **2006**, *18*, 4259. c) Lartia, R.; Allain, C.; Bordeau, G.; Schmidt, F.; Fiorini-Debuisschert, C.; Charra, F.; Teulade-Fichou, M. P. *J. Org. Chem.* **2008**, *73,* 1732.
15. Guldi, D. M.; Swartz, A.; Luo, C.; Gomez, R.; Segura, J. L.; Martin, N. *J. Am. Chem. Soc.* **2002**, *124*, 10875.
16. Messmore, B. W.; Hulvat, J. F.; Sone, E. D.; Stupp, S. I. *J. Am. Chem. Soc.* **2004**, *126*, 14452.
17. a) Jørgensen, M.; Krebs, F. C. *J. Org. Chem.* **2005**, *70*, 6004. b) Zheng, S.; Barlow, S.; Parker, T. C.; Marder, S. R. *Tetrahedron Lett.* **2003**, *44*, 7989. c) Jen, A. K. Y.; Rao, V. P.; Wong, K. Y.; Drost, K. J. *J. Chem. Soc., Chem. Commun* **1993**, 90.

18. Pretsch, E.; Bühlmann, P.; Affolter, C. *Structure Determination of Organic Compounds*. Springer-Verlag: Berlin, 2000.

19. Ko, C.-W.; Tao, Y.-T.; Danel, A.; Krzeminska, L.; Tomasik, P. *Chem. Mater.* **2001**, *13*, 2441.

20. a) Chi, C.; Wegner, G. *Macromol. Rapid Comm.* **2005**, *26*, 1532. b) Chi, C.; Im, C.; Enkelmann, V.; Ziegler, A.; Lieser, G.; Wegner, G. *Chem. Eur. J.* **2005**, *11*, 6833.

21. a) Xu, C.; Webb, W. W. *J. Opt. Soc. Am. B* **1996**, *13*, 481. b) Tian, N.; Xu, Q.-H. *Adv. Mater.* **2007**, *19*, 1988.

22. Xu, C.; Williams, R. M.; Zipfel, W.; Webb, W. W. *Bioimaging* **1996**, *4*, 198.

23. a) Luo, Y.; Norman, P.; Macak, P.; Agren, H. *J. Phys. Chem. A* **2000**, *104*, 4718. b) Wang, C.-K.; Zhao, K.; Su, Y.; Ren, Y.; Zhao, X.; Luo, Y. *J. Chem. Phys.* **2003**, *119,* 1208. c) Ray, P. C.; Leszczynski, J. *J. Phys. Chem. A* **2005**, *109,* 6689. d) Terenziani, F.; Painelli, A.; Katan, C.; Charlot, M.; Blanchard-Desce, M. *J. Am. Chem. Soc.* **2006**, *128,* 15742. e) Paterson, M. J.; Kongsted, J.; Christiansen, O.; Mikkelsen, K. V.; Nielsen, C. B. *J. Chem. Phys.* **2006**, *125,* 184501. f) Zhao, K.; Ferrighi, L.; Frediani, L.; Wang, C.-K.; Luo, Y. *J. Chem. Phys.* **2007**, *126,* 204509. g) Easwaramoorthi, S.; Shin, J. Y.; Cho, S.; Kim, P.; Inokuma, Y.; Tsurumaki, E.; Osuka, A.; Kim, D. *Chem. Eur. J.* **2009**, *15,* 12005.

24. a) Johnsen, M; Ogilby, P. R. *J. Phys. Chem. A* **2008**, *112,* 78319. b) Fitilis, I.; Fakis, M.; Polyzos, I.; Giannetas, V.; Persephonis, P.; Mikroyannidis. J. *J. Phys.*

Chem. A. **2008**, *112,* 4742.

25. Woo, H. Y.; Liu, B.; Kohler, B.; Korystov, D.; Mikhailovsky, A.; Bazan G. C. *J. Am. Chem. Soc*. **2005**, *127,* 14721.

26. a) Corredor, C. C.; Belfield, K. D.; Bondar, M. V.; Przhonska, O.V.; Yao, S. *J. Photochem.Photobiol. A: Chem.* **2006,** *184*, 105. b) Wang, X; Nguyen, D, M; Yanez, C, O; Rodriguez, L; Ahn, H-Y; Bondar, M. V; Belfield, K. D. *J. Am. Chem. Soc.*, **2010**, *132,* 12237. c) Wang, X; Yao, S. Ahn, H-Y; Zhang, Y; Bondar, M. V; Torres, J. A; Belfield, K. D;. *Biomed. Opt. Express* **2010**, *1,* 453

Chapter 3

Linear and Star-shaped Pyrazine-containing Acene Dicarboximides with High Electron-affinity

3.1 Introduction

As mentioned in chapter 1, organic conjugated molecules are of great importance and interest from the viewpoint of their fundamental electronic and optoelectronic properties and their potential applications, such as for two-photon absorption(see chapter 2), organic field-effect transistors (OFETs).[1] After large success on hole-transporting (*p*-type) organic semiconductors,[2] recently there is increasing interest in the development of high performance electron-transporting (*n*-type) semiconductors, which are desirable for the fabrication of *p*–*n* junction diodes, bipolar transistors, and complementary integrated circuits.[3] The general design approaches to achieve *n*-type semiconductors include (1) attachment of electron-withdrawing substituents (e.g. fluorine,[4] carboximide,[5] cyano-[6]) onto the traditional *p*-type semiconductors (e.g. acene, oligothiophene) and/or (2) replacement of the carbon atoms in the framework by electron-deficient atoms (e.g. imine nitrogen[7]). Following this guidance, some *n*-type semiconductors have been successfully synthesized and used in *n*-channel OFETs.[8]

Linear acene and star-shaped angularly fused acene (i.e., starphene) are good candidates for organic semiconductors and recently electron-deficient n-type acenes[4d,5f,g,6e,7a–f] and starphenes[7m–o,9] have been reported by several groups including us. The substitution by electron-withdrawing dicarboximide groups stabilized the electron-rich acene molecules and also improved their solubility.[5] Replacement of one or more benzene rings in acene and starphene with an

electron-deficient pyrazine ring not only increased the electron affinity, but also enhanced intermolecular interactions and improved their kinetic stability towards H_2O and O_2.[7a–e,10] To further increase the electron affinity, herein we are interested in combining both approaches together to design and synthesize new pyrazine-containing acene and starphene dicarboximide derivatives such as the dibenzo-tetraazahexacene[7m, 11] bis(dicarboximide)s **3-1a**–**b** and **3-2a**–**b**, and hexaazatrinaphthylene tris(dicarboximide) **3-3** (Figure 3.1). High electron affinity is expected for these molecules, which is a pre-requisite for a good n-type semiconductor. Different alkyl chains are used to tune their solubility and thermal behavior in the solid state.

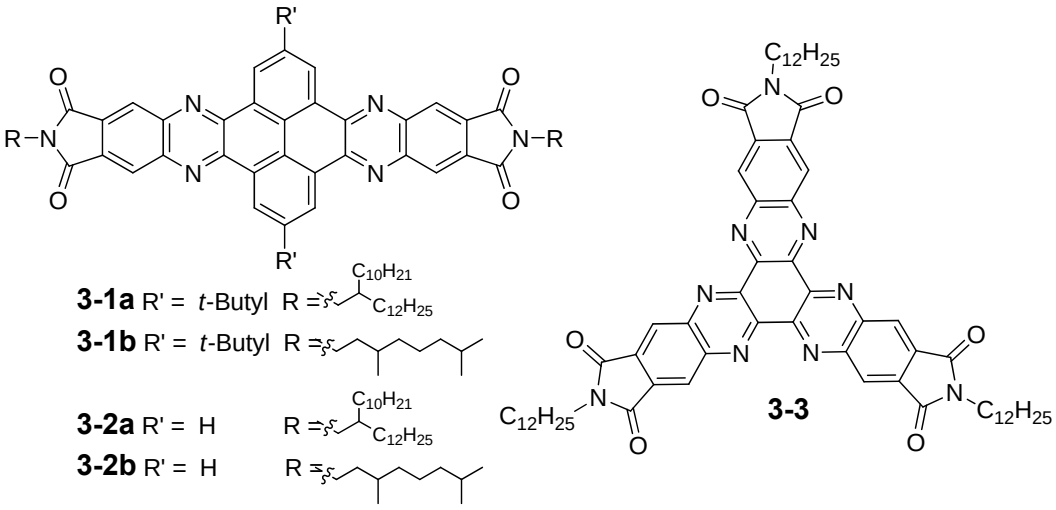

Figure 3.1 Chemical structures of nitrogen-rich dibenzohexacene diimides (**3-1a**–**b**, **3-2a**–**b**) and trinaphthylene trisimide (**3-3**).

3.2 Results and Discussion

3.2.1 Synthesis

The synthesis of these electron-deficient compounds is shown in Scheme 3.1.

The formation of pyrazine rings is based on a condensation reaction between *o*-diamine and dione. The key intermediate compounds are the 1,2-diamino-4,5-phthalimides **3-12a**–**c** with different alkyl chains which have never been reported previously. The synthesis started from the protection of *o*-phenylenediamine **3-4** with *p*-toluenesulfonyl chloride (TsCl) in dry pyridine to afford **3-5** in 93% yield. Bromination of **3-5** with Br_2 in HOAc gave compound **3-6** in 89% yield, and subsequent deprotection was conducted by heating **3-6** in 95% sulfuric acid at 110 °C for about 15 min to give the diamine **3-7** in 95% yield. Prolongation of the reaction time to 2 h as reported in the literature[12] led to an unknown black solid without **3-7** at all. The diamine **3-7** was reacted with $SOCl_2$–Et_3N in DCM to give 5,6-dibromobenzo[*c*][1,2,5]thiadiazole **3-8** in 96% yield, which was refluxed with CuCN-CuI in nitrobenzene for 6 h, followed by treatment with $FeCl_3$ in HCl solution to give compounds **3-9** and **3-10** in 60% and 10% yield, respectively.[13] **3-9** could be hydrolyzed under acid conditions ($FeCl_3$–HCl) to give **3-10** in 28% yield. Alkylation of **3-10** with 1-bromo-3,7-dimethyloctane, 11-(bromomethyl)tricosane,[14] and 1-bromododecane in the presence of K_2CO_3 afforded compounds **3-11a**, **3-11b**, and **3-11c** in 90%, 88%, and 90% yield, respectively.[15] In addition, **3-11** can also be prepared by treating **3-9** with the corresponding alkyl amine in *o*-DCB catalyzed by $ZnBr_2$ in around 50% yield. Reduction of **3-11** was first attempted by using reducing agents such as $NaBH_4$, Zn powder[16] and tin powder, however, all

attempts failed to give the desired diamine **3-12**. Alternatively, a mild reductant, Fe powder, turned out to be an appropriate reductant and the diamines **3-12a–c** were prepared in 90–93% yields from **3-11a–c**. Interestingly, all these diamine compounds show good environmental stability in contrast to many other electron-rich diamines.

Scheme 3.1 Synthetic scheme for **3-1a**–**b**, **3-2a**–**b**, and **3-3**.

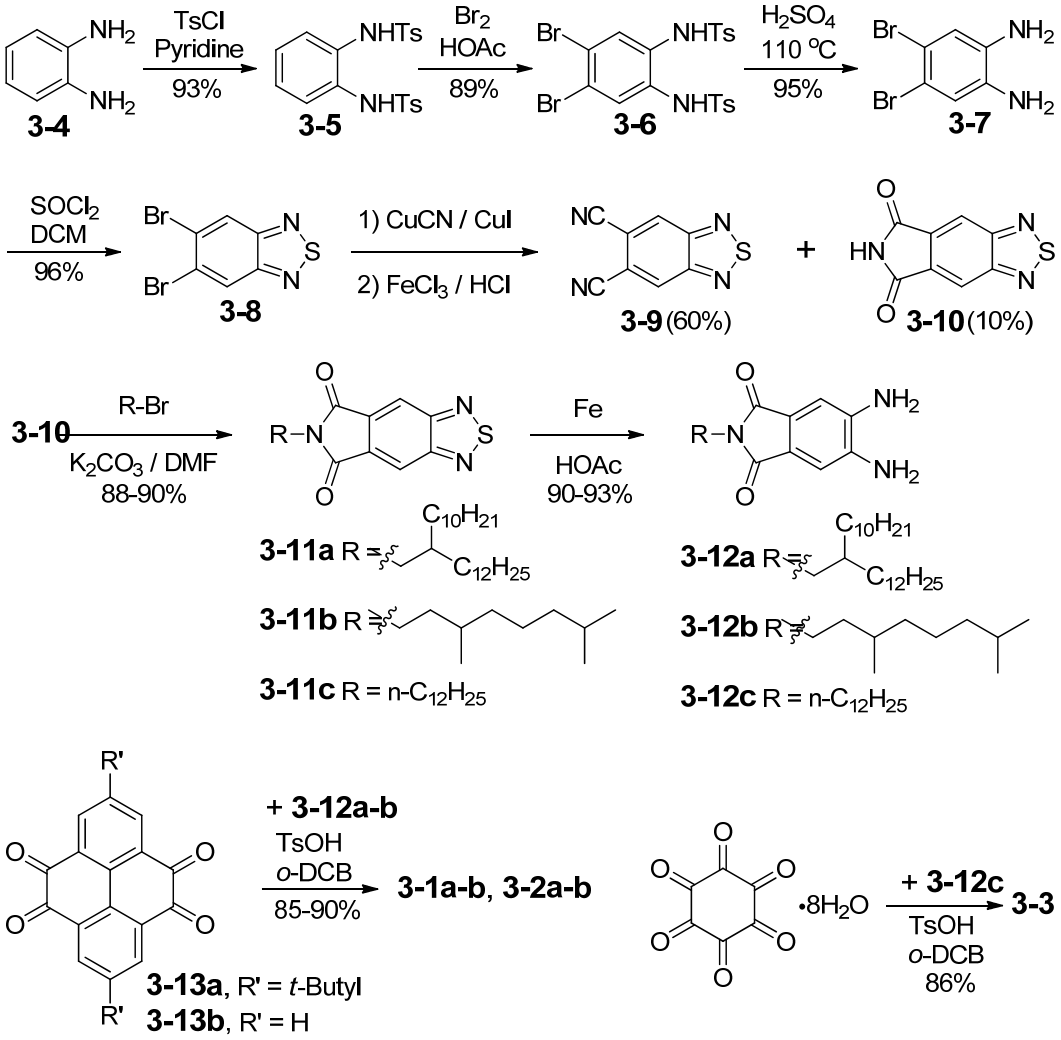

The linear compounds **3-1a** and **3-1b** were then synthesized in 85% and 90% yield, respectively, by a condensation reaction between 2,7-di-*tert*-butylpyrene-4,5,9,10-tetraone (**3-13a**)[17] and 2.2 equivalents of **3-12a–b** in refluxing *o*-DCB in the presence of a catalytic amount of TsOH. Similarly, compounds **3-2a**–**b** were prepared under the same conditions from compounds **3-13b** and **3-12a**–**b** in 85% and 90% yield, respectively. The *tert*-butyl group was supposed to facilitate the solubility of **3-1a**–**b**,[18] however, to our surprise, **3-2a** (**3-2b**) have better solubility than **3-1a** (**3-1b**). Condensation between **3-13a**–**b** and **3-12c** gave insoluble materials. The star-shaped hexaaza-trinaphthylene trisimide **3-3** was prepared in 86% yield by a similar condensation reaction between hexaketocyclohexane octahydrate and 3.3 equivalents of **3-12c**. Compound **3-3** showed excellent solubility, such as in DCM, THF, and even in hexane, which allows us to perform various characterizations in solution. ^{1}H NMR, ^{13}C NMR spectroscopy, mass spectrometry (HR-EI MS and MALDI-TOF MS), and elemental analysis were used to identify the chemical structure and purity of all the new compounds.

3.2.2 Photophysical Properties

The UV-vis absorption and photoluminescence (PL) spectra of compounds **3-1a–b**, **3-2a–b**, and **3-3** were recorded in THF solution. It was found that the alkyl chains had almost no effect on the spectra profiles (Figure 3.2). All of the

these compounds show well-resolved UV-vis absorption and emission bands, with the longest absorption maximum at 431, 431, 429, 429 and 399 nm and the emission maxima at 457, 457, 447, 447 and 504 nm for **3-1a**, **3-1b**, **3-2a**, **3-2b**, and **3-3**, respectively (Table 3.1). The absorption spectra of **3-1 – 3-3** in thin film showed a similar profile to that in solution but with a 12–16 nm red-shift and accompanied with a long tail to the near infrared region, indicating strong intermolecular interactions in the solid state (Figure 3.3).

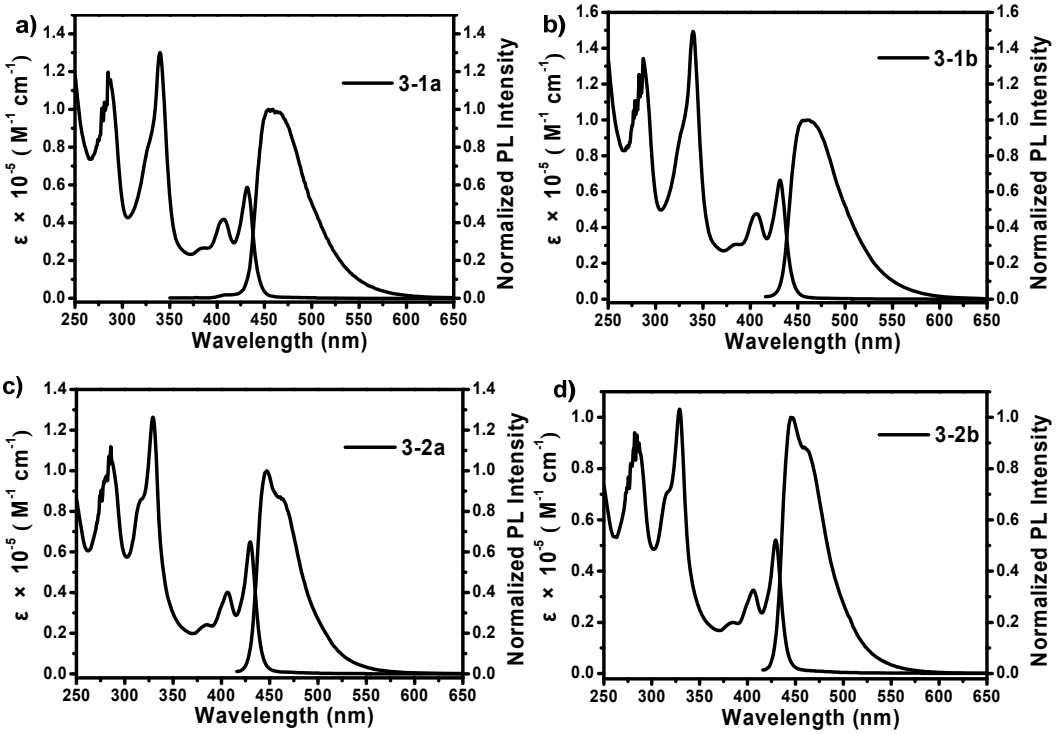

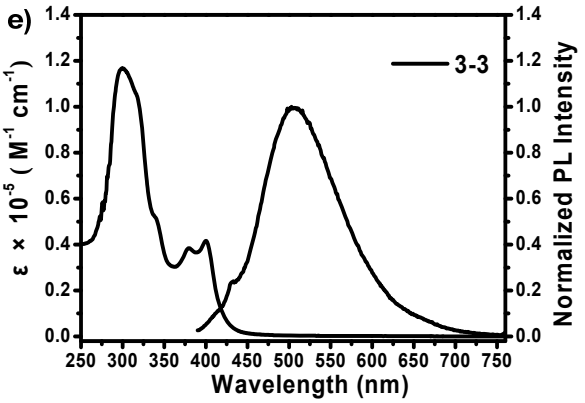

Figure 3.2 Normalized absorption spectra and emission spectra of compounds **3-1a**–**b**, **3-2a**–**b** and **3-3** in THF. The emission spectra of **3-1a**–**b**, **3-2a**–**b** and **3-3** were recorded under the excitation wavelength of 340, 406, 406, 406 and 380 nm, respectively.

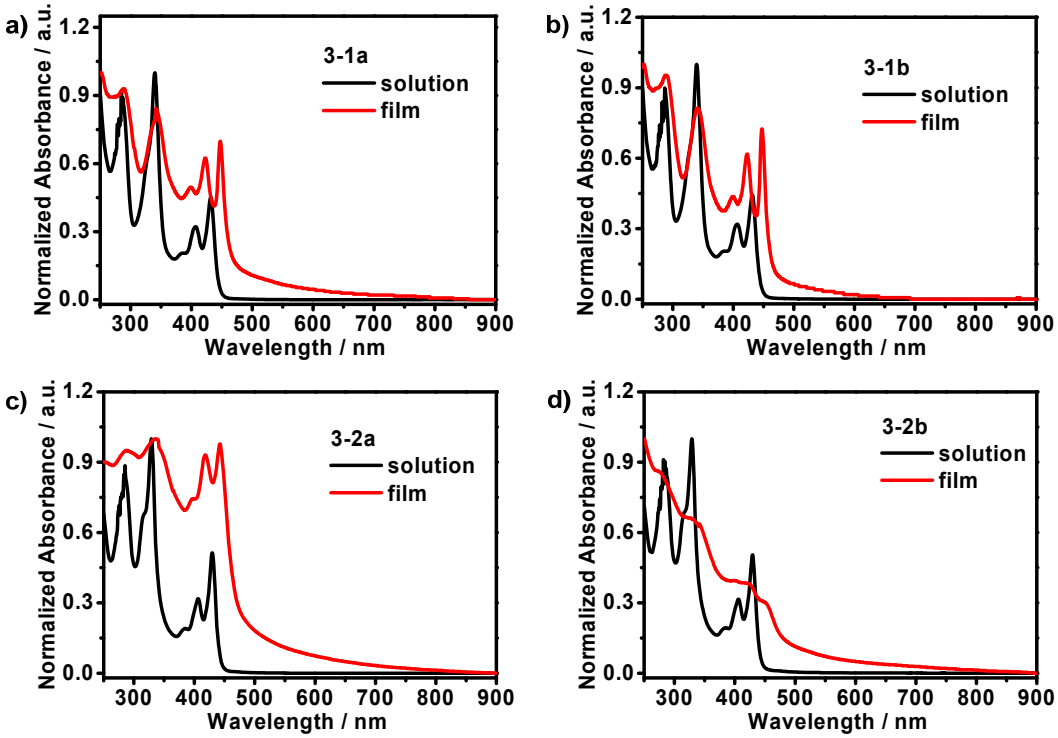

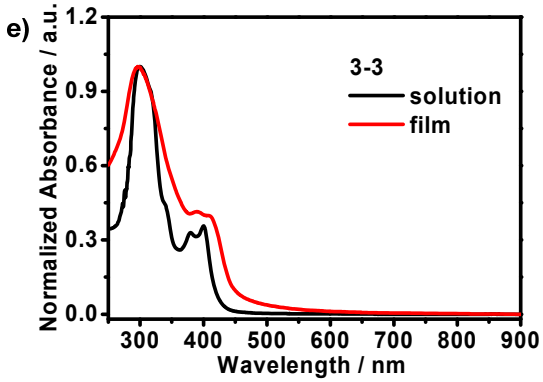

Figure 3.3 Normalized absorption spectra in THF solution and solid film (spin-coated from $CHCl_3$ solution) for compounds **3-1a**–**b**, **3-2a**–**b**, and **3-3**

Table 3.1 UV-vis and PL data for compounds **3-1a**–**b**, **3-2a**–**b**, and **3-3**

	Solution			Film
	λ_{abs} / nm	ε_{max} / M^{-1} cm^{-1}	λ_{PL} / nm	λ_{abs} / nm
3-1a	431	5800	457	447
3-1b	431	6500	457	447
3-2a	429	6400	447	442
3-2b	429	5200	447	443
3-3	399	4100	504	411

3.2.3 Electrochemical Properties

The electrochemical properties of **3-1a–b**, **3-2a–b** and **3-3** were investigated by cyclic voltammetry (CV) and differential pulse voltammetry (DPV) in DCM solution. As shown in Figure 3.4, three quasi-reversible reduction waves were observed for **3-1a**–**b**, **3-2a**–**b**, and **3-3**, with the onset reduction potential (E_{red}^{onset})

at -1.37, -1.36, -1.31, -1.30 and -0.79 V, respectively (Table 3.2). Again, the different alkyl chains and *tert*-butyl group have shown little effect on the redox behavior. No obvious redox waves were observed upon oxidation up to 1.80 V. The LUMO energy level (electron-affinity) derived from the onset of reduction potential is -3.43, -3.44, -3.49, -3.50 and -4.01 eV for **3-1a**–**b**, **3-2a**–**b**, and **3-3**, respectively.[19] Accordingly, the respective HOMO energy levels are deducted as -6.22, -6.23, -6.29, -6.31 and -6.96 eV for **3-1a**–**b**, **3-2a**–**b**, and **3-3**, respectively, based on the equation HOMO = LUMO - E_g^{opt}, where E_g^{opt} is the optical energy gap determined from the lowest energy absorption onset. Compared with the trinaphthylene tris(dicarboximide)s,[9] after the introduction of six N atoms, the LUMO energy level of **3-3** was lowered by 0.33 eV from -3.68 eV to -4.01 eV. The electron affinities of **3-1a**–**b** and **3-2a**–**b** are also increased to ca. 0.20 eV compared to their analogs without dicarboximide substituents.[11c] The low-lying LUMO energy level (i.e., large electron affinity) of all compounds indicates that they can serve as promising candidates for n-type devices with good air stability.[8,20]

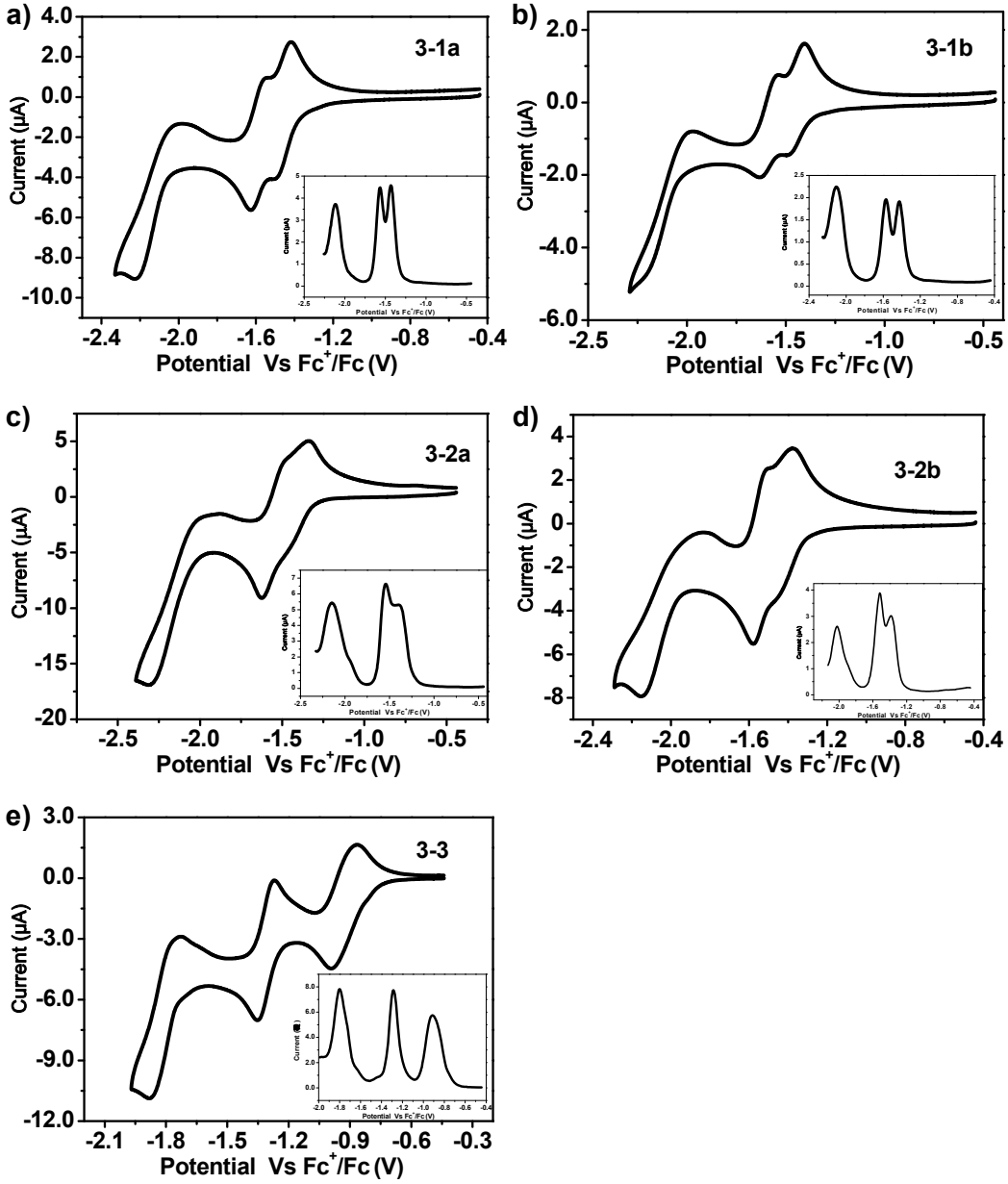

Figure 3.4 Cyclic voltammetry (CV) and differential pulse voltammetry (DPV) curves (inset) for compounds **3-1a**–**b**, **3-2a**–**b**, and **3-3** in DCM with 0.1 M Bu_4NPF_6 as supporting electrolyte, a gold electrode with a diameter of 2 mm, a Pt wire, and an Ag/AgCl electrode were used as the working electrode, the counter electrode, and the reference electrode, respectively, with a scan rate at 100 mV/s.

Table 3.2 Cyclic voltammetry data for compounds **3-1a**–**b**, **3-2a**–**b**, and **3-3**

Cpd	$E_{1/2}^{red(1)}$	$E_{1/2}^{red(2)}$	$E_{1/2}^{red(3)}$	E_{red}^{onset}	E_g [a]	HOMO[b]	LUMO[c]

	/ V	/ V	/ V	/ V	/ V	/ eV	/ eV
3-1a	-1.43	-1.56	-2.12	-1.37	2.79	-6.22	-3.43
3-1b	-1.42	-1.57	-2.10	-1.36	2.79	-6.23	-3.44
3-2a	-1.38	-1.54	-2.15	-1.31	2.80	-6.29	-3.49
3-2b	-1.39	-1.52	-2.03	-1.30	2.81	-6.31	-3.50
3-3	-0.91	-1.29	-1.80	-0.79	2.95	-6.96	-4.01

[a] E_g was estimated from the absorption edge in solution; [b] LUMO was calculated according to the equation, LUMO = – (4.80 + E_{red}^{onset}); [c] HOMO was estimated according to the equation, HOMO = E_g – LUMO.

3.2.4 Thermal Properties

The thermal behavior and self-assembly of **3-1a**–**b**, **3-2a**–**b**, and **3-3** in the solid state were investigated by thermogravimetric analysis (TGA), differential scanning calorimetry (DSC), polarizing optical microscopy (POM) and X-ray diffraction (XRD). TGA measurements revealed that all compounds were thermally stable over 390 °C with 5% weight loss (see Figure 3.5). DSC curves of **3-1a**, **3-1b** and **3-2b** showed one endothermic transition from the crystalline phase to an isotropic phase (Figure 3.6), which was confirmed by POM measurements (Figure 3.7). The detailed packing structure at room temperature can not be simply concluded from their powder XRD patterns (Figure 3.8). DSC curves of **3-2a** exhibited three endothermic transitions at 127, 154 and 167 °C upon heating and three exothermic transitions at 165, 134 and 103 °C upon cooling (Figure 3.6).

POM measurements disclosed that the compound entered an isotropic phase at around 170 °C. Upon slow cooling, a typical fan-type texture was observed at 160 °C (Figure 3.7), indicating an ordered columnar liquid crystalline phase. Upon further cooling below 135 °C, some defects were observed in the fan-type texture, corresponding to the second exothermic transition. Upon further cooling below 103 °C, crystalline domains were observed. The XRD pattern of **3-2a** recorded at room temperature (Figure 3.8) revealed that **3-2a** has an orthorhombic arrangement with lattice parameter a = 2.68 nm, b = 1.05 nm and γ = 90°. However, the broad reflection peaks in the XRD patterns recorded at 160 °C and 130 °C (Figure 3.9) limited detailed analysis of the mesophases. Compound **3-3** entered into a columnar liquid crystalline phase after 317 °C as demonstrated by the bright focal conic texture recorded at 345 °C upon heating (Figure 3.7). XRD pattern of **3-3** at room temperature showed only one major reflection peak at 2θ = 2.943° and thus the accurate packing structure cannot be figured out.

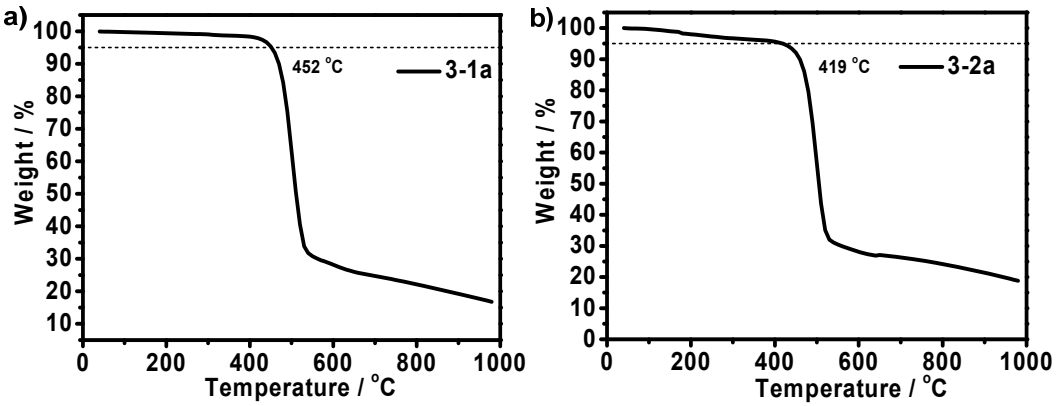

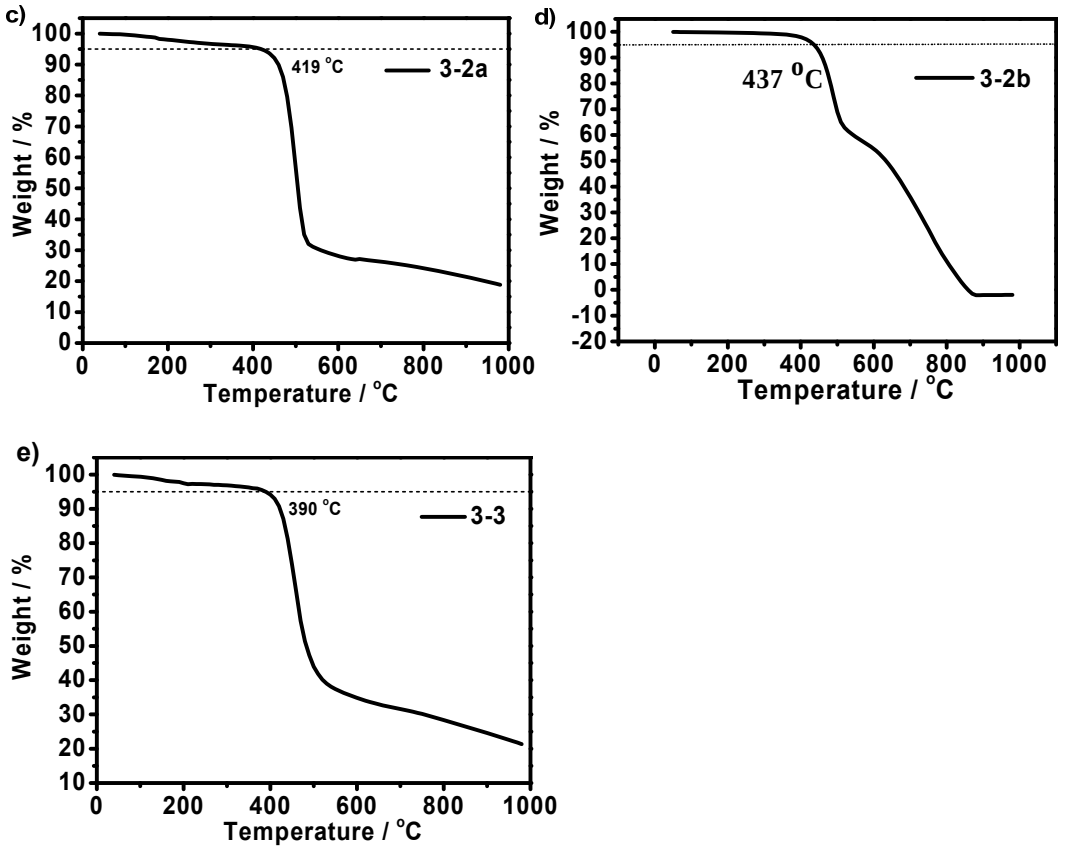

Figure 3.5 Thermogravimetric analysis (TGA) curves for compounds **3-1a**–**b**, **3-2a**–**b**, and **3-3** with a heating rate of 10 °C/min under nitrogen.

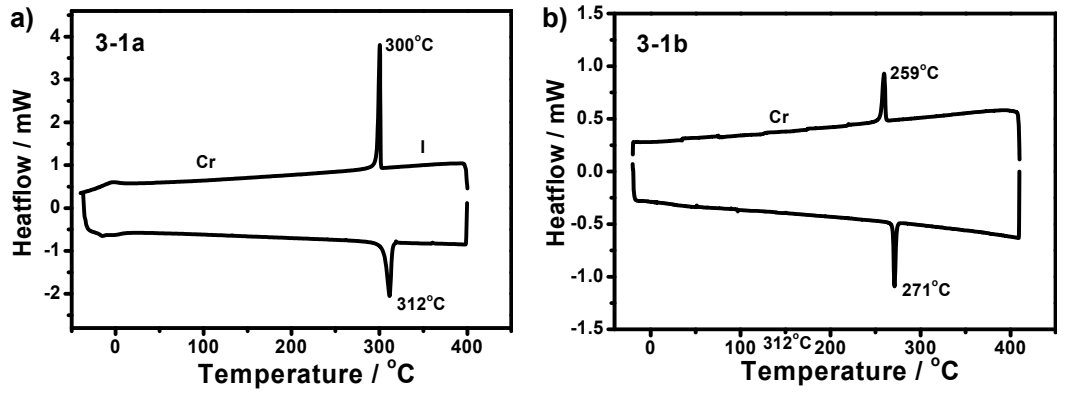

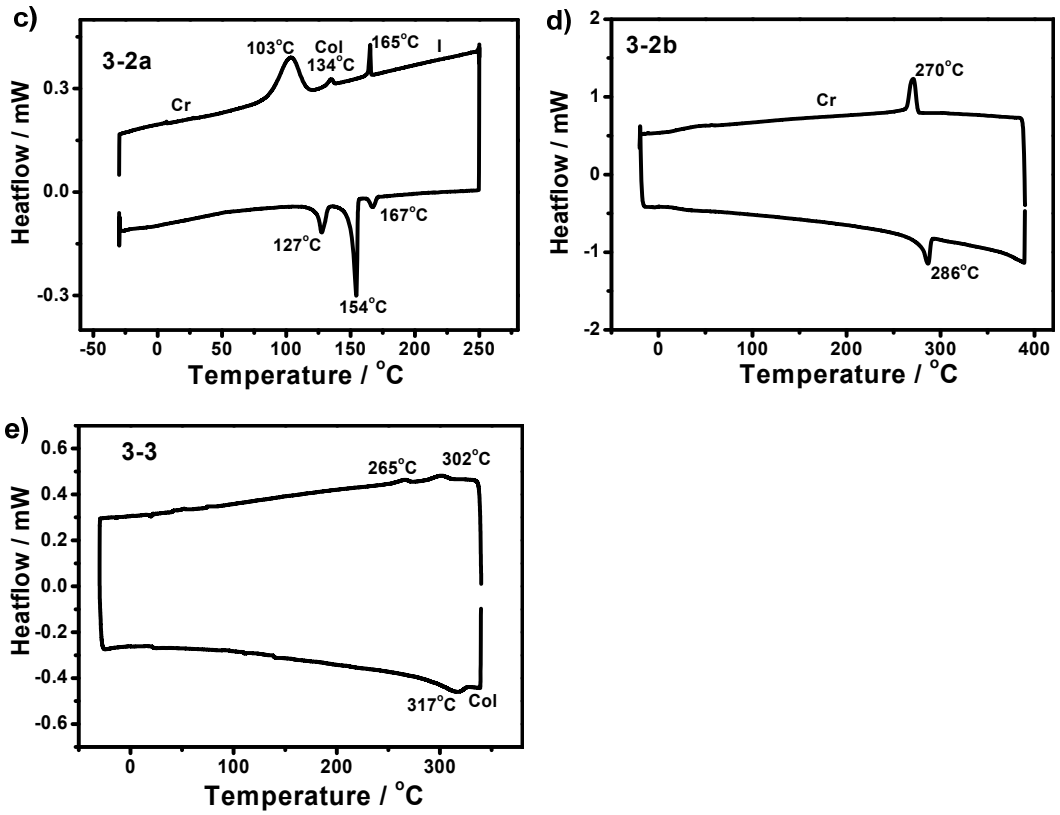

Figure 3.6 DSC curves for compounds **3-1a**–**b**, **3-2a**–**b**, and **3-3** with a heating/cooling scan rate of 10 °C/min under nitrogen. (Cr = crystalline phase, I = isotropic phase, Col = columnar crystalline phase)

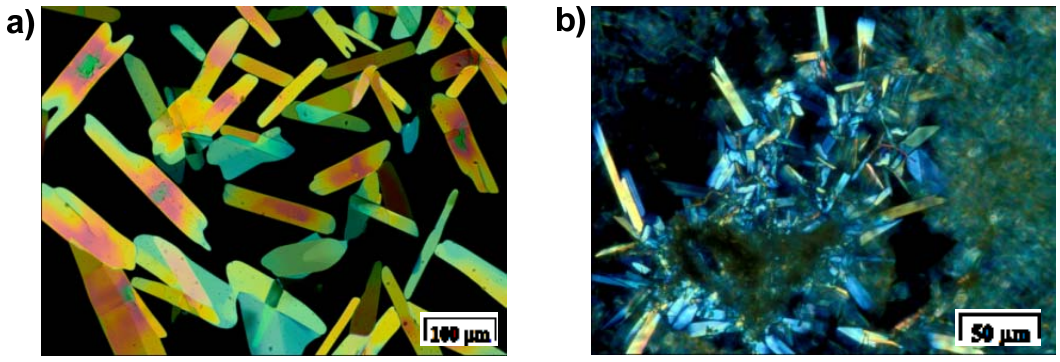

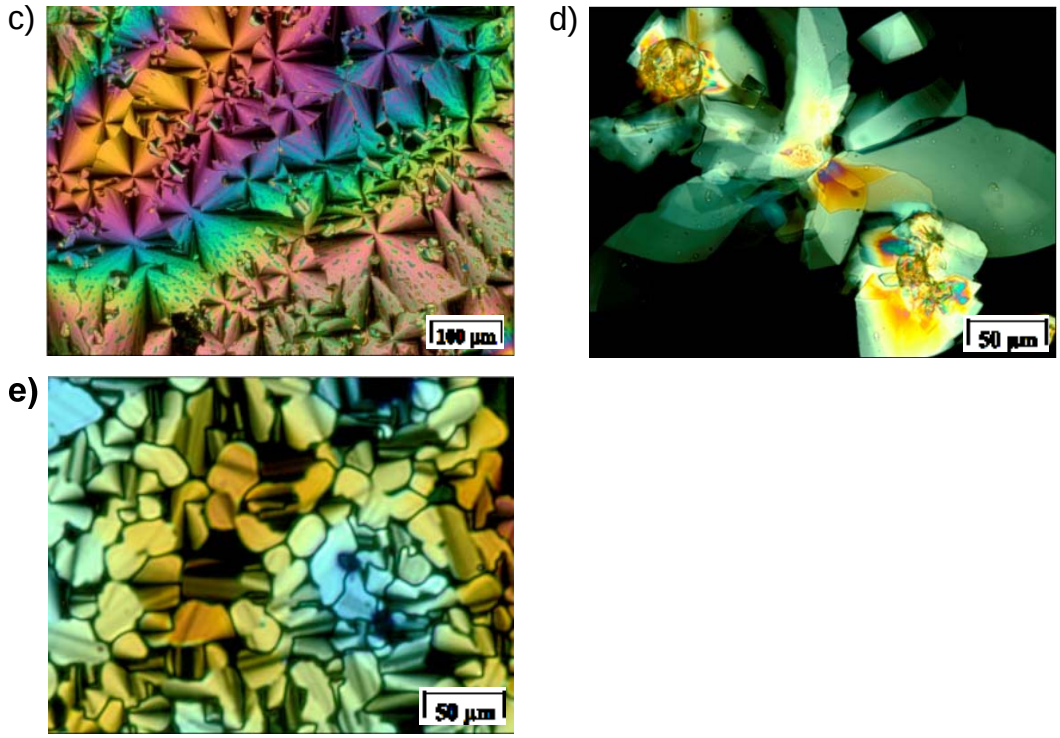

Figure 3.7 POM images for **3-1a**–**b**, **3-2a**–**b** and **3-3**. a) **3-1a**, upon slow cooling at 250 °C; b) **3-1b**, upon slow cooling at 260 °C; c) **3-2a** at 160 °C upon cooling; d) **3-2b**, upon slow cooling at 315 °C; and e) **3-3** at 345 °C upon heating.

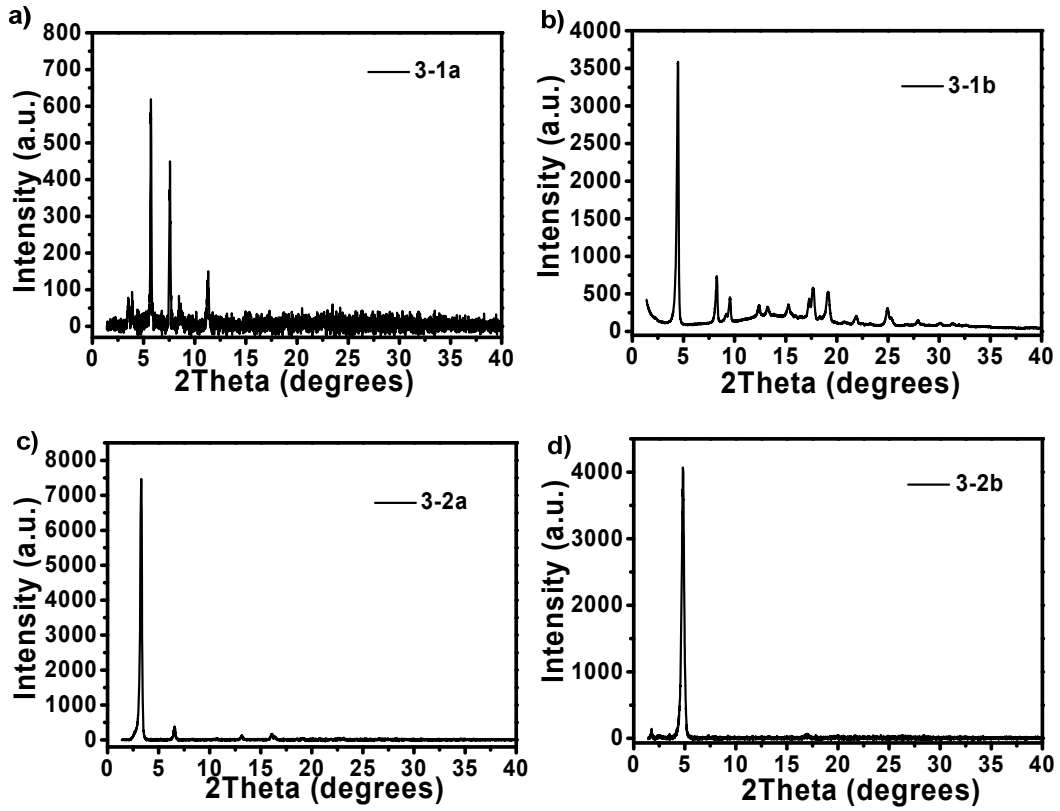

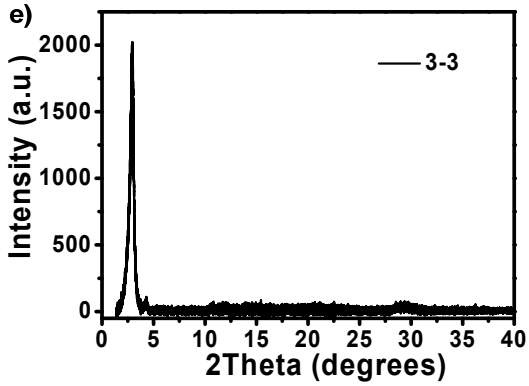

Figure 3.8 Powder XRD patterns for **3-1a**–**b, 3-2a**–**b,** and **3-3**

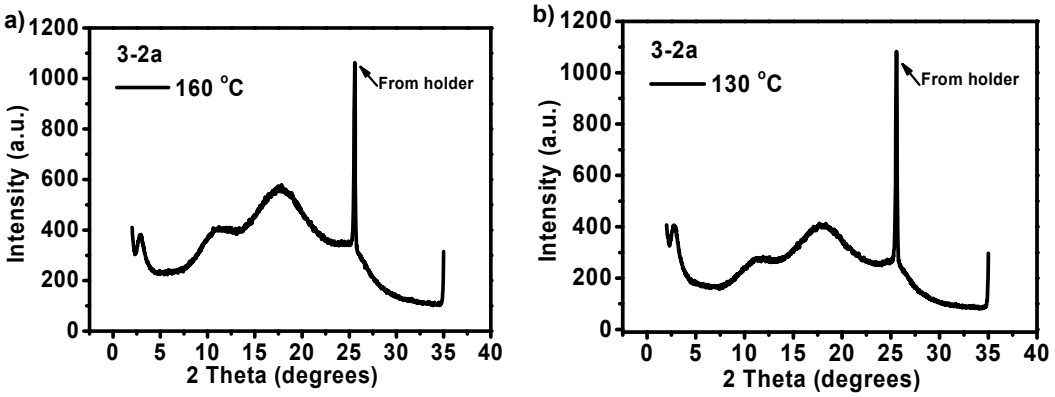

Figure 3.9 Variable-Temperature Powder XRD (VT-XRD) patterns for **3-2a** at 160 ^{o}C and 130 ^{o}C.

3.2.5 Space-Charge Limited-Current (SCLC) Mobility

Charge carrier mobilities of **3-1a-b**, **3-2a-b**, and **3-3** in thin films were estimated via space-charge limited-current (SCLC) technique by using a diode device configuration of ITO–PEDOT:PSS–Al(2 nm)–material–Al. The SCLC is described by $J = 9/8\varepsilon_0\varepsilon_r\mu V^2/ d^3$, where ε_0 is the permittivity of free space, ε_r is the relative dielectric constant of the active material estimated from capacitance measurements (assumed to be 3), d is the film thickness, μ is electron mobility, V

is the voltage drop across the device, $V = V_{appl} - V_r - V_{bi}$, V_{appl} is the applied voltage to the device, V_r is the voltage drop due to contact resistance and series resistance across the electrodes, V_{bi} is the built-in voltage due to the difference in work function of the two electrodes. The resistance of the device was measured using a blank configuration ITO– PEDOT–Al and was found to be about 10–20 Ω. The V_{bi} was determined from the transition between the ohmic region and SCL region and is found to be about 1 V. The film thickness was measured by surface profilometer. The fabricated device was tested in a nitrogen filled glovebox and dark conditions. The current density–voltage (*J*–V) curves were measured using a Keithley 2400 source measurement unit. The SCLC electron mobilities were found to be 3-7 × 10^{-4} cm^2 V^{-1} s^{-1} for **3-1a**–**b**, **3-2a**–**b**, and 3.4 × 10^{-5} cm^2 V^{-1} s^{-1} for **3-3** (Figure 3.10). Unfortunately, our preliminary results show that solution processed thin films of all these compounds only show very weak field effect transistor activity which was also observed for other imine nitrogen-containing semiconductors.[8]

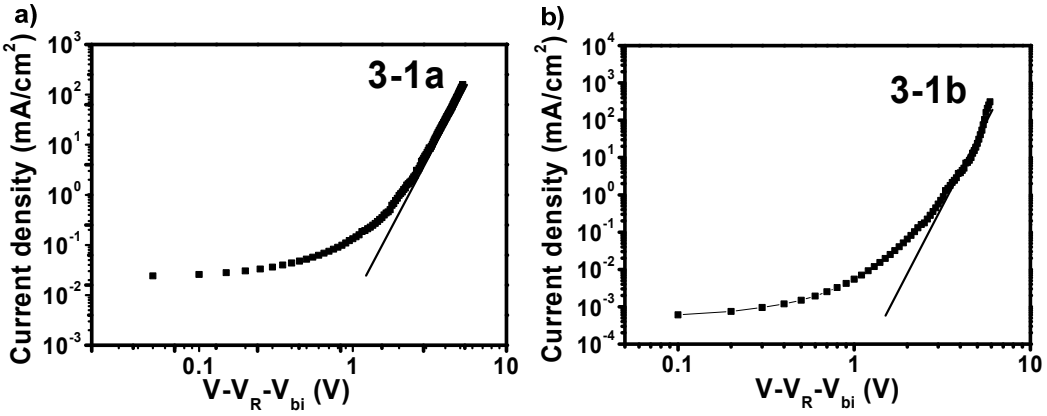

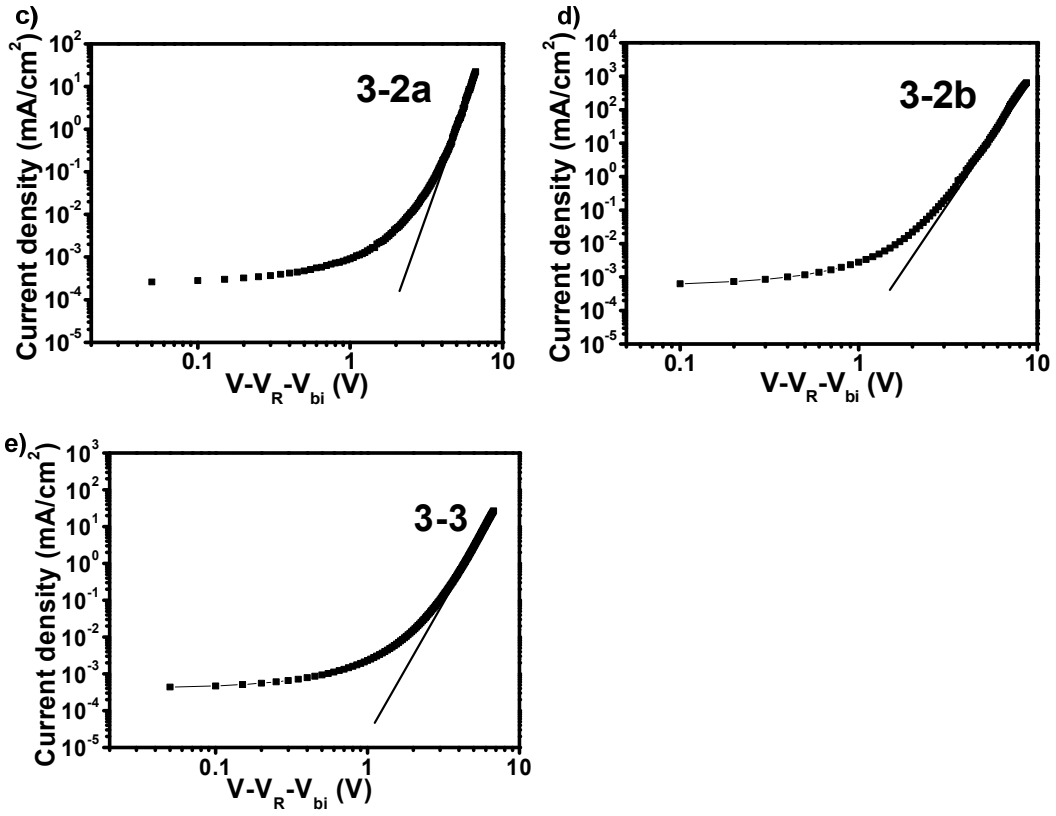

Figure 3.10 Double logarithmic plot of the current density (*J*) versus applied voltage (*V*) curves for **3-1a**–**b**, **3-2a**–**b**, and **3-3**

3.3 Conclusions

In summary, a series of electron-deficient pyrazine-containing linear and star-shaped acene and starphene molecules end functionalized with dicarboximide groups have been successfully synthesized, and their optical properties, electrochemical properties and thermal behavior were investigated. Due to the attachment of electron-withdrawing carboximide groups and the fusion of pyrazine rings, these new compounds showed high electron affinities. Moderate electron mobilities in thin films were also measured via the SCLC technique. The observed high electron affinity of these molecules suggests that they can be used

as potential electron transporting materials in organic electronic devices.

3.4 Experimental

3.4.1 General

Anhydrous tetrahydrofuran (THF) and dichloromethane (DCM) were obtained by distillation over sodium and calcium hydride, respectively. 2,7-Di-*tert*-butylpyrene-4,5,9,10-tetraone,[17] pyrene- 4,5,9,10-tetraone,[17] and 11-(bromomethyl)-tricosane[14] were prepared according to the literature procedures. All other chemicals were purchased from commercial supplies and used without further purification.

All NMR spectra were recorded on Bruker AMX500 at 500 MHz and Bruker ACF300 at 300 MHz spectrometers. ^{1}H NMR and ^{13}C NMR spectra were recorded in $CDCl_3$ and DMSO-d^6. All chemical shifts are quoted in ppm, using the residual solvent peak as a reference standard. Mass spectra were recorded in EI mode and high resolution mass spectra were recorded with EI source. Matrix-assisted laser desorption ionization time-of-flight (MALDI-TOF) analysis was performed on a Bruker Autoflex II MALDI-TOF instrument by using 1,8,9-trihydroxyanthracene as matrix and Pepmix as internal standard or external standard. UV-vis absorption and fluorescence spectra were recorded on Shimadzu UV-1700 and RF-5301 spectrometers in HPLC pure solvents. Cyclic voltammetry was performed on a CHI 620C electrochemical analyzer with a three-electrode

cell in a solution of 0.1 M tetrabutylammonium hexafluorophosphate (Bu_4NPF_6) dissolved in dry DCM at a scan rate of 100 mV s^{-1}. A gold electrode with a diameter of 2 mm, a Pt wire and an Ag/AgCl electrode were used as the working electrode, the counter electrode and the reference electrode, respectively. The potential was calibrated against the ferrocene/ferrocenium couple. Thermogravimetric analysis was carried out on a TA instrument 2960 at a heating rate of 10 °C min^{-1} under N_2 flow, differential scanning calorimetry was performed on a TA instrument 2920 at a heating–cooling rate of 10 °C min^{-1} under N_2 flow. The initial phase transitions and corresponding temperatures for these compounds were determined by an OLYMPUS BX51 polarizing optical microscope equipped with a Linkam TP94 programmable hot stage. VT X-ray diffraction studies were carried out on a Bruker-AXS D8 ADVANCE Powder X-ray diffractometer with Anton Paar Model HTK 1200 High Temperature Chamber and room temperature XRD measurements were performed on a Bruker-AXS D8 DISCOVER with GADDS Powder X-ray diffractometer, both with Cu Kα radiation.

3.4.2 Detailed Synthetic Procedures and Characterization Data

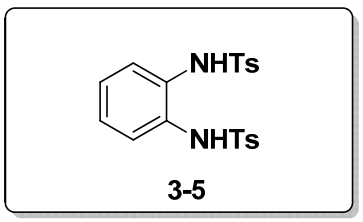

3-5

N,N'-(1,2-phenylene)bis(4-methylbenzenesulfonamide)

o-phenylenediamine (540 mmol, 58.5 g) was added slowly to a solution of *p*-toluenesulfonyl chloride (2 eq, 1.080 mol, 205.9 g) in dry pyridine (500 mL) which was cooled to -10 ^{o}C in a NaCl/ice bath. The resulted mixture was stirred at room temperature for 18 h. By slow addition of 15% aqueous HCl, a precipitate was formed. The solid were dissolved in EtOH (1400 mL) and refluxed for 1 h, and then stored in a refrigerator overnight for crystallization. After filtration, compound **3-5** was obtained as a faint solid (210.2 g, 93%). ^{1}H NMR (500 MHz, $CDCl_3$): δ ppm = 7.57 (d, *J* = 8.2 Hz, 4 H), 7.22 (d, *J* = 8.2 Hz, 4 H), 7.04 - 7.01 (m, 2 H), 6.98 – 6.94 (m, 2 H), 6.91 (br, 2 H), 2.39 (s, 6 H); ^{13}C NMR (125 MHz, $CDCl_3$): δ ppm = 144.15, 135.46, 130.76, 129.60, 127.53, 127.23, 125.96, 21.57. HR-EI-MS (m/z): calcd. for $C_{20}H_{20}N_2O_4S_2$: 416.0864; found 416.0860 (error = -1.0 ppm).

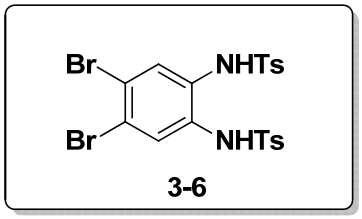

3-6

N,N'-(4,5-dibromo-1,2-phenylene)bis(4-methylbenzenesulfonamide)

Bromine (19.2 g, 0.180 mol) was added drop-wise to an ice-cooled and stirred suspension of **3-5** (37.5 g, 0.090 mol) and anhydrous NaOAc (15.0 g*)* in glacial acetic acid (150 mL). The mixture was stirred and heated at 110 ^{o}C for 3 hr., then

cooled and poured into ice water (400 mL), and then stirred for additional 1hr, and EtOH (200 mL) was added. After filtration, the precipitate gave fine colorless powder of **3-6** (45.990 g, 89%). ^{1}H NMR (500 MHz, $CDCl_3$): δ ppm = 7.60 (d, *J* = 8.2 Hz, 4 H), 7.28 (d, *J* = 8.2 Hz, 4 H), 7.20 (s, 2 H), 6.75 (br, 2 H), 2.42 (s, 6 H). ^{13}C NMR (125 MHz, $CDCl_3$): δ ppm = 144.83, 135.34, 130.89, 130.09, 129.92, 127.64, 122.59, 21.55. HR-EI-MS (m/z): calcd. for $C_{20}H_{18}Br_2N_2O_4S_2$: 571.9075; found 571.9055. (error = -3.5 ppm).

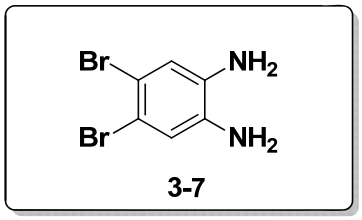

3-7

4,5-dibromobenzene-1,2-diamine

The preceding **3-6** (45.2 g, 78.7 mmol) was heated in concentrated sulphuric acid (90.0 mL) at 110 °C for about 15 min. After cooling to room temperature, the reaction mixture was poured into ice-water and neutralized with 50% NaOH solution until the color of the solution is off-white and lots of precipitate was formed. After filtration, the precipitate gave off-white powder of **3-7** (19.3 g, 95%). ^{1}H NMR (500 MHz, $CDCl_3$): δ ppm = 6.92 (s, 2 H), 3.40 (br, 4 H). ^{13}C NMR (125 MHz, $CDCl_3$): δ ppm = 135.47, 120.65, 113.62. HR-EI-MS (m/z): calcd. for $C_6H_6Br_2N_2$: 263.8898; found 263.8893 (error = -1.9 ppm).

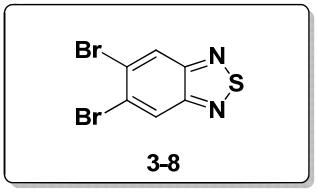

3-8

5,6-dibromobenzo[*c*][1,2,5]thiadiazole

To a solution of **3-7** (5.32 g, 20.0 mmol) and Et_3N (4.15 eq, 12 mL, 83 mmol) in dry DCM (60 mL) was added, in an ice-cooled condition, a solution of thionyl chloride (2.55 eq, 3.80 mL, 51 mmol) in DCM (10 mL). After addition was complete, the reaction mixture was stirred for 5 hr under reflux. After cooling to room temperature, the reaction mixture was filtered, the filtrate was collected while discarding the solid residue, and the solvent was removed under vacuum and purified with column chromatography using pure DCM as the eluent to give product **3-8** as a pink-white solid (5.645 g, 96%). ^{1}H NMR (300 MHz, $CDCl_3$): δ ppm = 8.38 (s, 2 H). ^{13}C NMR (125 MHz, $CDCl_3$): δ ppm = 153.82, 127.14, 124.90. EI-MS (m/z): calcd. for $C_6H_2Br_2N_2S$: 291.8305; found 291.8305 (error = 0 ppm).

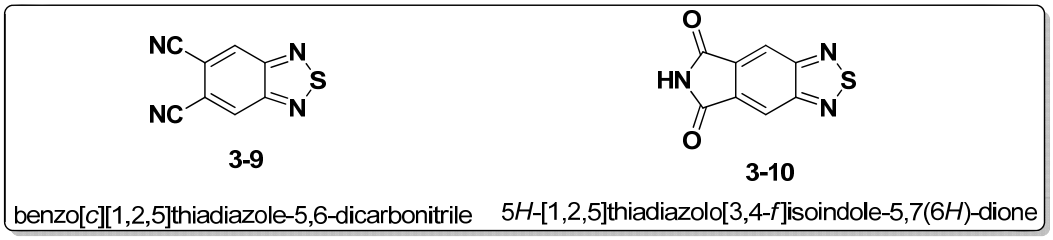

3-9 benzo[*c*][1,2,5]thiadiazole-5,6-dicarbonitrile

3-10 5*H*-[1,2,5]thiadiazolo[3,4-*f*]isoindole-5,7(6*H*)-dione

A mixture of nitrobenzene (40 mL) and dry DMF (120 mL) was added to a stirred mixture of **3-8** (5.88 g, 20.0 mmol), CuCN (4.1 eq, 82.0 mmol, 7.30 g) and CuI (1.36 g, 7.2 mmol). The mixture was stirred under reflux condition for 6 hr,

cooled and poured into a mixture of hydrated $FeCl_3$ (6.8 g), 37% HCl (1.7 mL) and water (10 mL). The suspension was heated at 70°C for 1h, and then removed the solvent under vacuum; the residue was dissolved with DCM and water, and extracted with DCM (100 mL). The combined organic phases were washed with HCl (6 M, 200 mL), saturated NaCl (200 mL), and saturated $NaHCO_3$ (200 mL), and was finally dried over Na_2SO_4, concentrated under reduced pressure to give a black residue and purified with column chromatography using eluent hexane/EA (5:1) to give **3-9** as a light yellow solid (2.234 g, 60%), and then THF/MeOH (1:1) to give **3-10** as a white solid (0.410 g, 10%).

Compound **3-9**: ^{1}H NMR (500 MHz, $CDCl_3$): δ ppm = 8.61 (s, 2 H); ^{13}C NMR (125 MHz, $CDCl_3$): δ ppm = 153.94, 129.81, 114.65, 113.88. HR-EI-MS (m/z): calcd. for $C_8H_2N_4S$: 186.0000; found 186.0008 (error = 4.3 ppm).

Compound **3-10**: ^{1}H NMR (300 MHz, DMSO-d^6): δ ppm = 11.88 (br, 1 H), 8.56 (s, 2 H); ^{13}C NMR (125 MHz, DMSO-d^6): δ ppm = 167.52, 156.16, 132.77, 117.42. HR-EI-MS (m/z): calcd. for $C_8H_3N_3O_2S$: 204.9946; found 204.9939 (error = -3.4 ppm).

General procedure for alkylation of compound 3-10

A mixture of **3-10** (8.0 mmol), K_2CO_3 (3.500 g, 24.0 mmol, 3.0 eq), and alkyl bromide (8.4 mmol, 1.05 eq) was heated under Ar(g) atmosphere to reflux in DMF (50 mL) for overnight. The reaction was stopped upon complete

consumption of the starting material **3-10** at which point the reaction was cooled and diluted with CH_2Cl_2 (100 mL) and washed with 10% aqueous HCl solution (100 mL × 2) and with saturated aqueous NaCl solution (100 mL × 2), dried over Na_2SO_4 and the solvent was removed under vacuum. The residue was purified by silica gel column chromatography using hexane/$CHCl_3$ (4:1~10:1) as the eluent to give the title compound **3-11a-c**.

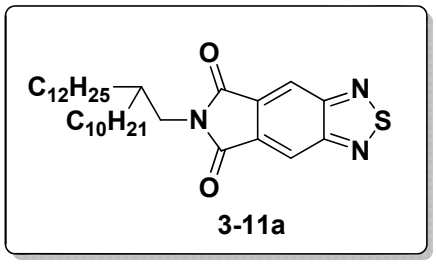

3-11a

6-(2-decyltetradecyl)-5H-[1,2,5]thiadiazolo[3,4-*f*]isoindole-5,7(6H)-dione

3-11a: Yield = 83%. White viscous oil. ^{1}H NMR (500 MHz, $CDCl_3$): δ ppm = 8.49 (s, 2 H), 3.67 (d, J = 7.0 Hz, 2 H), 1.94 (br, 1 H), 1.45 - 1.23 (m, 40 H), 0.89 – 0.86 (m, 6 H); ^{13}C NMR (125 MHz, $CDCl_3$): δ ppm = 166.61, 156.66, 131.54, 118.04, 43.07, 40.51, 36.87, 31.85, 31.84, 31.51, 30.92, 29.86, 29.63, 29.61, 29.56, 29.51, 29.29, 26.86, 26.22, 22.61, 14.01. HR-EI-MS (m/z): calcd. for $C_{32}H_{51}N_3O_2S$: 541.3702; found 541.3708 (error = 1.1 ppm).

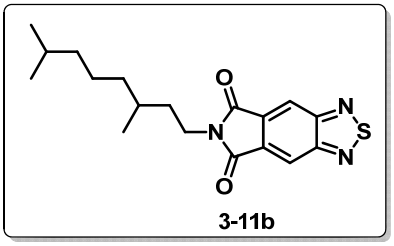

3-11b

6-(3,7-dimethyloctyl)-5H-[1,2,5]thiadiazolo[3,4-*f*]isoindole-5,7(6H)-dione

3-11b: Yield = 91%. White solid. ^{1}H NMR (500 MHz, $CDCl_3$): δ ppm = 8.49 (s, 2 H), 3.83 - 3.76 (m, 2 H), 1.78 - 1.73 (m, 1 H), 1.54 - 1.49 (m, 4 H), 1.36 - 1.13 (m, 5 H), 1.00 - 0.85 (m, 9 H); ^{13}C NMR (125 MHz, $CDCl_3$): δ ppm = 166.27, 156.60, 131.62, 117.97, 39.09, 37.11, 36.86, 35.17, 30.73, 27.81, 24.45, 22.56, 22.49, 19.30. HR-EI-MS (m/z): calcd. for $C_{18}H_{27}N_3O_2S$: 345.1511; found 345.1513 (error = 0.6 ppm)

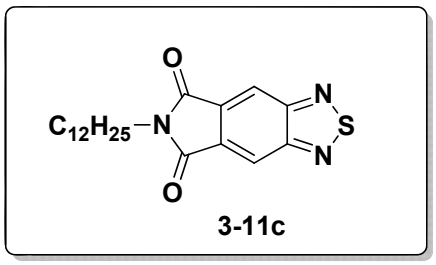

3-11c

6-dodecyl-5H-[1,2,5]thiadiazolo[3,4-*f*]isoindole-5,7(6H)-dione

3-11c: Yield = 90%. White solid. ^{1}H NMR (500 MHz, $CDCl_3$): δ ppm = 8.50 (s, 2 H), 3.78 (t, *J* = 7.3 Hz, 2 H), 1.76 - 1.70 (q, 2 H), 1.35 - 1.25 (m, 18 H), 0.87 (t, *J* = 7.0 Hz , 3 H); ^{13}C NMR (125 MHz, $CDCl_3$): δ ppm = 166.49, 156.71, 131.66, 118.15, 38.93, 31.87, 29.58, 29.51, 29.43, 29.29, 29.13, 28.33, 26.87, 22.64, 14.06. HR-EI-MS (*m/z)*: calcd. for $C_{20}H_{27}N_3O_2S$: 373.1824; found 373.1823 (error = -0.3 ppm)

General procedure for reduction of 3-11a-c to compound 3-12a-c

A mixture of **3-11** (2.0 mmol), ion powder (1.344 g, 24.0 mmol, 12 eq), and glacial acetic acid (20 mL) was heated under reflux for 15-30 min. It was then cooled to room temperature, basified with a solution of NaOH, and extracted with ether. The combined ether extract was washed with a solution of NaOH and water, dried over anhydrous Na_2SO_4, and the solvent was removed to afford a yellow residue and purified with column chromatography using Hex/THF (1:1~3:1) to give the final product **3-12a-c.**

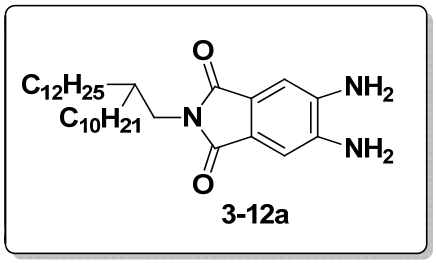

3-12a

5,6-diamino-2-(2-decyltetradecyl)isoindoline-1,3-dione

3-12a: Yield = 92%. Yellow powder. ^{1}H NMR (500 MHz, $CDCl_3$): δ ppm = 7.09 (s, 2 H), 3.83 (br, 4 H), 3.47 (d, *J* = 7.5 Hz, 2 H), 1.83 - 1.82 (br, 1 H), 1.33 - 1.23 (m, 40 H), 0.89 - 0.86 (m, 6 H); ^{13}C NMR (125 MHz, $CDCl_3$): δ ppm = 169.51, 139.40, 124.20, 109.98, 41.92, 37.06, 31.81, 31.42, 29.91, 29.59, 29.56, 29.53, 29.52, 29.24, 26.25, 22.57, 13.99. HR-EI-MS (m/z): calcd. for $C_{32}H_{55}N_3O_2$: 513.4294; found 513.4273 (error = 4.1 ppm)

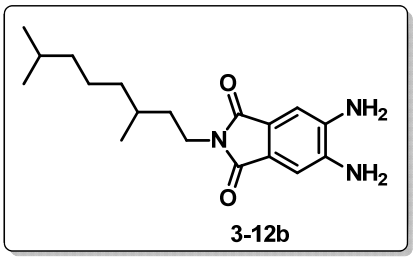

3-12b

5,6-diamino-2-(3,7-dimethyloctyl)isoindoline-1,3-dione

3-12b: Yield = 93%. Yellow powder. ^{1}H NMR (500 MHz, $CDCl_3$): δ ppm = 7.09 (s, 2 H), 3.83 (br, 4 H), 3.62 - 3.59 (m, 2 H), 1.68 - 1.61 (m, 1 H), 1.53 - 1.10 (m, 9 H), 0.94 (d, *J* = 6.3 Hz, 3 H), 0.84 (d, *J* = 6.9 Hz, 6 H); ^{13}C NMR (125 MHz, $CDCl_3$): δ ppm = 169.01, 139.29, 124.98, 110.26, 39.24, 37.06, 36.06, 35.70, 30.74, 27.91, 24.55, 22.64, 22.57, 19.40. HR-EI-MS (m/z): calcd. for $C_{18}H_{27}N_3O_2$: 317.2103; found 317.2102 (error = 0.3 ppm).

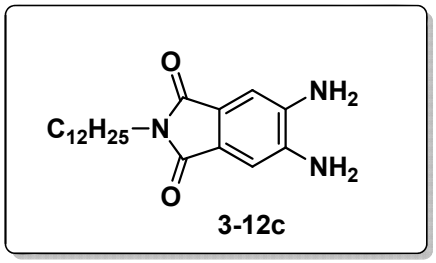

3-12c

5,6-diamino-2-dodecylisoindoline-1,3-dione

3-12c. Yield = 93%. Golden yellow powder. ^{1}H NMR (500 MHz, $CDCl_3$): δ ppm = 7.08 (s, 2 H), 3.83 (br, 4 H), 3.57 (t, *J* = 7.5 Hz, 2 H), 1.63 - 1.60 (q, 2 H), 1.30 - 1.24 (m, 18 H), 0.87 (t, *J* = 7.5 Hz , 3 H); ^{13}C NMR (125 MHz, $CDCl_3$): δ ppm = 169.09, 139.30, 124.90, 110.28, 37.79, 31.90, 29.69, 29.60, 29.57, 29.51, 29.32, 29.24, 28.77, 26.89, 22.67, 14.09. HR-EI-MS (*m/z)*: calcd. for $C_{20}H_{31}N_3O_2$:

345.2416; found 345.2421 (error = -1.4 ppm)

General procedure of diamine and dione condensation reaction:

For **3-1a-b** and **3-2a-b**

Diamine **3-12a-b** (0.22 mmol, 2.2 eq) and 2,7-di-*tert*-butylpyrene-4,5,9,10-tetraone or pyrene-4,5,9,10-tetraone (0.1 mmol) were suspended in *o*-DCB (8 mL). Catalytic amount of *p*-toluenesulfonic acid (2 mg) was added. The pH of the solution should be little acidic at this stage. The resulted solution was stirred and refluxed for overnight under Ar (g) atmosphere. The *o*-DCB was removed under vacuum and the residue was dissolved in DCM and saturated NaCl, extracted with DCM. The combined organic phases were washed with saturated $NaHCO_3$ (200 mL), and then the solvent was removed under reduced pressure to give yellow residue. The solid residue was added $CHCl_3$ (10 mL), and stirred for 30 min, and then purified with column chromatography using Hex/$CHCl_3$ (1:1~1:5) to give the final product **3-1a-b** and **3-2a-b**.

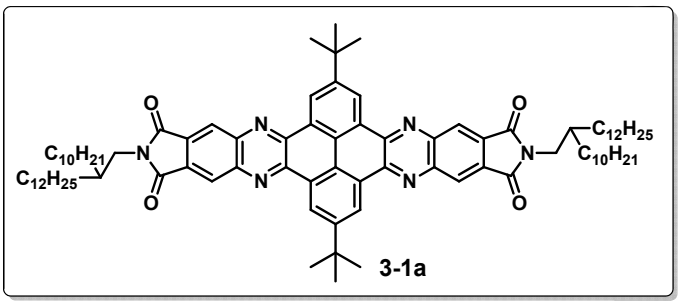

2,12-di-tert-butyl-7,17-bis(2-decyltetradecyl)pyrrolo[3,4-*i*]pyrrolo[3'',4'':6',7']quinoxalino[2',3':9,10]phenanthro[4,5-*abc*]phenazine-6,8,16,18(7H,17H)-tetraone

3-1a: Yield = 81%. Yellow powder. ^{1}H NMR (500 MHz, $CDCl_3$): δ ppm = 9.66 (s, 4 H), 8.55 (s, 4 H), 3.46 (d, *J* = 5.2 Hz, 4 H), 1.88 - 1.82 (m, 20 H), 1.24 - 1.23 (m, 80 H), 0.87 - 0.84 (m, 12 H); ^{13}C NMR (125 MHz, $CDCl_3$): δ ppm = 166.88, 151.77, 144.03, 143.90, 130.80, 128.26, 126.33, 126.12, 125.67, 42.83, 36.97, 36.01, 31.91, 31.81, 31.57, 29.97, 29.68, 29.65, 29.59, 29.35, 26.28, 22.67, 14.09. MALDI-TOF MS: *m/z*= 1329.9659 ([*M* + H]$^+$); calculated exact mass: 1329.9762. ([*M* + H]$^+$) Elemental Analysis: calcd. for $C_{64}H_{76}N_6O_4$: C, 79.47; H 9.40; N, 6.32; found: C, 79.17; H 9.38; N, 6.30;

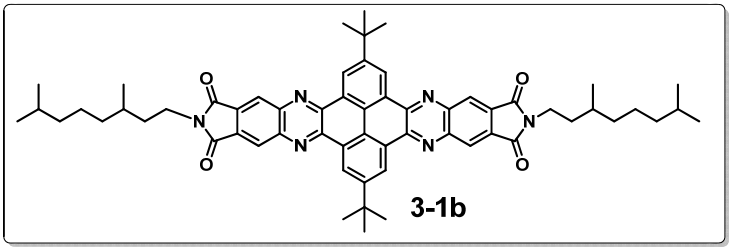

3-1b

2,12-di-tert-butyl-7,17-bis(3,7-dimethyloctyl)pyrrolo[3,4-*i*]pyrrolo[3'',4'':6',7']quinoxalino[2',3':9,10]phenanthro[4,5-*abc*]phenazine-6,8,16,18(7H,17H)-tetraone

3-1b: Yield = 86%. Yellow powder. ^{1}H NMR (500 MHz, $CDCl_3$, 323K): δ ppm = 9.83 (s, 4 H), 8.81 (s, 4 H), 3.82 (d, *J* = 7.5 Hz, 4 H), 1.83 - 1.54 (m, 20 H), 1.42 - 1.19 (m, 8 H + 10 H), 1.04 (d, *J* = 6.3 Hz, 6 H), 0.90 (d, *J* = 6.9 Hz, 12 H); ^{13}C

NMR (125 MHz, $CDCl_3$, 323K): δ ppm = 166.96, 152.08, 144.51, 144.47, 131.45, 128.82, 126.69, 126.53, 125.97, 39.36, 37.20, 37.13, 36.07, 35.53, 31.79, 31.10, 28.00, 24.64, 22.65, 22.59, 19.49. MALDI-TOF MS: *m/z*= 937.5888 ($[M + H]^+$); calculated exact mass: 937.5380. ($[M + H]^+$) Elemental Analysis: calcd. for $C_{64}H_{76}N_6O_4$: C, 76.89; H, 7.31; N, 8.97; found: C, 76.90; H, 7.29; N, 9.00.

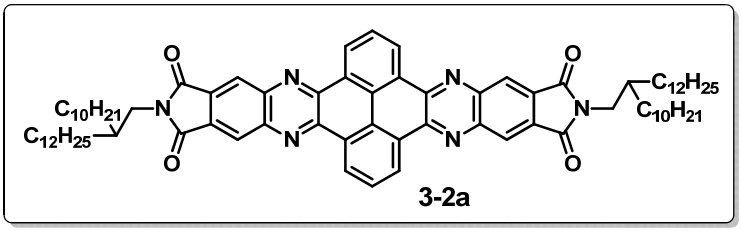

3-2a

7,17-bis(2-decyltetradecyl)pyrrolo[3,4-*i*]pyrrolo[3'',4'':6',7']quinoxalino[2',3':9,10]phenanthro[4,5-*abc*]phenazine-6,8,16,18(7H,17H)-tetraone

3-2a: Yield = 88%. Yellow powder. ^{1}H NMR (500 MHz, $CDCl_3$): δ ppm = 8.39 (d, *J* = 7.0 Hz, 4 H), 7.71(s, 4 H), 7.36 (t, *J* = 7.0 Hz, 2H), 3.52(d, *J* = 5.1 Hz, 4 H), 1.90 (br, 2 H), 1.40 - 1.26 (m, 80 H), 0.89 - 0.86 (m, 12 H); ^{13}C NMR (125 MHz, $CDCl_3$): δ ppm = 166.35, 143.08, 141.45, 130.75, 128.01, 127.52, 127.07, 125.84, 124.56, 42.89, 37.08, 31.96, 31.94, 31.89, 31.49, 30.12, 29.77, 29.72, 29.66, 29.63, 29.42, 29.39, 29.33, 26.28, 22.70, 22.68, 14.09. MALDI-TOF MS: *m/z*= 1217.7934 ($[M + H]^+$); calculated exact mass: 1217.8510. ($[M + H]^+$) Elemental Analysis: calcd. for $C_{64}H_{76}N_6O_4$: C, 78.90; H, 8.94; N, 6.90; found: C, 78.75; H, 8.93; N, 6.92.

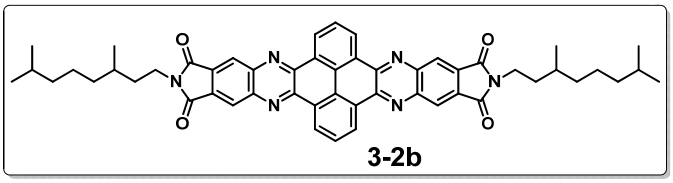

3-2b

7,17-bis(3,7-dimethyloctyl)pyrrolo[3,4-*i*]pyrrolo[3'',4'':6',7']quinoxalino[2',3':9,10]phenanthro[4,5-*abc*]phenazine-6,8,16,18(7H,17H)-tetraone

3-2b: Yield =87%. Yellow powder.^{1}H NMR (500 MHz, $CDCl_3$, 323K): δ ppm = 8.48 (d, *J* = 7.5 Hz, 4 H), 7.77 (s, 4 H), 7.44 (t, *J* = 7.0 Hz, 2H), 3.67 (t, *J* = 7.5 Hz, 4 H), 1.79 - 1.20 (m, 2 H + 18 H), 1.40 (d, *J* = 6.3 Hz, 6 H), 0.93 (d, *J* = 6.9 Hz, 12 H); ^{13}C NMR (125 MHz, $CDCl_3$, 323K): δ ppm = 166.09, 143.28, 141.73, 131.06, 128.21, 127.70, 127.33, 126.16, 124.63, 39.39, 37.13, 35.42, 31.18, 28.03, 24.68, 22.71, 22.64, 19.44. MALDI-TOF MS: *m/z*= 825.4212 ([*M* + H] $^{+}$); calculated exact mass: 825.4128 ([*M* + H] $^{+}$). Elemental Analysis: calcd. for $C_{64}H_{76}N_6O_4$: C, 75.70; H, 6.35; N, 10.19; found: C, 75.57; H, 6.34; N, 10.17.

For **3-3**

Diamine **3-12c** (0.33 mmol, 114 mg, 3.3 eq) and hexaketocyclohexane octahydrate (0.1 mmol, 31 mg) were suspended in *o*-DCB (8 mL). Catalytic amount of *p*-toluenesulfonic acid (2 mg) was added. The pH of the solution should be little acidic at this stage. The resulted solution was stirred and refluxed for overnight under Ar (g) atmosphere. The *o*-DCB was removed under vacuum and the residue was dissolved in DCM and saturated NaCl, extracted with DCM. The combined organic phases were washed with saturated $NaHCO_3$ (50 mL), and

then the solvent was removed under reduced pressure to give yellow residue, and then purified with column chromatography using Hex/THF (1:3~1:1) to give the final product **3-1c** as a yellow green solid.

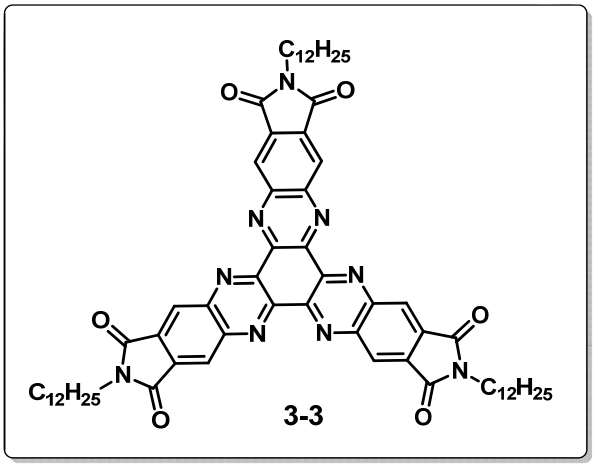

2,9,16-tridodecyl-1H-pyrrolo[3,4-i]pyrrolo[3',4':6,7]quinoxalino[2,3-*a*]pyrrolo[3',4':6,7]quinoxalino[2,3-*c*]phenazine-1,3,8,10,15,17(2H,9H,16H)-hexaone

3-3: 80 mg, yield = 82%. Yellow green powder. ^{1}H NMR (500 MHz, $CDCl_3$): δ ppm = 9.12 (s, 6 H), 3.86 (t, *J* = 7.5 Hz, 6 H), 1.83 - 1.77 (m, 6 H), 1.46 - 1.26 (m, 54 H), 0.87 (t, *J* = 7.0 Hz, 9 H); ^{13}C NMR (125 MHz, $CDCl_3$): δ ppm = 165.84, 145.76, 143.97, 133.77, 126.53, 39.15, 31.87, 29.60, 29.58, 29.56, 29.47, 29.30, 29.16, 28.40, 26.96, 22.63, 14.05. MALDI-TOF MS: *m/z*= 1096.7280 ([*M* + H]$^{+}$); calculated exact mass: 1096.6388. ([*M* + H]$^{+}$. Elemental Analysis: calcd. for $C_{64}H_{76}N_6O_4$: C, 72.30; H, 7.45; N, 11.50; found: C, 72.51; H, 7.44; N, 11.53.

3.5 References

1. For a recent review, see a) Bendikov, M.; Wudl, F.; Perepichka, D. F. *Chem.*

Rev. **2004**, *104*, 4891; b) Wu, J. *Curr. Org. Chem.* **2007**, *11*, 1220; c) Wu, J.; Pisula, W.; Müllen, K. *Chem. Rev.* **2007**, *107*, 718; d) Murphy, A. R.; Fréchet, J. M. J. *Chem. Rev.* **2007**, *107*, 1066; e) Zaumseil, J.; Sirringhaus, H. *Chem. Rev.* **2007**, *107*, 1296; f) Mas-Torrent, M.; Rovira, C. *Chem. Soc. Rev.* **2008**, *37*, 827;

2. For a recent review, see a) Katz, H. E.; Bao, Z.; Gilat, S. L. *Acc. Chem. Res.* **2001**, *34*, 359; b) Pascal, R. A. Jr. *Chem. Rev.* **2006**, *106*, 4809; c) Anthony, J. E. *Chem. Rev.* **2006**, *106*, 5028; d) Anthony, J. E. *Angew. Chem. Int. Ed.* **2008**, *47*, 452.
3. a) Yoon, M.-H.; Dibeneddetto, S. A.; Facchetti, A.; Marks, T. J. *J. Am. Chem. Soc.* **2005**, *127*, 1348. b) Sun, Y.; Liu, Y.; Zhu, D. *J. Mater. Chem.* **2005**, *15*, 53. c) Di, C.; Yu, G.; Liu, Y.; Zhu, D. *J. Phys. Chem. B* **2007**, *111*, 4083. (d) Murphy, A. R.; Frechet, J. M. J. *Chem. Rev.* **2007**, *107*, 1066. (e) Zaumseil, J.; Sirringhaus, H. *Chem. Rev.* **2007**, *107*, 1296.
4. a) Bao, Z.; Lovinger, A. J.; Brown, J. *J. Am. Chem. Soc.* **1998**, *120*, 207. b) Sakamoto, Y.; Shingo, K.; Suzuki, T. *J. Am. Chem. Soc.* **2001**, *123*, 4643. c) Facchetti, A.; Yoon, M. H.; Stern, C. L.; Hutchison, G. R.; Ratner, M. A.; Marks, T. J. *J. Am. Chem. Soc.* **2004**, *126*, 13480. d) Qu, H.; Chi, C. *Org. Lett.*, **2010**, *12*, 3360.
5. a) Katz, H. E.; Lovinger, A. J.; Johnson, J.; Kloc, C.; Siegrist, T.; Li, W.; Lin, Y.-Y.; Dodabalapur, A. *Nature* **2000**, *404*, 478. b) Gregg, B. A.; Cormier, R.

A. *J. Am. Chem. Soc.* **2001**, *123*, 7959. c) Jones, B. A.; Facchetti, A.; Wasielewski, M. R.; Marks, T. J. *J. Am. Chem. Soc.* **2007**, *129*, 15259. d) Wang, Z.; Kim, C.; Facchetti, A.; Marks, T. J. *J. Am. Chem. Soc.* **2007**, *129*, 13362. e) Guo, X.; Ortiz, R. P.; Zheng, Y.; Hu,Y.; Noh, Y-Y.; Baeg, K-J.; Facchetti, A.; Marks, T. J. *J. Am. Chem. Soc.* **2011**, *133*, 1405. f) Qu, H.; Cui, W.; Li, J.; Shao, J.; Chi, C. *Org. Lett.*, **2011**, *13*, 924. g) Ye, Q.; Chang, J.; Huang, K-W.; Chi, C. *Org. Lett.* **2011**, *13*, 5960. h) Ramanan, C.; Smeigh, A. L.; Anthony, J. E.; Marks, T. J. Wasielewski M. R. *J. Am. Chem. Soc.*, **2012**, *134*, 386.

6. a) Usta, H.; Facchetti, A.; Marks, T. J. *J. Am. Chem. Soc.*, **2008**, *130*, 8580. b) Gao, X.; Di, C.; Hu, Y.; Yang, X.; Fan, H.; Zhang, F.; Liu, Y.; Li H.; Zhu, D. *J. Am. Chem. Soc.*, **2010**, *132*, 3697. c) Hu,Y.; Gao, X.; Di, C.; Yang, X.; Zhang, F.; Liu, Y.; Li H.; Zhu, D. *Chem. Mater.*, **2011**, *23*, 1204. d) Qiao,Y.; Guo,Y.; Yu, C.; Zhang, F.; Xu,W.; Liu, Y.; Zhu, D. *J. Am. Chem. Soc.*, **2012**, *134*, 4084. e) Li, J.; Chang, J-J.; Tan, H. S.; Jiang, H.; Chen,X.; Chen, Z.; Zhang J.; Wu, J. *Chem. Sci.*, **2012**, *3*, 8.

7. a) Tang, Q.; Liu, J.; Chan, H. S.; Miao, Q. *Chem.; Eur. J.* **2009**, *15*, 3965. b) Liang, Z.; Tang, Q.; Mao, R.; Liu, D.; Xu, J.; Miao, Q. *Adv. Mater.* **2011**, *23*, 5514. c) Li, Z.; Du, J.; Tang, Q.; Wang, F.; Xu, J.; Yu, J. C.; Miao, Q. *Adv. Mater.* **2010**, *22*, 3242. d) Liang, Z.; Tang, Q.; Xu, J.; Miao, Q. *Adv. Mater.* **2011**, *23*, 1535. e) Wang, C.; Liang, Z.; Liu, Y.; Wang, X.; Zhao, N.; Miao, Q.;

Hu, W.; Xu, J. *J. Mater. Chem.* **2011**, *21*, 15201. f) He, Z.; Liu, D.; Tang, Q.; Zhang, D.; Wang, S.; Ke, N.; Xu, J.; Yu, J. C.; Miao, Q. *Chem. Mater.* **2009**, *21*, 1400. g) Liang, Z.; Tang, Q.; Liu, J.; Li, J.; Yan, F.; Miao, Q. *Chem. Mater.* **2010**, *22*, 6438. h) Mao, R.; Tang, Q.; Miao, Q. *Org. Lett.*, **2012**, 14, 1050. i) Bunz, U. H. F. *Chem.; Eur. J.* **2009**, *15*, 6780. j) Miao, S.; Appleton, A. L.; Berger, N.; Barlow, S.; Marder, S. R.; Hardcastle, K. I.; Bunz, U. H. F. *Chem.; Eur. J*. **2009**, *15*, 4990. k) Bunz, U. H. F. *Pure Appl. Chem.* **2010**, *82*, 953. l) Appleton, A. L.; Brombosz, S. M.; Barlow, S.; Sears, J. S.; Bredas, J. L.; Marder, S. R.; Bunz, U. H. F. *Nat. Commun.* **2010**, *1*, 91. m) Miao, S.; Brombosz,S. M.; Schleyer, P.v.R.; Wu, J. I.; Barlow, S; Marder, S. R.; Hardcastle, K. I.; Bunz, U. H. F. *J. Am. Chem. Soc.* **2008**, *130*, 7339. n) Tverskoy, O.; Rominger, F.; Peters, A.; Himmel, H. J.; Bunz, U. H. F. *Angew. Chem.* **2011**, *50*, 3557. o) Lindner, B. D.; Engelhart, J. U.; Tverskoy, O.; Appleton, A. L.; Rominger, F.; Peters, A.; Himmel, H. J.; Bunz, U. H. F. *Angew. Chem.* **2011**, *50*, 8588. p) Wu, J. I.; Wannere, C. S.; Mo, Y. R.; Schleyer, P. v. R.; Bunz, U. H. F. *J. Org. Chem*. **2009**, *74*, 4343. q) Engelhart, J. U.; Lindner, B. D.; Tverskoy, O.; Rominger, F.; Bunz, U. H. F. *Org. Lett.*, **2012**, 14, 1008. r) Tong, C.; Zhao, W.; Jing Luo, Mao,H.; Chen, W.; Chan, H.S. O.; Chi, C. *Org. Lett.*, **2012**, *14*, 494.

8. Wang, C.; Dong, H.; Hu, W.; Liu, Y.; Zhu, D. *Chem. Rev.* **2012**, 112, 2208.
9. a) Yin, J.; Qu, H.; Zhang, K.; Luo, J.; Zhang, X.; Chi, C.; Wu, J. *Org. Lett*.

2009, *11*, 3028. b) Chang, T.-H.; Wu, R.-R.; Chiang, M. Y.; Liao, S.-C.; Ong, C. W.; Hsu, H.-F.; Lin, S.-Y. *Org. Lett.* **2005**, *7*, 4075. c) Kaafarani, B. R.; Kondo, T.; Yu, J.; Zhang, Q.; Dattilo, D.; Risko, C.; Jones, S. C.; Barlow, F.; Domercq, B.; Amy, F.; Kahn, A.; Bre´das, J.-L.; Kippelen, B.; Marder, S. R. *J. Am. Chem. Soc.* **2005**, *127*, 16358. d) Ishi-i, T.; Yaguma, K.; Kuwahara, R.; Taguri, Y.; Mataka, S. *Org. Lett.* **2006**, *8*, 585. e) Yip, H.-L.; Zou, J.; Ma, H.; Tuan, Y.; Tucker, N. M.; Jen, A. K.-Y. *J. Am. Chem. Soc.* **2006**, *128*, 13042.

10. a) Winkler, M.; Houk, K. N. *J. Am. Chem. Soc*. **2007**, *129*, 1805. b) Payne, M. M.; Odom, S. A.; Parkin, S. R.; Anthony, J. E. *Org. Lett*. **2004**, *6*, 3325. c) Payne, M. M.; Parkin, S. R.; Anthony, J. E.; Kuo, C.; Jackson, T. N. *J. Am. Chem. Soc.* **2005**, *127*, 8028.
11. a) Hu, J.; Zhang, D.; Jin, S.; Cheng, S. Z. D.; Harris, F. W. *Chem. Mater.* **2004**, *16*, 4912. b) Kaafarani, B. R.; Kondo, T.; Yu, J.; Zhang, Q.; Dattilo, D.; Risko, C.; Jones, S. C.; Barlow, F.; Domercq, B.; Amy, F.; Kahn, A.; Bre´das, J.-L.; Kippelen, B.; Marder, S. R. *J. Am. Chem. Soc.* **2005**, *127*, 16358. c) Miao, S.; Smith, M. D.; Bunz, U. H. F. *Org. Lett.* **2006**, *8*, 757. d) Gao, B.; Wang, M.; Cheng, Y.; Wang, L.; Jing, X.; Wang, F. *J. Am. Chem. Soc.* **2008**, *130*, 8297.
12. Cheeseman, G. W. H. *J. Chem. Soc.*, **1962**, *1170*.
13. Mørkved, E. H; Neset, S. M; Bjørlo, O; Kjøsen, H; Hvistendahl, G; Mo. F. *Acta Chemica Scandinavica*.**1995**, *49*, 658.
14. Qu, H; Luo, J; Zhang, X; Chi, C. *J. Polym. Sci. Part A: Polym Chem.,* **2010**,

48, 186.

15. a) Zhao, B; Liu, B; Png, R. Q; Zhang, K; Lim, K. A. Luo, J. Shao, J. Ho, P. K. H; Chi, C; Wu, J. *Chem. Mater.*, **2010**, *22*, 435.b) Shao, J.; Guan, Z.; Yan, Y.; Jiao, C.; Xu, Q-H.; Chi, C. *J. Org. Chem.* **2011**, *76*, 780.
16. a) Lindgren, L. J.; Zhang, F.; Andersson, M.; Barrau, S.; Hellstrom, S.; Mammo, W.; Perzon, E.; Inganas, O.; Andersson, M. R. *Chem. Mater*. **2009**, *21*, 3491. b) Hong, D-J.; Lee, E.; Jeong, H.; Lee, J-K.; Zin, W-C.; Nguyen,T. D.; Glotzer, S. C.; Lee, M. *Angew. Chem. Int. Ed.* **2009**, *48*, 1664.
17. Hu, J.; Zhang, D.; Harris, F. W. *J. Org. Chem.* **2005**, 70, 707.
18. a) Jang, B. B.; Lee, S. H.; Kafafi, Z. H. *Chem. Mater.* **2006**, *18*, 449. b) Brusso, J. L.; Hirst, O. D.; Dadvand, A.; Ganesan, S.; Cicoira, F.; Robertson, C. M.; Oakley, R. T.; Rosei, F.; Perepichka, D. F. *Chem. Mater.* **2008**, *20*, 2484.
19. a) Chi, C.; Wegner, G. *Macromol. Rapid Commun.* **2005**, *26*, 1532. b) Chi, C.; Im, C.; Enkelmann, V.; Ziegler, A.; Lieser, G.; Wegner, G. *Chem.;Eur. J.* **2005**, *11*, 6833.
20. Constantinides, C. P.; Koutentis, P. A.; Schatz, J. *J. Am. Chem. Soc*. **2004**, *126*, 16232.

Chapter 4

Unsymmetrical Naphthalene Imides with High Electron Affinity for Air-stable and Solution-Processible n-Channel Field Effect Transistors

4.1 Introduction

In chapter 3, a series of n-type semiconductors have been successfully synthesized; however, they exhibit only moderate charge carrier mobility via SCLC technique, probably due to their poor molecular arrangements in the solid state. To achieve efficient n-type semiconductors, molecules with strong intermolecular π-π interaction and low-lying LUMO energy level are required. As a result, the building block naphthalene diimide (NDI) come into our sight.

Naphthalene diimide (NDI) is a promising building block, which has been widely employed to construct *n*-type semiconductors with high performance and good air-stability. Based on core-expansion or core-substitution strategy,[1] considerable NDI derivatives with symmetrical structures have been designed and synthesized for *n*-channel OFETs. For instance, two core-expanded naphthalene diimides fused with 2-(1,3-dithiol-2-ylidene)malonitrile groups were reported to exhibit high electron mobility (μ_e) of 0.51 $cm^2 V^{-1} s^{-1}$ in ambient air.[2] Nevertheless, the unsymmetrical naphthalene diimide derivatives were rarely synthesized and used for *n*-channel OFETs.[3] Marks' group reported a series of unsymmetrical naphthalene imide derivative, the naphthaleneamidinemonoimide-fused oligothiophenes, which showed electron mobility up to 0.35 $cm^2 V^{-1} s^{-1}$ based on vapor deposited thin films. However, the solution processed films gave the electron mobility of only 4×10^{-5} to 3×10^{-3} $cm^2 V^{-1}s^{-1}$ under vacuum.[4] For large scale fabrication of low-cost devices, solution based film deposition processes

with high charge carrier mobility are highly desirable.[5] In this chapter, we will demonstrate the synthesis of a family of unsymmetrical naphthalene imide derivatives **4-1a**, **4-1b** and **4-2** – **4-5** (Figure 4.1) with high electron affinity, and their applications in solution processed, air-stable *n*-channel OFETs. Compared with the symmetric NDIs, one imide group in these unsymmetric naphthalene imides was annulated with benzoimidazole or imidazole unit carrying various electron withdrawing substituents (e.g. imide, cyano-, and nitro- group). Thus these new molecules are expected to show high electron affinity with tunable lowest unoccupied molecular orbital (LUMO) energy levels, which are essential for air-stable *n*-channel OFETs.

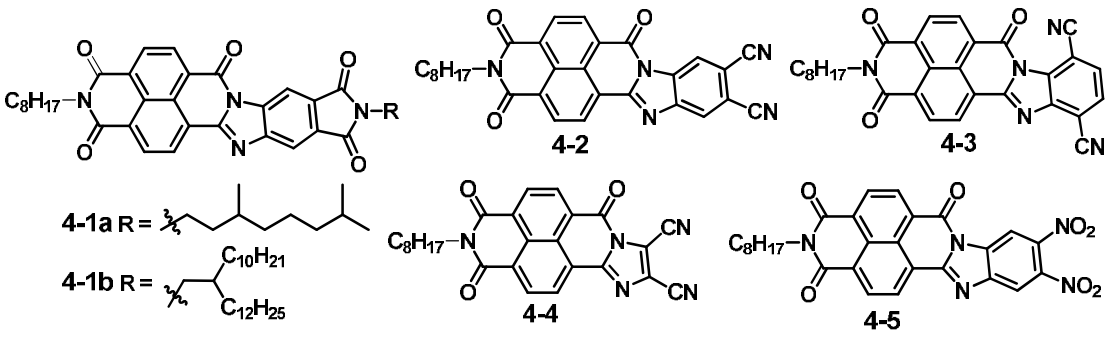

Figure 4.1. Chemical structures of unsymmetrical naphthalene imide derivatives (**4-1a**–**b**, **4-2** – **4-5**).

4.2 Results and Discussion

4.2.1 Synthesis

The synthesis of these electron-deficient organic semiconductors is shown in

Scheme 4.1. The key reaction is the condensation between the naphthalene monoanhydride **4-6** and different diamines (**4-7a**, **4-7b**, **4-9**, **4-11** – **4-13**). Naphthalene monoanhydride **4-6**, the diamines **4-7a**, **4-7b** and **4-13** were prepared according to reported literature procedures.[5] To synthesize 4,5-diaminophthalonitrile **4-9**, $NaBH_4$ was first employed to reduce benzothiadiazole-4,7-dicarbonitrile **4-8**,[5b] however, the yield was only 12%. Later Fe powder[5b] was applied to reduce **4-8** in refluxing acetic acid, and **4-9** was obtained in 80% yield. Similarly, 2,3-diaminoterephthalonitrile **4-11** was prepared from **4-10** under the same condition in 85% yield.[6] The naphthalene imide derivatives **4-1** – **4-5** were then prepared by condensation between **4-6** and the diamines **4-7**, **4-9**, **4-11** – **4-13**, respectively, in 81-88% yields.

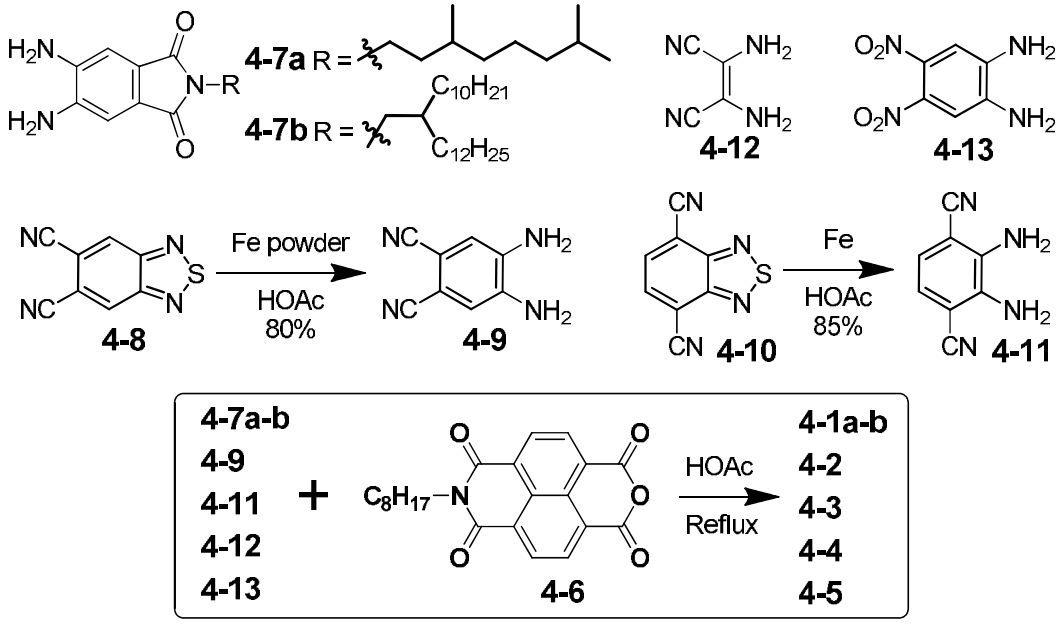

Scheme 4.1. Synthetic scheme for **4-1a**–**b** and **4-2** – **4-5**

Compounds **4-1a**, **4-1b** and **4-2** – **4-5** showed good solubility in normal organic solvents such as DCM and THF, which allows us to perform various characterizations in solution, and makes it possible to fabricate OFET devices by convenient solution processing techniques. ^{1}H NMR, ^{13}C NMR spectroscopy, mass spectrometry (HR-EI MS and MALDI-TOF MS), and elemental analysis were used to identify the chemical structure and purity of all the new compounds.

4.2.2 Photophysical Properties

The UV-vis absorption and photoluminescence spectra of compounds **4-1a**–**b** and **4-2** – **4-5** were recorded in chloroform solution (Figure 4.2, Table 4.1). For **4-1a** and **4-1b**, the alkyl chains had no effect on the spectra profiles, and both showed absorption maximum ($l_{\mathrm{abs}}{}^{\mathrm{max}}$) at 432 nm and the emission maximum ($l_{\mathrm{em}}{}^{\mathrm{max}}$) at 528 nm. For **4-2** and **4-3**, the position of the two cyano groups has little effect on the absorption profiles, with the same $l_{\mathrm{abs}}{}^{\mathrm{max}}$ at 416 nm and $l_{\mathrm{em}}{}^{\mathrm{max}}$ at 500 nm. For **4-4**, although with one benzene ring less than **4-2**, it exhibited similar $l_{\mathrm{abs}}{}^{\mathrm{max}}$ at 416 nm and $l_{\mathrm{abs}}{}^{\mathrm{max}}$ at 498 nm. For **4-5**, in which two cyano groups were replaced by two nitro groups compared to **4-2**, the absorption and emission maxima are almost the same as those of **4-2**. It is worth to note that all of these compounds show moderate-to-high photoluminescence quantum yields ranging from 41% to 81% (Table 4.1).

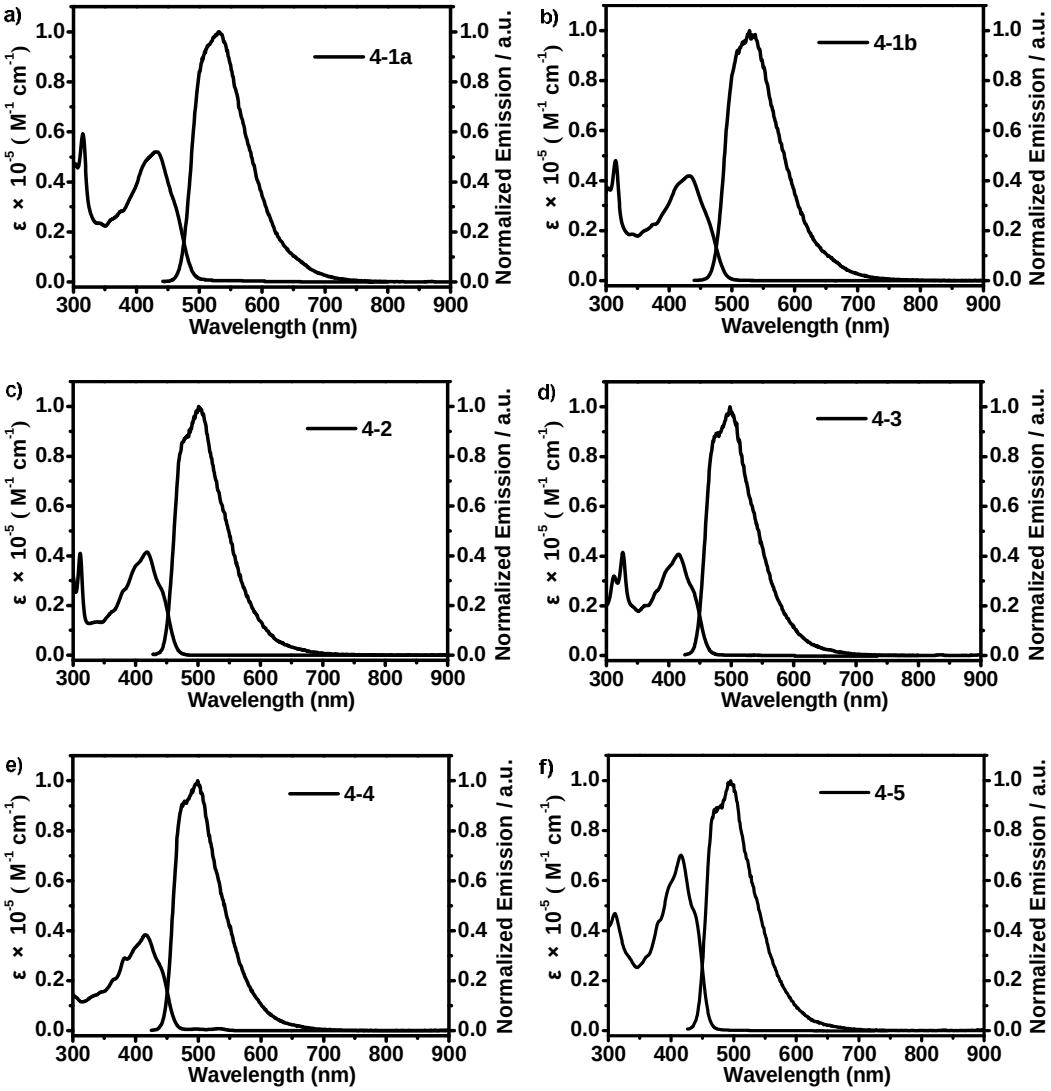

Figure 4.2. Absorption spectra (c = 1 × 10^{-5} M) and normalized emission spectra (c = 1 × 10^{-6} M) of compounds **4-1a** (a), **4-1b** (b), **4-2** (c), **4-3** (d), **4-4** (e), **4-5** (f) in $CHCl_3$ solution. The emission spectra were recorded under the excitation wavelength of 432, 432, 416, 416, 416 and 416 nm, respectively.

Table 4.1. UV and PL data for compounds **4-1a**, **4-1b** and **4-2** – **4-5**

	λ_{abs} [a] / nm	ε_{max} [b] / M^{-1} cm^{-1}	λ_{PL} [c] / nm	QY[d]
4-1a	432	42300	528	65%
4-1b	432	42000	528	66%

4-2	416	41000	500	81%
4-3	416	40500	500	45%
4-4	416	41600	498	42%
4-5	416	41900	498	41%

[a] UV-vis absorption maximum, the experimental uncertainty is ±1 nm; [b] Molar extinction coefficient at the absorption maximum; [c] Photo-luminescence maximum, the experimental uncertainty is ±1 nm; [d] Fluorescence quantum yields by using fluorescein (pH ≈ 11, NaOH aqueous solution) as a standard; the experimental uncertainty is ±5-10%.

4.2.3 Electrochemical Properties

The electrochemical properties of **4-1a**, **4-1b**, **4-2** – **4-5** were investigated by cyclic voltammetry and differential pulse voltammetry in DCM solution (Figure 4.3, Table 4.2). Three quasi-reversible reduction waves were observed for **4-1a** and **4-1b**, with the half-wave potential ($E_{red}^{1/2}$) at -0.95, -1.35 and -2.41 V for **4-1a** (*vs* Fc^+/Fc), and the different alkyl chains showed less effect on the redox behaviors. The LUMO energy level derived from the onset of the reduction potential (E_{red}^{onset}) is -3.90 and -3.92 eV for **4-1a** and **4-1b**, respectively. Accordingly, the respective HOMO energy levels are deducted as -6.43 eV and -6.46 eV for **4-1a** and **4-1b**, respectively, based on the equation HOMO = LUMO - E_g^{opt}, where E_g^{opt} is the optical energy gap determined from the lowest energy absorption onset.[7]

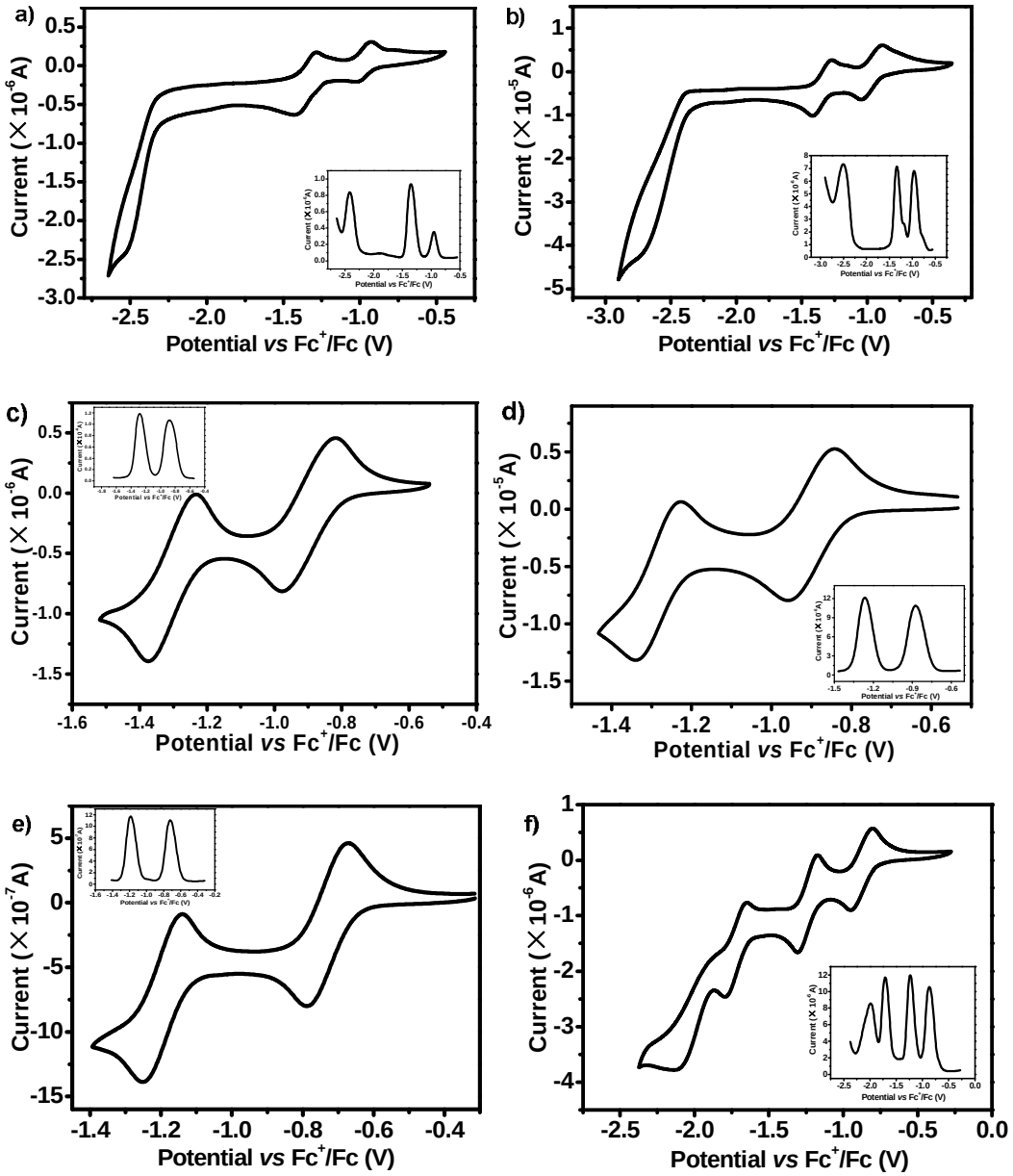

Figure 4.3. CV curves and DPV curves (inset) for compounds **4-1a** (a), **4-1b** (b), **4-2** (c), **4-3** (d), **4-4** (e), **4-5** (f) in dry DCM with 0.1 M Bu_4NPF_6 as supporting electrolyte, a gold electrode with a diameter of 2 mm, a Pt wire, and an Ag/AgCl electrode were used as the working electrode, the counter electrode, and the reference electrode, respectively, with a scan rate at 50 mV/s.

For **4-2**, **4-3** and **4-4**, two quasi-reversible reduction waves were observed with $E_{red}^{1/2}$ at -0.88 and -1.28 V for **4-2**, -0.95 and -1.35 V for **4-3**, -0.75 and -1.19 V for **4-4**. The LUMO energy level derived from E_{red}^{onset} is -4.00, -3.90 and -4.15

eV, respectively, and the HOMO energy level was calculated to be -6.68, -6.58 and -6.73 eV, respectively. By changing the position of the two cyano groups, the LUMO energy level was shifted by 0.10 eV (**4-2** *vs* **4-3**), and by removal of one benzene moiety from **4-2** to **4-4**, the LUMO energy level was lowered around 0.15 eV.

Table 4.2. Cyclic voltammograms data for compounds **4-1a**–**b** and **4-2** – **4-5**

cpd	$E_{re}^{1/2}$ / V				E_{re}^{onset} / V	LUMO [a] / eV	HOMO [b] /eV	E_g [c] / eV
4-1a	-0.95	-1.35	-2.41	--	-0.90	-3.90	-6.43	2.53
4-1b	-0.96	-1.33	-2.51	--	-0.88	-3.92	-6.46	2.54
4-2	-0.88	-1.28	--	--	-0.80	-4.00	-6.68	2.68
4-3	-0.95	-1.35	-2.42	--	-0.90	-3.90	-6.58	2.68
4-4	-0.75	-1.19	-0.65	--	-0.65	-4.15	-6.73	2.68
4-5	-0.86	-1.24	-1.71	-1.99	-0.78	-4.02	-6.70	2.68

[a] LUMO was calculated according to the equation, LUMO = – (4.80 + E_{red}^{onset}); [b] HOMO was estimated according to the equation, HOMO = LUMO – E_g; [c] E_g was estimated from the absorption edge in solution.

For compound **4-5**, four quasi-reversible reduction waves were observed with $E_{red}^{1/2}$ at -0.86, -1.24, -1.71 and -1.99 V. Hence the LUMO and HOMO were calculated to be -4.02 and -6.70 eV, respectively. For all compounds, no obvious redox waves were observed upon oxidation up to 1.80 V. The low-lying LUMO

energy level (i.e., large electron affinity) of these compounds indicates that they can serve as promising candidates for *n*-channel OFETs with good air stability.[8]

4.2.4 Thermal Properties

The thermal behavior and self-assembly of **4-1a**, **4-1b**, **4-2** – **4-5** in solid state were investigated by a combination of thermogravimetric analysis (TGA), differential scanning calorimetry (DSC), polarizing optical microscopy (POM) and powder X-ray diffraction (XRD) techniques (Figure 4.4, Figure 4.5, Figure 4.6 and Figure 4.7). TGA measurements revealed that all compounds were thermally stable over 320 ^{o}C with 5% weight loss. Compounds **4-1a**, **4-1b** and **4-3** all show a crystalline phase-to-liquid crystalline phase transition at 31, -0.5 and 64 ^{o}C, respectively, from their DSC and POM studies. An obvious XRD peak at 3.31 Å correlated to intermolecular π-π stacking was observed for **4-3**, indicating the existence of long-range ordered π-stacking. Compounds **4-2** and **4-4** both are crystalline materials at room temperature with melting point at 245 ^{o}C and 200 ^{o}C, respectively. Compound **4-5** turned out to be an amorphous solid at room temperature with melting point at 197 ^{o}C. The liquid crystalline properties of **4-1a**, **4-1b** and **4-3** may facilitate formation of self-healed, ordered thin films in OFET devices.

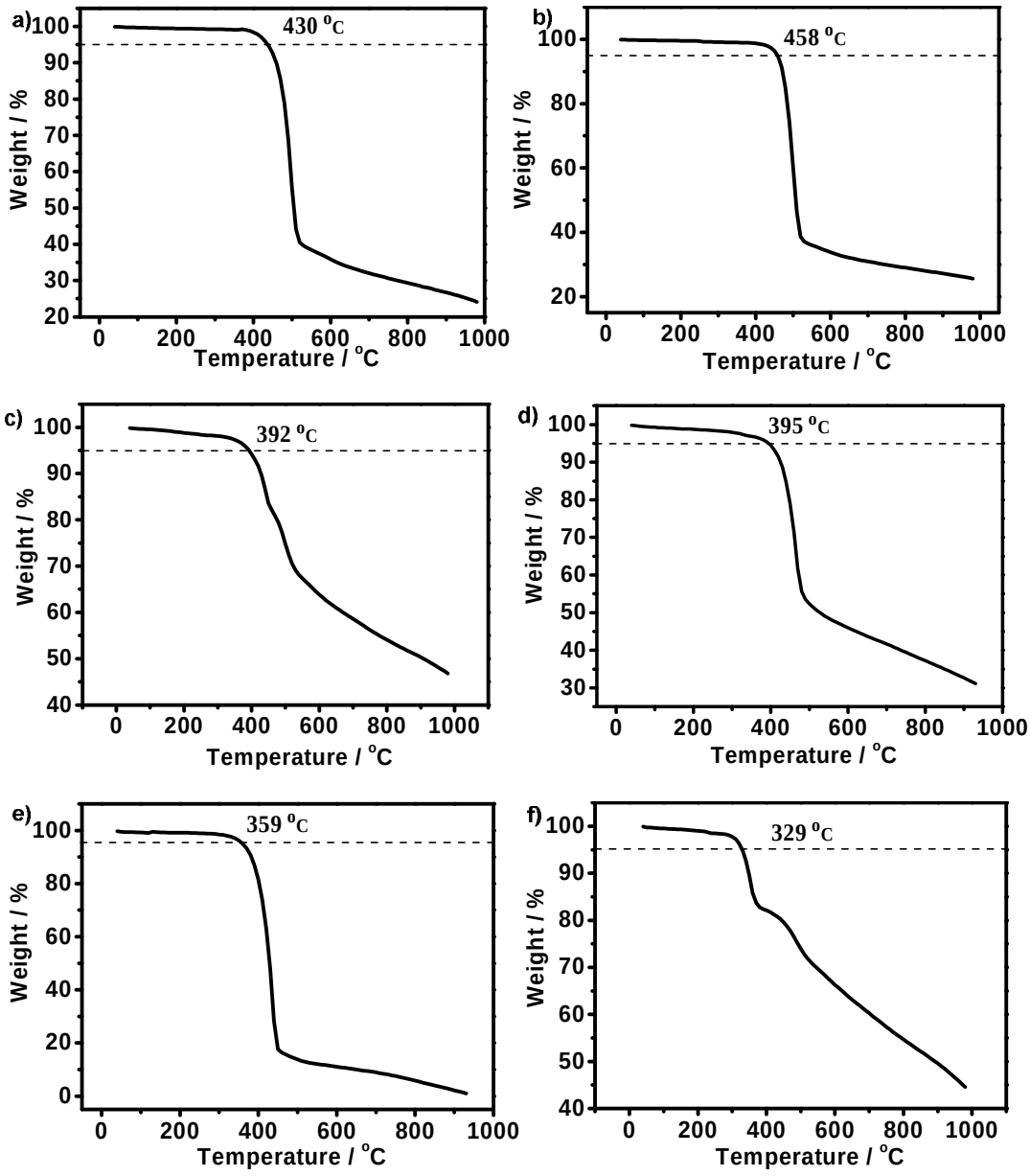

Figure 4.4. Thermogravimetric analysis (TGA) curves for compounds **4-1a** (a), **4-1b** (b), **4-2** (c), **4-3** (d), **4-4** (e), **4-5** (f) with a heating rate of 10 °C/min under nitrogen.

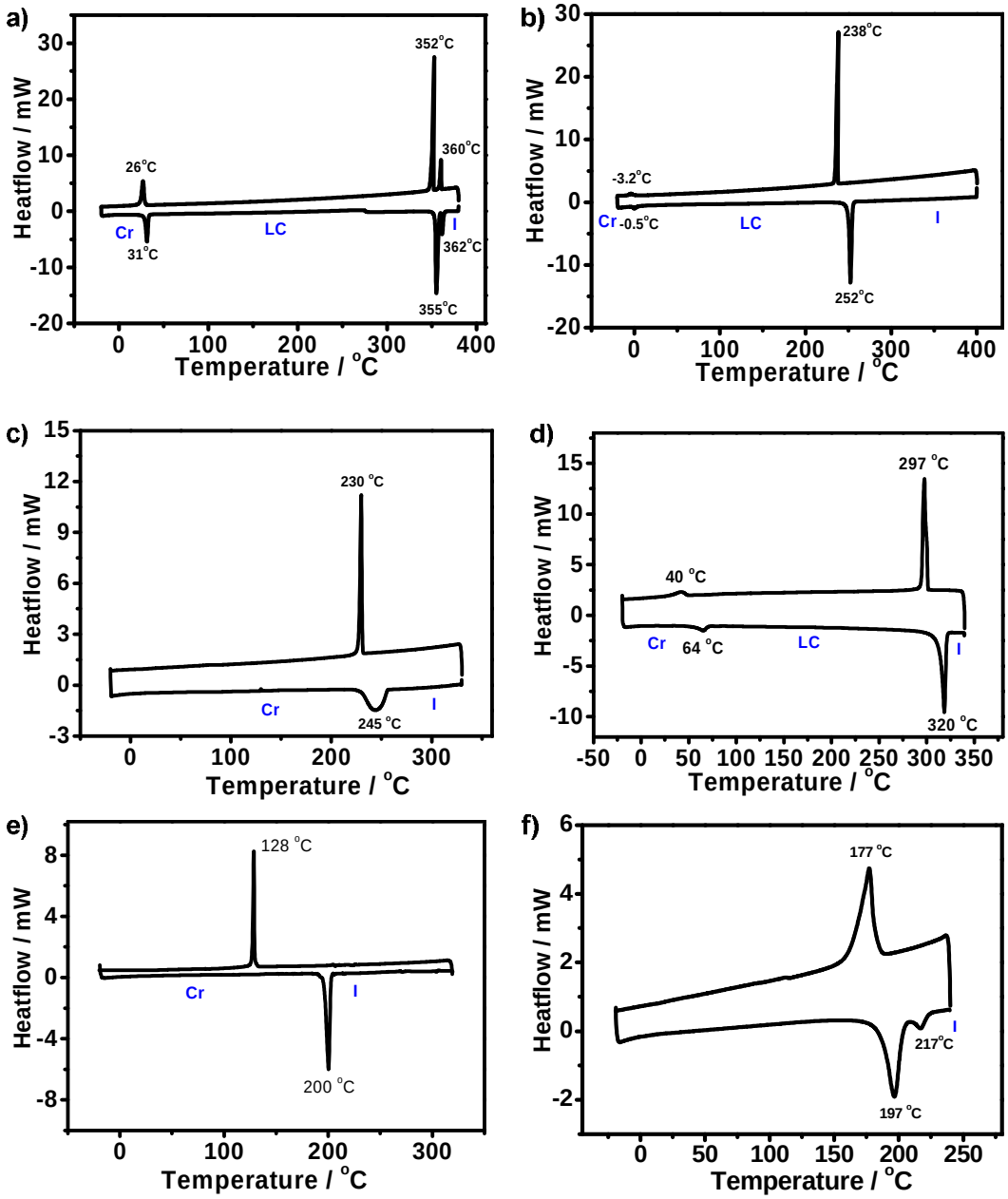

Figure 4.5. DSC curves for compounds **4-1a** (a), **4-1b** (b), **4-2** (c), **4-3** (d), **4-4** (e), **4-5** (f) with a heating/cooling scan rate of 10 °C/min under nitrogen. (Cr = crystalline phase, LC = liquid crystal phase, I = isotropic phase).

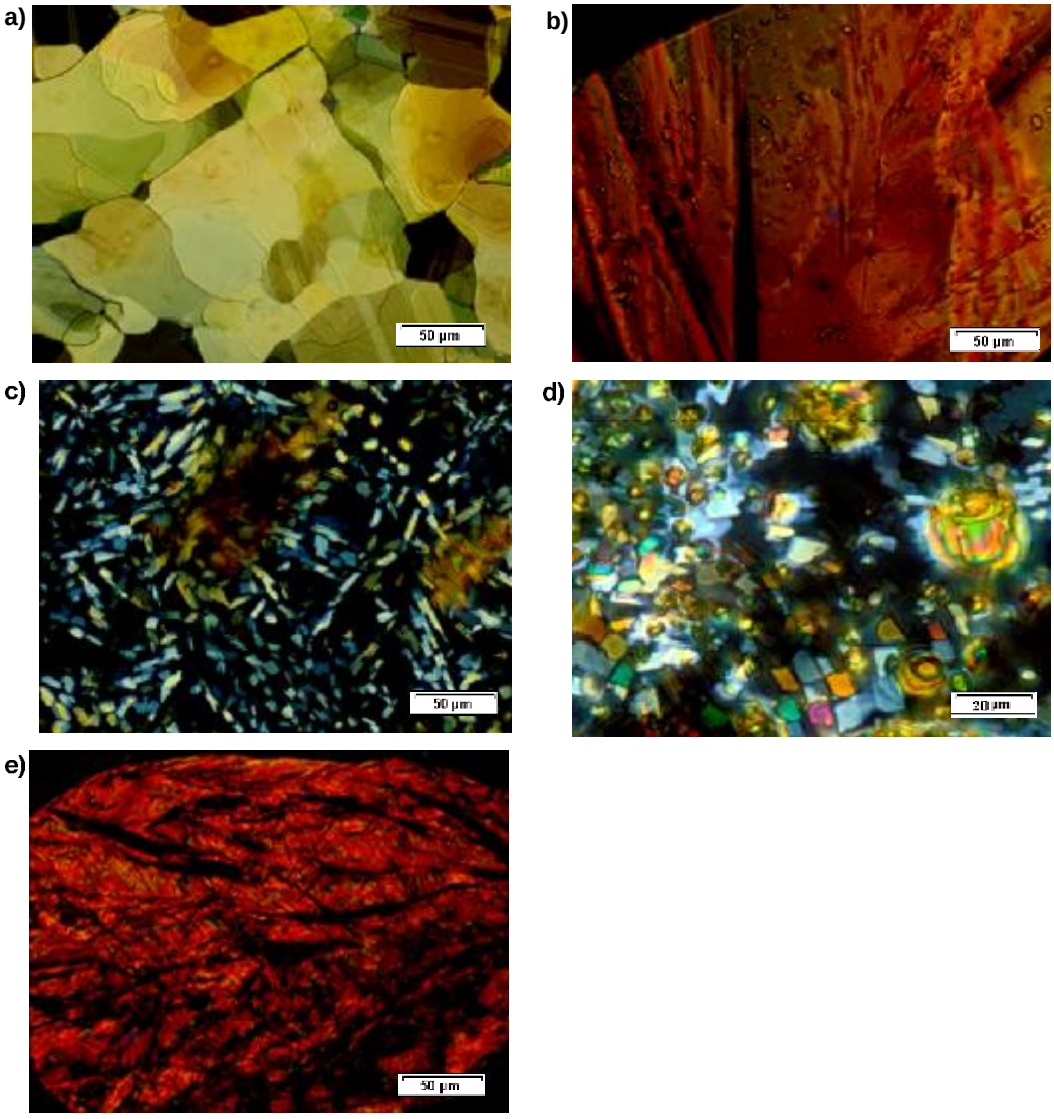

Figure 4.6. POM images for **4-1a**–**b** and **4-2** – **4-4**. a) **4-1a**, at 338 °C upon slow cooling from the melt; b) **4-1b**, at 227 °C upon slow cooling from the melt; c) **4-2**, at 205 °C upon slow cooling from the melt; d) **4-3**, at 270 °C upon slow cooling from the melt; e) **4-4**, at 100 °C upon slow cooling from the melt.

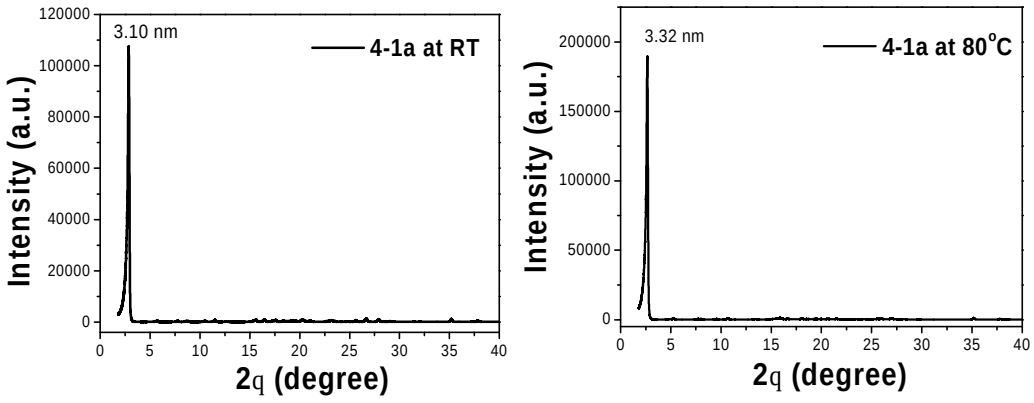

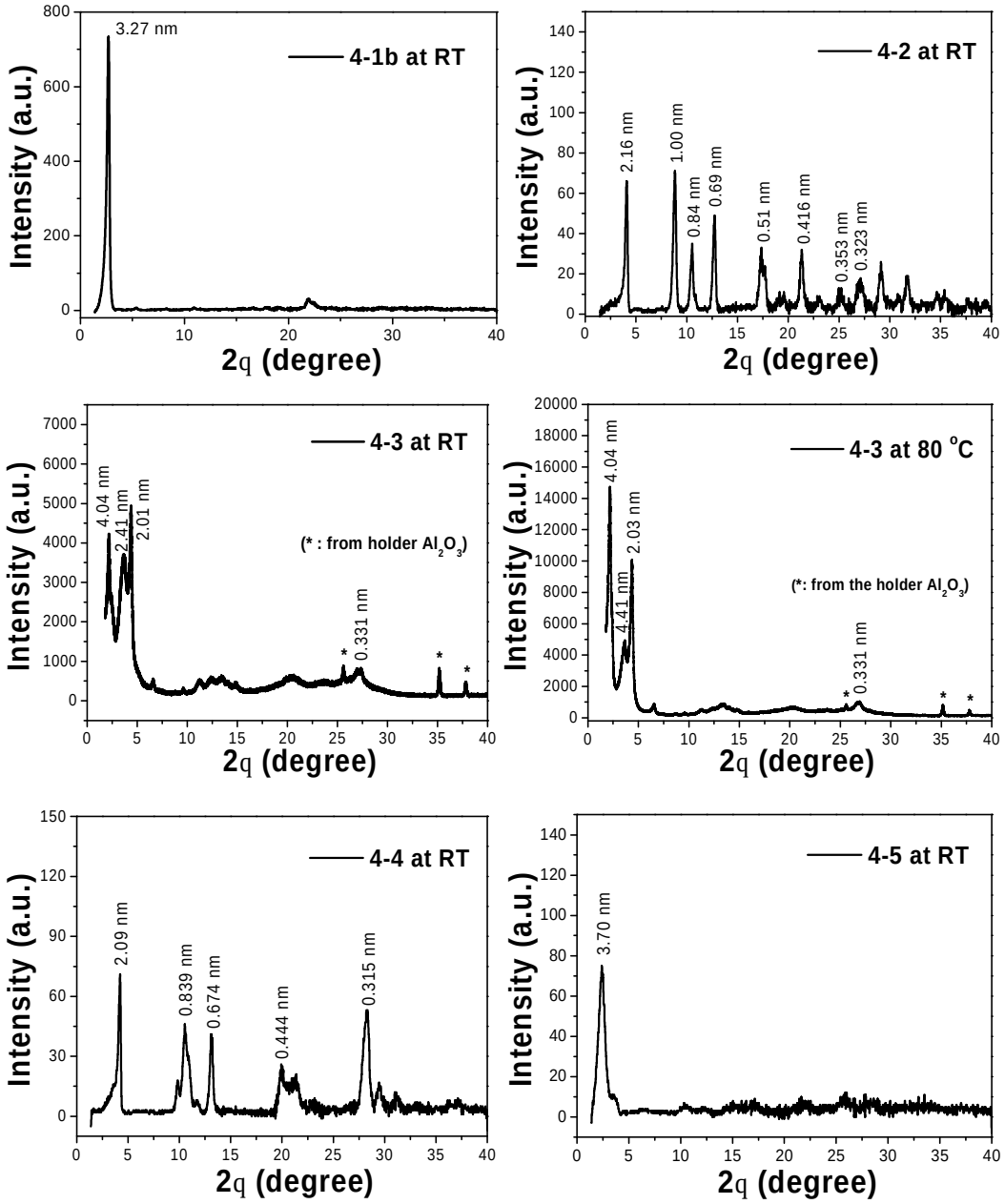

Figure 4.7. Powder X-ray diffraction (XRD) patterns of compounds **4-1a**, **4-1b**, **4-2** – **4-5** at different temperatures.

4.2.5 OFET device measurement

The charge transport properties of **4-1a**, **4-1b**, and **4-2** – **4-5** were characterized using OFETs. Bottom-gate top-contact OFETs were fabricated on p^+-Si/SiO_2 substrates by spin casting 0.8-1.0 wt% chloroform solution onto

octadecyltrimethoxysilane (OTMS) or octadecyltrichlorosilane (ODTS) treated substrates. The thin films were then annealed at selective temperatures for 30 min under vacuum. Au source/drain electrodes (80 nm) were patterned on the organic layer through a shadow mask. All devices were characterized in a N_2 atmosphere. The typical transfer and output curves are shown in Figure 4.8. Thin film of **4-5** did not show any field effect behaviors in this study, presumably due to its amorphous character in solid state.

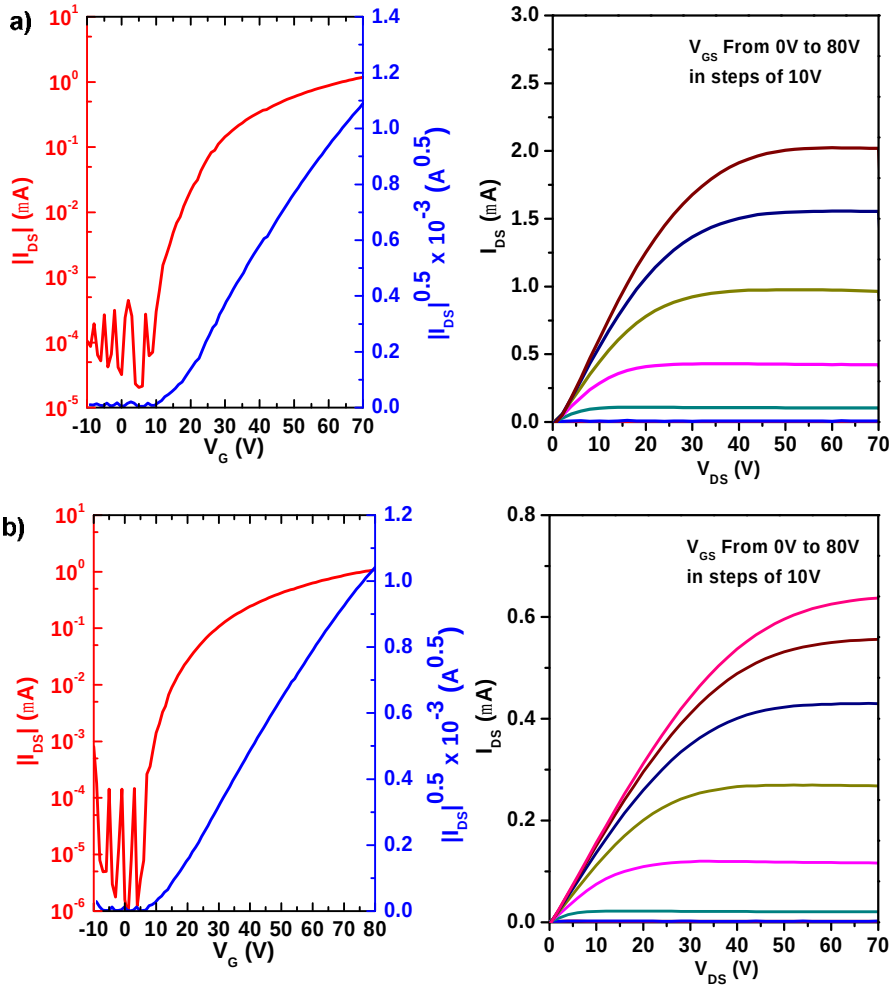

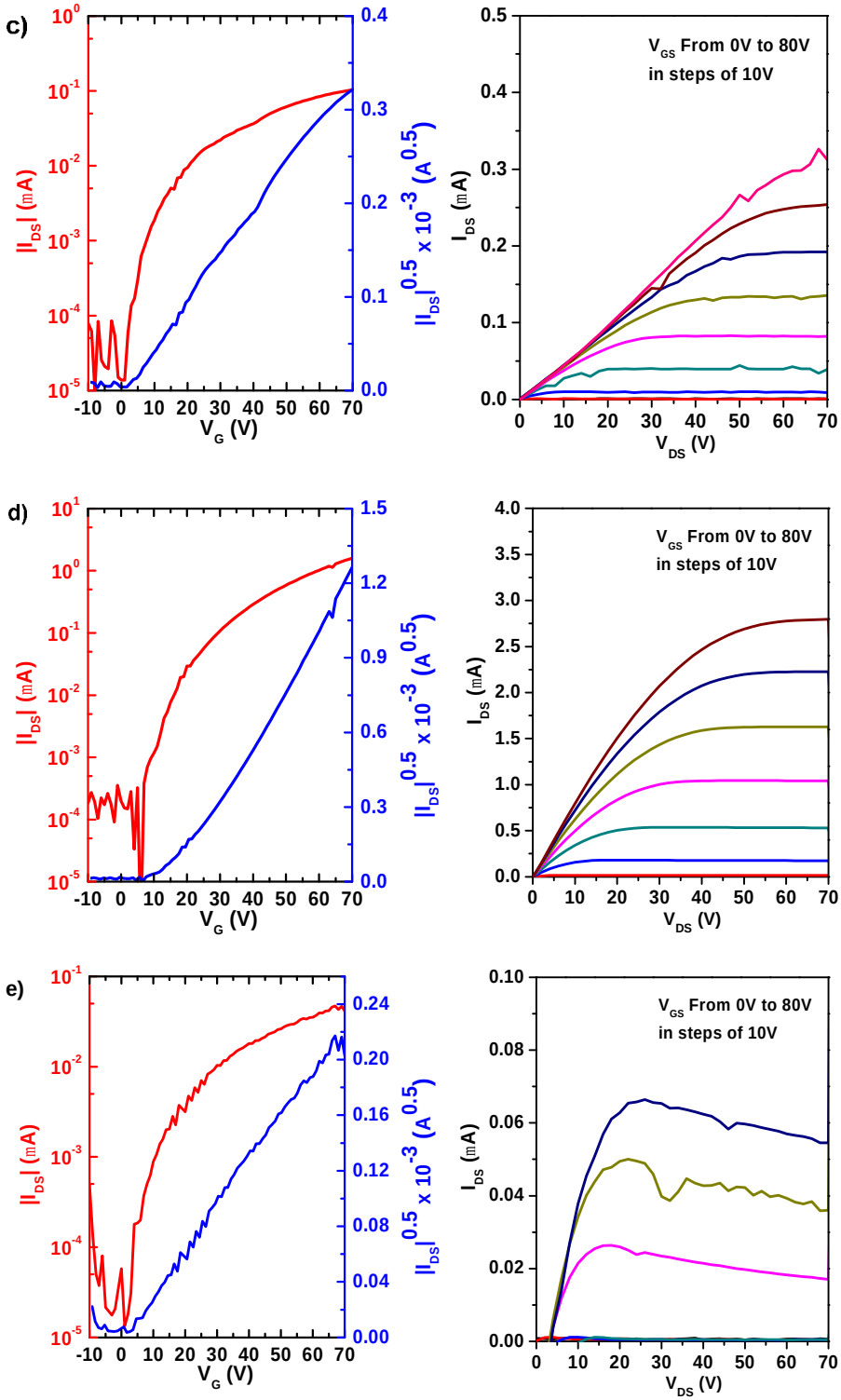

Figure 4.8.Transfer (V_D = 70 V, left) and output (right) characteristics of OFET devices from **4-1a** (a), **4-1b** (b), **4-2** (c), **4-3** (d) and **4-4** (e).

The devices of **4-1a**, **4-1b** and **4-2** – **4-4** all operate in *n*-channel region, and

their characteristic data are summarized in Table 4.3. The as-spun thin film devices based on **4-1a** and **4-1b** on OTMS treated substrate showed high electron mobilities of about 0.01-0.012 $cm^2V^{-1}s^{-1}$, which renders them attractive for low temperature process and facilitates device fabrication for organic electronics. Upon thermal annealing, the device performance slightly decreases. For thin films of **4-2** and **4-3**, when annealing at 150 ^oC, the devices exhibited relatively higher average electron mobilities (0.0028 $cm^2V^{-1}s^{-1}$ for **4-2**, and 0.016 $cm^2V^{-1}s^{-1}$ for **4-3** on OTMS treated substrate) compared to the as deposited devices. Nonetheless, upon annealing at 100 ^oC, thin films of **4-4** showed much lower electron mobility (about 4×10^{-4} $cm^2V^{-1}s^{-1}$). The current on/off ratio for all the devices is about 10^4 – 10^5, and threshold voltage is around 10-20 V.

Table 4.3. The electron mobilities (μ_e), threshold voltages (V_T), and current on/off ratios ($I_{on/off}$) of OFET devices based on **4-1a**–**b** and **4-2** – **4-4** measured in nitrogen and in air.

	Surface treatment	T_{Anneal} / ^oC	In N_2			In air		
			μ_e / $cm^2V^{-1}s^{-1}$	V_T / V	$I_{on/off}$	μ_e / $cm^2V^{-1}s^{-1}$	V_T / V	$I_{on/off}$
4-1a	ODTS	As-spun	0.006	15	10^5	0.0008	45	10^4
	OTMS	As-spun	0.012	15	10^5	0.002	25	10^4
4-1b	ODTS	As-spun	0.0064	20	10^5	5×10^{-5}	26	10^4
	OTMS	As-spun	0.01	15	10^5	0.002	36	10^4

4-2	ODTS	150	0.001	10	10^4	0.0002	8	10^3
	OTMS	150	0.0028	10	10^4	0.001	12	10^4
4-3	ODTS	150	0.004	10	10^4	0.001	20	10^5
	OTMS	150	0.016	18	10^5	0.006	16	10^5
4-4	ODTS	100	2×10^{-5}	5	10^3	5×10^{-6}	20	10^3
	OTMS	100	4×10^{-4}	5	10^4	1×10^{-4}	20	10^3

Thin film morphology and solid state microstructure were characterized by tapping-mode atomic force microscopy (AFM) and XRD. The thin films of **4-1a**, **4-1b** and **4-2** – **4-4** exhibited intense and sharp Bragg reflections in XRD patterns (Figure 4.9), which are correlated to a lamellar packing structure with interlayer distance of 3.15, 3.45, 3.29, 1.94 and 2.1 nm, respectively. AFM images of the thin films revealed polycrystalline grains with different shapes (Figure 4.10). Thin films of and **4-2** and **4-4** exhibited relatively larger grain boundary, and thus poor FET performance. On the other hand, the liquid crystalline **4-1a**, **4-1b** and **4-3** showed more continuous thin films and higher charge carrier mobilities. The devices operated in air showed slight decrease of electron mobility and on/off ratio (Table 4.3). For **4-2** and **4-3**, the threshold voltage almost did not shift when tested in air after storing (Figure 4.11). The good device stability must be ascribed to the low-lying LUMO energy levels of these naphthalene imide derivatives.

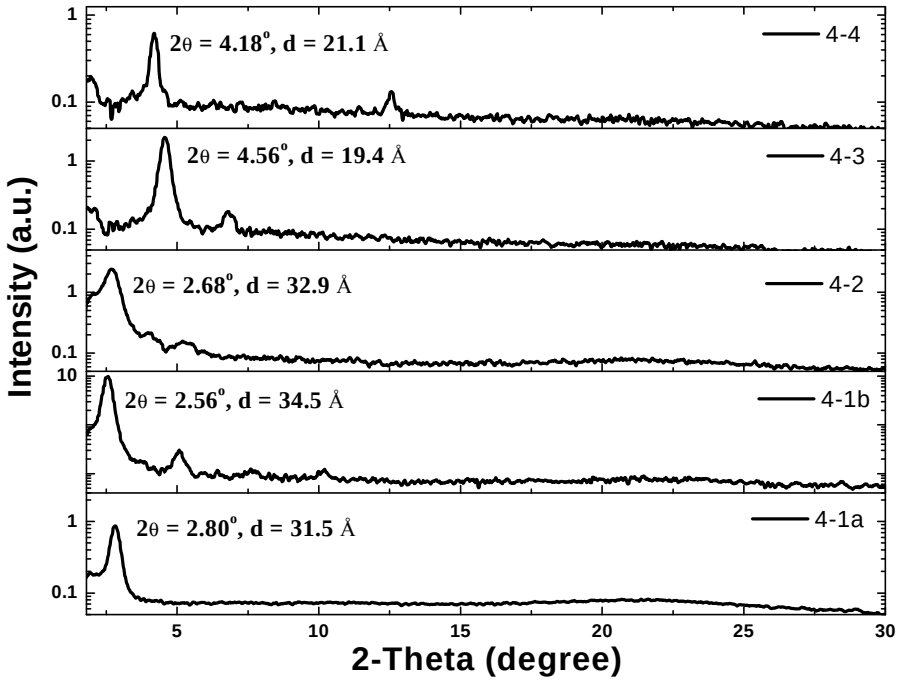

Figure 4.9. X-ray diffraction patterns for the thin films of **4-1a**, **4-1b** (as-spun), **4-2** – **4-3** (annealed at 150 °C) and **4-4** (annealed at 100 °C).

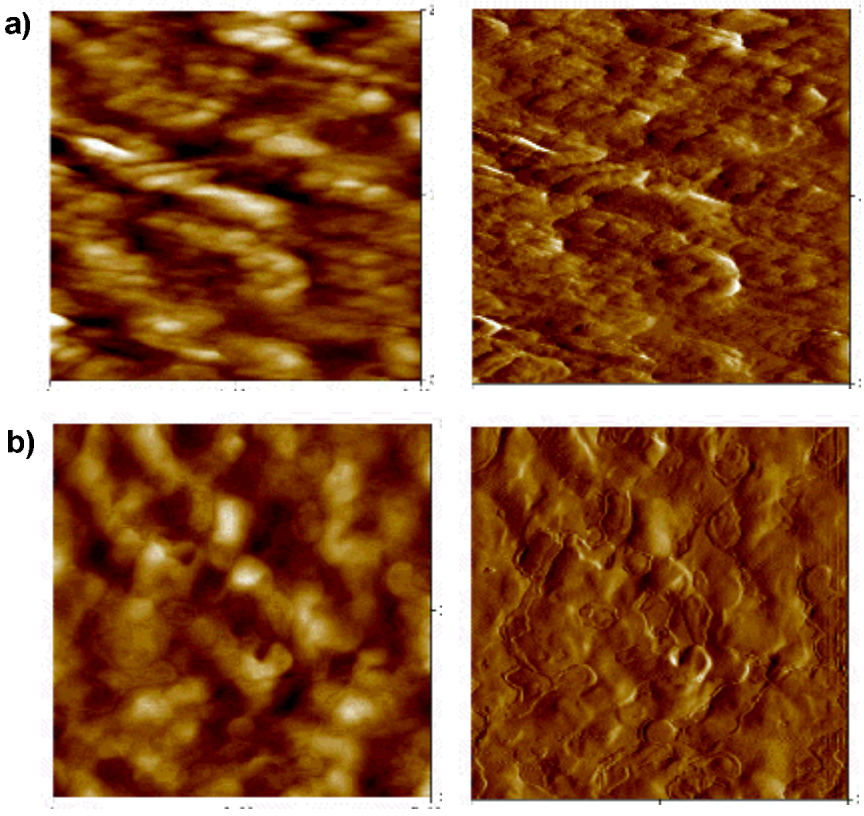

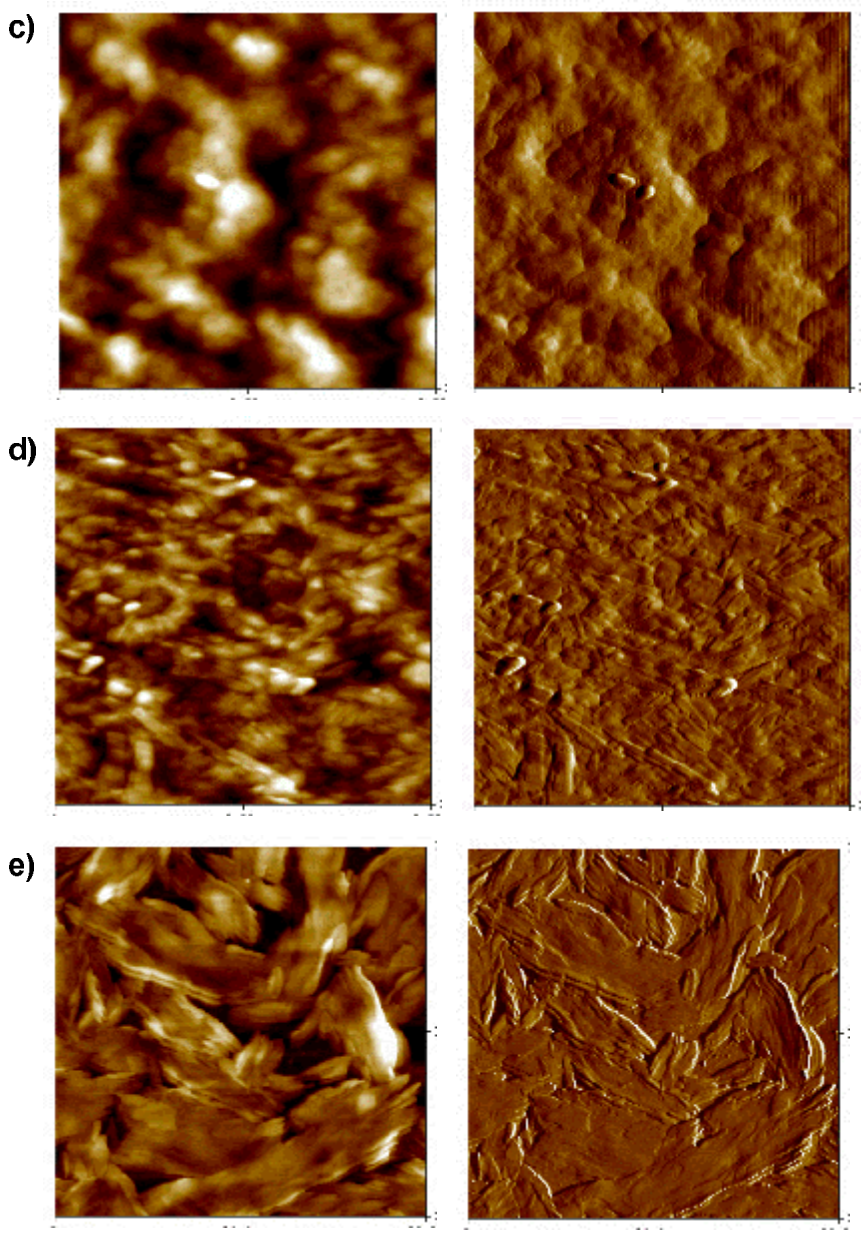

Figure 4.10. AFM images (height and amplitude images, 2μm×2μm) of the thin films of a) **4-1a** (as-spun), b) **4-1b** (as spun), c) **4-2** (annealed at 150 ^{o}C), d) **4-3** (annealed at 150 ^{o}C) and e) **4-4** (annealed at 100 ^{o}C).

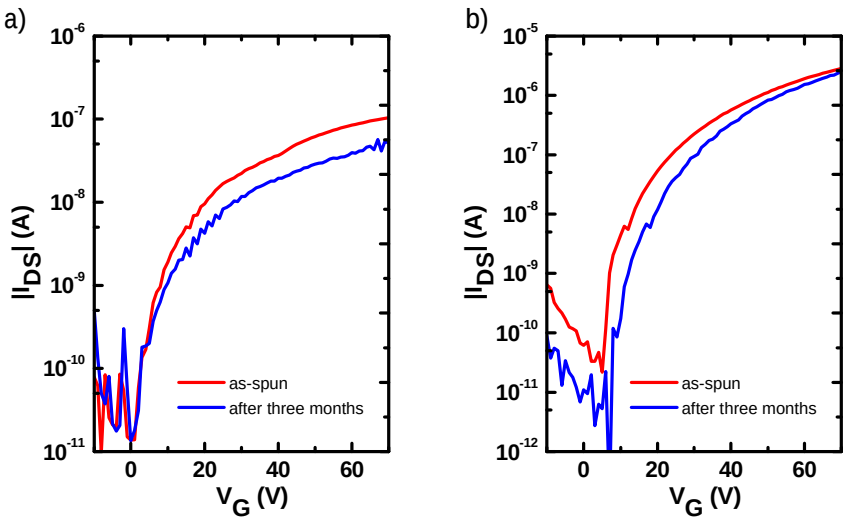

Figure 4.11. Transfer characteristics of thin films **4-2** (a) and **4-3** (b) on OTMS treated substrates annealed at 150 ^{o}C for as spun conditions (red) and after storing in N_2 for three months (blue).

4.3 Conclusions

In summary, a series of unsymmetric naphthalene imide derivatives **4-1a**, **4-1b** and **4-2** – **4-5** with high electron affinities were synthesized and used in air-stable n-channel OFETs. It was found that liquid crystalline compounds **4-1a**, **4-1b** and **4-3** showed good performance with electron mobility up to 0.016 cm^2 $V^{-1}s^{-1}$ and current on/off ratios of 10^4-10^5. These compounds can be easily processed from solution at low temperature, indicating their promising applications in solution processed organic electronics.

4.4 Experimental

4.4.1 General

7-octyl-1H-isochromeno[6,5,4-*def*]isoquinoline-1,3,6,8(7H)-tetraone (**4-6**), di-amine 5,6-diamino-2-(3,7-dimethyloctyl)isoindoline-1,3-dione (**4-7a**), 5,6-diamino-2-(2-decyltetradecyl)isoindoline-1,3-dione (**4-7b**), benzo[*c*][1,2,5]thiadiazole-5,6-dicarbonitrile (**4-8**), benzo[*c*][1,2,5]thiadiazole-4,7-dicarbonitrile (**4-10**) and 4,5-dinitrobenzene-1,2-diamine (**4-13)** were prepared according to literature procedure.[5-6]

All NMR spectra were recorded on Bruker AMX500 at 500 MHz and Bruker ACF300 at 300 MHz spectrometers. ^{1}H NMR and ^{13}C NMR spectra were recorded in CDCl3 and DMSO-d^{6}. All chemical shifts are quoted in ppm, using the residual solvent peak as a reference standard. Mass spectra were recorded in EI mode and high resolution mass spectra were recorded with EI source. Matrix-assisted laser desorption ionization time-of-flight (MALDI-TOF) analysis was performed on a Bruker Autoflex II MALDI-TOF instrument by using 1,8,9-trihydroxyanthracene as matrix and Pepmix as internal standard or external standard. UV-vis absorption and fluorescence spectra were recorded on Shimadzu UV-1700 and RF-5301 spectrometers in HPLC pure solvents. Cyclic voltammetry was performed on a CHI 620C electrochemical analyzer with a three-electrode cell in a solution of 0.1 M tetrabutylammonium hexafluorophosphate (Bu_4NPF_6) dissolved in dry DCM at a scan rate of 100 mV s^{-1}. A gold electrode with a diameter of 2 mm, a Pt wire and an Ag/AgCl electrode were used as the working

electrode, the counter electrode and the reference electrode, respectively. The potential was calibrated against the ferrocene/ferrocenium couple. Thermogravimetric analysis was carried out on a TA instrument 2960 at a heating rate of 10 °C/min under N_2 flow, differential scanning calorimetry was performed on a TA instrument 2920 at a heating/cooling rate of 10 °C/min under N_2 flow. The initial phase transitions and corresponding temperatures for these compounds were determined by an OLYMPUS BX51 polarizing optical microscope equipped with a Linkam TP94 programmable hot stage. VT X-ray diffraction studies were carried out on a Bruker-AXS D8 ADVANCE Powder X-ray diffractometer with Anton Paar Model HTK 1200 High Temperature Chamber and room temperature XRD measurements were performed on a Bruker-AXS D8 DISCOVER with GADDS Powder X-ray diffractometer, both with Cu Kα radiation.

Top-contact, bottom-gate OFET devices were prepared on the p+ silicon wafer and 200 nm thermal SiO_2 layer serves as the gate dielectric. The SiO_2/Si substrate was cleaned with acetone and isopropanol, then immersed in a piranha solution for 8 minutes, and washed by deionized water. The clean substrate was then treated with octadecyltrimethoxysilane (OTMS) spin coated from 10 mM trichloroethylene solution followed by treatment with ammonia for 7h, or with octadecyltrichlorosilane (ODTS) immersed in 3 mM hexadecane solution for 16h in N_2. The semiconductor layer was deposited on top of the OTMS or ODTS-modified dielectric surface by spin-casting from the solution of active

component in chloroform (0.8-1 wt%). Subsequently, gold source/drain electrodes were deposited by thermal evaporation through a metal shadow mask to create a series of FETs (W = 1 mm, L = 50-100 um). The FET devices were then characterized using a Keithley SCS-4200 semiconductor parameter analyzer in the N_2 glovebox. The FET mobility was extracted using the following equation in the saturation regime from the gate sweep: $I_D = W/(2L)C_i\mu(V_G - V_T)^2$, where I_D is the drain current, μ is the field-effect mobility, C_i is the capacitance per unit area of the gate dielectric layer (SiO_2, 200 nm, C_i = 17 nF cm^{-2}), and V_G and V_T are gate voltage and threshold voltage, respectively. W and L are respectively channel width and length.

4.4.2 Synthesis of the intermediates and target molecules

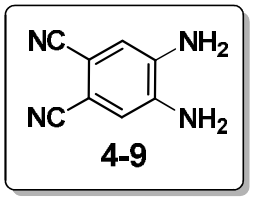

4-9

4,5-diaminophthalonitrile

A mixture of benzo[*c*][1,2,5]thiadiazole-5,6-dicarbonitrile **4-8** (0.930 g, 5.0 mmol), ion powder (3.360 g, 60 mmol, 12 eq), and glacial acetic acid (20 mL) was heated under reflux for around 30 min. It was then cooled to room temperature, basified with a solution of NaOH, and extracted with ether. The combined ether extract was washed with a solution of NaOH and water, dried over anhydrous Na_2SO_4, and the solvent was removed to afford a yellow residue

and purified with column chromatography using Hex/THF (1:1) to give the final product **4-9** as white solid (0.632 g,. 80%). ^{1}H NMR (500 MHz, DMSO-d^6): δ ppm = 6.87 (s, 2H) 5.87 (br, 4H); ^{13}C NMR (125 MHz, DMSO-d^6): δ ppm = 139.06, 117.82, 115.52, 101.39. EI-MS (m/z): calcd. for $C_8H_6N_4$: 158.0592; found 158.1.

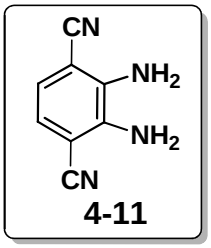

4-11

2,3-diaminoterephthalonitrile

A mixture of benzo[*c*][1,2,5]thiadiazole-4,7-dicarbonitrile **4-10** (0.930 g, 5.0 mmol), ion powder (3.360 g, 60 mmol, 12 eq), and glacial acetic acid (20 mL) was heated under reflux for around 30 min. It was then cooled to room temperature, basified with a solution of NaOH, and extracted with ether. The combined ether extract was washed with a solution of NaOH and water, dried over anhydrous Na_2SO_4, and the solvent was removed to afford a yellow residue and purified with column chromatography using Hex/THF (1:1) to give the final product **4-11** as white solid (0.672 g, 85%). ^{1}H NMR (500 MHz, DMSO-d^6): δ ppm = 6.71 (s, 2H), 6.06, (br, 4H); ^{13}C NMR (125 MHz, DMSO-d^6): δ ppm = 139.62, 118.48, 117.66, 95.05. HR-EI-MS (m/z): calcd. for $C_8H_6N_4$: 158.0592; found 158.0586 (error = -0.4 ppm). Elemental Analysis: calcd. for $C_{64}H_{76}N_6O_4$: C,

60.75; H, 3.82; N, 35.42; found: C, 60.47; H, 3.89; N, 35.19.

General procedure for condensation reaction between anhydride and diamine

A mixture of **4-6** (1.0 equiv), and diamine (1.0 equiv) were refluxed in HOAc under Ar(g) atmosphere for overnight. Upon cooling, the suspension was dissolved with DCM and water, and extracted with DCM. The combined organic phases were washed with saturated NaCl (aq), and was finally dried over Na_2SO_4, concentrated under reduced pressure to give a residue and purified with column chromatography to give the title product.

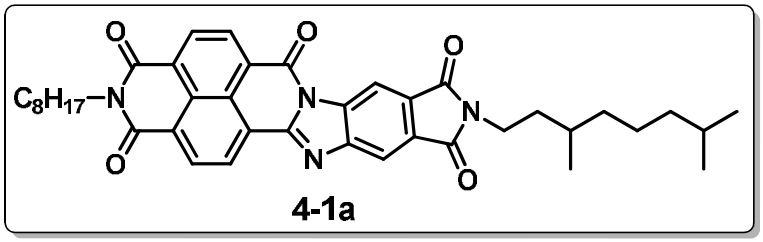

4-1a

10-(3,7-dimethyloctyl)-2-octyl-1H-benzo[*lmn*]isoindolo[5',6':4,5]imidazo[2,1-*b*][3,8]phenanthroline-1,3,6,9,11(2H,10H)-pentaone

4-6 (0.4 mmol, 152 mg), diamine **4-7a** (0.4mmol, 127 mg). **4-1a**, Golden yellow solid (230 mg, 87%).

^{1}H NMR (500 MHz, $CDCl_2CDCl_2$, 373 K): δ ppm = 9.07 (d, *J* = 8.0 Hz, 2H), 9.01 – 8.98 (m, 2H), 8.88 - 8.83 (m, 2H), 8.34 (s, 1H), 4.26 (t, *J* = 7.0 Hz, 2H), 3.81 (d, *J* = 7.5 Hz, 2H), 1.87- 1.81 (m, 2H), 1.64 - 1.23 (m, 20H), 1.05 (d, *J* = 6.5 Hz, 3H),

0.96 - 0.92 (m, 9H); ^{13}C NMR (125 MHz, $CDCl_2CDCl_2$, 373K): δ ppm = 167.10, 162.22, 162.05, 158.72, 150.44, 147.80, 135.25, 131.70, 131.19, 130.56, 130.26, 129.96, 128.28, 127.61, 127. 24, 126.36, 125.79, 125.63, 124.35, 120.13, 116.02, 111.42, 40.88, 39.04, 36.84, 36.66, 35.28, 31.43, 30.76, 28.91, 28.77, 27.88, 27.59, 26.82, 24.23, 22.27, 22.22. MALDI-TOF-MS (m/z): calcd. for $C_{40}H_{44}N_4O_5$: 660.3312; found 661.3343 $[M+H]^+$. Elemental Analysis: calcd. for $C_{64}H_{76}N_6O_4$: C, 72.70; H, 6.71; N, 8.48; found: C, 72.57; H, 6.61; N, 8.61.

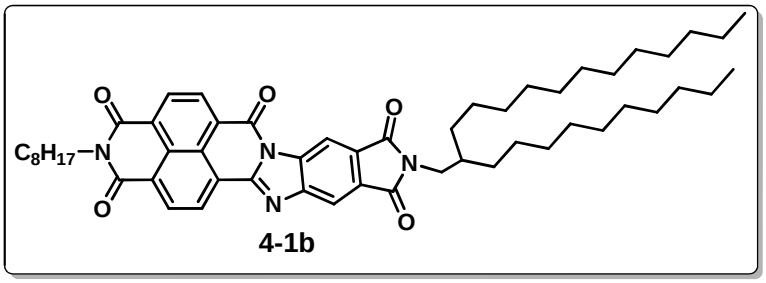

4-1b

10-(2-decyltetradecyl)-2-octyl-1H-benzo[*lmn*]isoindolo[5',6':4,5]imidazo[2,1-*b*][3,8]phenanthroline-1,3,6,9,11(2H,10H)-pentaone

4-6 (0.375 mmol, 143 mg), diamine **4-7b** (0.375 mmol, 192 mg). **4-1b**, Golden yellow solid (282 mg, 88%).

^{1}H NMR (500 MHz, $CDCl_3$, 323 K): δ ppm = 8.94 - 8.91 (m, 2H), 8.84 (s, 1H), 8.81 - 8.76 (m, 2H), 8.17 (s, 1H), 4.21 (t, *J* = 8.0 Hz, 2H), 3.63 (d, *J* = 7.0 Hz, 2H), 1.93 (br, 1H), 1.81 - 1.75(m, 2H), 1.49 - 1.24 (m, 50H), 0.90 - 0.85 (m, 9H); ^{13}C NMR (125 MHz, $CDCl_3$, 323 K): δ ppm = 167.75, 167.73, 162.50, 162.34, 158.84, 150.52, 147.84, 135.33, 132.07, 131.52, 130.88, 130.31, 130.02, 128.45, 127.82, 127.42, 126.46, 125.91, 125.83, 124.43, 116.18, 111.73, 42.88, 41.15, 37.22,

31.92, 31.82, 29.98, 29.68, 29.65, 29.63, 29.59, 29.32, 29.28, 29.18, 28.16, 27.15, 26.45, 22.64, 22.61, 13.99. HR-EI-MS (m/z): calcd. for $C_{54}H_{72}N_4O_5$: 856.5503; found 856.5536 (error = 3.9 ppm). Elemental Analysis: calcd. for $C_{64}H_{76}N_6O_4$: C, 75.66; H, 8.47; N, 6.54; found: C, 75.37; H, 8.29; N, 6.38.

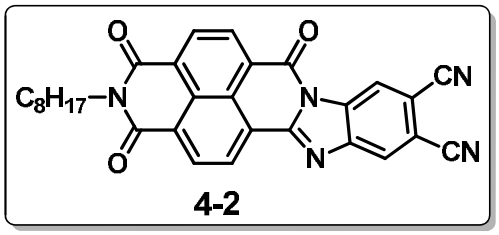

2-octyl-1,3,6-trioxo-1,2,3,6-tetrahydrobenzo[*lmn*]benzo[4,5]imidazo[2,1-*b*][3,8]phenanthroline-9,10-dicarbonitrile

4-6 (0. 50 mmol, 190 mg), diamine **4-9** (0.50 mmol, 79 mg). **4-2**, Yellow solid (202 mg, 81%).

^{1}H NMR (500 MHz, $CDCl_3$, 273K): δ ppm = 9.08 (d, *J* = 7.5 Hz, 1H), 9.04 – 9.02 (m, 2H), 8.91 - 8.88 (m, 2H), 8.35 (s, 1H), 4.22 (t, *J* = 7.5 Hz, 2H), 1.79 - 1.73 (br, 2H), 1.56 - 1.28(m, 10H), 1.49 - 1.24 (m, 50H), 0.88 (t, *J* = 6.5 Hz, 3H); ^{13}C NMR (125 MHz, $CDCl_3$, 323K): δ ppm = 162.40, 162.25, 159.04, 152.45, 146.20, 134.06, 132.66, 131.65, 131.12, 128.97, 128.82, 127.58, 126.70, 126.64, 126.28, 126.05, 123.80, 121.82, 115.49, 115.33, 113.42, 112.58, 41.25, 31.80, 29.26, 29.16, 28.16, 27.12, 22.60, 13.96. HR-EI-MS (m/z): calcd. for $C_{30}H_{23}N_5O_3$: 501.1801; found 501.1814 (error = 2.6 ppm). Elemental Analysis: calcd. for $C_{64}H_{76}N_6O_4$: C, 71.84; H, 4.62; N, 13.96; found: C, 71.99; H, 4.89; N, 13.68.

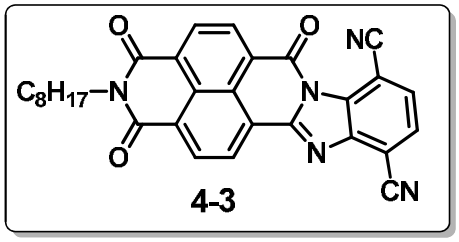

2-octyl-1,3,6-trioxo-1,2,3,6-tetrahydrobenzo[*lmn*]benzo[4,5]imidazo[2,1-*b*][3,8]phenanthroline-8,11-dicarbonitrile

4-6 (0. 5 mmol, 190 mg), diamine **4-11** (0.5 mmol, 79 mg). **4-3**, Yellow solid (210 mg, 84%).

^{1}H NMR (500 MHz, $CDCl_3$, 273K): δ ppm = 9.17 (d, *J* = 8.0 Hz, 1H), 9.05 (d, *J* = 7.5 Hz, 1H), 8.89 - 8.86 (m, 2H), 7.98 (d, *J* = 8.0 Hz, 1H) 7.92 (d, *J* = 8.0 HZ, 1H), 4.21 (t, *J* = 7.5 Hz, 2H), 1.79 - 1.73 (br, 2H), 1.46 - 1.25(m, 10H), 0.88 (t, *J* = 7.5 Hz, 3H); ^{13}C NMR (125 MHz, $CDCl_3$, 273K): δ ppm = 162.42, 162.25, 158.73, 151.30, 146.49, 133.02, 132.59, 131.70, 131.18, 130.99, 130.05, 129.13, 128.64, 127.24, 126.36, 125.93, 125.76, 123.59, 115.83, 114.52, 109.13, 104.88, 41.15, 31.79, 29.27, 29.16, 28.09, 27.06, 22.62, 14.07. HR-EI-MS (m/z): calcd. for $C_{30}H_{23}N_5O_3$: 501.1801; found 501.1814 (error = 2.6 ppm). Elemental Analysis: calcd. for $C_{64}H_{76}N_6O_4$: C, 71.84; H, 4.62; N, 13.96; found: C, 71.77; H, 4.91; N, 13.77.

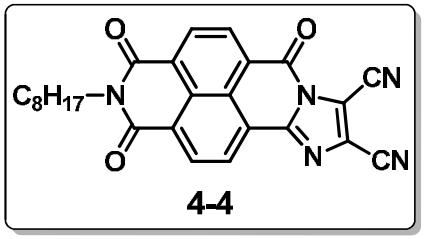

4-4

2-octyl-1,3,6-trioxo-1,2,3,6-tetrahydrobenzo[*lmn*]imidazo[2,1-*b*][3,8]phenanthroline-8,9-dicarbonitrile

4-6 (0. 5 mmol, 190 mg), diamine **4-12** (0.5 mmol, 79 mg). **4-4**, Yellow solid (210 mg, 84%).

^{1}H NMR (500 MHz, $CDCl_3$, 273 K): δ ppm = 9.04 (d, *J* = 7.5 Hz, 1H), 8.92 (d, *J* = 7.5 Hz, 1H), 8.90 (d, *J* = 8.0 Hz, 1H), 8.05 (d, *J* = 7.5 Hz, 1H), 4.20 (t, *J* = 7.5 Hz, 2H), 1.78 - 1.71 (m, 2H), 1.46 - 1.25 (m, 10H), 0.87 (t, *J* = 7.0 Hz, 3H); ^{13}C NMR (125 MHz, $CDCl_3$, 273 K): δ ppm = 162.12, 161.96, 156.68, 147.44, 134.29, 131.84, 131.10, 129.64, 128.75, 127.31, 127.14, 126.44, 125.09, 124.31, 122.37, 110.50, 109.38, 107.20, 41.23, 31.76, 29.22, 29.14, 28.05, 27.04, 22.60, 14.06. HR-EI-MS (m/z): calcd. for $C_{30}H_{23}N_5O_3$: 501.1801; found 501.1814 (error = 2.6 ppm). Elemental Analysis: calcd. for $C_{64}H_{76}N_6O_4$: C, 69.17; H, 4.69; N, 15.51; found: C, 69.36; H, 4.92; N, 15.53.

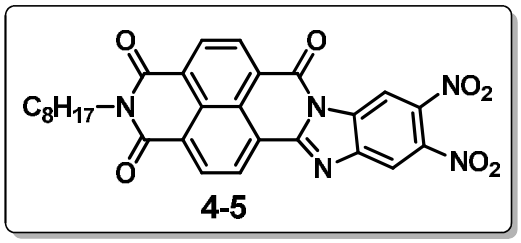

4-5

9,10-dinitro-2-octylbenzo[*lmn*]benzo[4,5]imidazo[2,1-*b*][3,8]phenanthroline-1

,3,6(2H)-trione

4-6 (0. 6 mmol, 228 mg), diamine **4-13** (0.6 mmol, 118 mg). **4-5**, Yellow solid (270 mg, 83%).

^{1}H NMR (500 MHz, $CDCl_3$, 273 K): δ ppm = 9.13 (s, 1H), 9.09 (d, *J* = 8.0 Hz, 1H), 9.04 (d, *J* = 8.0 Hz, 1H), 8.91 - 8.88 (m, 2H), 8.43 (s, 1H), 4.23 (t, *J* = 8.0 Hz, 2H), 1.80- 1.74 (br, 2H), 1.32 - 1.29(m, 10H), 0.88 (t, *J* = 7.0 Hz, 3H); ^{13}C NMR (125 MHz, $CDCl_3$, 273 K): δ ppm = 162.36, 162.20, 158.90,153.41, 145.47, 142.02, 141.13, 132.94, 132.78, 131.64, 131.11, 129.02, 128.86, 127.55, 126.75, 126.21, 125.84, 123.66, 117.57, 113.32, 41.25, 31.80, 29.26, 29.16, 28.15, 27.11, 22.60, 13.97. HR-EI-MS (m/z): calcd. for $C_{28}H_{23}N_5O_7$: 541.1597; found 541.1617 (error = 3.7 ppm). Elemental Analysis: calcd. for $C_{64}H_{76}N_6O_4$: C, 62.10; H, 4.28; N, 12.93; found: C, 62.28; H, 4.28; N, 12.83.

4.5 Reference

1. a) Hu, Y.; Gao, X.; Di, C-A.; Yang, X.; Zhang, F.; Liu, Y.; Li, H.; Zhu, D. Chem. Mater. **2011**, *23*, 1204. b) Chang, J.; Ye, Q.; Huang, K.-W.; Zhang, J.; Chen, Z.-K. ; Wu, J.; Chi, C. *Org. Lett.*, **2012**, *14*, 2964. c) Yue, W.; Lv, A.; Gao, J.; Jiang, W.; Hao, L.; Li, C.; Li, Y.; Polander, L. E.; Barlow, S.; Hu, W.; Di Motta, S.; Negri, F.; Marder, S. R.; Wang, Z. *J. Am. Chem. Soc.* **2012**, *134*, 5770.
2. Gao, X.; Di, C.-A.; Hu, Y.; Yang, X.; Fan, H.; Zhang, F.; Liu, Y.; Li, H.; Zhu,

D. *J. Am. Chem. Soc.* **2010**, *132,* 3697.

3. a) Deng, P.; Yan, Y.; Wang S.-D.; Zhang, Q. *Chem. Commun.*, **2012**, *48,* 2591. b) Ortiz, R. P.; Herrera, H.; Seoane, C.; Segura, J. L. ; Facchetti;A.; Marks, T. J. *Chem.–Eur. J.*, **2012**, *18*, 532.
4. Ortiz, R. o. P.;Herrera,H.; Blanco, R. l.;Huang,H.; Facchetti, A.; Marks, T. J.; Zheng, Y.; Segura, J. L. J. *Am. Chem. Soc*. **2010**, *132*, 8440.
5. a) Greenfield, S. R.; Svec, W. A.; Gosztola, D.; Wasielewisky, M. R. *J. Am. Chem. Soc*. **1996**, *118*, 6767. b) Shao, J.; Chang, J.; Chi. C. *Org. Biomol. Chem.*, **2012**, *10*, 7045. c) Cheeseman, G. W. H. *J. Chem. Soc.*, **1962**, 1170.
6. Pilgram, K.; Skiles, R. D.; *J. Heterocyclic Chem.*, **1974**, *11*, 777.
7. a) Chi, C.; Wegner, G. *Macromol. Rapid Commun.* **2005**, *26*, 1532. b) Chi, C.; Im, C.; Enkelmann, V.; Ziegler, A.; Lieser, G.; Wegner, G. *Chem-Eur. J.* **2005**, *11*, 6833.
8. Constantinides, C. P.; Koutentis, P. A.; Schatz, J. *J. Am. Chem. Soc*. **2004**, *126*, 16232.

Chapter 5

A Phthalimide-fused Naphthalene Dimide with High Electron Affinity for High Performance n-Channel Field Effect Transistor

5.1 Introduction

In chapter 4, a series of electron-deficient unsymmetrical naphthalene imide derivatives have been successfully synthesized, and the fabricated devices exhibit electron mobility of up to 0.016 $cm^2\ V^{-1}s^{-1}$, with current on/off ratios of 10^4-10^5, and threshold voltages of 10-20 V. However, the charge mobility still needs to be improved based on the unsymmetrical naphthalene imide derivatives.

Many results have proved that NDIs with electron-withdrawing groups can increase electron affinity and ambient stability of the device.[1-2] Previously, core-expanded NDIs along the naphthalene moiety have been extensively studied, and exhibited superior OFET performances based on the solution processed devices.[3-7] However, only few examples of expanded NDIs with an aromatic unit fused at the imide sites have been reported,[8-13] and most of them showed larger electron affinity compared to the unsubstituent NDIs. Among them, only few of them were applied for OFETs. For example, NDIs fused with thieno[3,4-*d*]imidazoles at the imide position showed high electron mobility of 0.35 $cm^2V^{-1}s^{-1}$ and NDIs fused with trifluoromethylbenzene group exhibited an electron mobility of 0.1 $cm^2V^{-1}s^{-1}$, both based on vacuum deposited films.[7,13] However, the performance of solution processed OFETs based on these materials was quite poor (μ_e = 4 × 10^{-5} to 3 × 10^{-3} $cm^2\ V^{-1}s^{-1}$) compared to vacuum deposited ones. Moreover, air stability of the devices was still a problem due to their low electron affinity. In order to develop new NDI-based *n*-type

semiconductor for air-stable, solution-processed *n*-channel OFETs, in this chapter, we show a new NDI derivative **NDIIC24** in which the two imide sites of the NDI are fused with diamino- phthalimide (Scheme 5.1). The molecular design is based on the following considerations: 1) extension of the π-conjugation length via fusion ensures the planar structure and promotes intermolecular π-π stacking, which is benefit for the efficient charge transport; 2) the electron-deficient imide groups and imine (=N-) units could increase the electron affinity, which is important for electron injection and air stability of the devices; 3) the *N*-alkyl chains at the end could tune the solubility and crystallinity of the materials.

5.2 Results and Discussion

Compound **NDIIC24** was synthesized as an orange solid in 93% yield by simple condensation reaction between the commercially available 1,4,5,8-naphthalenetetracarboxylic dianhydride **5-1** and the diamine 5,6-diamino-2-(2-decyltetradecyl)isoindoline-1,3-dion **5-2** which was recently reported by us (Scheme 5.1), the synthesis of **5-2** was also shown in chpter 3.[14] **NDIIC24** showed moderate solubility in $CHCl_3$ and THF, which allows us to perform various characterizations in solutions and fabricate OFET devices by convenient solution-based techniques. ^{1}H NMR spectrum showed that two isomers, *cis*-/*trans*-**NDIIC24**, coexist in an approximately 1:1 ratio, which however cannot be separated by column chromatography (see Appendix).

Replacement of the branched 2-decyltetradecyl chain by shorter chains such as 2-hexyldecyl or 3,7-dimethyloctyl led to insoluble materials, indicating the strong intermolecular interaction between the rigid cores.

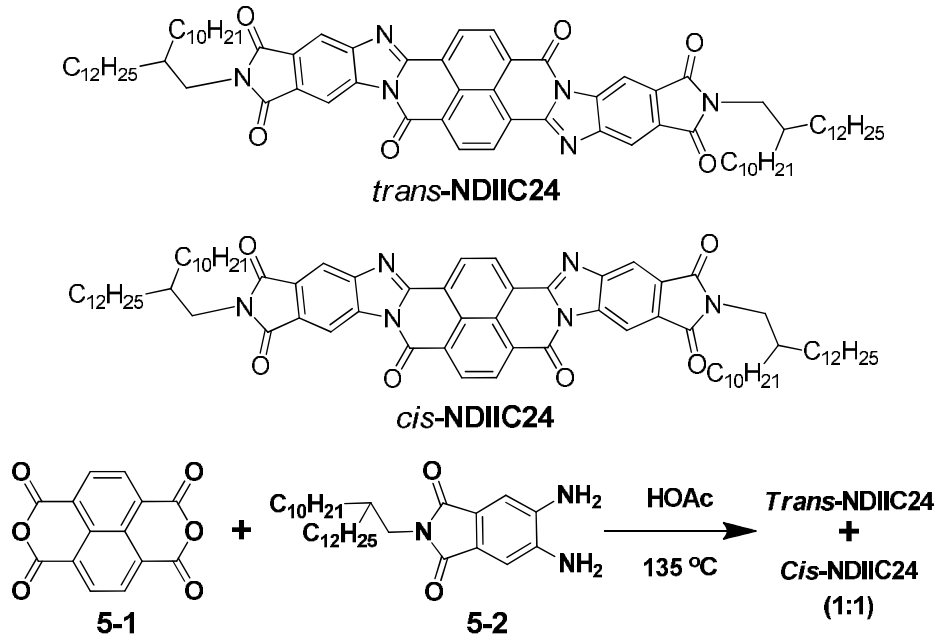

Scheme 5.1 Synthetic route for **NDIIC24**.

NDIIC24 shows well-resolved UV-vis absorption and emission bands in chloroform solution, exhibiting the longest absorption maximum at 532 nm and emission maximum at 548 nm (Figure 5.1). It is interesting to note that **NDIIC24** shows high fluorescence quantum yield of 44% in $CHCl_3$. Moreover, the strong fluorescence could even be observed in the solid state.

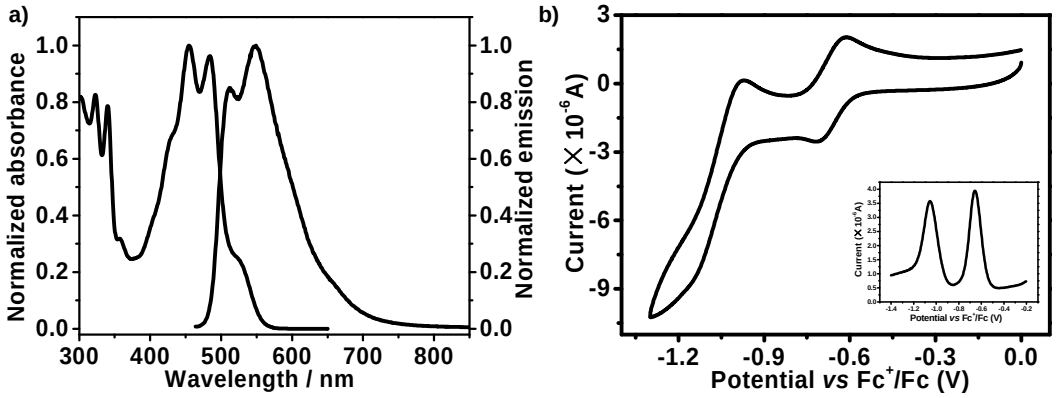

Figure 5.1 (a) UV-vis absorption and emission spectra of **NDIIC24** in chloroform; (b) Cyclic voltammograms of **NDIIC24** in dry DCM with 0.1 M Bu_4NPF_6 as supporting electrolyte, a gold electrode with a diameter of 2 mm, a Pt wire, and an Ag/AgCl electrode were used as the working electrode, the counter electrode, and the reference electrode, respectively, with a scan rate at 50 mV/s.

The electrochemical properties of **NDIIC24** were investigated by cyclic voltammetry (CV) and differential pulse voltammetry (DPV) in dichloromethane (DCM). As shown in Figure 5.1, two quasi-reversible reduction waves were observed for **NDIIC24**, with half-wave potential $E_{red}^{1/2}$ at -0.66 V and -1.06 V (*vs* Fc^+/Fc). The LUMO energy level was derived as -4.21 eV from the onset of the first reduction wave.[15] No obvious redox waves were observed upon anodic scan up to 1.80 V due to the electron deficient character of this compound. The low-lying LUMO energy level (i.e., high electron affinity) of this compound indicates that it can serve as promising candidate for *n*-channel OFETs with good air stability.[16] Thermogravimetric analysis of **NDIIC24** revealed that it was thermally stable up to 443 ^oC with 5% weight loss (Figure 5.2).

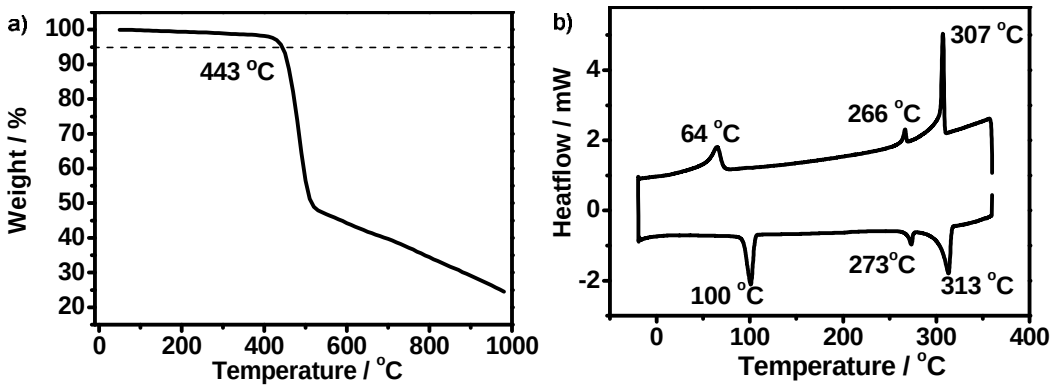

Figure 5.2 a) TGA plot of **NDIIC24** with a heating rate of 10 °C/min in nitrogen; b) DSC plot of **NDIIC24** with a heating/cooling rate of 10 °C/min in nitrogen

Bottom-gate, top-contact OFETs were fabricated on p+-Si wafer with 200 nm thermal grown SiO_2 as the dielectric layer. The dielectric surface was treated with (octadecyltrimethoxysilane (OTMS) or octadecyltrichlorosilane (ODTS), and then thin film of **NDIIC24** were deposited by spin coating from 0.6-1.0 wt% $CHCl_3$ solution. The devices were completed by patterning the Au source/drain electrodes using a shadow mask. The devices exhibited typical *n*-type behavior with an average electron mobility of 0.056 $cm^2V^{-1}s^{-1}$ for the devices on OTMS-treated substrate measured in nitrogen (Table 5.1). This value is one order of magnitude higher than that of solution processed devices based on thieno[3,4-*d*]imidazole fused NDIs (μ_e = 0.003 $cm^2V^{-1}s^{-1}$).[7] The devices on ODTS-modified substrate generally gave lower mobilities. The current on/off ratio is around 10^6, and threshold volatge (V_T) is about 10-20 V. The output and transfer characteristics of the device are shown in Figure 5.3. Well defined saturation behavior could be observed in the output plot, and almost linear

behavior at low voltage indicated a small injection barrier between Au electrodes and active layer. The transfer curves exhibited a small hysteresis between forward and reverse curves due to less trap density on the dielectric surface.

Table 5.1 OFET device performance based on **NDIIC24** measured under different conditions.

Surface treatment	T_{aneal} / °C	In N_2			In air		
		μ / $cm^2 V^{-1} s^{-1}$	V_T / V	$I_{On/off}$	μ / $cm^2 V^{-1} s^{-1}$	V_T / V	$I_{On/off}$
OTMS	As spun	0.056	9-12	1×10^6	0.05	22-26	3×10^6
OTMS	100	0.038	12-15	4×10^3	0.036	21-24	1×10^6
ODTS	As spun	0.012	8-10	1×10^5	0.006	22-24	2×10^5
ODTS	100	0.008	14-16	4×10^3	0.003	24-27	3×10^3

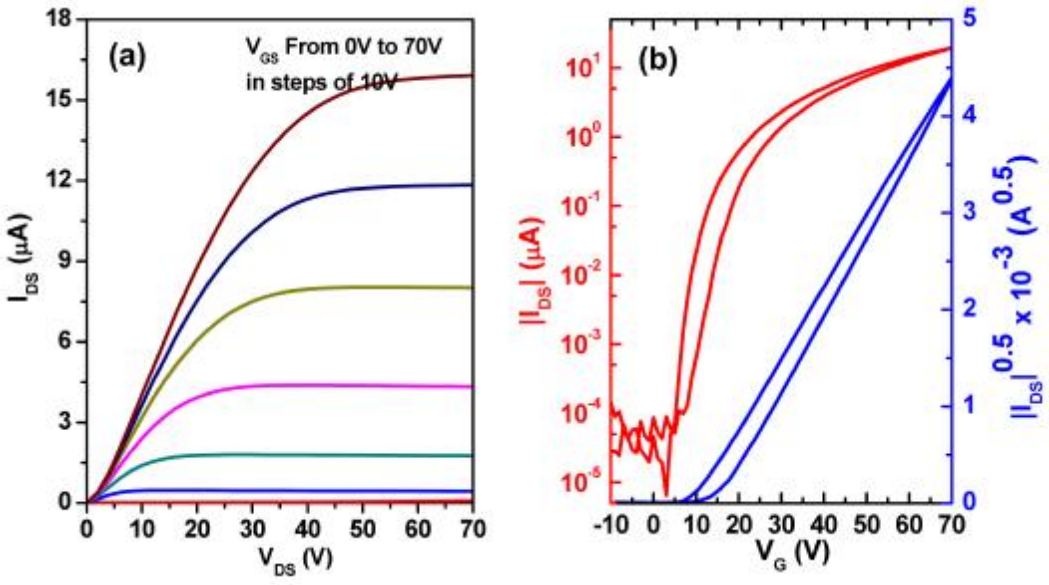

Figure 5.3 Output and transfer (V_{DS} = 70 V) characteristics of a typical OFET device based on **NDIIC24**.

The air stability of OFET devices based on **NDIIC24** was checked in the ambient conditions. When device exposed to air, the transfer curve showed almost no shift due to its high electron affinity, as well as the electron mobility (Figure 5.4 and Table 5.1). After the device storing in N_2 atmosphere for 6 months, electron mobility of 0.04 $cm^2V^{-1}s^{-1}$ was still maintained (70% of the pristine value) with a stable on/off current ratio of 10^5 (Figure 5.5). The bias stress stability of the device was studied with a constant gate bias of 20 V. Small V_T shift was observed upon stress conditions (Figure 5.4), indicating good stress stability of this material. The current on/off cycle test of OFET devices of this compound was also evaluated for 1200 s, and only slight current degradation in the initial stage was observed (Figure 5.4), indicating good operating stability of this material.

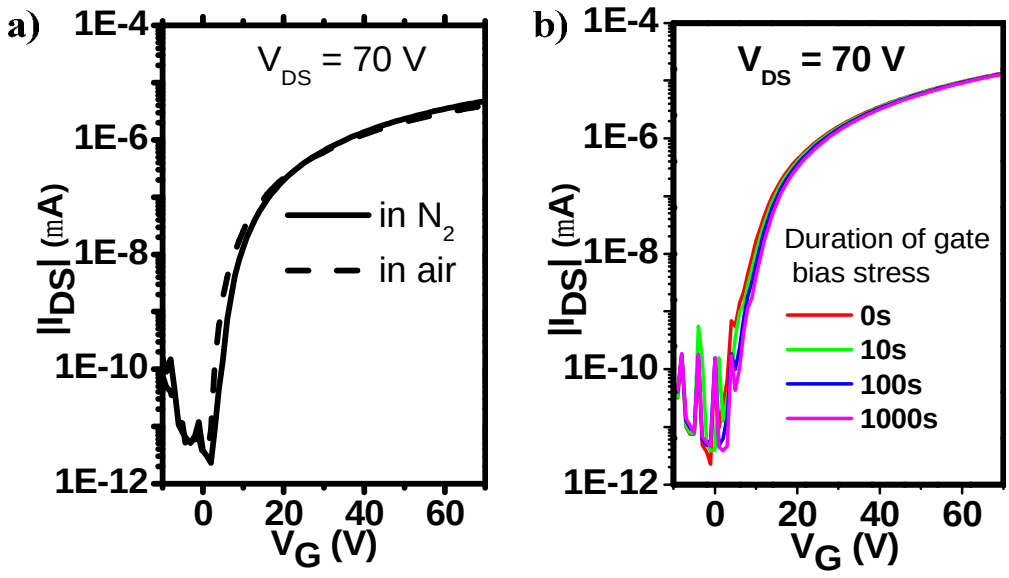

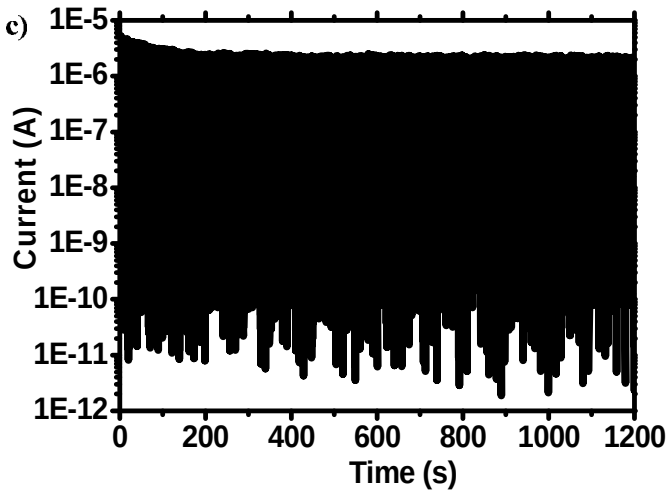

Figure 5.4 (a) Transfer characteristics of an OFET device based on **NDIIC24** measured in N_2 and air conditions; (b) stability of transfer characteristics of the device under different bias stress conditions; (c) cyclic stability of the device during continuous on/off cycles for 1200 s (V_{ON} = 60 V, V_{OFF} = 0 V).

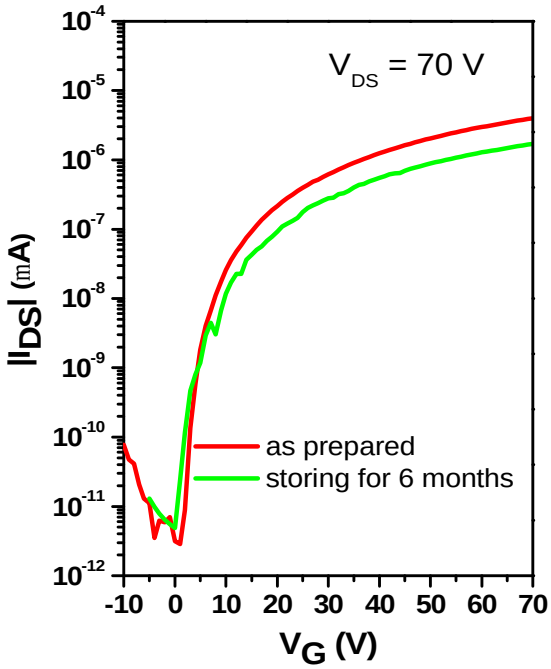

Figure 5.5 The transfer characteristics of the OFET device tested after storing in N_2 for 6 months.

The film morphology and microstructure of the spin-coated thin film were characterized by tapping-mode AFM and X-ray diffraction (XRD), respectively

(Figure 5.6). AFM measurements showed that the thin film exhibited uniform and interconnected grains with grain sizes around 400 nm. After thermal annealing at 100 ^{o}C, no obvious change was observed for the surface morphology. However, XRD patterns of the thin film showed an detectable shift of the *d*-spacing of primary peak from 28.1 Å to 26.7 Å, probably due to increased molecular tilting on the dielectric surface and/or larger degree of *N*-alkyl chain interdigitation. In addition, annealing did not improve the device performance in this case (Table 5.1).

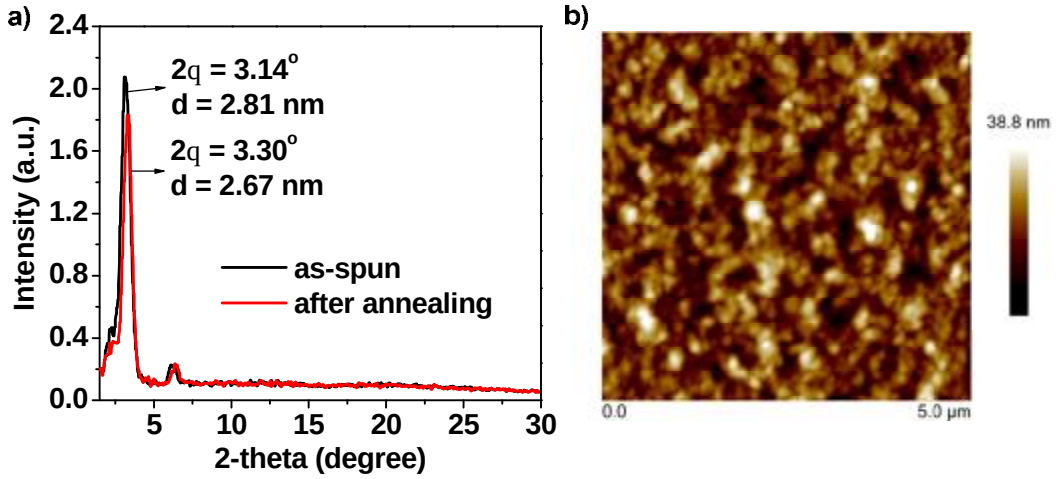

Figure 5.6 (a) X-ray diffraction patterns of spin coated thin films of **NDIIC24** on OTMS-treated substrates before and after thermal annealing at 100 ^{o}C; (b) tapping mode AFM images (height mode) of the thin films of **NDIIC24** on OTMS modified SiO_2/Si substrate.

CMOS inverters were accomplished by combining two transistors with *n*-type **NDIIC24** as *n*-mos and *p*-type TIPS-pentacene as *p*-mos through solution processed methods (Figure 5.7). Due to the difference in mobility between

NDIIC24 (~0.05 $cm^2V^{-1}s^{-1}$) and TIPS-pentacene (~0.8 $cm^2V^{-1}s^{-1}$), the *n*-channel transistor size was designed 10× larger than that of the *p*-channel transistor ($(W/L)_p$: $(W/L)_n$ of 1 : 10). The inverter shows good response, with V_{OUT} of the inverter exhibiting a sharp inversion at V_{IN} of ~53 V and at V_{DD} of 80 V, which corresponds to a maximum voltage gain ($-dV_{OUT}/dV_{IN}$) of 64.

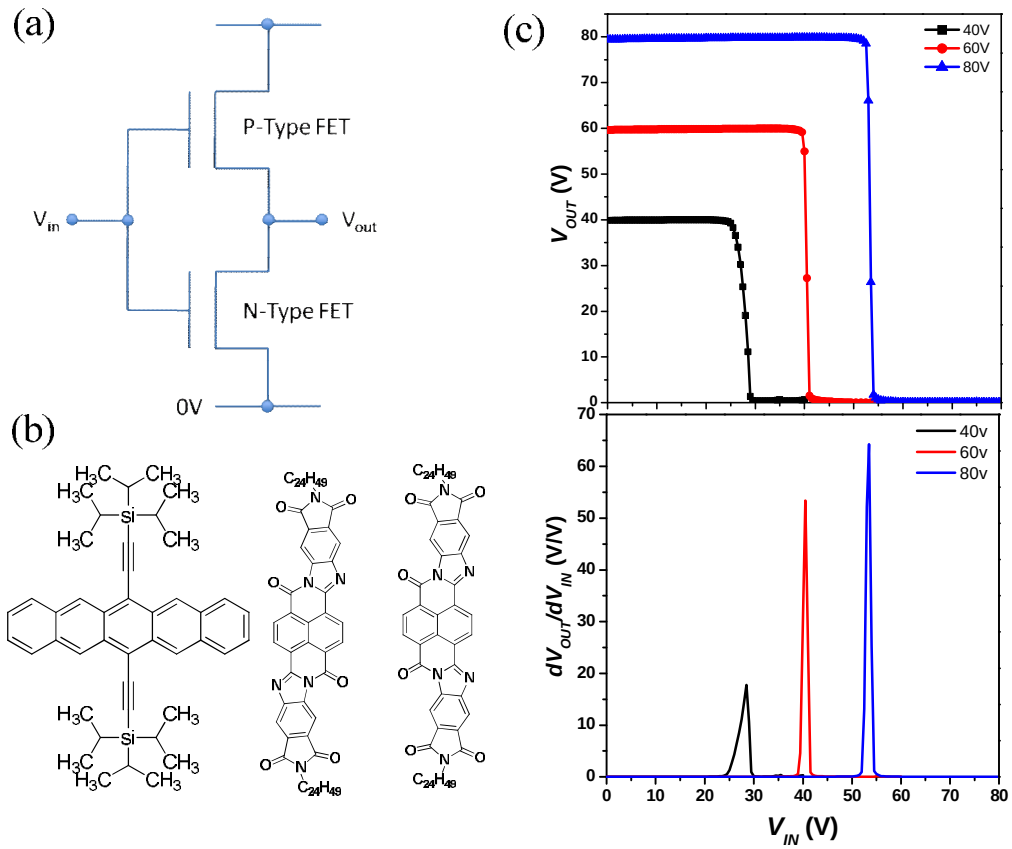

Figure 5.7 (a) Schematic representation of the inverter; (b) Chemical structures of the TIPS-pentacene and **NDIIC24**; (c) Voltage transfer characteristics of a complementary inverter with various supplied voltages and the plots of gains ($-dV_{OUT}/dV_{IN}$) that correspond to the voltage transfer curves.

5.3 Conclusions

In summary, **NDIIC24** as a highly electron-deficient semiconductor was prepared in a simple way and used for high performance *n*-channel OFETs and complementay inverters. The OFETs were conveniently fabricated *via* solution processing, and high electron mobility and high on/off current ratio were achived. Due to the low-lying LUMO energy level, the OFET devices displayed very good air stability and operating stability, which is essential for practical applications. As a demonstration, complementary inverters based on *n*-type **NDIIC24** and *p*-type TIPS-pentacene gave a large voltage gain.

5.4 Experimental

5.4.1 General

NMR spectra were recorded on Bruker AMX500 at 500 MHz spectrometers. ^{1}H NMR spectrum was recorded in $CDCl_3$. All chemical shifts are quoted in ppm, using the residual solvent peak as a reference standard. Matrix-assisted laser desorption ionization time-of-flight (MALDI-TOF) analysis was performed on a Bruker Autoflex Ⅲ MALDI-TOF instrument by using 1,8,9-trihydroxyanthracene as matrix and Pepmix as internal standard or external standard.

UV-vis absorption and fluorescence spectra were recorded on Shimadzu UV-1700 and RF-5301 spectrometers in HPLC pure solvents. Cyclic voltammetry was performed on a CHI 620C electrochemical analyzer with a three-electrode cell in a solution of 0.1M tetrabutylammonium hexafluorophosphate (Bu_4NPF_6)

dissolved in dry DCM at a scan rate of 50 mV s^{-1}. A gold electrode with a diameter of 2 mm, a Pt wire and an Ag/AgCl electrode were used as the working electrode, the counter electrode and the reference electrode, respectively. The potential was calibrated against the ferrocene/ferrocenium couple. Thermogravimetric analysis (TGA) was carried out on a TA instrument 2960 at a heating rate of 10ºC/min under N_2 flow.

Top-contact, bottom-gate TFTs were prepared. A heavily p+-doped silicon wafer (100, Silicon Quest International, resistivity < 0.005 Ωcm^{-1}) with a 200-nm thermal silicon dioxide (SiO_2) was used as the substrate/gate electrode, with the SiO_2 layer serving as the gate dielectric. The SiO_2/Si substrate was cleaned with acetone, IPA. It was then immersed in a piranha solution ($V(H_2SO_4)$: $V(H_2O_2)$ = 2:1) for 20 minutes, followed by rinsing with deionized water, and then treated with octadecyltrimethoxysilane (OTMS) spin coated from 10 mM trichloroethylene solution, and treated with ammonia for 7h, or octadecyltrichlorosilane (ODTS) immersed in 3 mM hexadecane solution for 16h in N_2. The semiconductor layer was deposited on top of the modified substrates by spin coating the 0.6-1 wt% solution in chloroform, firstly annealed at 60 ^{o}C for 10 min to remove the solvent, then the devices annealed at selective temperatures for 0.5 h. Subsequently, gold source/drain electrode pairs were deposited by thermal evaporation through a metal shadow mask to create a series of TFTs with various channel length (L = 100/150 μm) and width (W = 1/4 mm) dimensions. The TFT

devices were characterized using a Keithley SCS-4200 probe station under N_2 or ambient conditions in the dark.

5.4.2 Detailed Synthetic Procedures and Characterization Data

2,12-bis(2-decyltetradecyl)benzo[lmn]isoindolo[5',6':4,5]imidazo[2,1-*b*]isoindolo[5',6':4,5]imidazo[2,1-*i*][3,8]phenanthroline-1,3,8,11,13,18(2H,12H)-hexaone isomers (NDIIC24)

A mixture of 1,4,5,8-naphthalenetetracarboxylic dianhydride (40 mg, 0.15 mmol, 1.0 equiv), and the diamine 5,6-diamino-2-(2-decyltetradecyl)isoindoline-1,3-dione (154 mg, 0.30 mmol, 2.0 equiv) were refluxed in HOAc (15 mL) under nitrogen atmosphere overnight. Upon cooling, the suspension was dissolved with $CHCl_3$ and water, and extracted with $CHCl_3$. The combined organic phases were washed with saturated NaCl (aq), and were finally dried over Na_2SO_4, concentrated under reduced pressure to give a residue which precipitated in MeOH. Reprecipitation in MeOH for another two times gave the title compound as an orange solid (170 mg, 93%). ^{1}H NMR (500 MHz, $CDCl_3$): δ ppm = 9.16 – 9.02 (m, 5H), 8.94 – 8.91 (m, 1H), 8.37 – 8.33 (m, 2H), 8.66 (d, *J* = 7.0 Hz, 4H), 1.95 (br, 2H), 1.57 – 1.24 (m, 80H), 0.86 – 0.85 (m, 12H). HR-MALDI-TOF-MS (m/z): calcd. for $C_{78}H_{106}N_6O_6$: 1223.7128; found 1224.8325 (error = 2.08 ppm). Elemental Analysis: calcd. for $C_{78}H_{106}N_6O_6$: C, 76.56; H, 8.73; N, 6.87; O, 7.84; found: C, 76.45; H, 8.63; N, 6.57.

5.5 References

1. Jones, B. A.; Facchetti, A.; Marks, T. J.; Wasielewski, M. R. *Chem. Mater.*, **2007**, *19*, 2703.
2. Chang, J.; Ye, Q.; Huang, K.; Zhang, J.; Chen, Z.; Wu, J.; Chi, C. *Org. Lett.*, **2012**, *14*, 2964.
3. Jones, B. A.; Facchetti, A.; Wasielewski, M. R.; Marks, T. J. *J. Am. Chem. Soc.*, **2007**, *129*, 15259.
4. Ye, Q.; Chang, J.; Huang K. W.; Chi, C. *Org. Lett.*, **2011**, *13*, 5960.
5. Gao, X.; Di, C.; Hu, Y.; Yang, X.; Fan, H.; Zhang, F.; Liu, Y.; Li, H.; Zhu, D. *J. Am. Chem. Soc.*, **2010**, *132*, 3697.
6. Hu, Y. B.; Gao, X. K.; Di, C. A.; Yang, X. D.; Zhang, F.; Liu, Y. Q.; Li, H. X.; Zhu, D. B. *Chem. Mater.*, **2011**, *23*, 1204.
7. Katsuta, S.; Tanaka, K.; Maruya, Y.; Mori, S.; Masuo, S.; Okujima, T.; Uno, H.; Nakayama, K.; Yamada, H. *Chem. Commun.*, **2011**, *47*, 10112.
8. Ortiz, R. P.; Herrera, H.; Blanco, R.; Huang, H.; Facchetti, A.; Marks, T. J.; Zheng, Y. ; Segura, J. L. *J. Am. Chem. Soc.*, **2010**, *132*, 8440.
9. Herrera, H.; Seoane, C.; Segura, J. L.; Facchetti, A.; Marks, T. J.. *Chem. Eur. J.*, **2012**, *18*, 532.
10. Gonzalez, S. R.; Casado, J.; Navarrete, J. L.; Blanco, R.; Segura, J. L. *J. Phys. Chem. A.*, **2008**, *112*, 6732.

11. Luo, M.; Wang, Q.; Wang, Z. Y. *Org. Lett.*, **2011**, *13*, 4092.

12. Mamada, M.; Bolivar, C. P.; Jr., P. A. *Org. Lett.*, **2011**, *13*, 4882.

13. Deng, P.; Yan, Y.; Wang, S.; Zhang, Q. *Chem. Commun.*, **2012**, *48*, 2591.

14. Shao, J.; Chang, J.; Chi, C. *Org. Biomol. Chem.*, **2012**, *10*, 7045.

15. Chi, C.; Wegner, G. *Macromol. Rapid Commun.* **2005**, *26*, 1532.

16. Constantinides, C. P.; Koutentis, P. A.; Schatz, J. *J. Am. Chem. Soc.* **2004**, *126*, 16232.

Chapter 6

Conclusion

The overall objective of this thesis was to design and synthesize π-conjugated molecules for two photon absorption (2PA) materials and organic field effect transistors (OFETs). It was found that octupolar molecules with D-π-A braches could achieve high 2PA cross section, and molecules with imide groups, CN groups, and imine (=N-, such as pyrazine) moieties could accomplish n-channel semiconductors. Considerable π-extended conjugated molecules with varied physical and optical properties have been successfully synthesized following above strategies.

Initial attempts to achieve two photon active molecules with high 2PA cross section were made based on a 'donor-acceptor' strategy using triazatruxene as the electron rich core. It was found that several electron withdrawing groups can be introduced onto the electron-rich triazatruxene core linked via double bond or thienylene vinylene as conjugation bridges. All newly synthesized chromophores **2-1** to **2-6** displayed high two-photon absorptivity with the maxima ranging from 280 GM to 1620 GM. Moreover, **2-5** and **2-6** exhibit large 2P action cross section (δΦ) with good thermal and photostability, so they could be the potential 2PF probes. Nonetheless, the 2PA cross section achieved was not high enough, and the construction of dendrimers based on the triazatruxene could be a good way.

In subsequent studies, a series of electron-deficient pyrazine-containing linear and star-shaped acene and starphene molecules end functionalized with dicarboximide groups were readily synthesized. Their optical properties,

electrochemical properties and thermal behavior were investigated in detail. Due to the attachment of electron-withdrawing carboximide groups and the fusion of pyrazine rings, these new compounds showed high electron affinities with the low-lying LUMO energy level of -4.01 eV. In particular, **3-2a** and **3-3** showed column liquid crystal property. Electron mobilities in thin films were measured via the SCLC technique; however, the charge mobilities obtained was only moderate, probably due to their poor molecule arrangements in the solid state. This result stimulates us to prepare more efficient n-channel semiconductors with dense molecular packing structure.

The building block, naphthalene diimide (NDI) exhibit strong π-π stacking in the solid state, and was selected as the functional core to build n-channel semiconductors. Thereby a series of electron-deficient naphthalene imide derivatives **4-1a**–**b** and **4-2** – **4-5** were readily synthesized via condensation reaction. Their optical properties, electrochemical properties, thermal behavior were fully investigated. The low-lying LUMO energy levels (-3.90 to -4.15 eV) located within the air stability window ensure air-stable n-channel operation. Semiconductors **4-1a**–**b** and **4-2** – **4-4** were used as active components for high performance, solution-processed *n*-channel organic field effect transistors. The fabricated devices exhibit electron mobility of up to 0.016 $cm^2 V^{-1}s^{-1}$, with current on/off ratios of 10^4-10^5, and threshold voltages of 10-20 V. Moreover, their excellent air and operating stability render them as a promising potential

candidate in organic electronics. However, the electron mobilities are still to be improved.

In pursuit of n-channel semiconductors with high electron mobility and good air stability, an electron deficient NDI derivative **NDIIC24** was designed and synthesized via condensation reaction, and applied for n-channel OFETs. The photophysical, electrochemical and thermal properties were carefully investigated. Thin film XRD and surface morphology indicate the formation of highly ordered microstructures on the dielectric surface. Due to the low-lying LUMO energy level (-4.21 eV), the OFET devices fabricated from solution processed film of **NDIIC24** exhibited high electron mobility up to 0.056 $cm^2V^{-1}s^{-1}$ with a current on/off ratio of 10^5 and a small threshhold voltage around 10 V. Complementary inverters based on n-type **NDIIC24** and p-type TIPS-Pentacene were also fabricated, demonstrating a maximum voltage gain ($-dV_{OUT}/dV_{IN}$) of 64.

Our approach opens opportunities to prepare a series of new conjugated molecules for 2PA materials and n-channel OFETs. Further structural optimization are still in demand, such as construction of dendrimers which could enhance the 2PA cross section, and introduction of electron withdrawing groups onto a building block with good molecular stacking which would improve the OFET performances and air stability.

Appendix

NMR Spectra of the Target molecules

^{1}H NMR spectrum of compound **2-1**

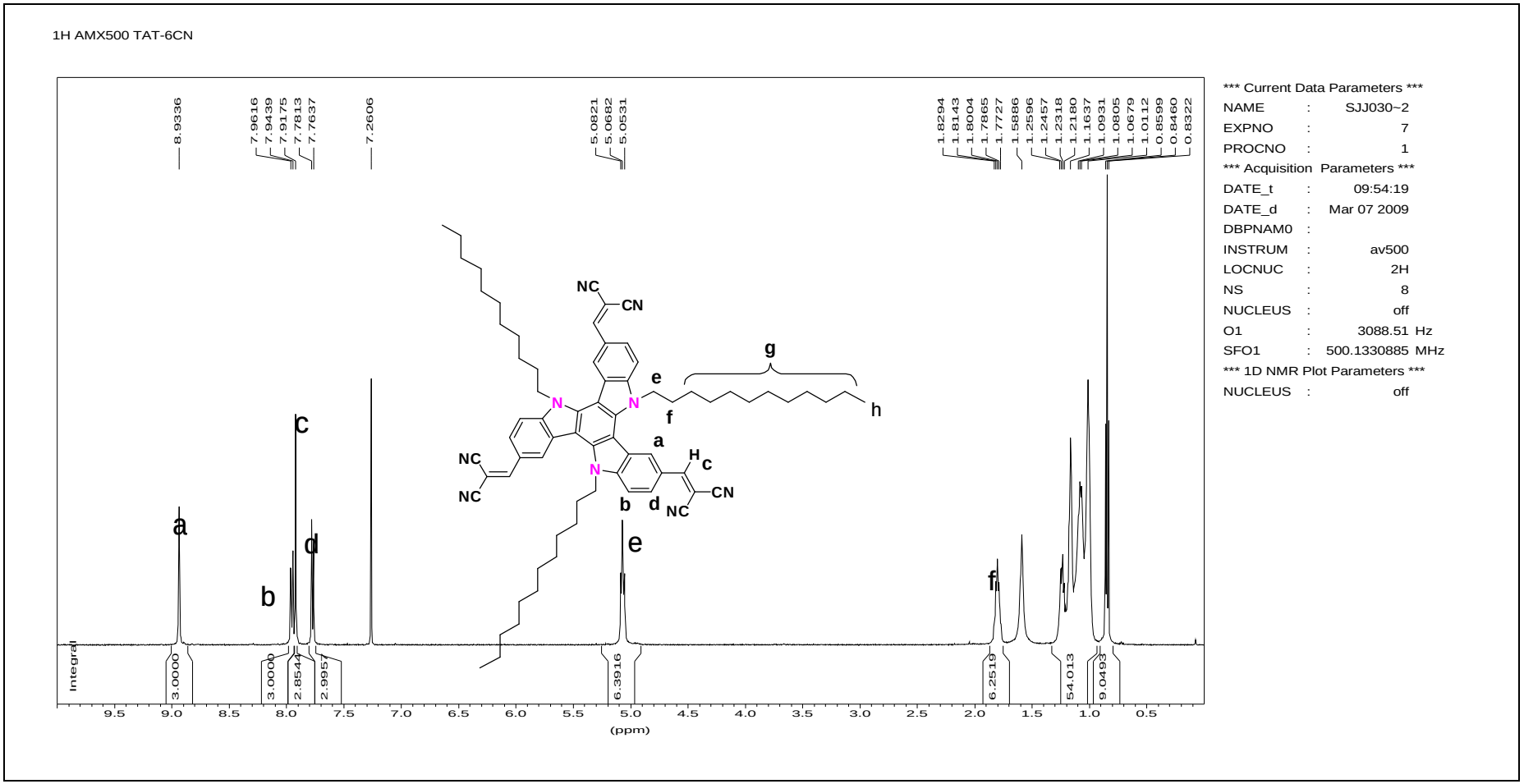

^{13}C NMR spectrum of compound **2-1**

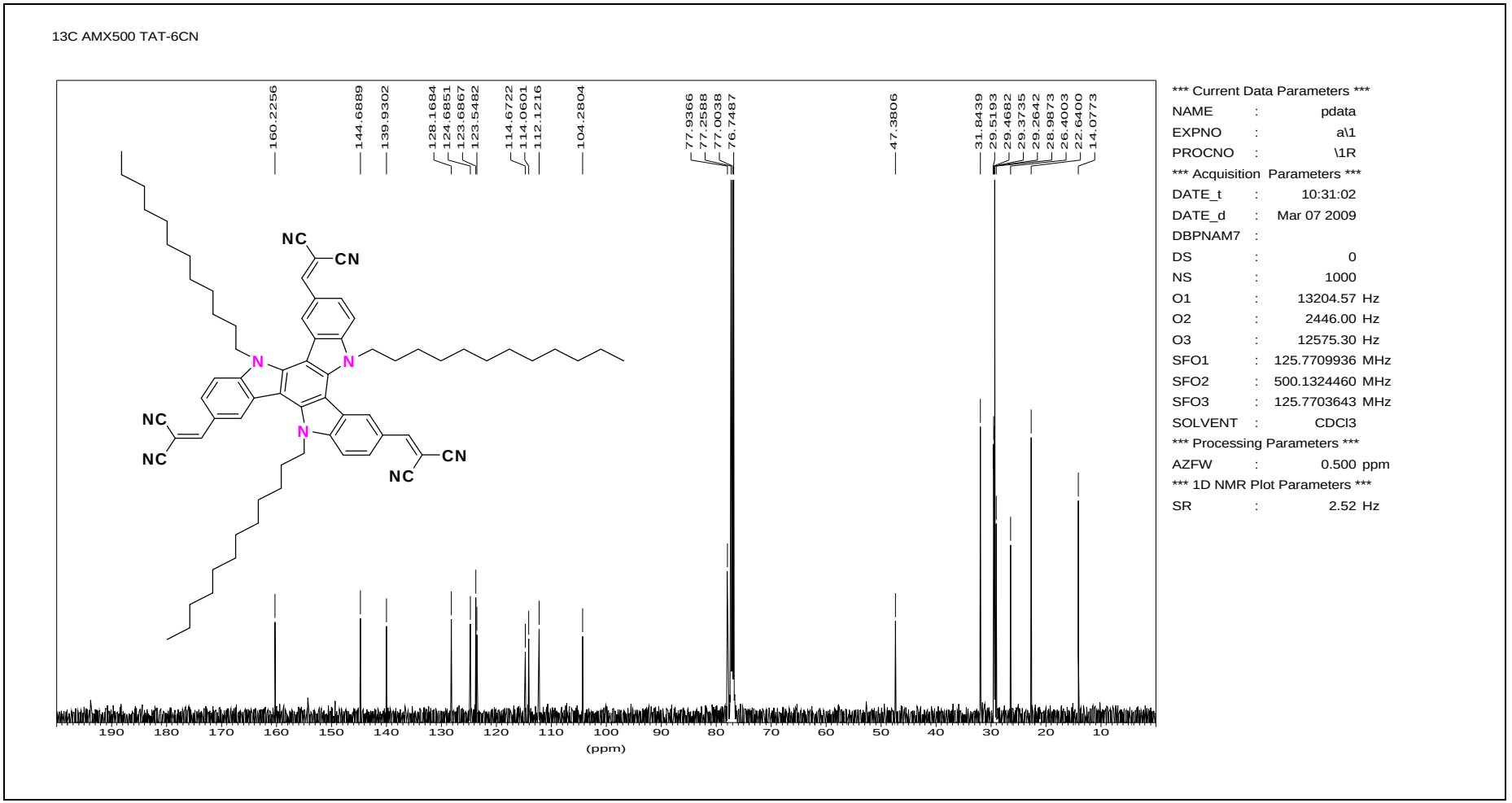

^{1}H NMR spectrum of compound **2-2**

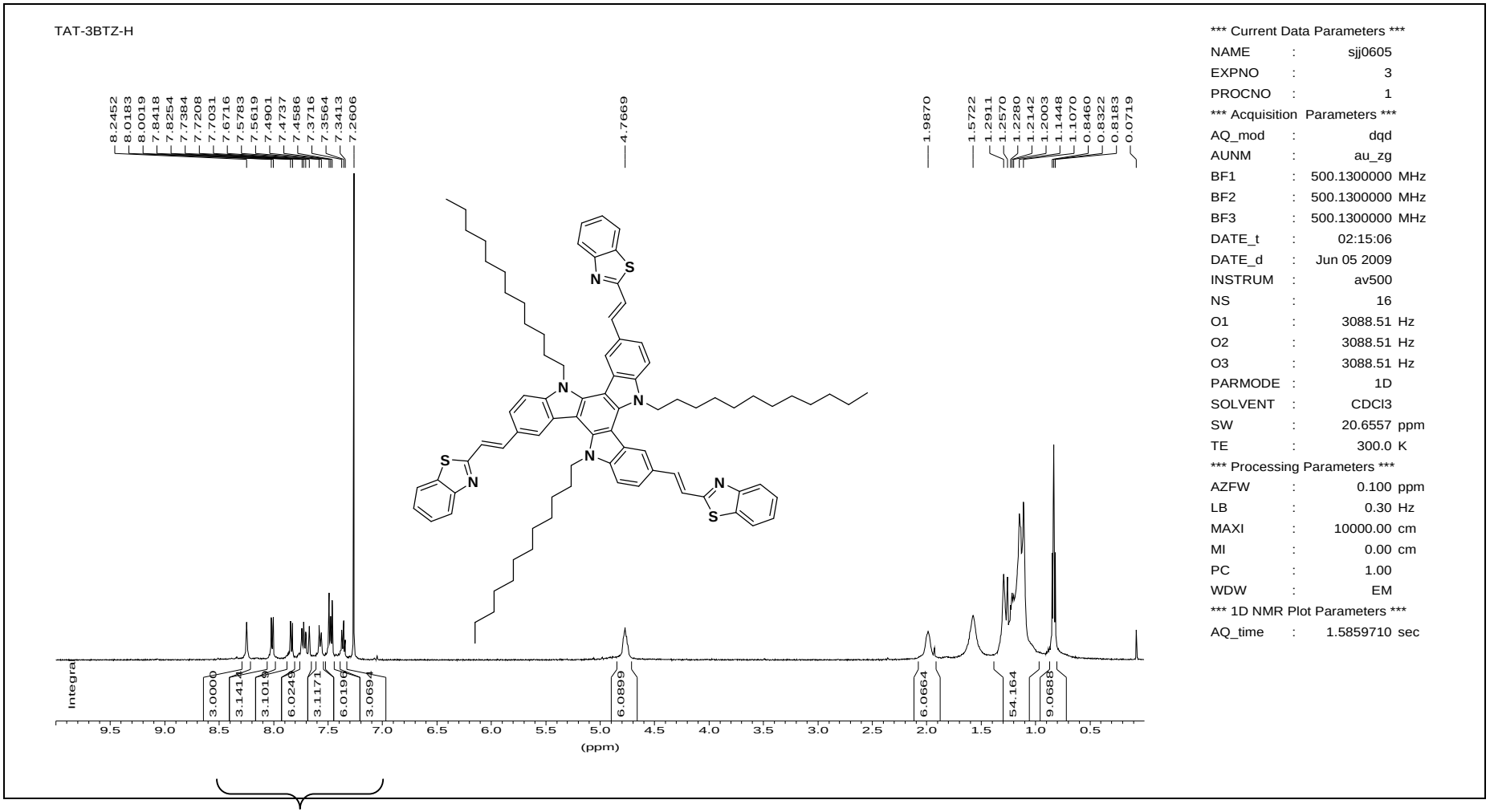

Enlarged part

Enlarged part:

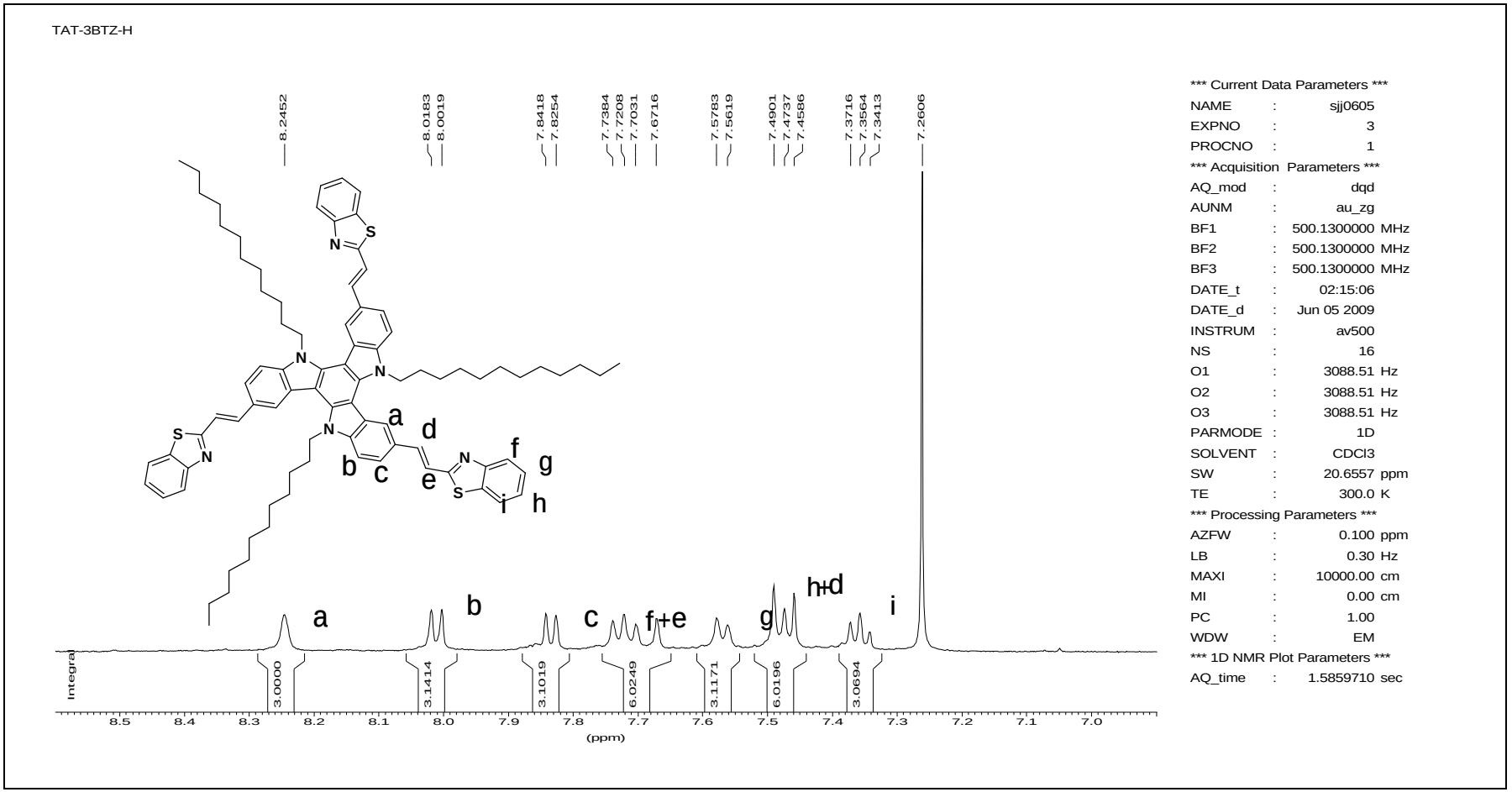

^{13}C NMR spectrum of compound **2-2**

13C AMX500 TAT-3BTZ

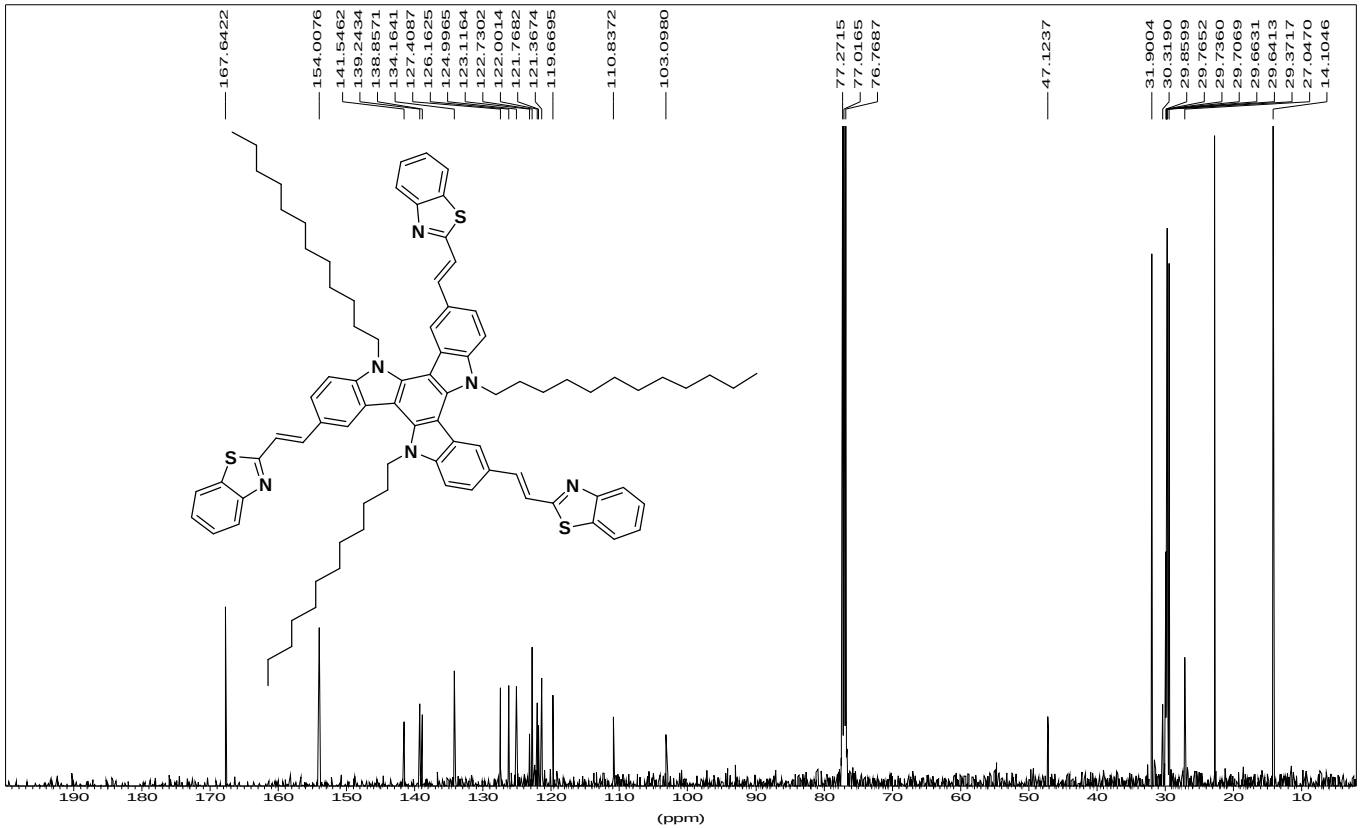

*** Current Data Parameters ***

NAME	:	10
EXPNO	:	10\
PROCNO	:	FID

*** Acquisition Parameters ***

DATE_t	:	11:51:30
DATE_d	:	Mar 07 2009
DBPNAM0	:	
INSTRUM	:	av500
LOCNUC	:	2H
NS	:	7728
NUCLEUS	:	off
O1	:	13204.57 Hz
SFO1	:	125.7709936 MHz

*** 1D NMR Plot Parameters ***

NUCLEUS	:	off

^{1}H NMR spectrum of compound **2-3**

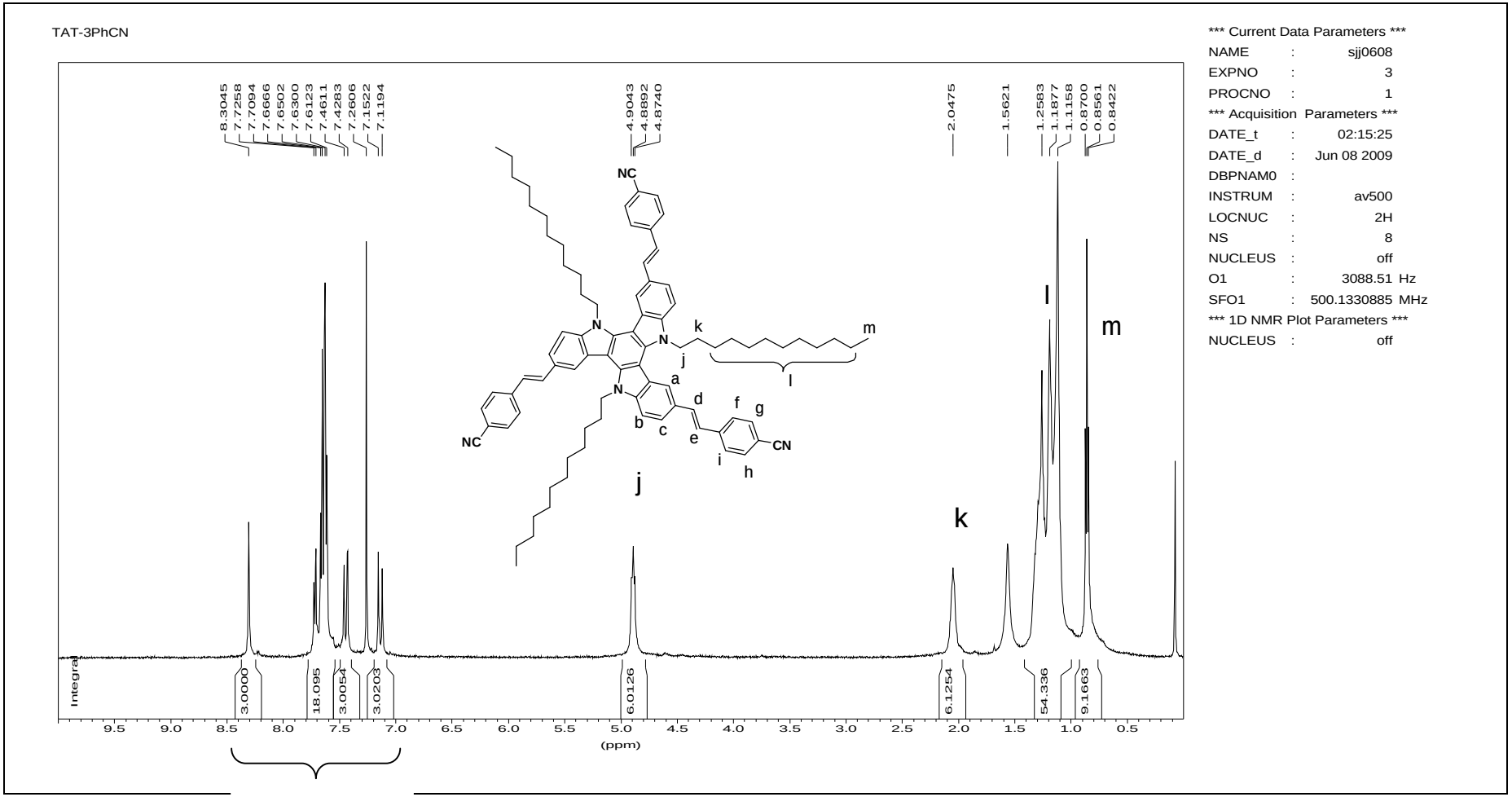

Enlarged part

Enlarged part:

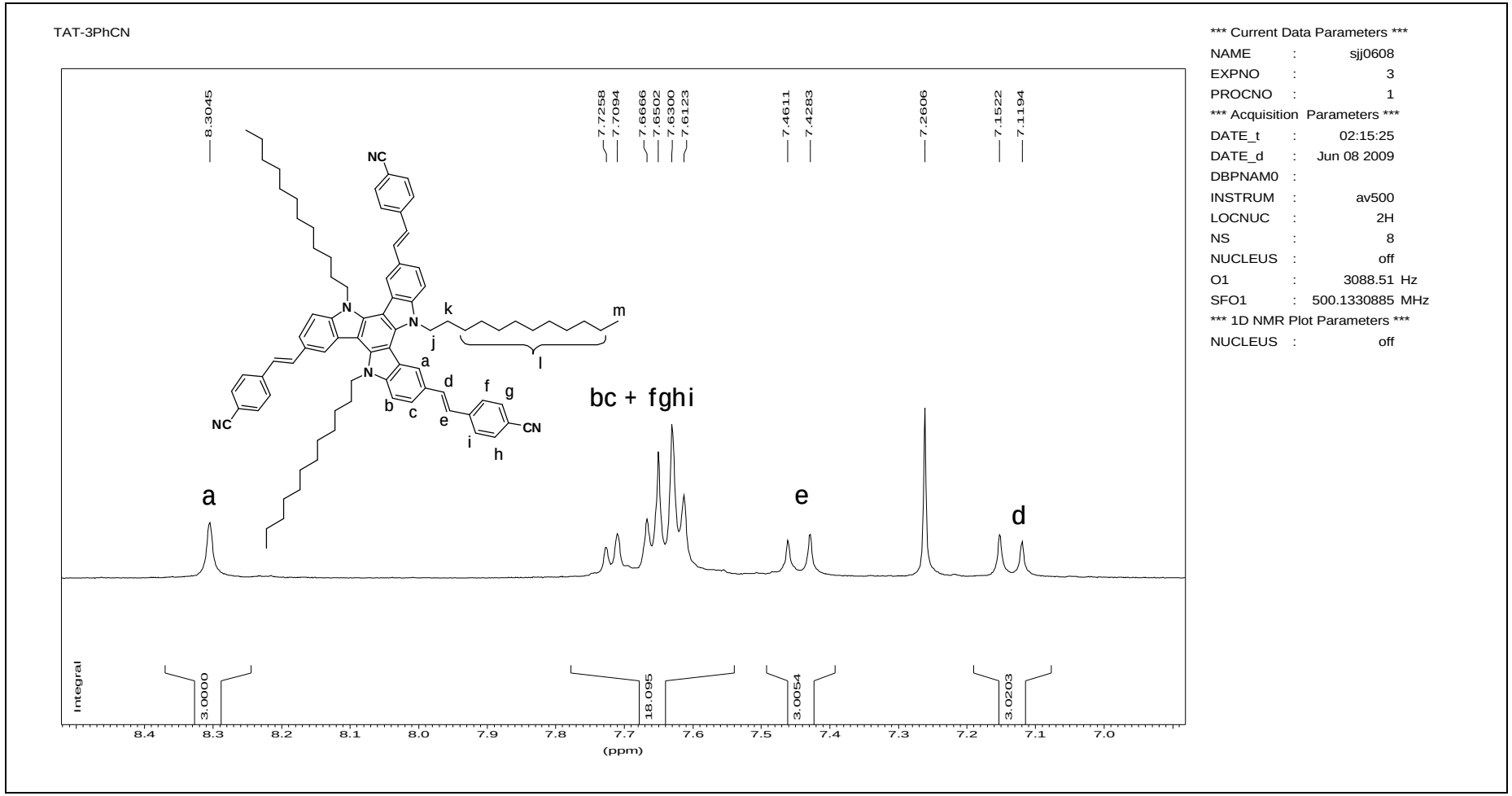

^{13}C NMR spectrum of compound **2-3**

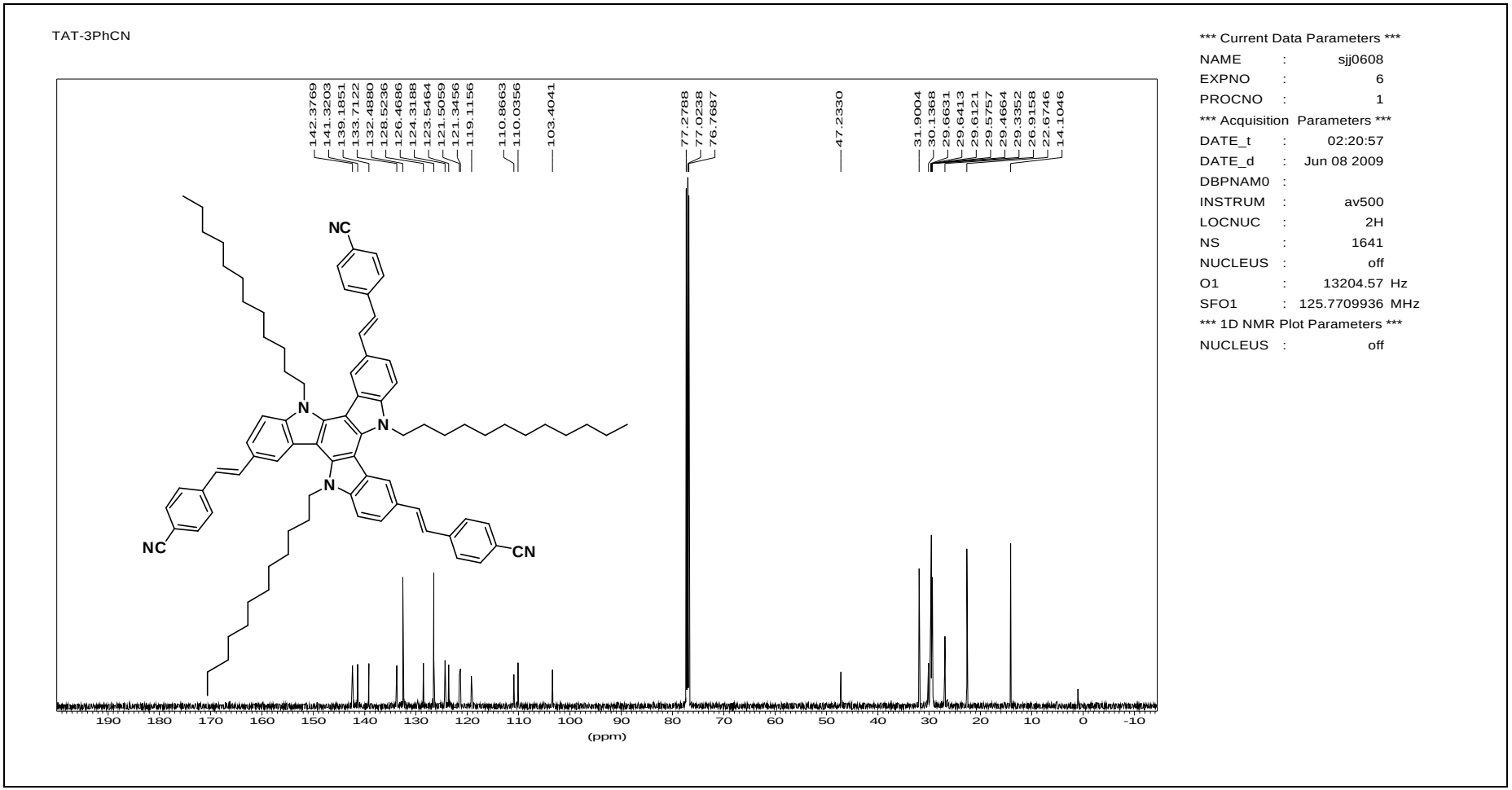

^{1}H NMR spectrum of compound **2-4**

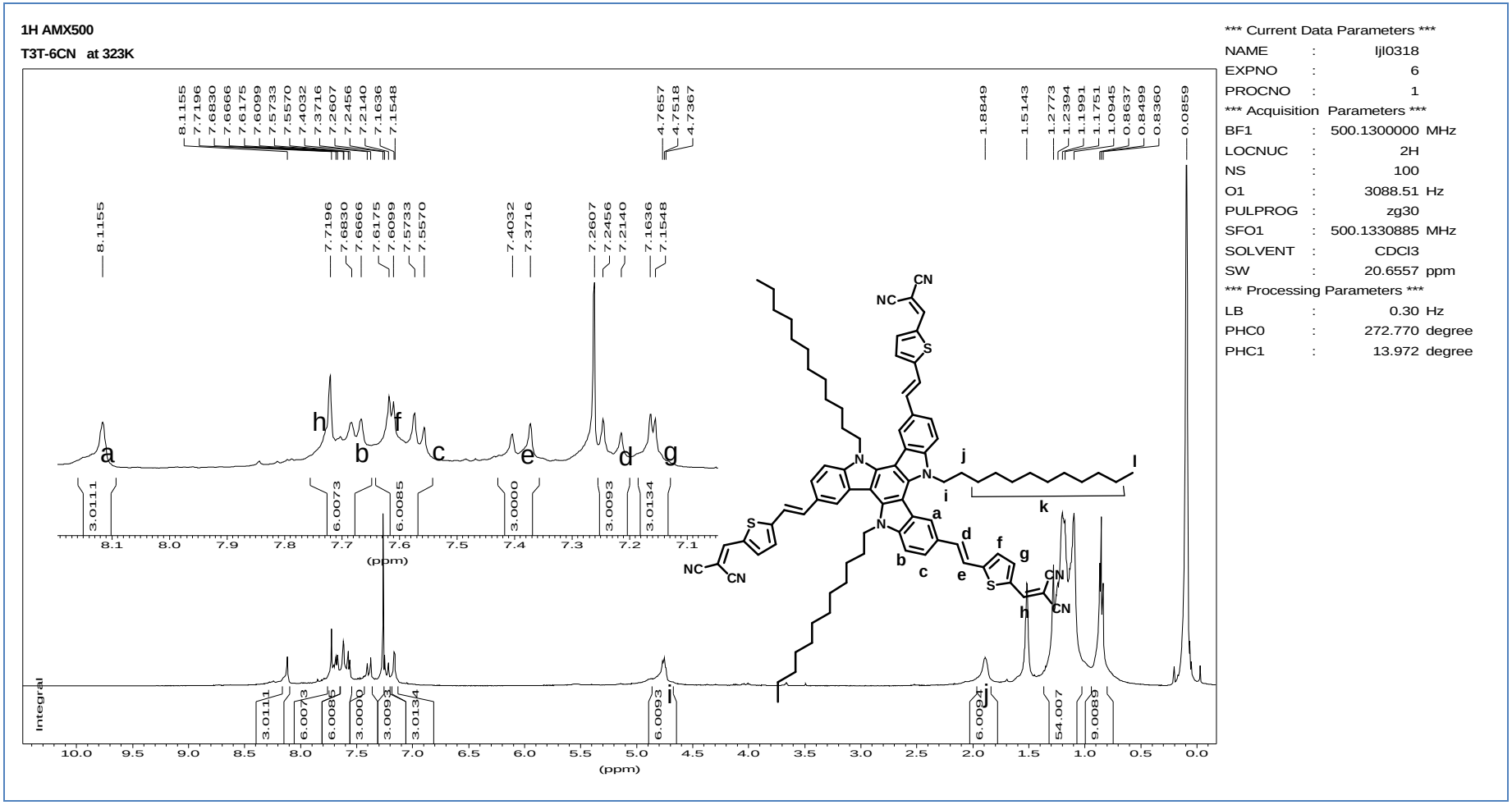

^{13}C NMR spectrum of compound **2-4**

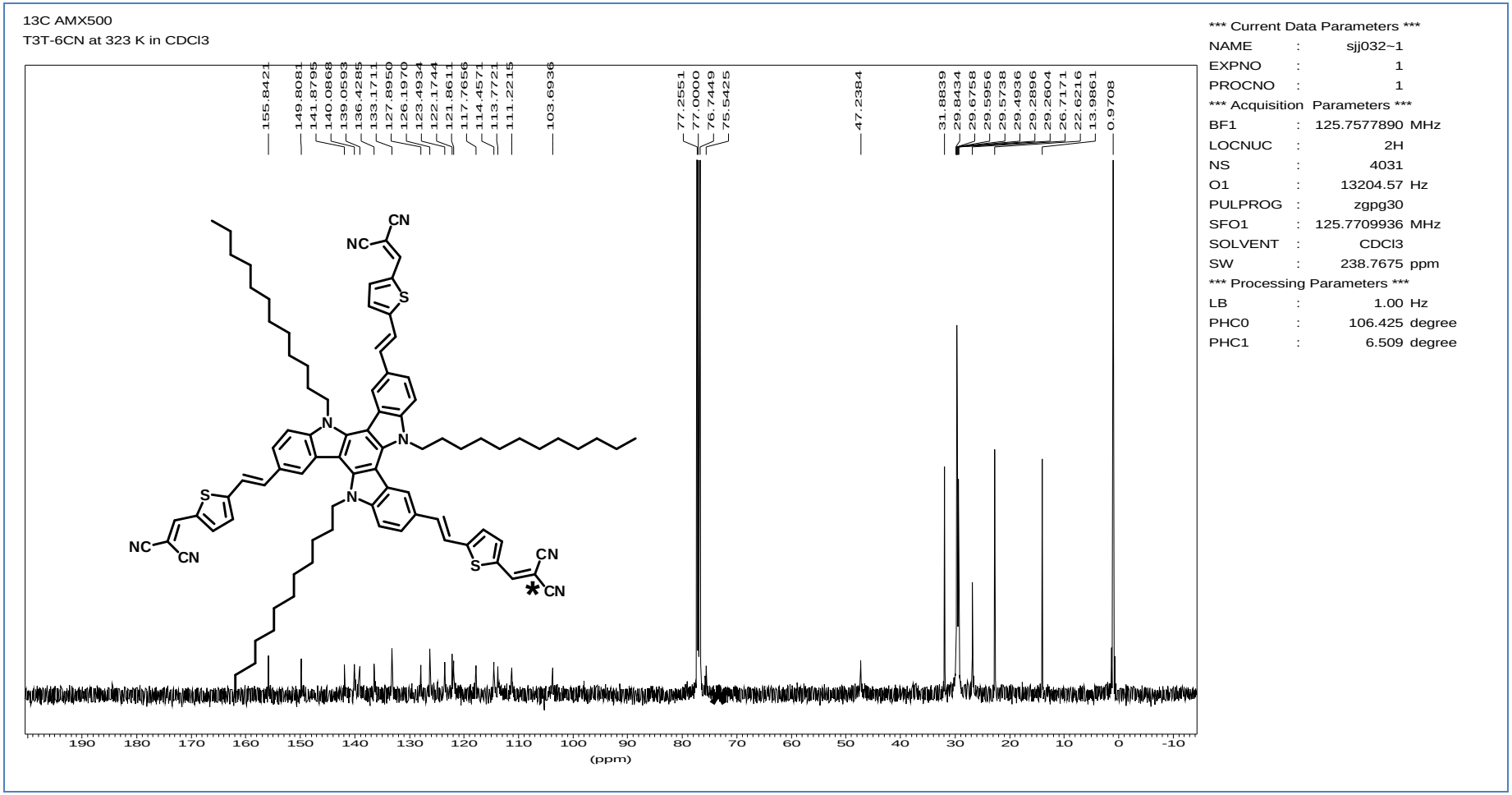

^{1}H NMR spectrum of compound **2-5**

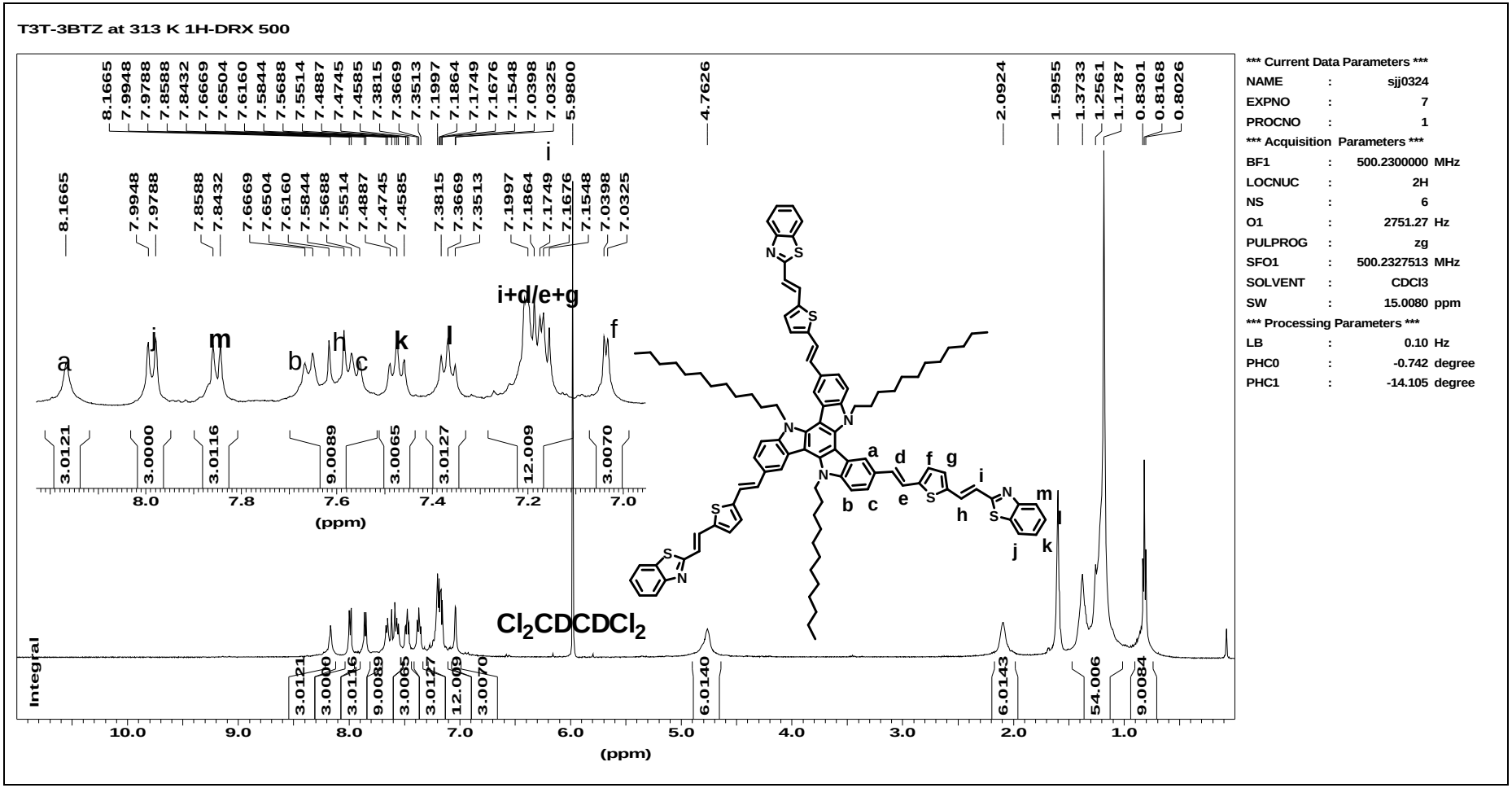

^{13}C NMR spectrum of compound **2-5**

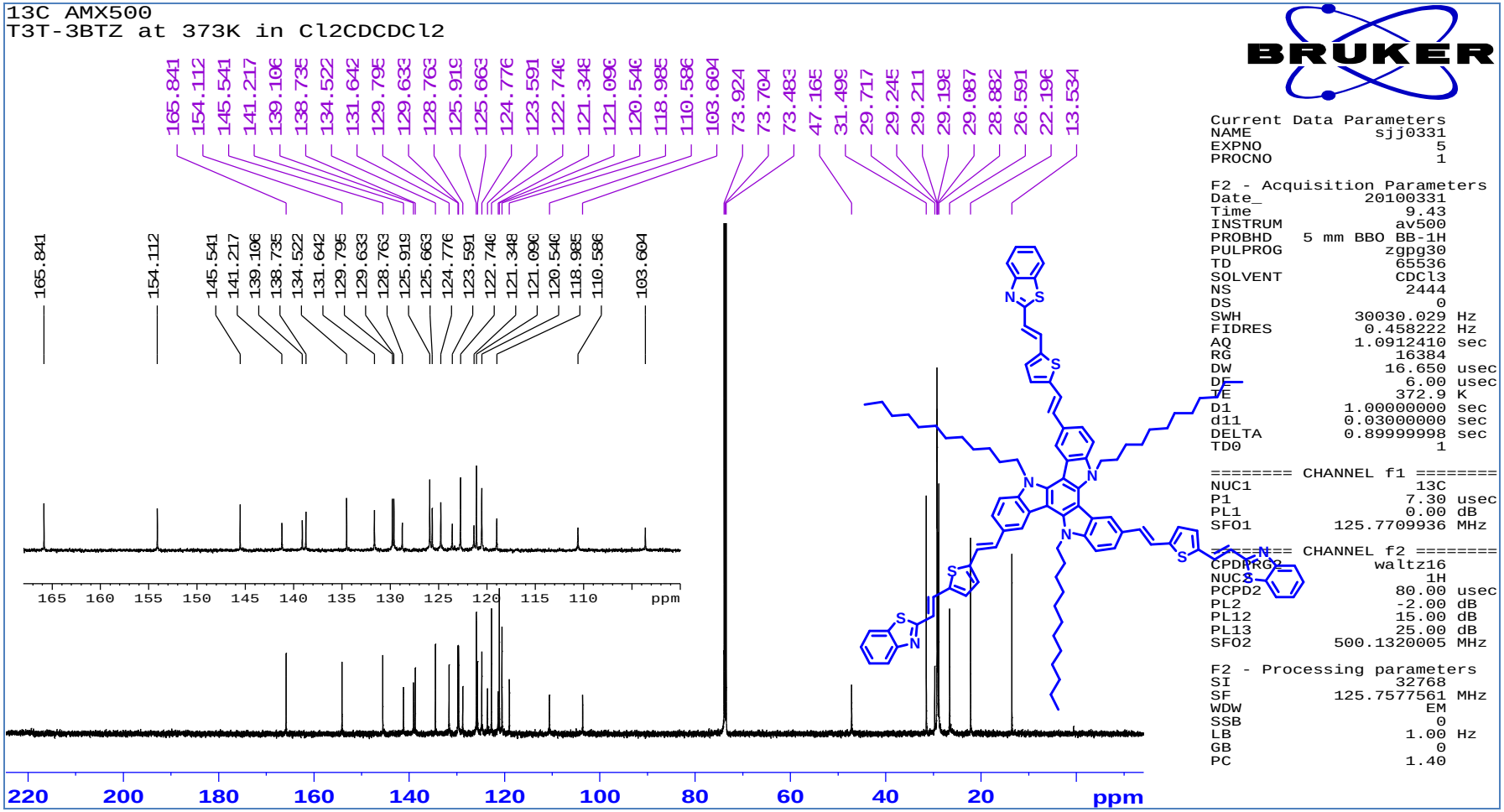

2D NMR spectrum of compound **2-5**

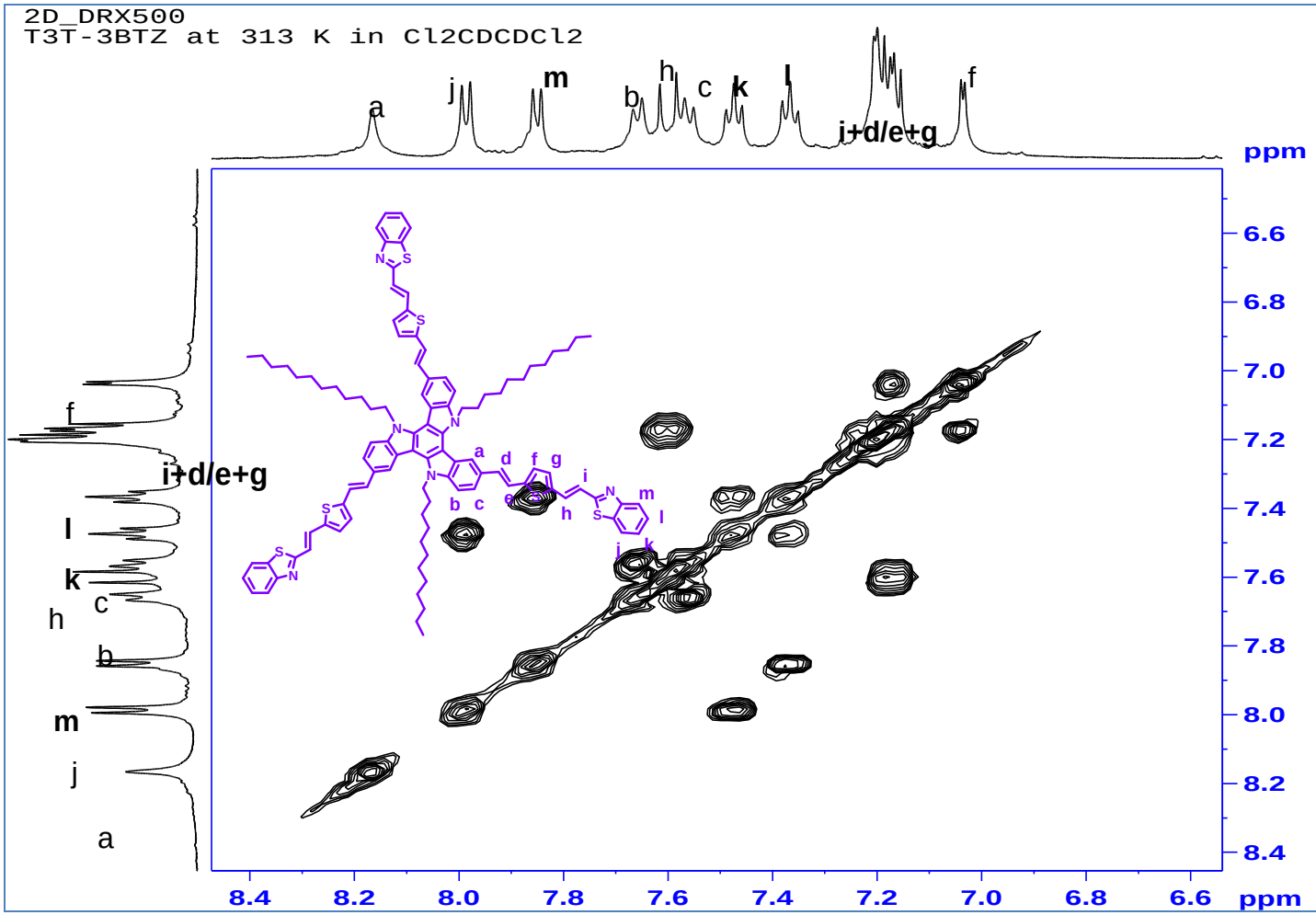


```
Current Data Parameters
NAME                  sjj0324
EXPNO                       9
PROCNO                      1

F2 - Acquisition Parameters
Date_                20100324
Time                    10.55
INSTRUM                spect
PROBHD    5 mm TXI 1H-13
PULPROG               cosygs
TD                      2048
SOLVENT                C6D6
NS                         8
DS                        16
SWH                 4464.286 Hz
FIDRES              2.179827 Hz
AQ                  0.2295380 sec
RG                        16
DW                   112.000 usec
DE                     6.00 usec
TE                    313.0 K
D0                0.00000300 sec
D1                1.50000000 sec
D13               0.00000300 sec
D16               0.00020000 sec
IN0               0.00022400 sec

======== CHANNEL f1 ========
NUC1                      1H
P0                     8.10 usec
P1                     8.10 usec
PL1                   -5.00 dB
SFO1           500.2317794 MHz

====== GRADIENT CHANNEL =====
P16                 1500.00 usec

F1 - Acquisition parameters
ND0                        1
TD                       256
SFO1                500.2318 MHz
FIDRES             17.438616 Hz
SW                     8.924 ppm
FnMODE             undefined

F2 - Processing parameters
SI                       512
SF             500.2296812 MHz
WDW                    SINE
SSB                       0
LB                     0.00 Hz
GB                        0
PC                     1.40

F1 - Processing parameters
SI                       512
MC2                       QF
SF             500.2296825 MHz
WDW                    SINE
SSB                       0
LB                     0.00 Hz
GB                        0
```

^{1}H NMR spectrum of compound **2-6**

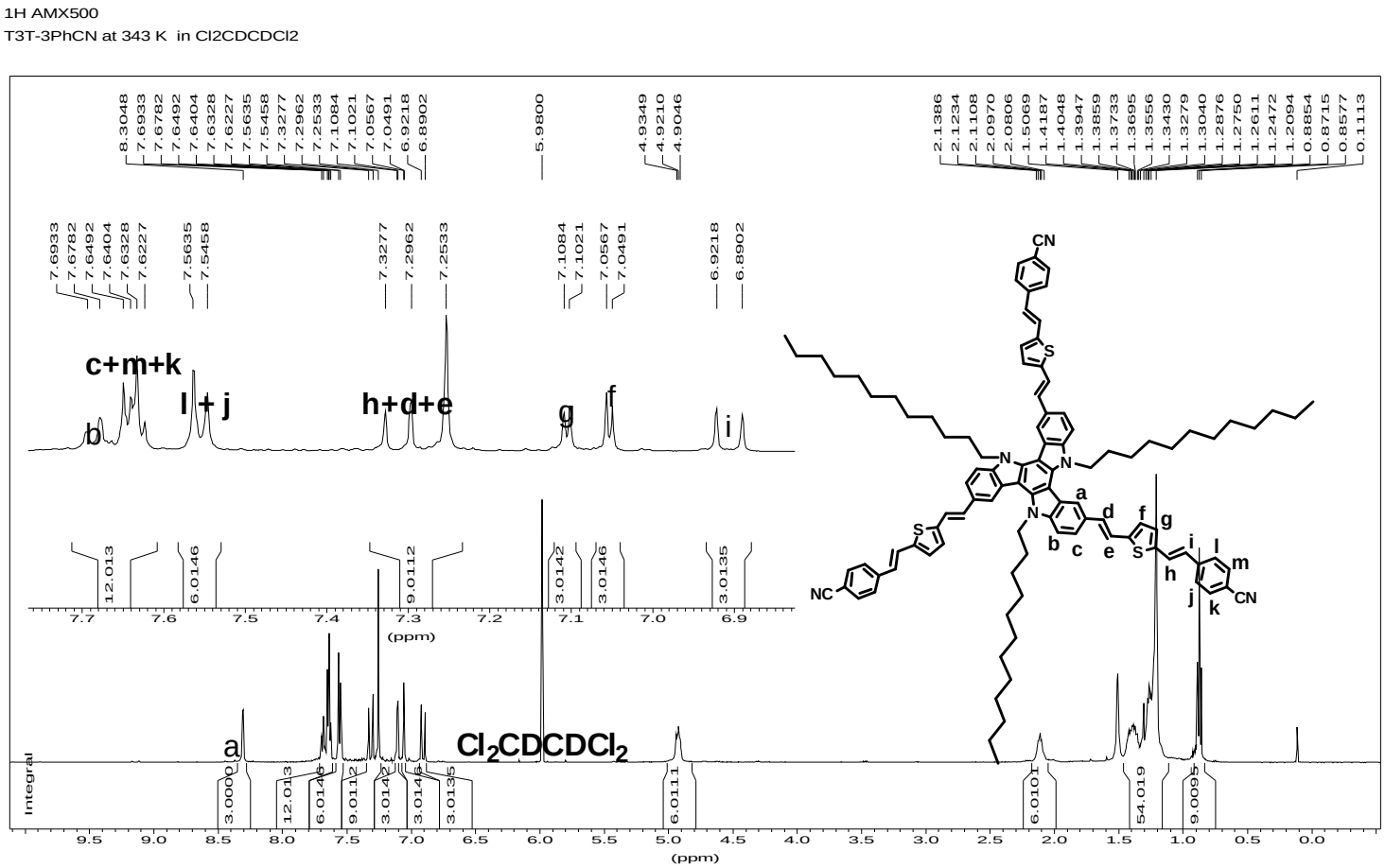


```
*** Current Data Parameters ***
NAME        :        sjj0331
EXPNO       :              9
PROCNO      :              1
*** Acquisition  Parameters ***
BF1         :  500.1300000 MHz
LOCNUC      :             2H
NS          :             32
O1          :     3088.51 Hz
PULPROG     :           zg30
SFO1        :  500.1330885 MHz
SOLVENT     :          CDCl3
SW          :     20.6557 ppm
*** Processing Parameters ***
LB          :      0.30 Hz
PHC0        :    273.401 degree
PHC1        :     -0.733 degree
```

2D NMR spectrum of compound **2-6**

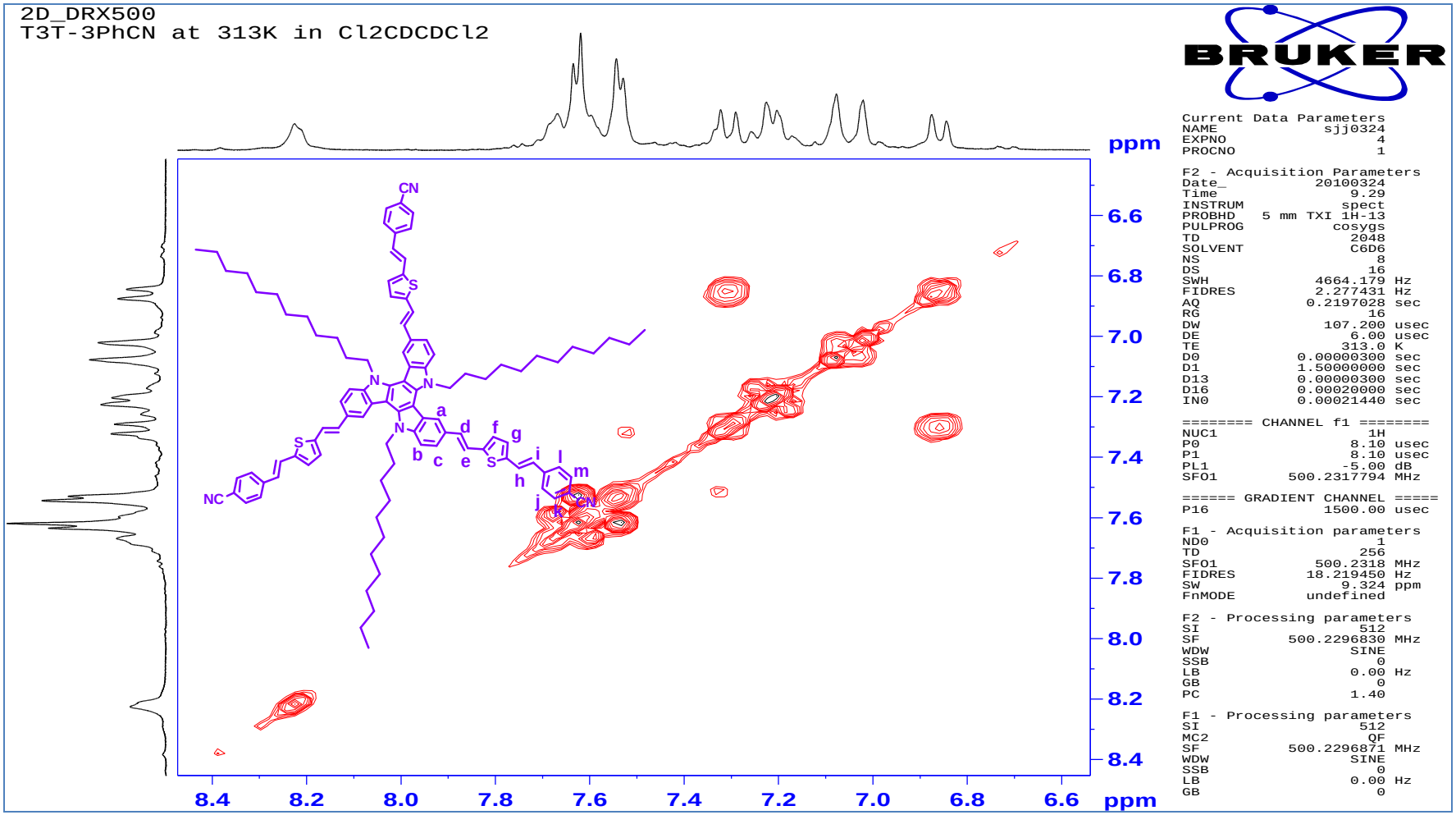

^{13}C NMR spectrum of compound **2-6**

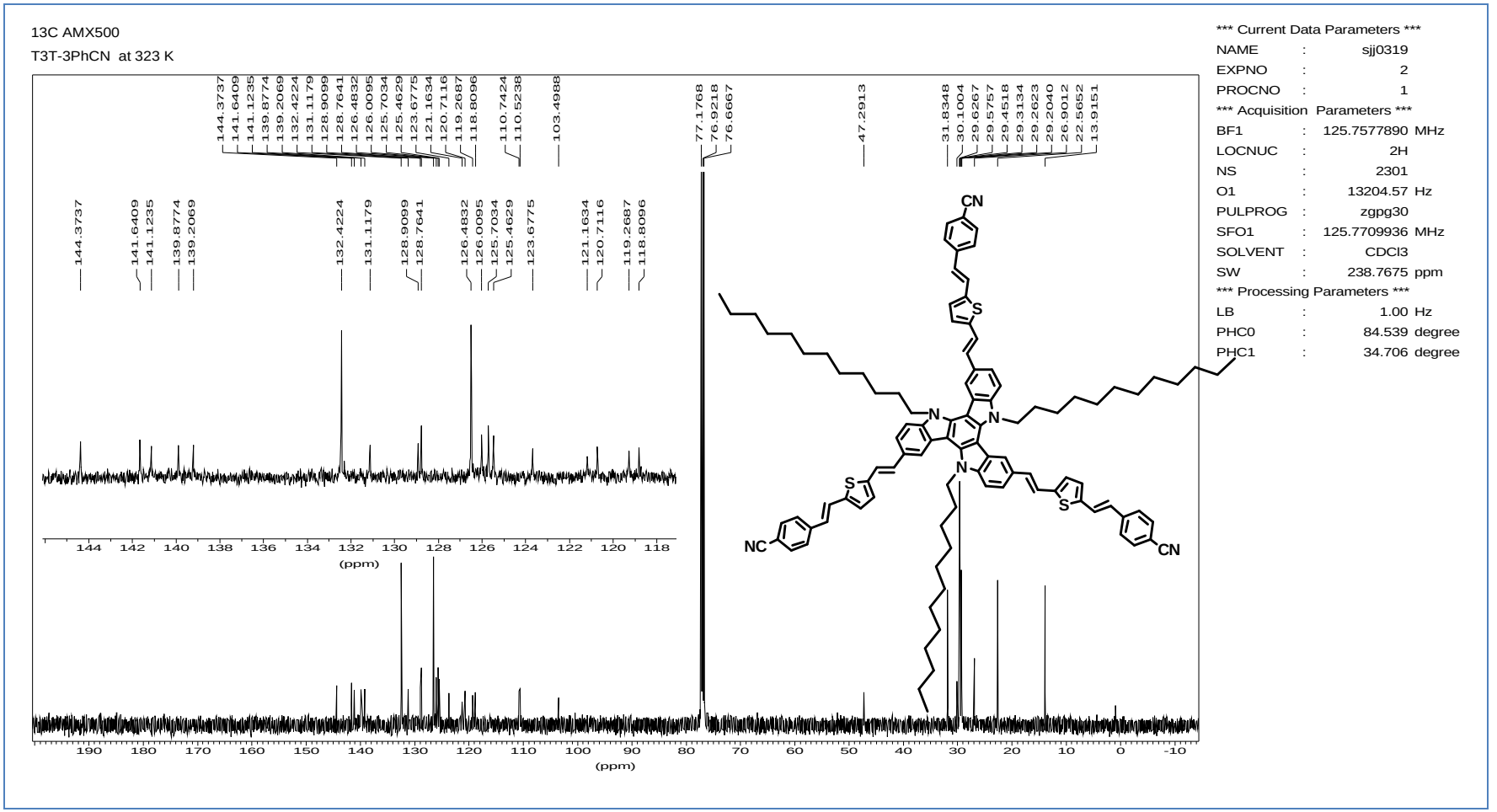

^{1}H NMR spectrum of compound **3-1a**

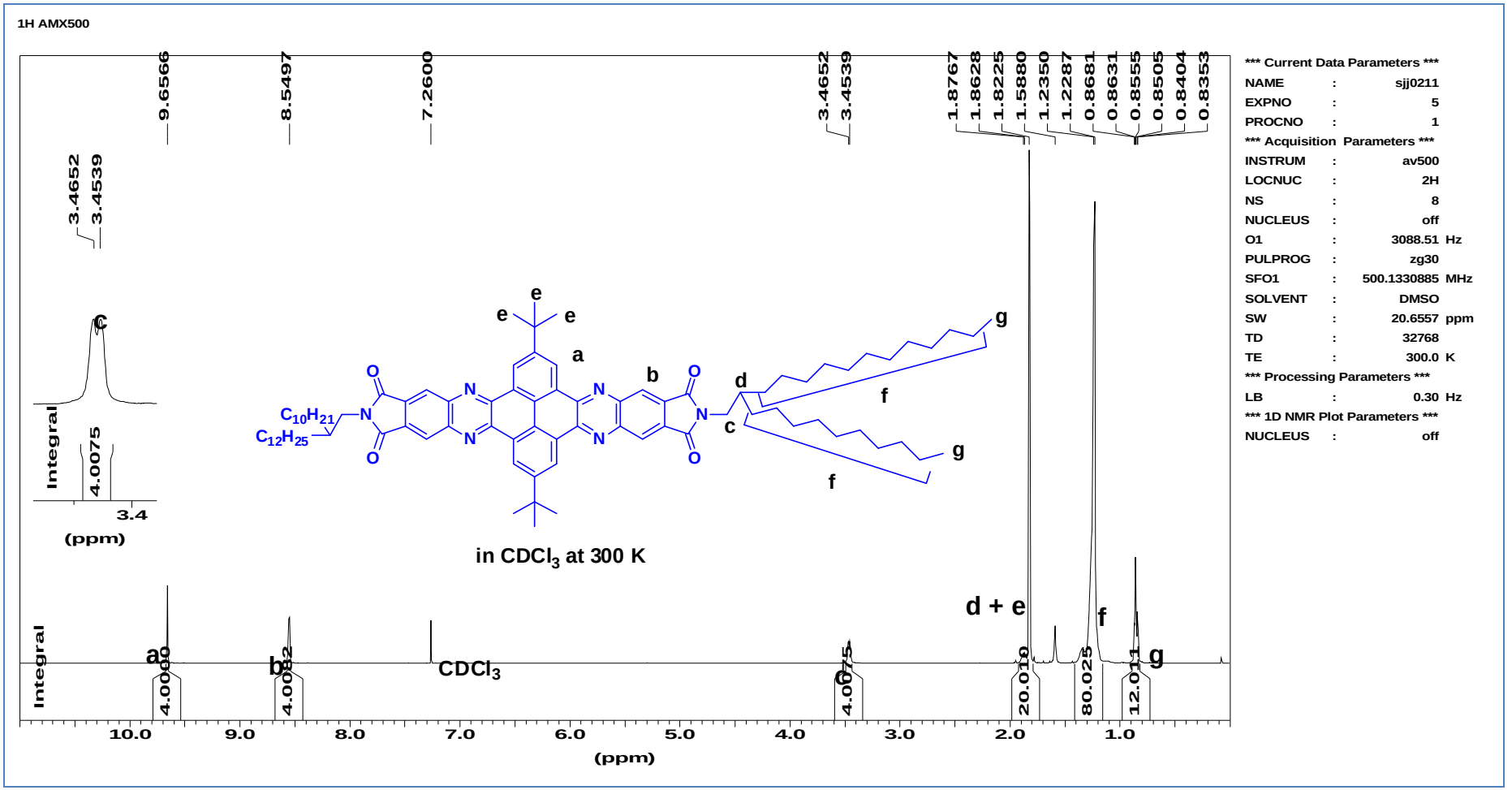

^{13}C NMR spectrum of compound **3-1a**

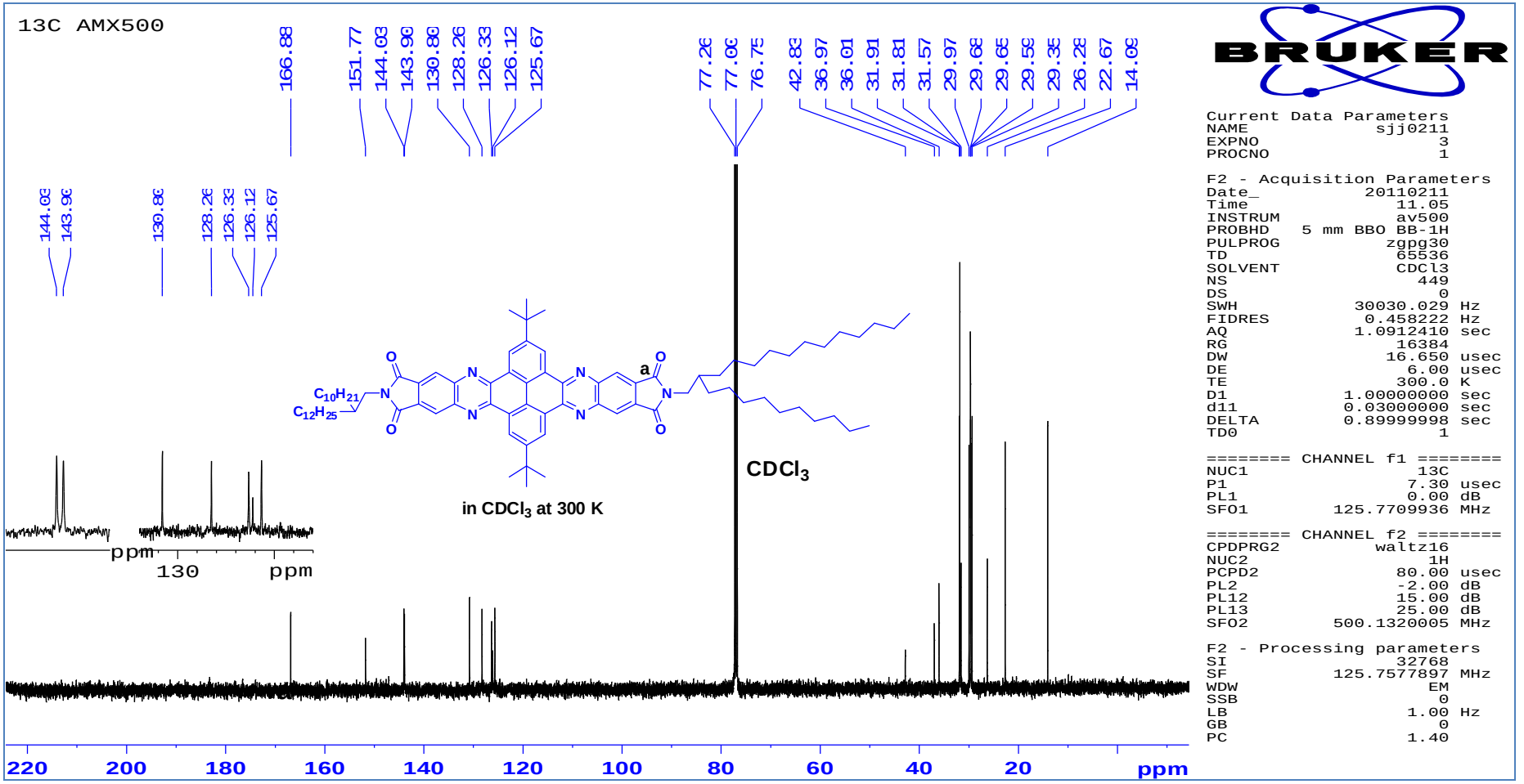

^{1}H NMR spectrum of compound **3-1b**

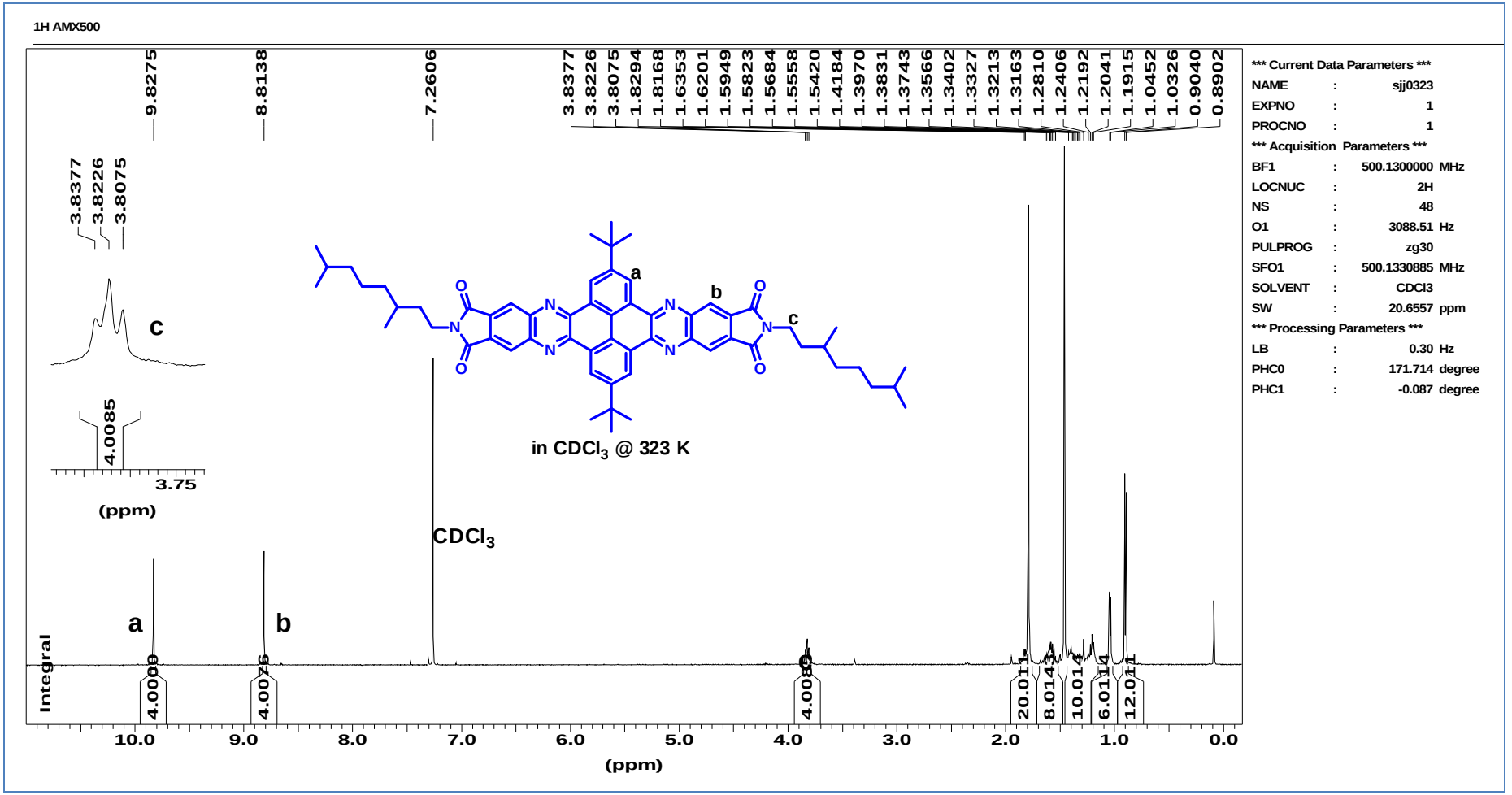

^{13}C NMR spectrum of compound **3-1b**

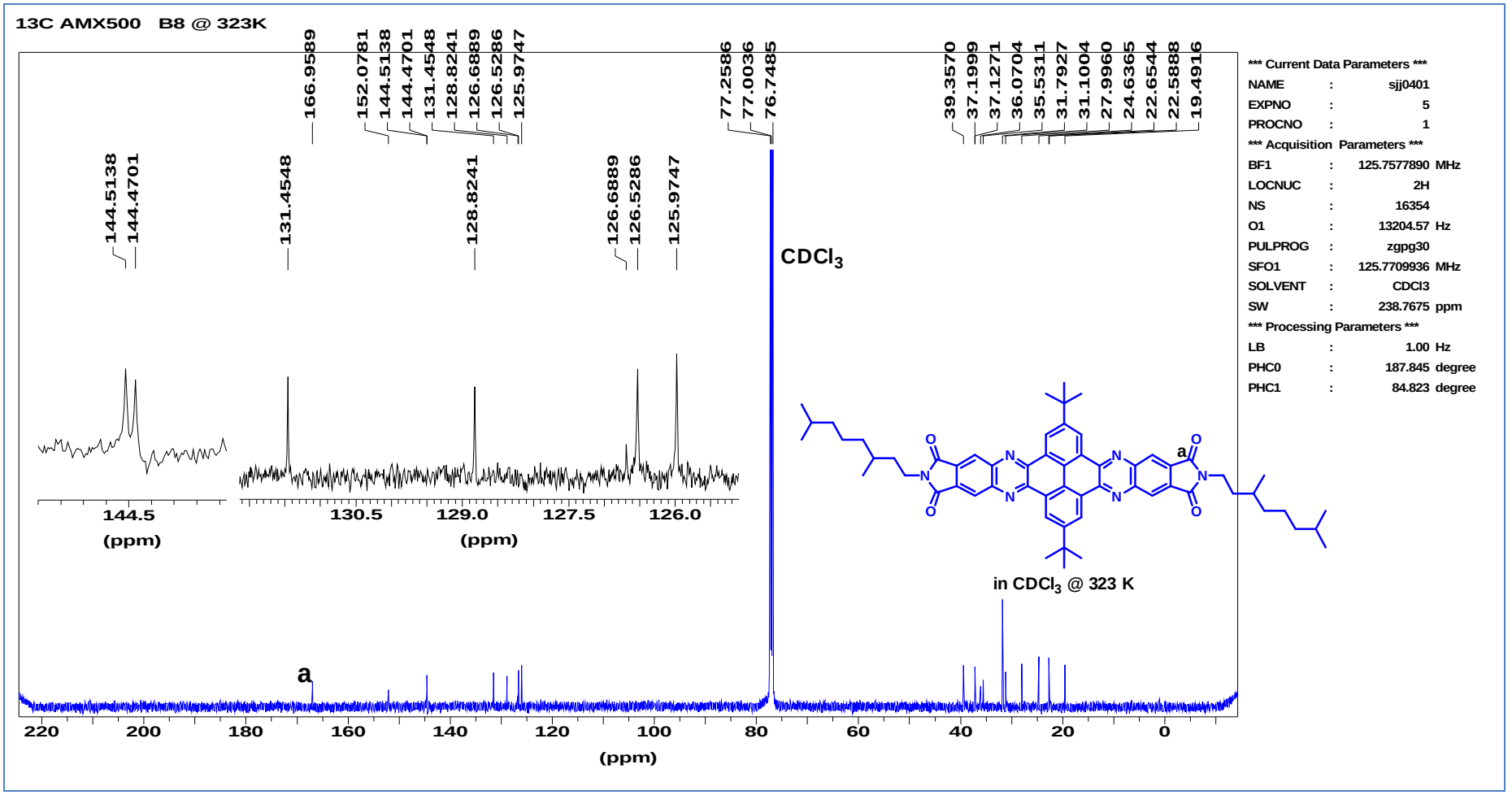

^{1}H NMR spectrum of compound **3-2a**

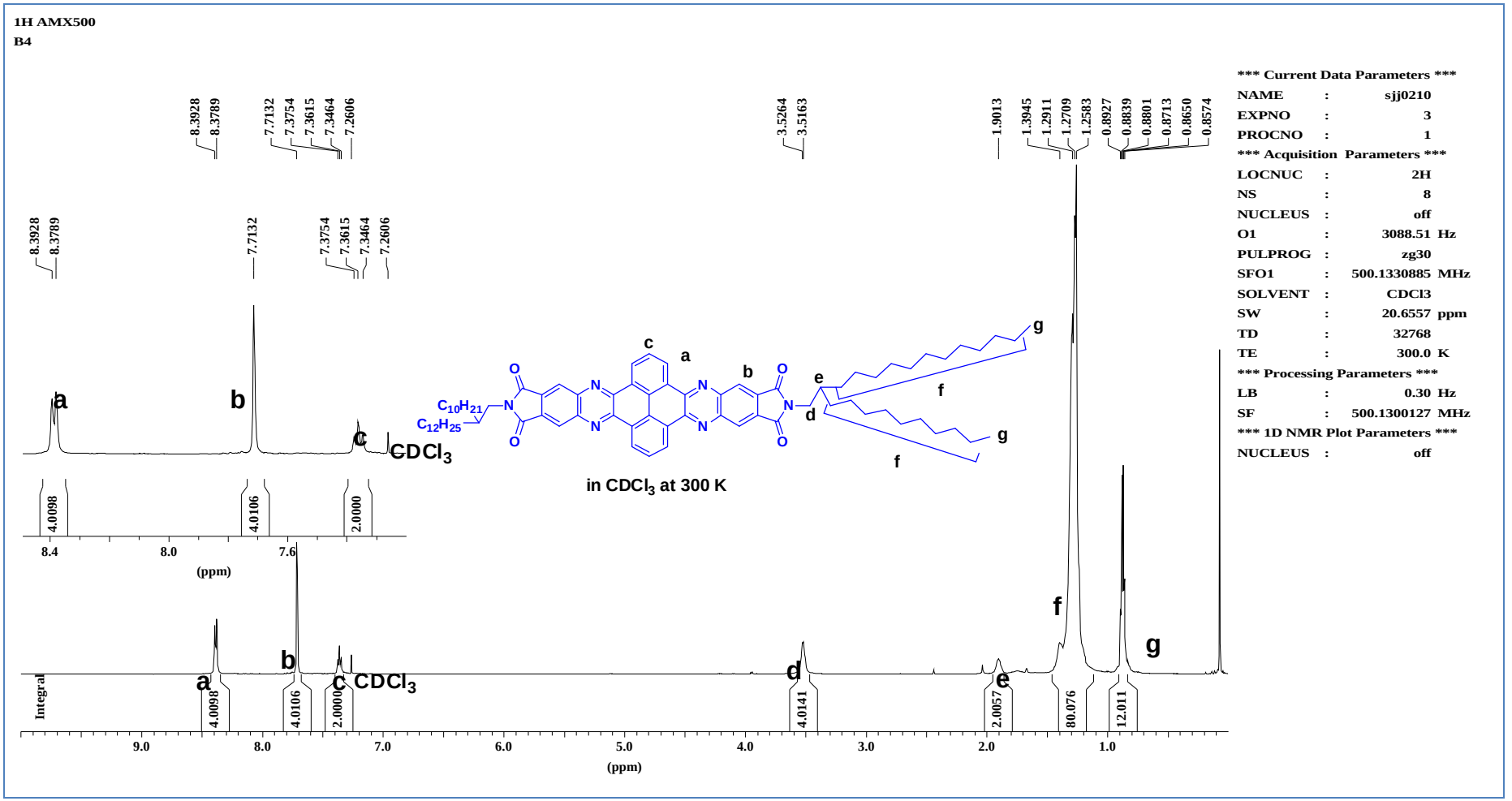

^{13}C NMR spectrum of compound **3-2a**

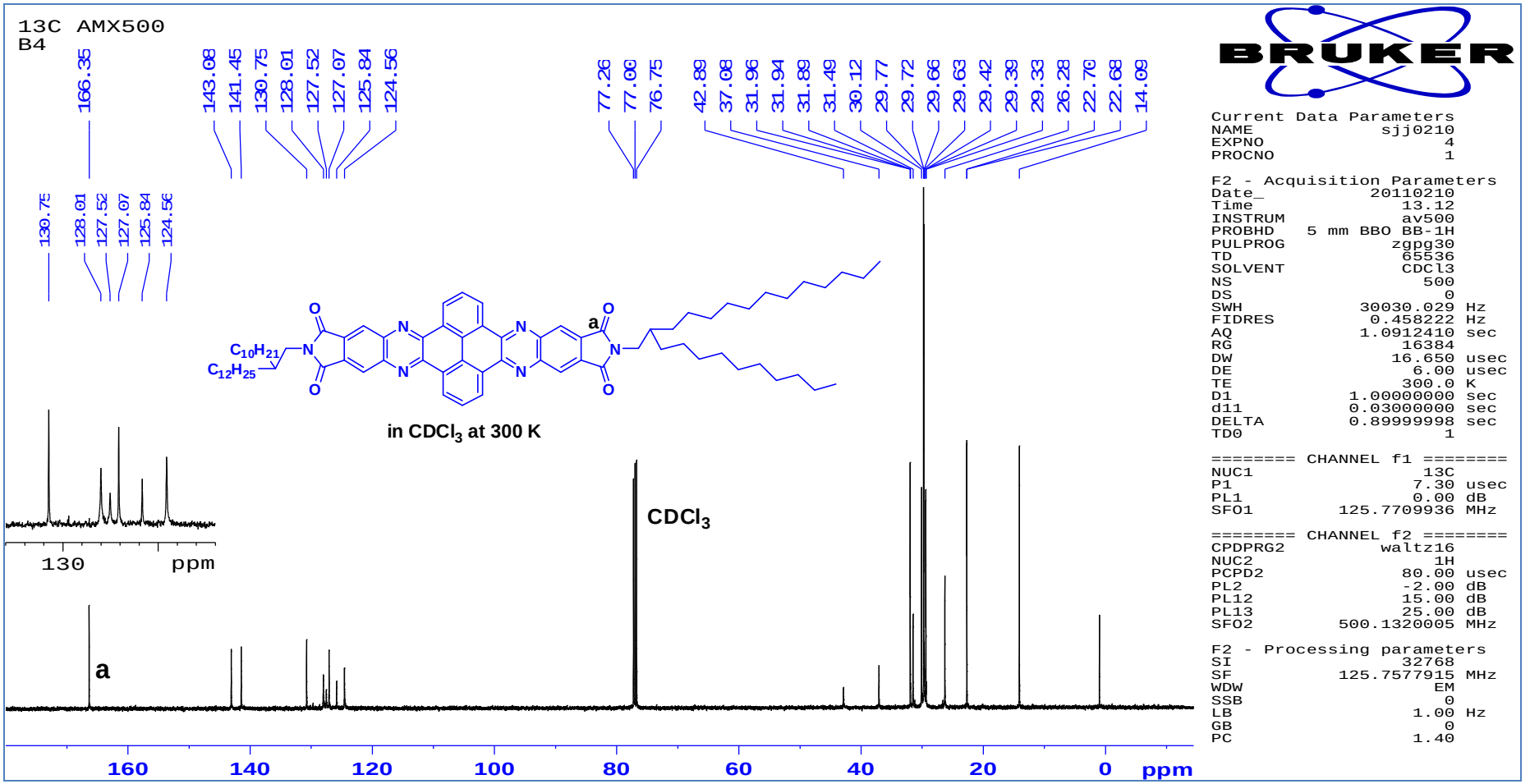

^{1}H NMR spectrum of compound **3-2b**

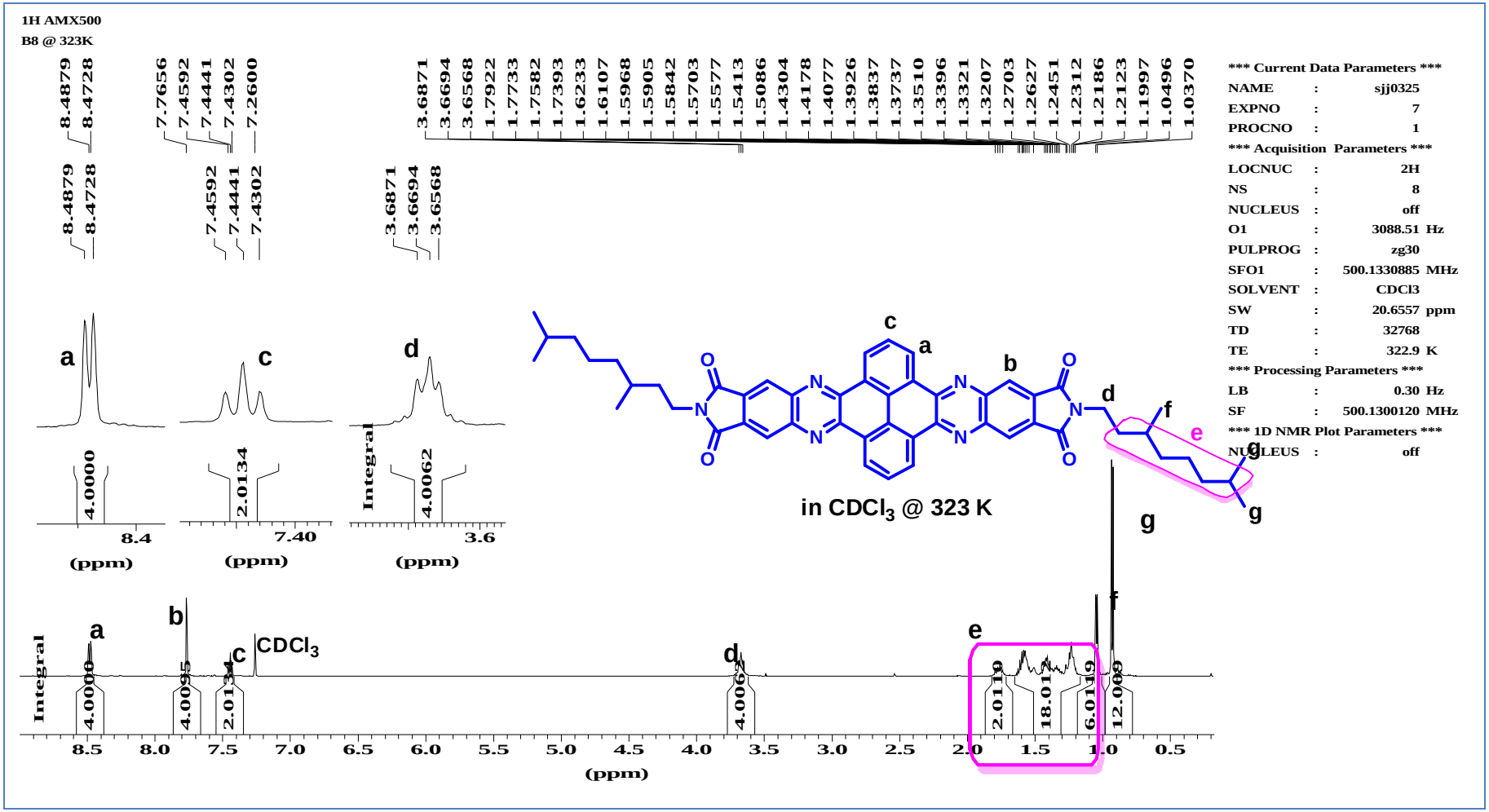

^{13}C NMR spectrum of compound **3-2b**

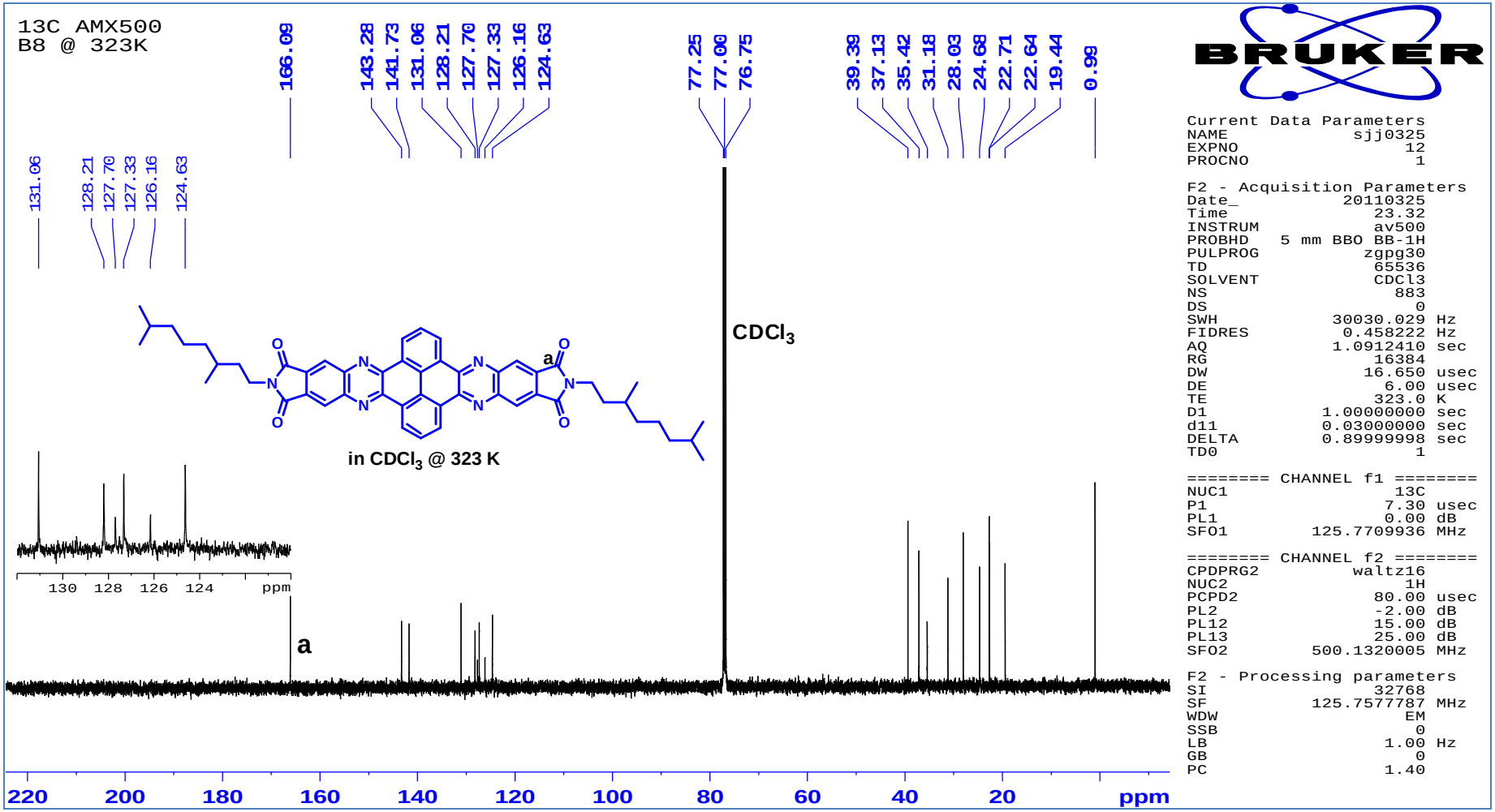

^{1}H NMR spectrum of compound **3-3**

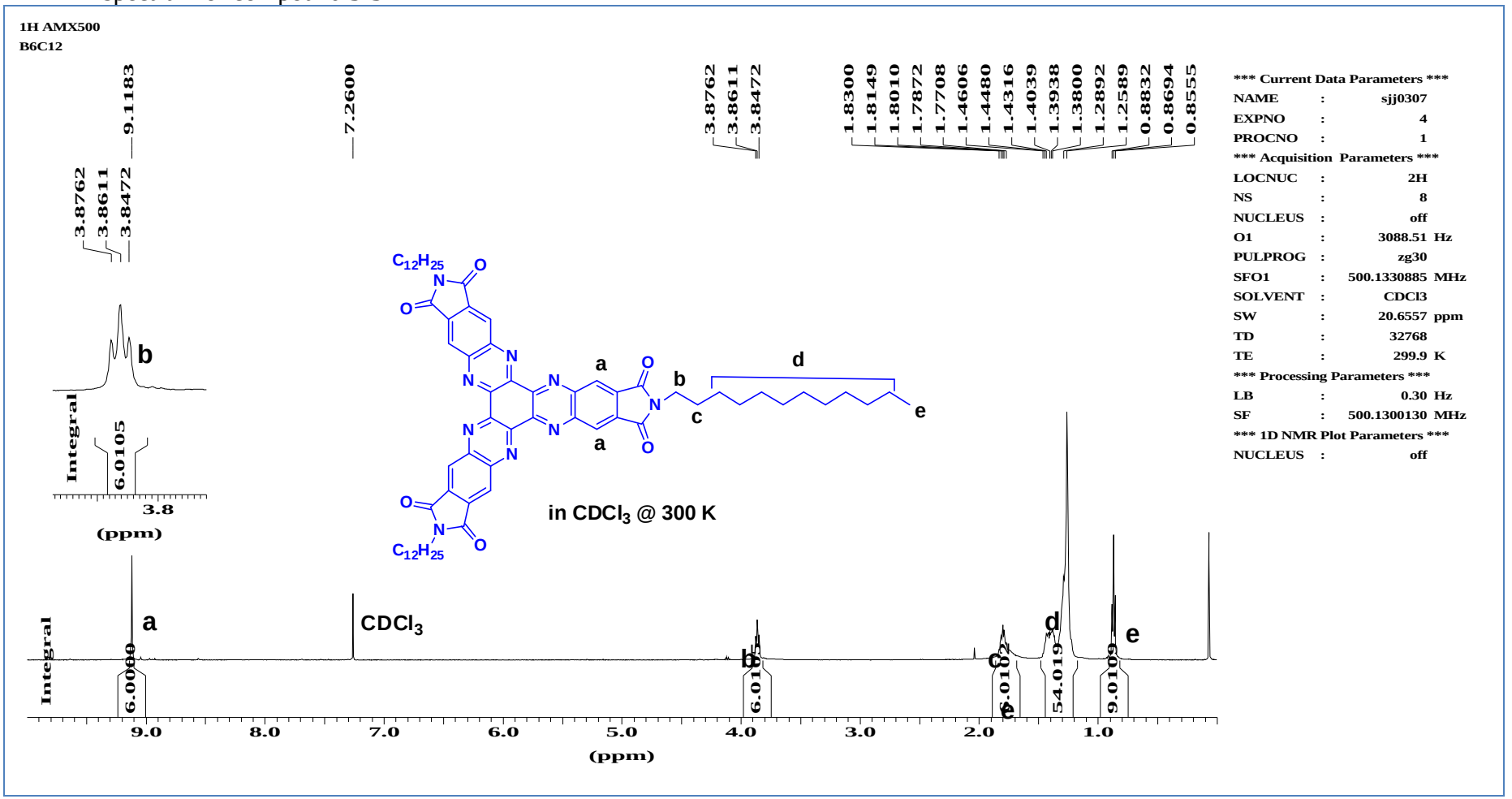

^{13}C NMR spectrum of compound **3-3**

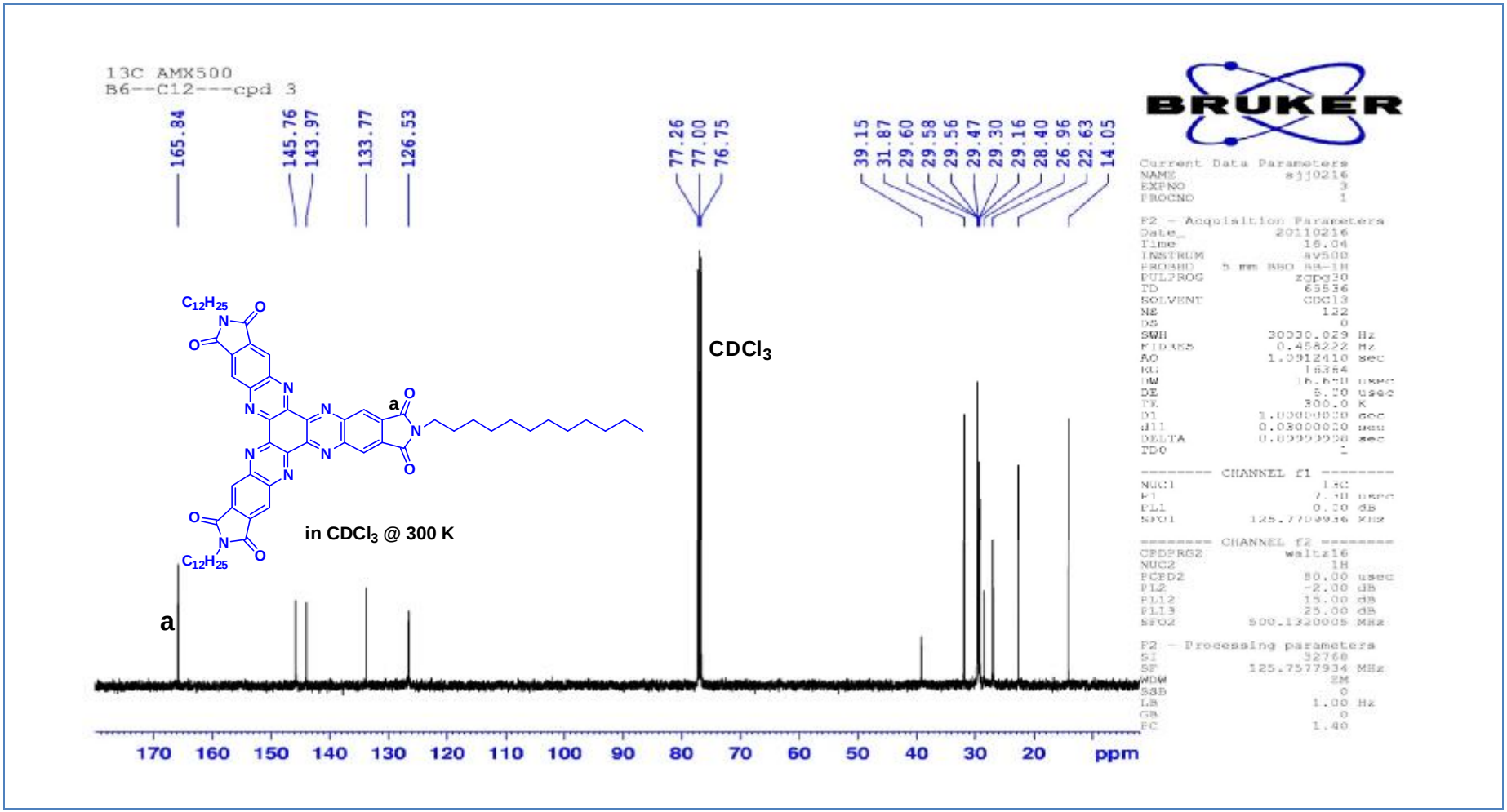

^{1}H NMR spectrum of compound **4-1a**

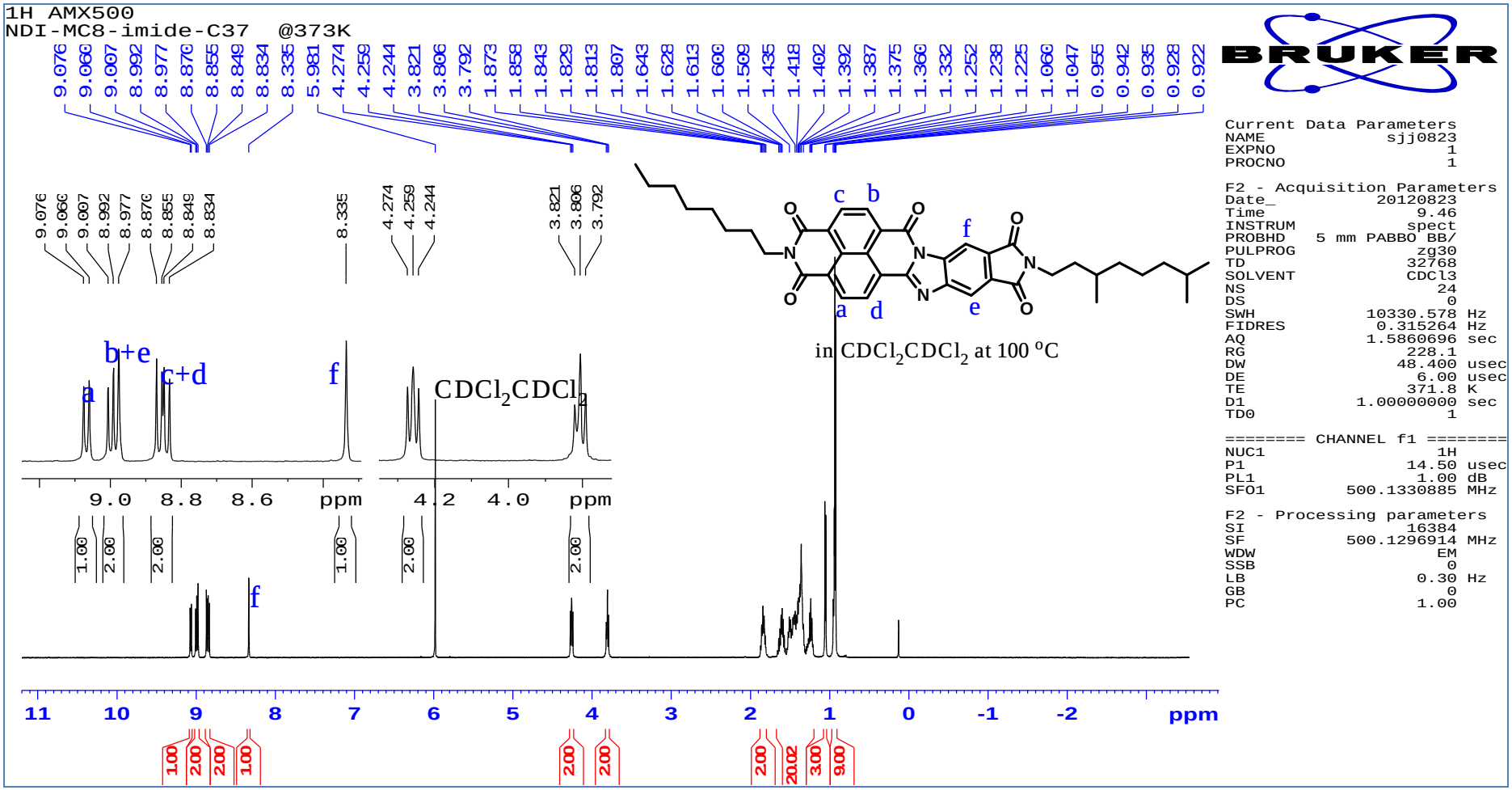

^{13}C NMR spectrum of compound **4-1a**

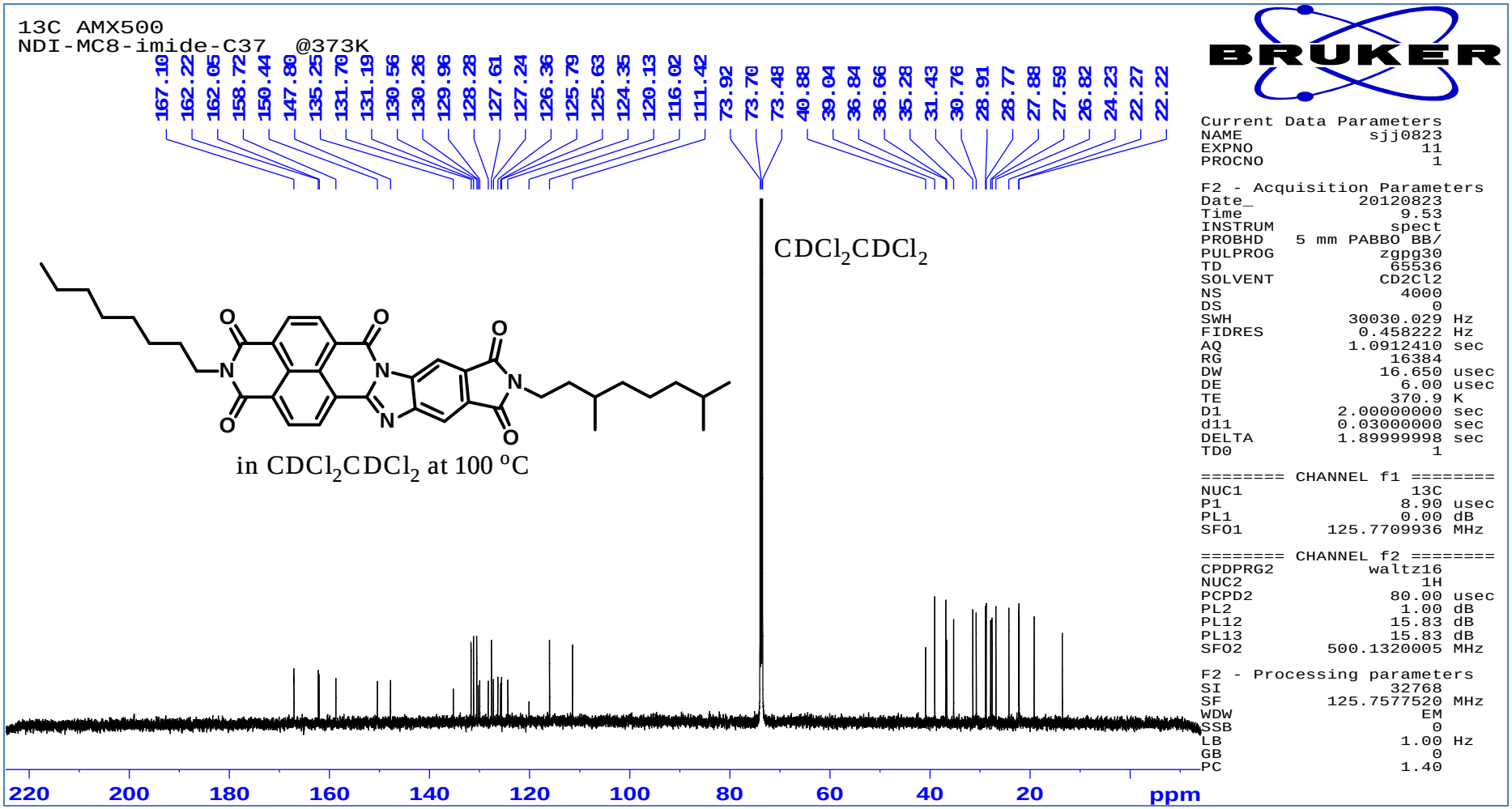

Enlarged part -- **4-1a**

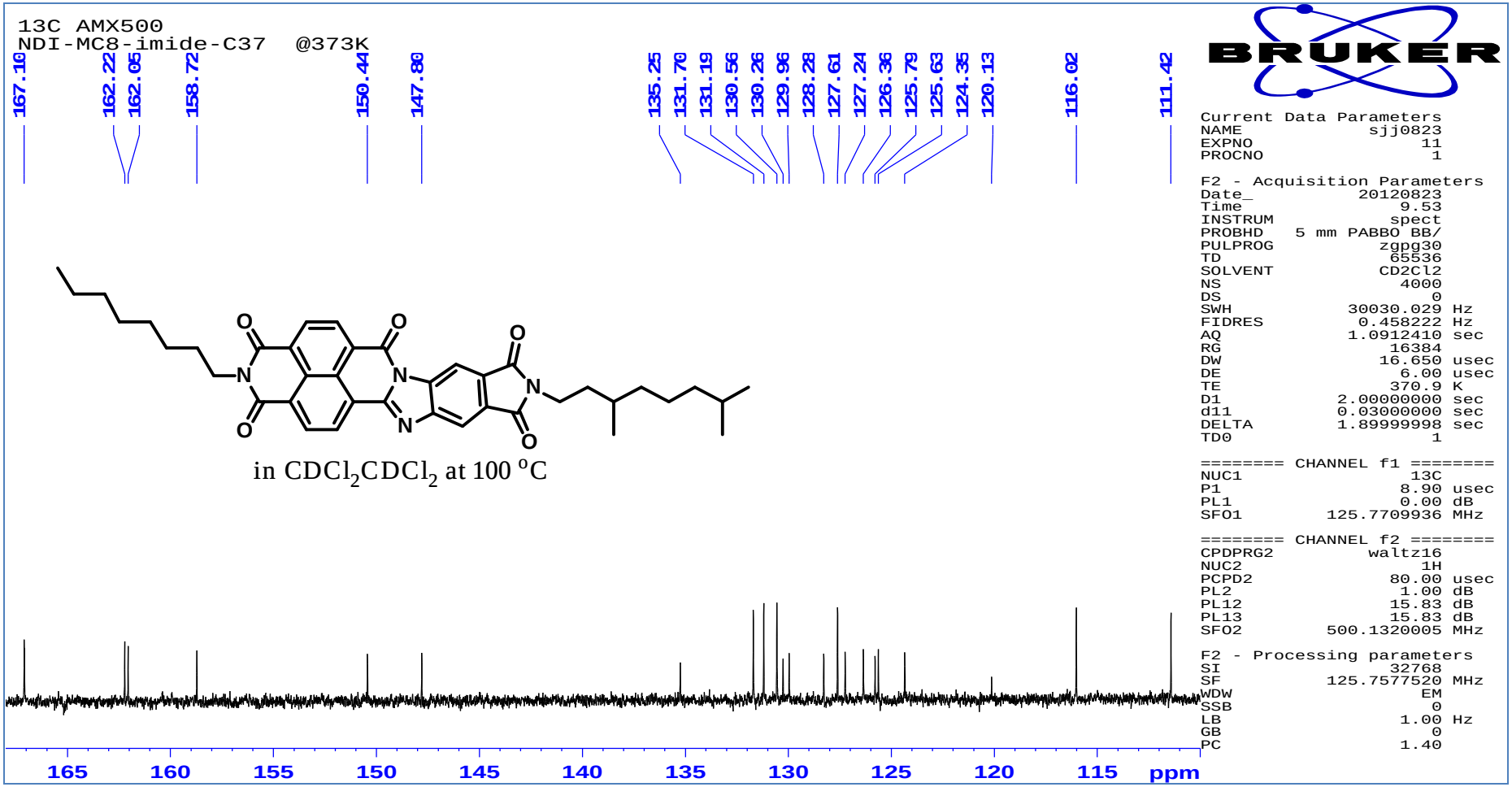

^{1}H NMR spectrum of compound **4-1b**

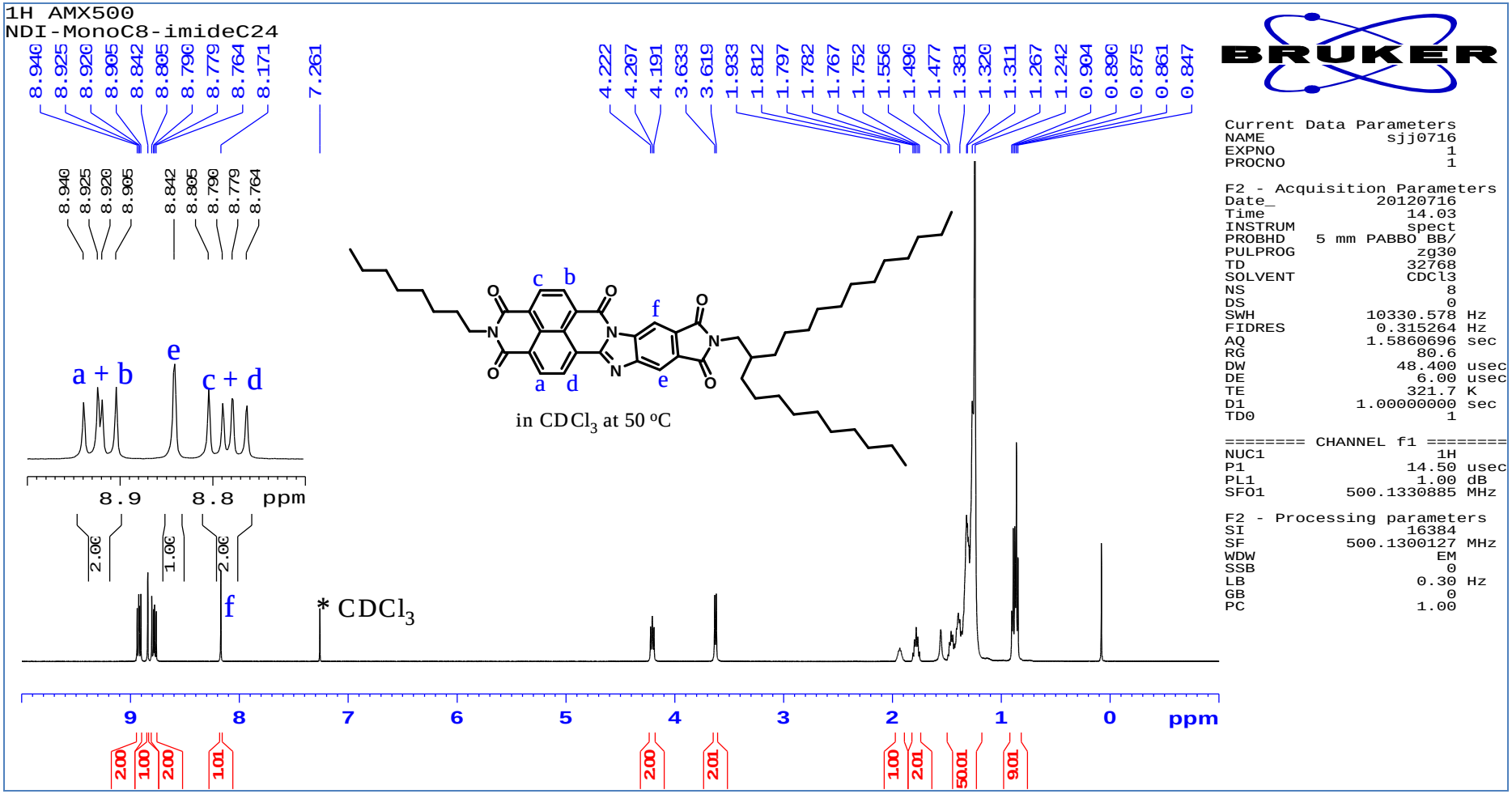

2D COSY spectrum of compound **4-1b**

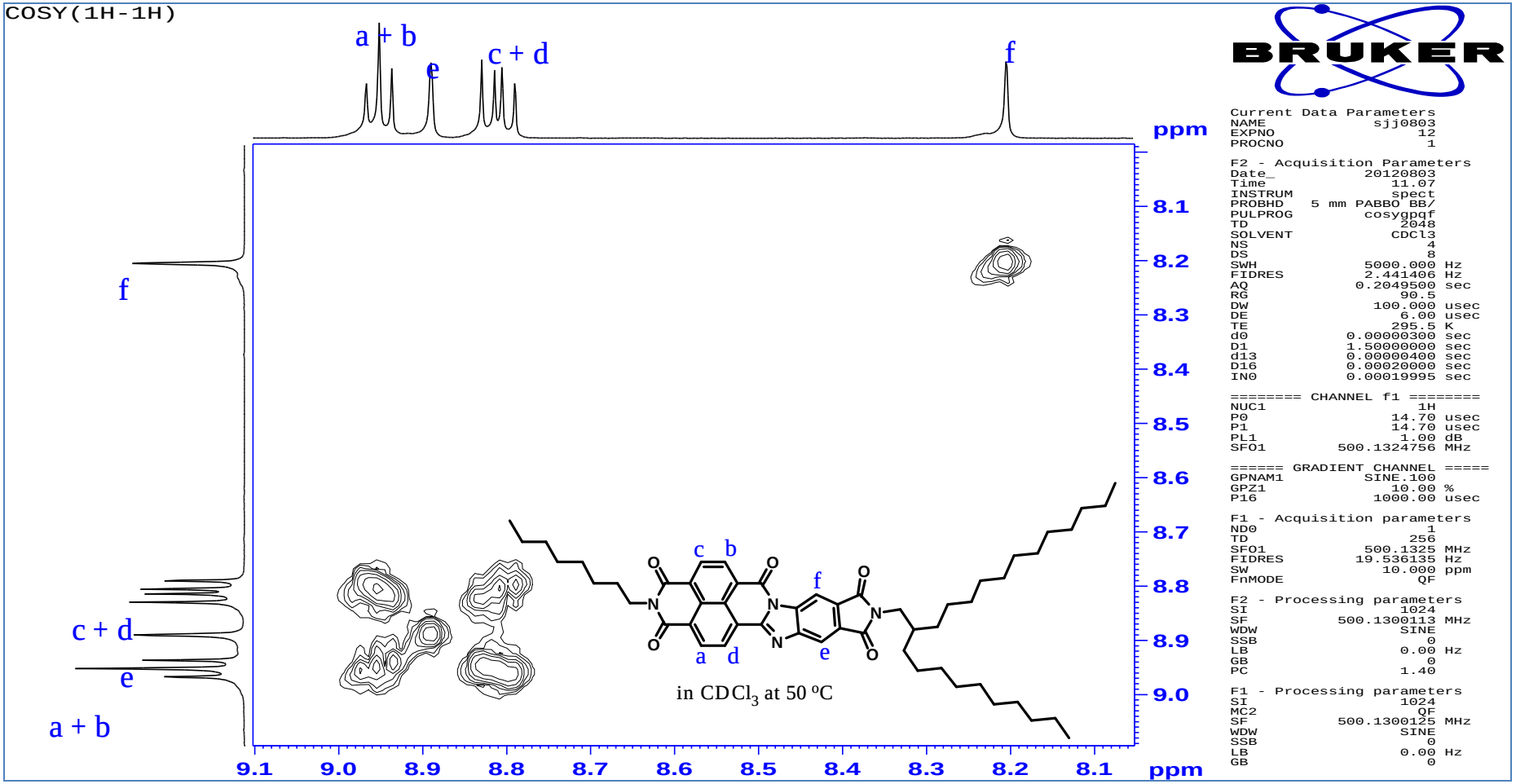

^{13}C NMR spectrum of compound **4-1b**

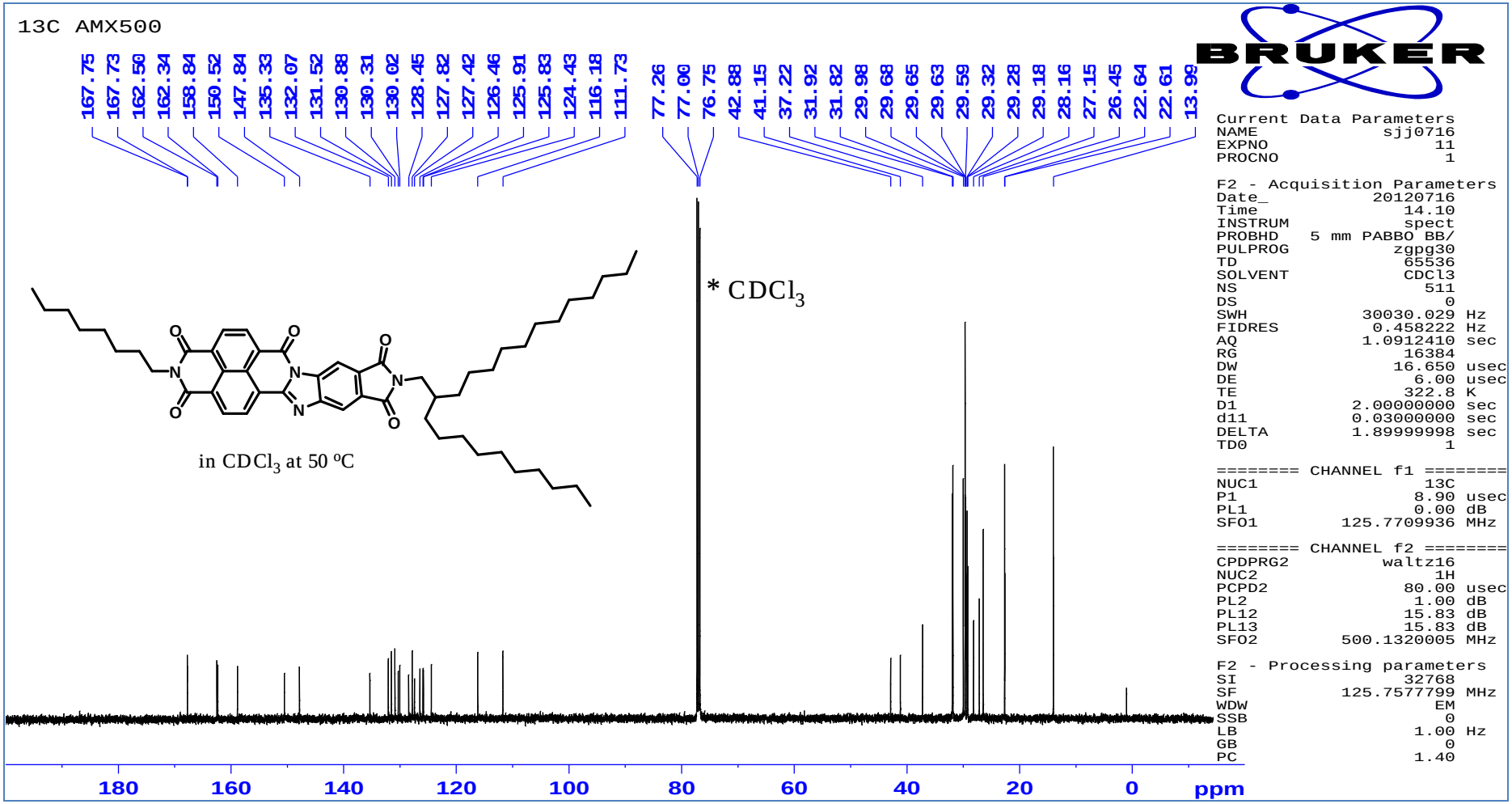

Enlarged part -- **4-1b**

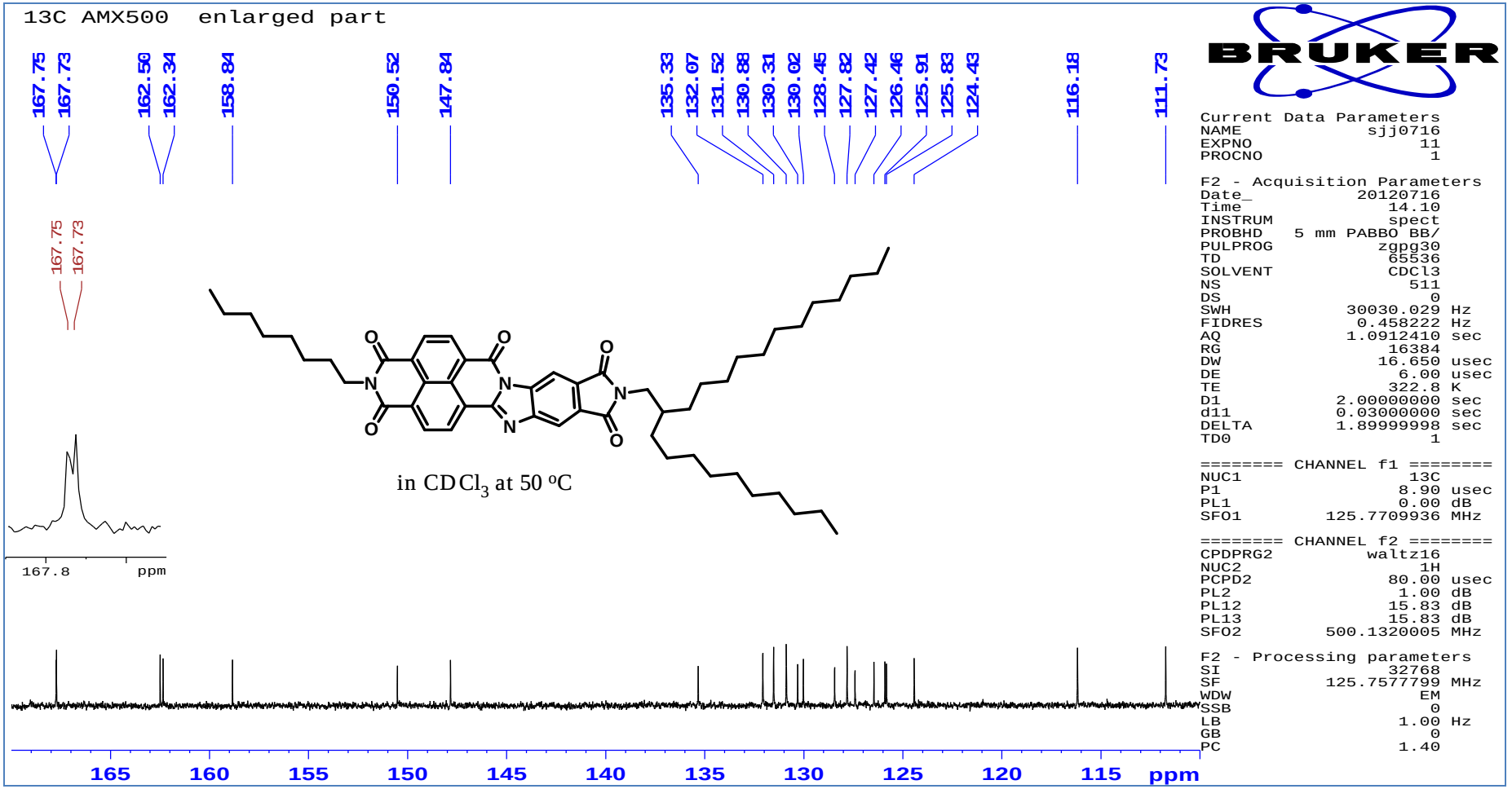

^{1}H NMR spectrum of compound **4-2**

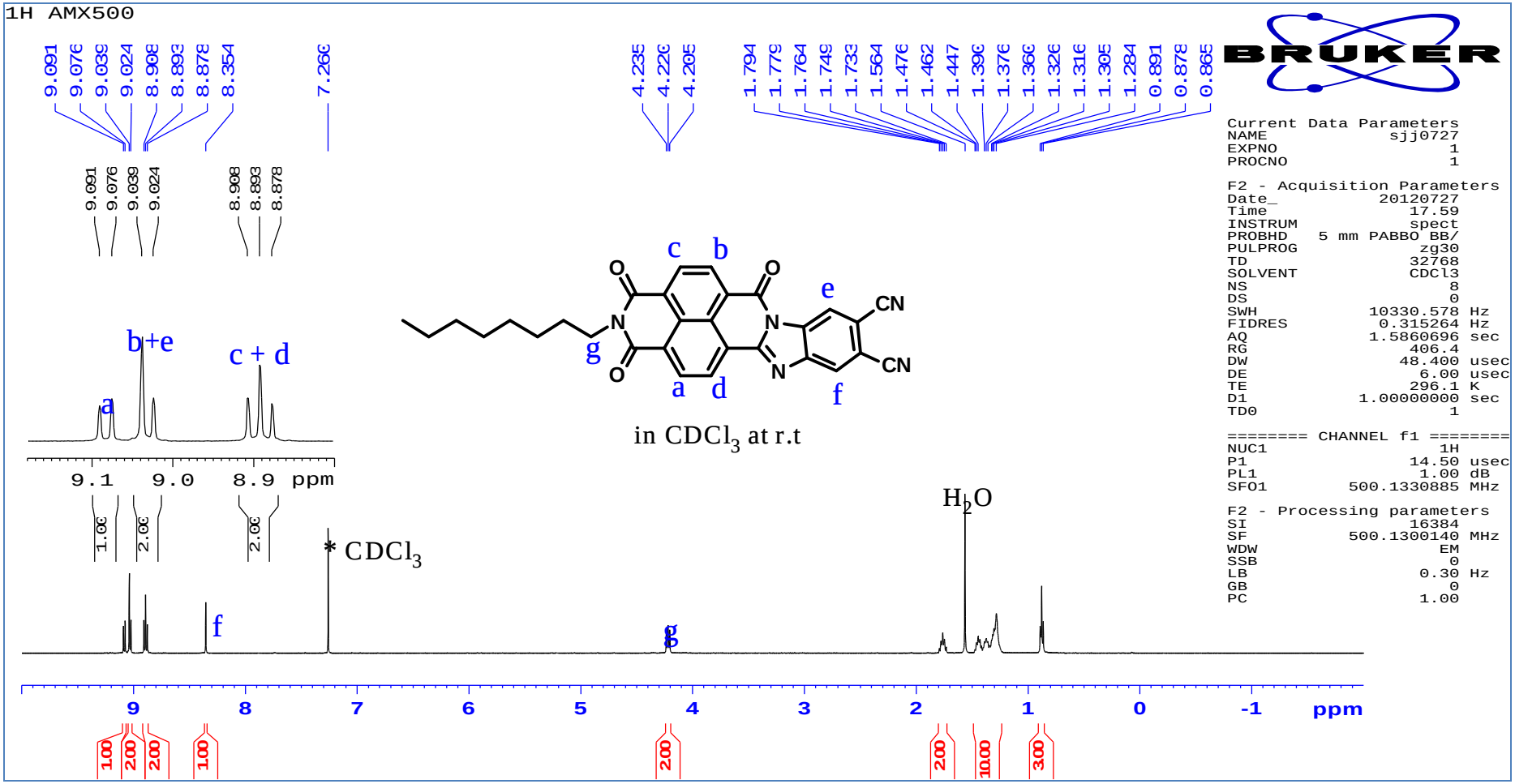

2D COSY spectrum of compound **4-2**

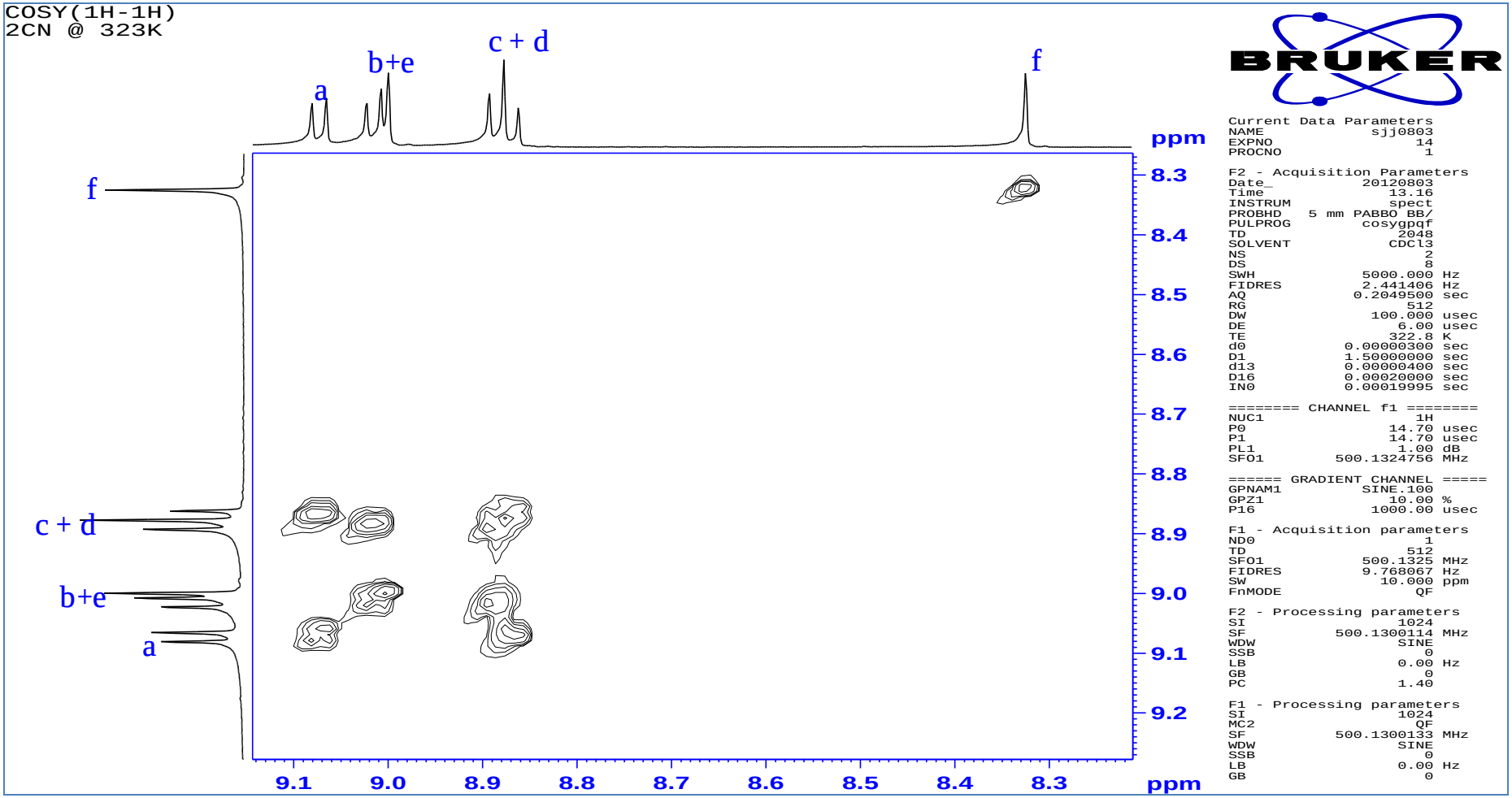

^{13}C NMR spectrum of compound **4-2**

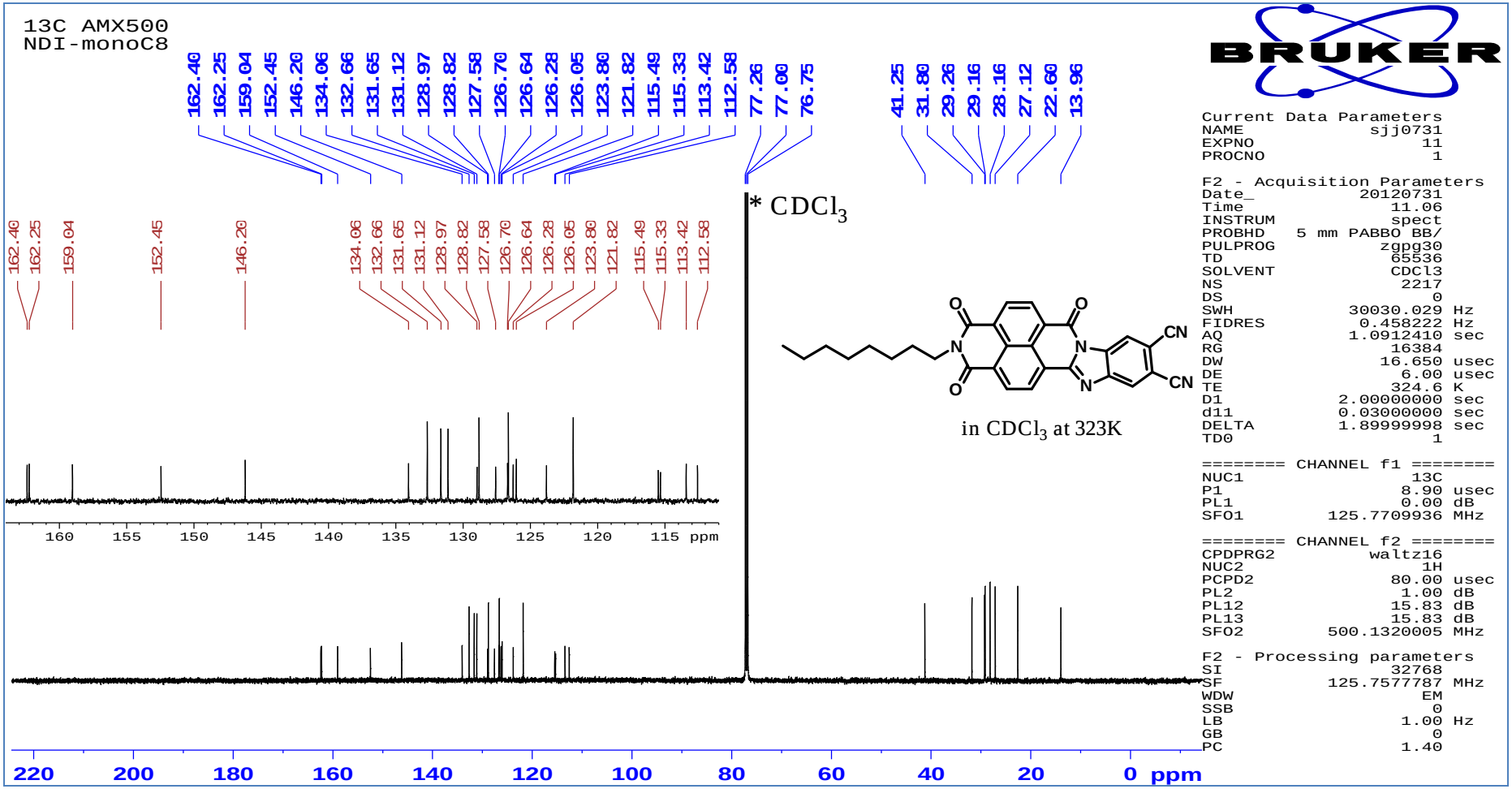

Enlarged part:-- **4-2**

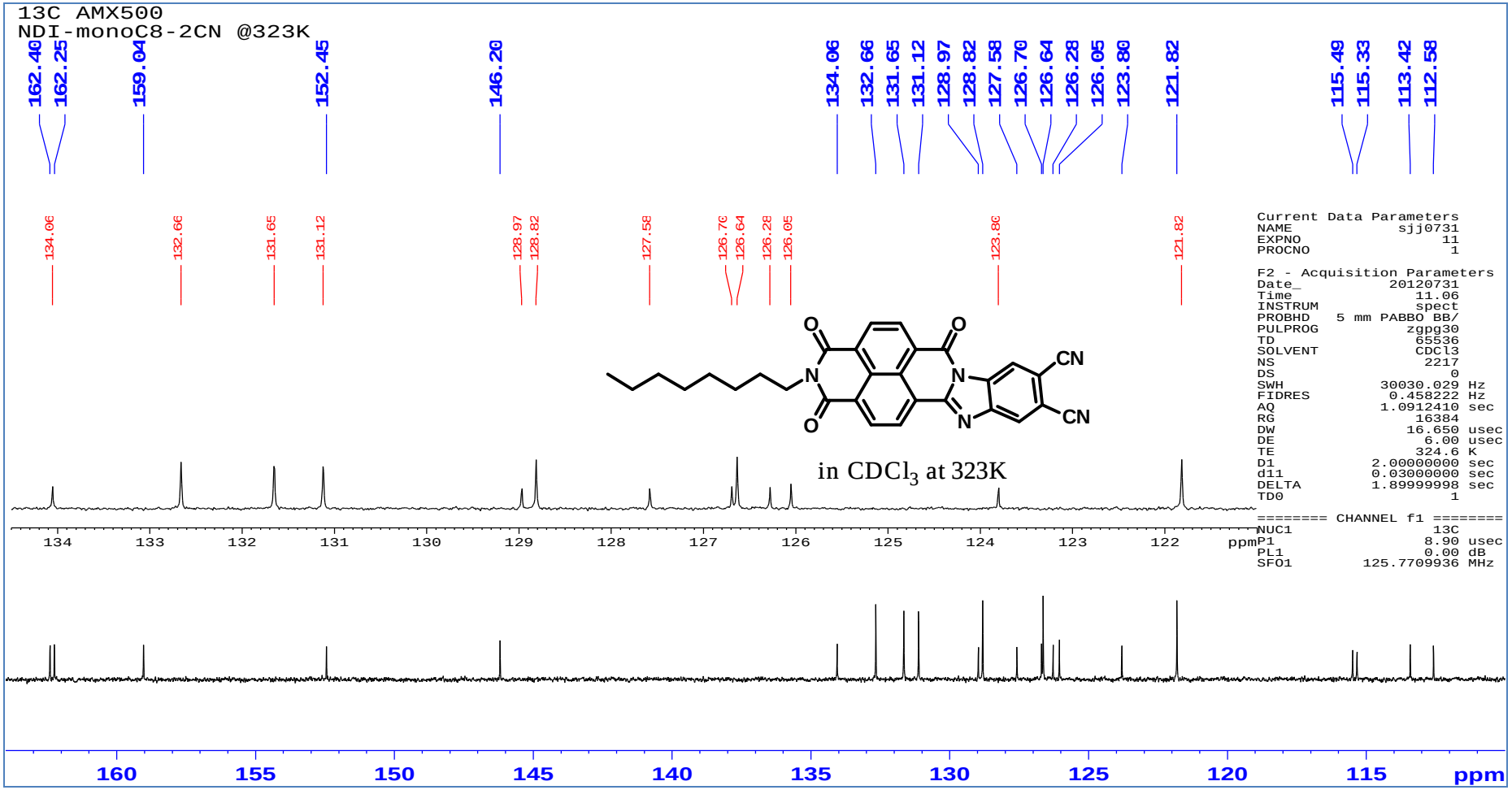

^{1}H NMR spectrum of compound **4-3**

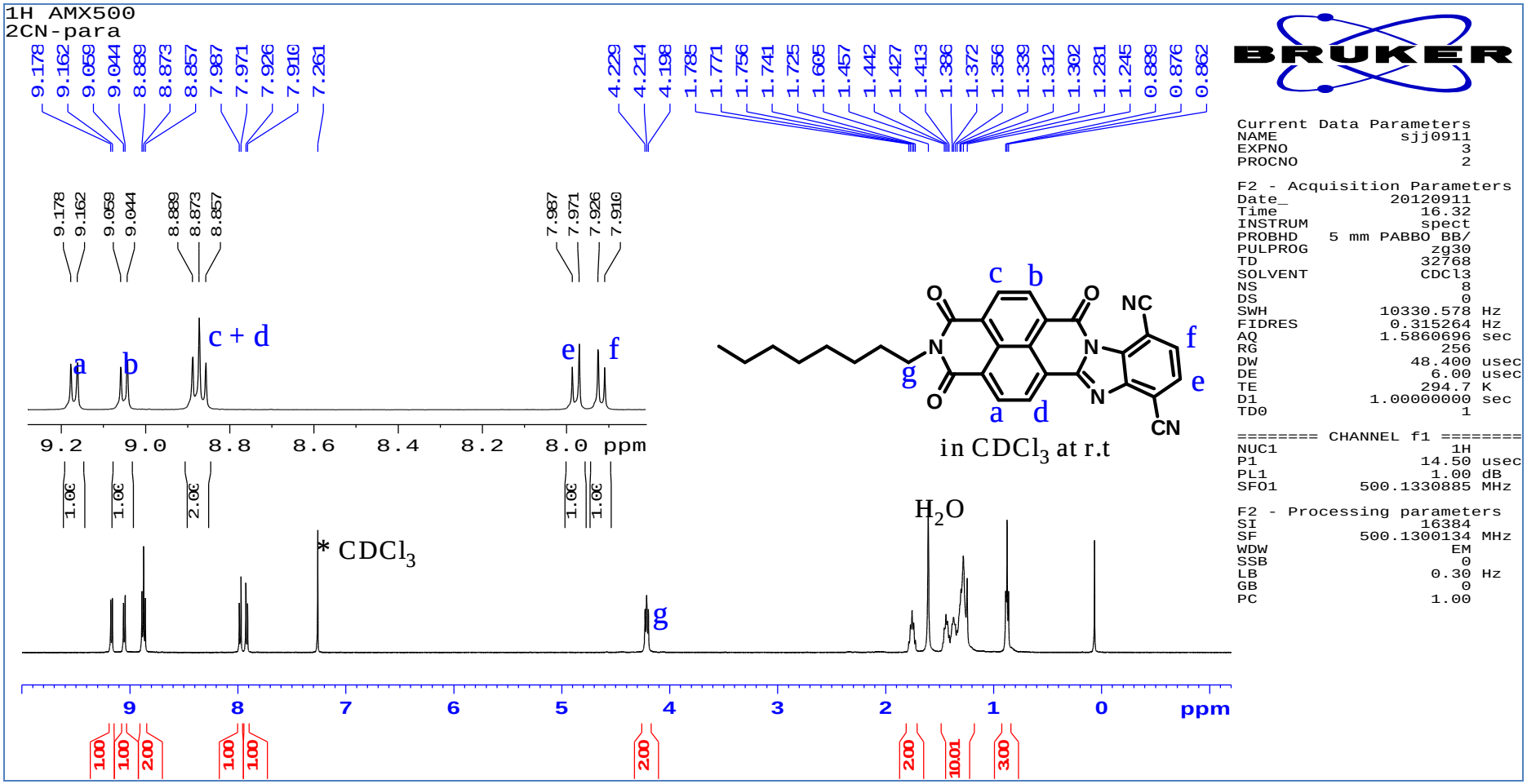

2D COSY (1H-1H) spectrum of compound **4-3**

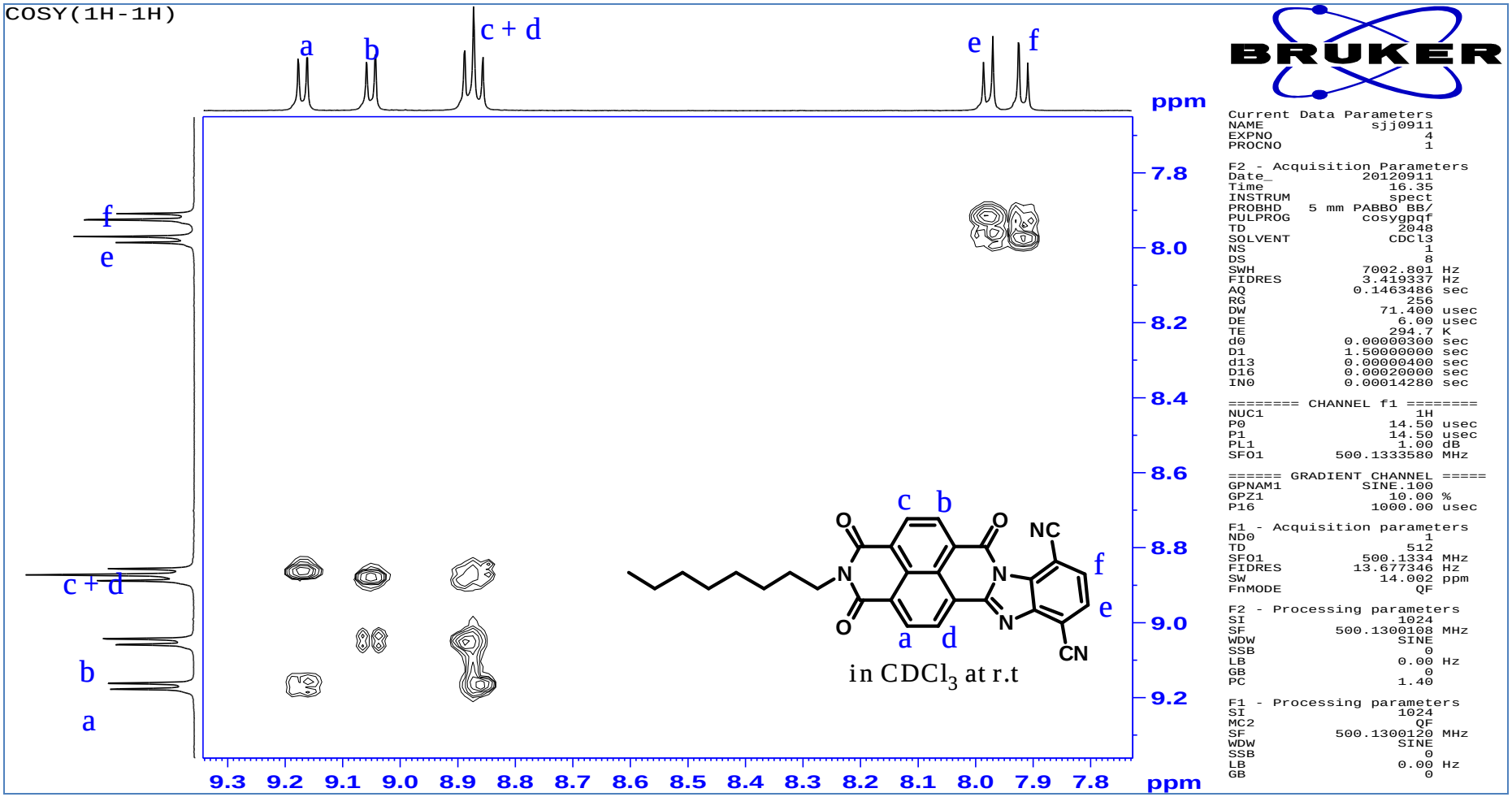

^{13}C NMR spectrum of compound **4-3**

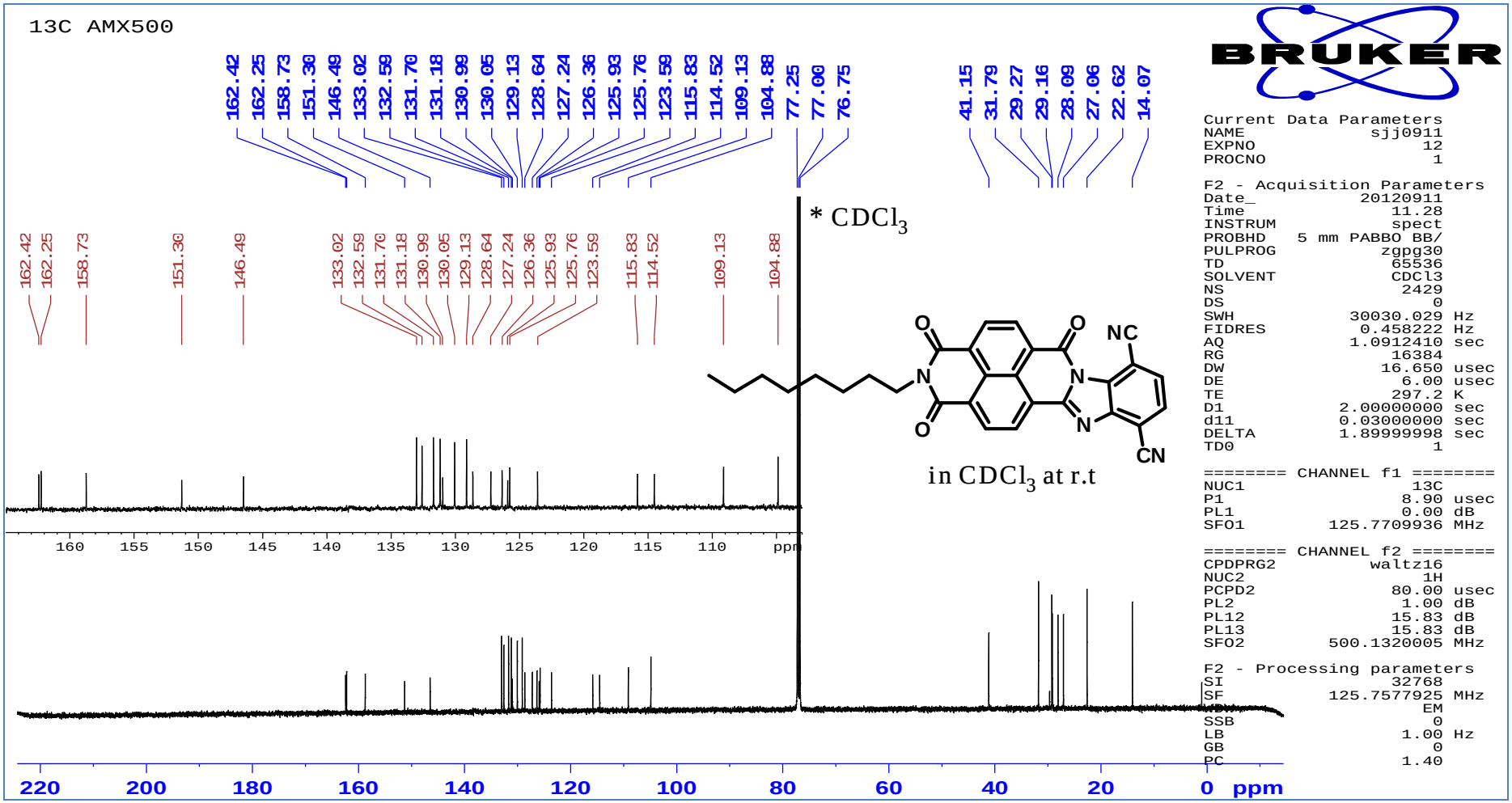

^{1}H NMR spectrum of compound **4-4**

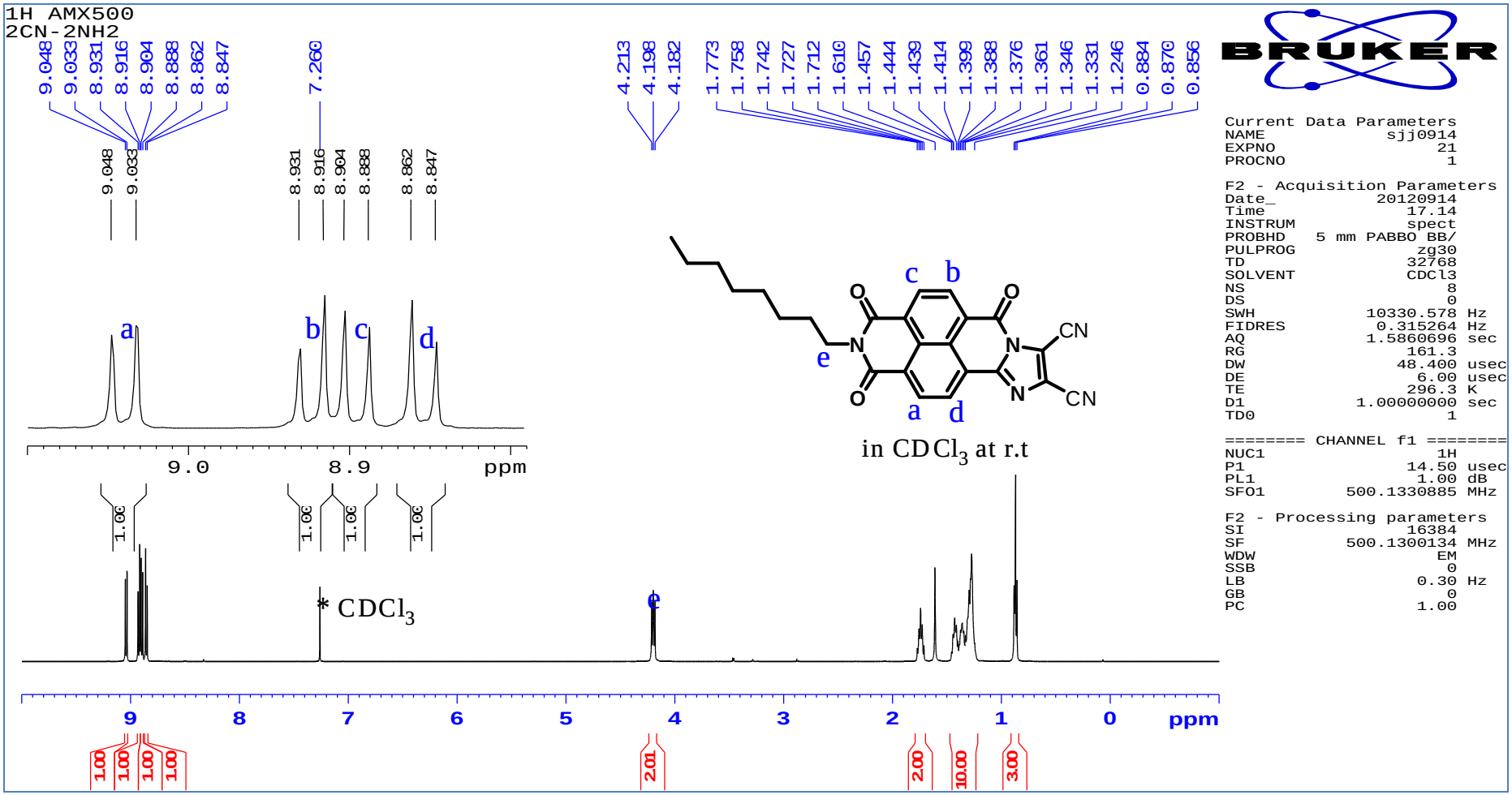

2D COSY spectrum of compound **4-4**

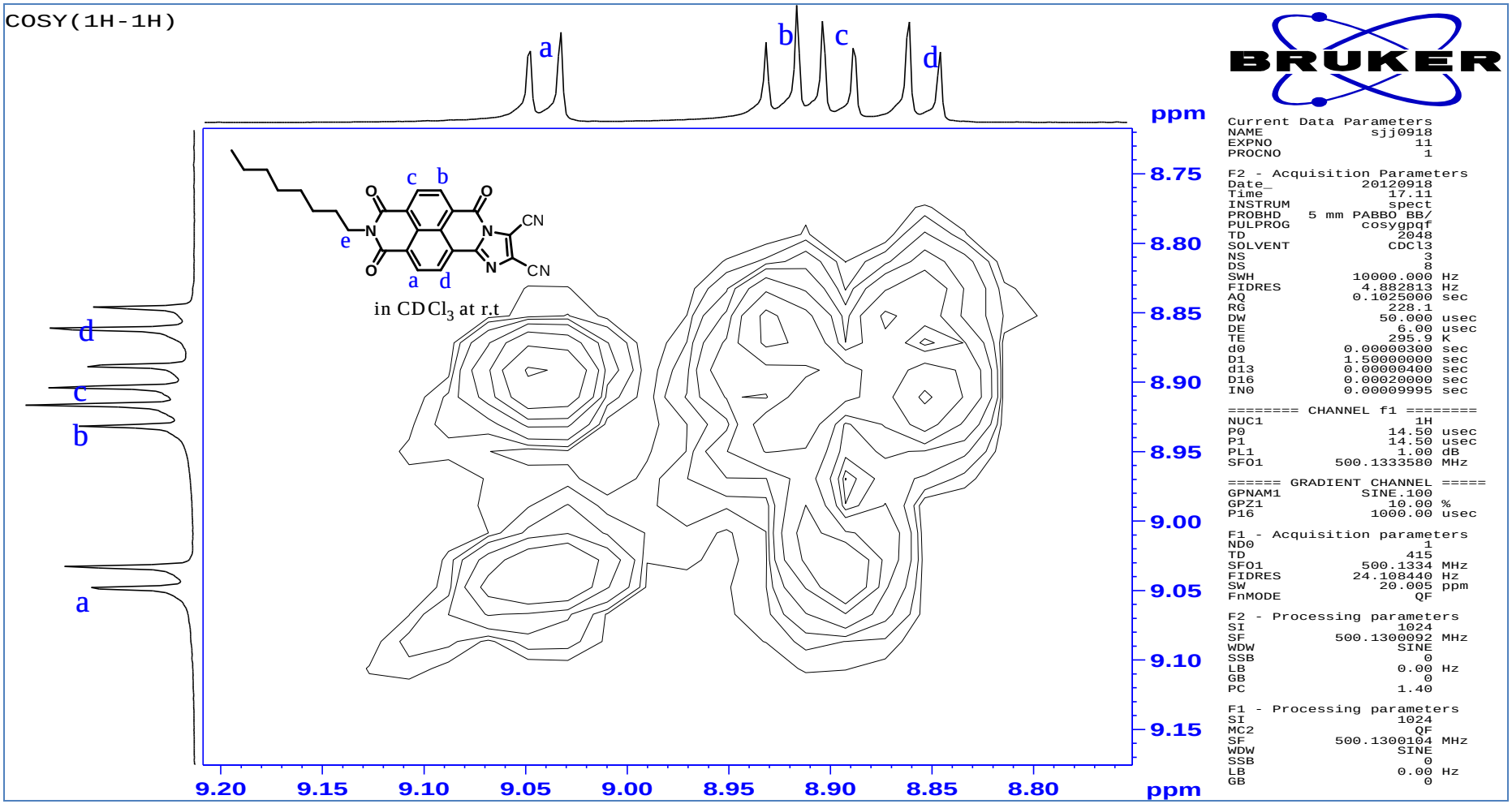

13C NMR spectrum of compound **4-4**

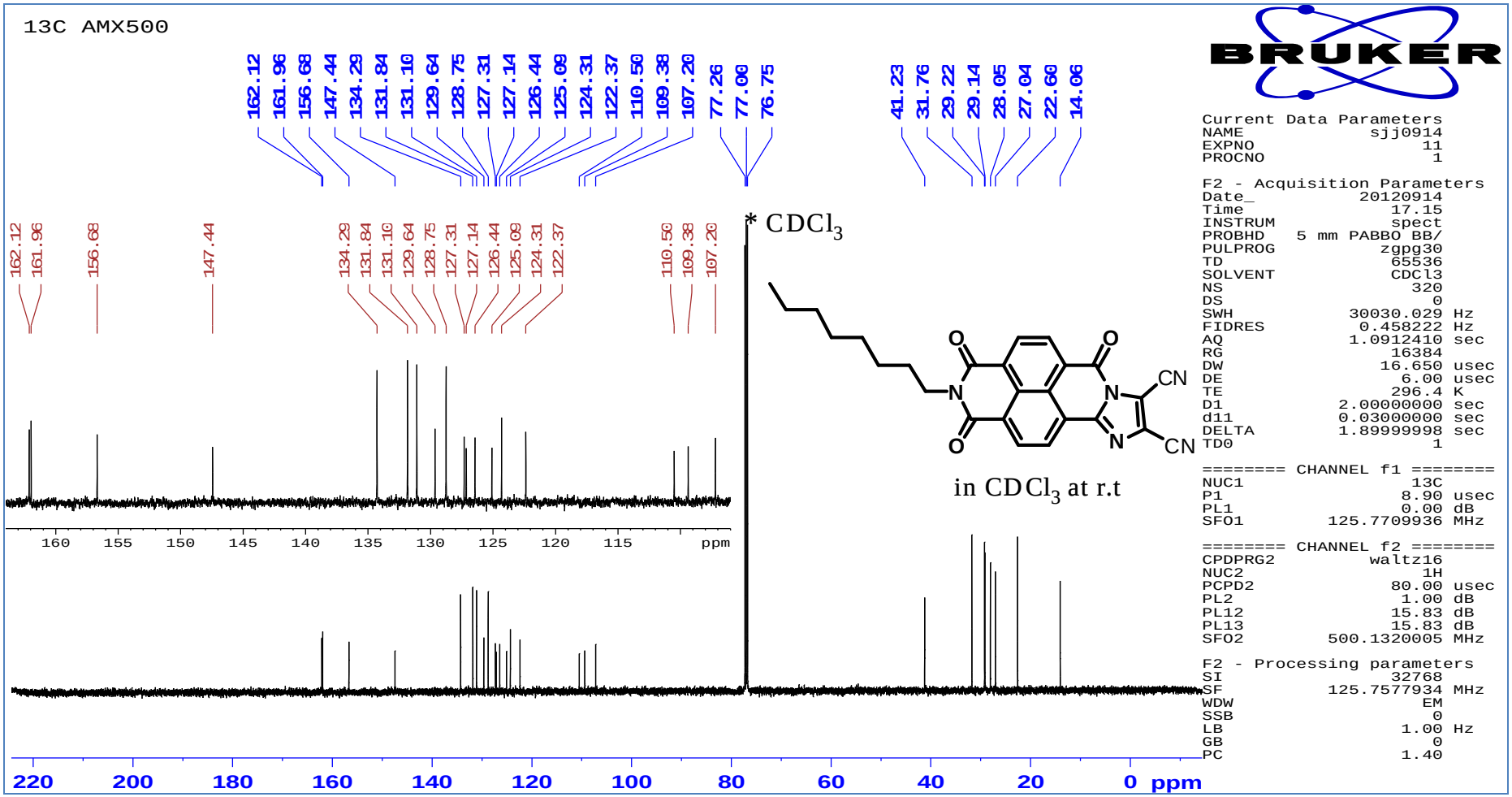

^{1}H NMR spectrum of compound **4-5**

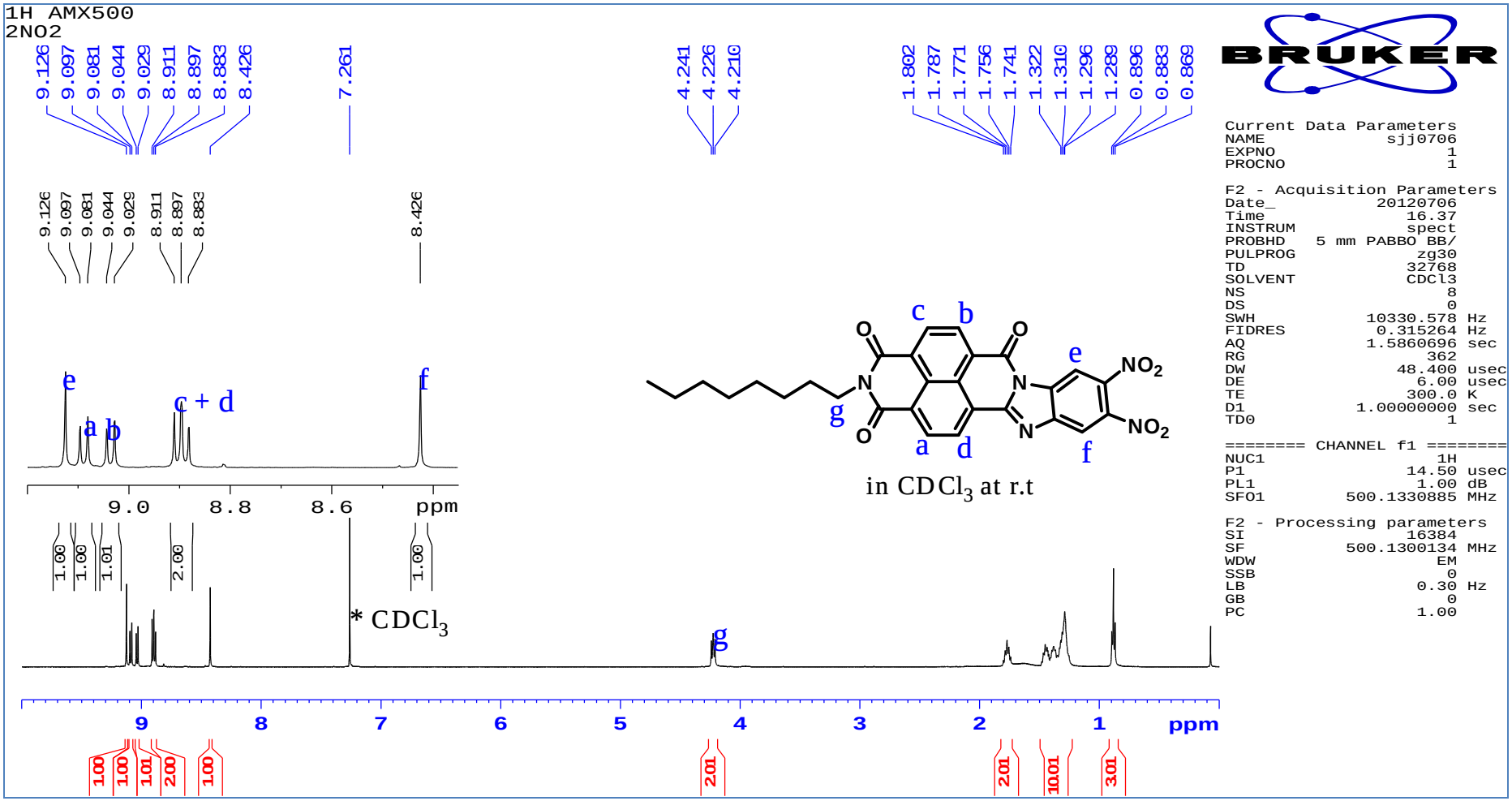

2D-COSY spectrum of compound **4-5**

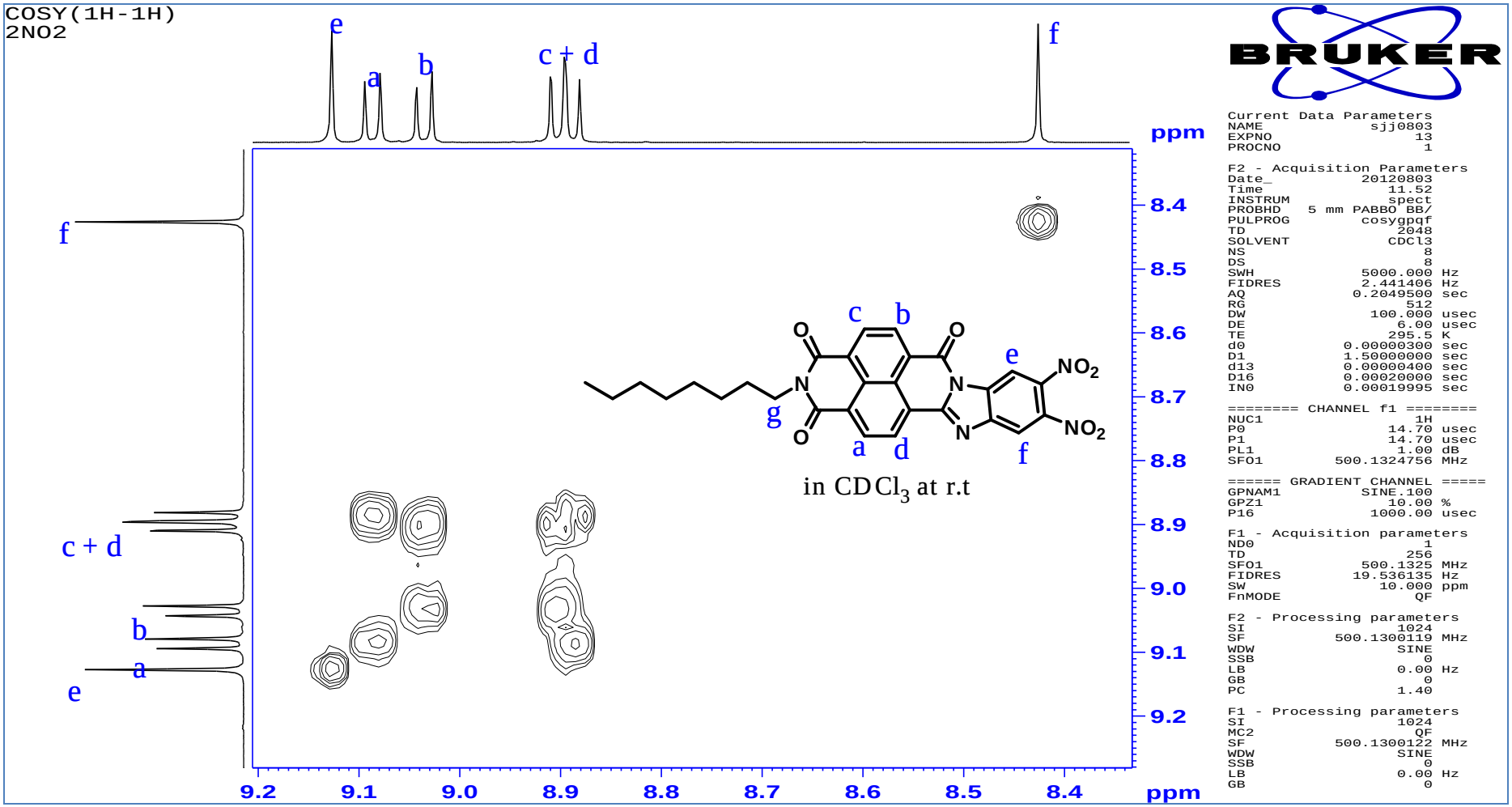

^{13}C NMR spectrum of compound **4-5**

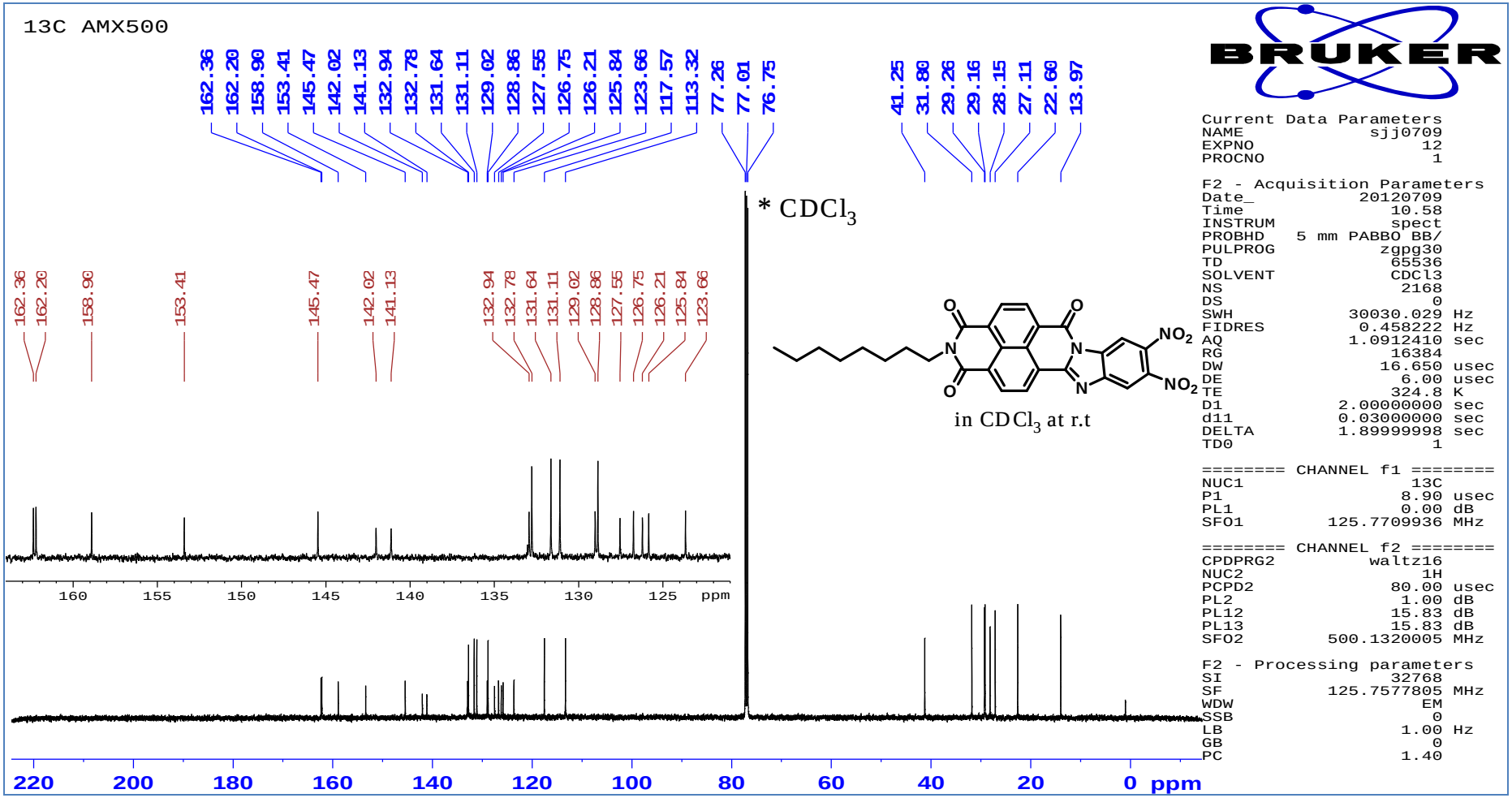

^{1}H NMR spectrum of **NDIIC24** (500 MHZ, $CDCl_3$)